Towards an Advanced Therapy Medicinal Product:
3D bioreactor culture of periosteal progenitor cells

Maarten Sonnaert

Examination committee

EM. Prof. Dr. Y.D. Willems	(Chair)
Prof. Dr. J. Van Humbeeck	(Promotor)
Dr. J. Schrooten	(Co-promotor)
Prof. Dr. F.P. Luyten	(Co-promotor)
Dr. I. Holsbeeks	(Co-promotor)
Prof. Dr. J.M. Aerts	
Prof. Dr. H. Van Oosterwyck	
Dr. F. Veraitch (University College London)	
Prof. Dr. A. Mantalaris (Imperial College London)	

Dissertation presented in partial fulfilment of the requirements for the degree of Doctor in Engineering Sciences

Sept 2015

Uitgegeven in eigen beheer, Maarten Sonnaert, O&N1, box 813, Herestraat 49, B-3000 Leuven

Dankwoord

Eind april 2010 stapte ik tijdens de laatste maand van mijn master thesis het bureau van Dr. Schrooten binnen met de vraag of ik na mijn studies als industrieel ingenieur kon beginnen aan een doctoraat binnen Prometheus. Het zou het begin zijn van een vijf jaar durende ontdekkingsreis in de wereld van weefsel engineering, stam cellen en bioreactoren. Zoals je op elke reis een einddoel voor ogen hebt, is deze thesis de eindbestemming van mijn doctoraat. De weg naar deze bestemming en de mensen die je op deze reis tegen komt, zijn echter minstens even belangrijk. Aangezien de rest van deze thesisverhandeling vooral het eindproduct is van deze reis, wil ik hier toch even de tijd nemen om de mensen die mij bij het tot stand komen hiervan hebben bijgestaan te bedanken.

Allereerst zou ik graag mijn promotoren, Dr. Schrooten, Prof. Luyten en Prof. Van Humbeeck willen bedanken om mij als industrieel ingenieur wegwijs te maken binnen de academische wereld. Toen ik vijf jaar geleden begon aan deze uitdaging, had ik absoluut geen idee wat mij te wachten stond. Jullie steun en begeleiding was van onschatbare waarde om dit doctoraat tot een goed einde te brengen. Dr. Schrooten, bedankt voor de interessante discussies en de vele manuscripten die vaak rood van de correcties en suggesties terugkwamen, zodat ik deze naar een hogen niveau kon tillen. Ook bedankt om mij de vrijheid te geven mijn eigen weg te zoeken in Prometheus met de daarbij horende interessante discussies, zowel op het labo over de bioreactoren als daarbuiten, onder meer over whisky. Prof. Luyten, bedankt om mij als ingenieur welkom te heten in het toenmalige labo voor skelet ontwikkeling en gewrichtsaandoeningen, voor uw kritische kijk en vragen omtrent de projecten van de bioreactor bench en uw waardevolle input voor de verschillende manuscripten. Prof. Van Humbeeck, bedankt voor het nalezen van mijn thesis manuscript en voor uw administratieve steun tijdens dit doctoraat.

Vervolgens zou ik ook mijn copromotor Dr. Inge Holsbeeks willen bedankten voor haar waardevolle input in het tot stand komen van deze thesis en om mij tijdens de lessen op Groep-T interesse te doen krijgen voor dit veld. Bij deze ook expliciet dank u wel aan

het hele team van Groep-T om mij bij hen welkom te heten het semester voor de toekenning van mijn IWT beurs wanneer er geen financiële middelen waren binnen Prometheus om mij te ondersteunen. Dat semester les geven was een zeer leerrijke ervaring waarvan ik nog lang de vruchten zal dragen.

Hartelijk dank ook aan Prof Yves Willems, Prof. Jean Marie Aerts en Prof Hans Van Oosterwyck om deel uit te maken van mijn jury en voor hun interesse in mijn onderzoekswerk. Thank you to the two external members of my jury, Prof Athanasios Mantalaris and Dr. Farlan Veraitch for making the trip to Leuven and for the interesting, critical, open minded discussions.

Het agentschap voor Innovatie door Wetenschap en Technologie (IWT) zou ik ook willen bedankten voor hun financiële steun bij het uitvoeren van dit doctoraat. Thank you also to the team of Octane for the very interesting research stay in Kingston, Canada.

Next, I would like to thank all my colleagues from Prometheus and SBE for all the assistance and interesting discussions as well as the nice evenings out and the great working atmosphere. Ioannis, thank you for all the interesting discussions, the never ending list of suggestions and the relentless commenting on all my manuscripts. Greet, thank you for introducing me to the world of CT and for opening my eyes to what was happening inside the bioreactor and the scaffolds. Both of you being motivated post-docs, each pushing me to give all I had and then a bit more still really helped me to get where I am now. Sometimes making me think twice if I came in to the lab with another overenthusiastic idea was really needed, as were the reminders that from time to time, occasionally the best way of forcing a breakthrough when getting stuck writing can be to just take the weekend off rather than keep on staring at the screen. Johanna and Wai, thank you for the moral support during the IWT writing back in the old lab. I think we put the foundations there for what is now a great working atmosphere in the office. Johanna, also thank you for making me start to run and although I'm not sure I'll be able to join you for your marathon this year, we'll get there sometime soon and who knows we can still convince Abhi to join again? The advantage of working in a multidisciplinary group is that on almost every topic there is an expert available to discuss your ideas with. Yoke Chin, Dennis, Toon, Johanna, Abhi, Luis and Gregory, thank you for being available for these discussions. And of course also thanks to everyone in the lab for the great working atmosphere and the many late nights both in the lab and in Leuven. Next to having a job you like, having a great atmosphere at your workplace is the best motivator to keep on going. I would like to think that these five years at the lab not only resulted in this thesis but also left me with a new group of friends whom, in the future, I hope to see much more often than this thesis.

Daarnaast wil ik ook Carla, Kathleen en al de andere techniekers bedanken voor hun uitstekende technische ondersteuning. Jullie hulp heeft het werk op regelmatige basis een heel stuk lichter gemaakt. Ook Jenny en Annemie verdienen hier een plaatsje voor al de administratieve ondersteuning. Er wordt vaak gezegd dat niemand onmisbaar is, maar ik heb toch sterk mijn twijfels over hoe lang het labo zou blijven draaien zonder jullie niet aflatende inzet.

Work hard, Play hard is de afgelopen vijf jaar mijn levensmotto geweest, of misschien was het *You only have one life to live so live it now*. Ik wil bij deze ook al mijn vrienden bedankten om het leven naast mijn doctoraat ook de moeite waard te maken. Bedankt voor alle toffe weekendjes, snooker avonden, etentjes, whisky tastings,… Ook al mijn reisgenoten van de verschillende mooie reizen die ik heb gemaakt, bedankt om deze één voor één tot onvergetelijke herinneringen te maken. Tijdens die paar weken per jaar kon ik echt mijn werk even volledig vergeten en in schitterend gezelschap ten volle genieten van het leven om dan vaak fysiek volledig uitgeput maar mentaal uitgerust terug thuis te komen.

Tot slot zou ik ook nog mijn familie willen bedanken voor al de steun en motivatie tijdens mijn doctoraat. Mama, Papa, bedankt voor alle goede zorgen en de warme thuis waar ik altijd weer terecht kon, zonder jullie had ik hier nu niet gestaan. Ook bedankt aan Jolijn, mijn zusje, om mij te blijven steunen en om van tijd tot tijd voor de nodige afleiding en koekjes te zorgen. Ik hoop dat ik binnen een 3-tal jaar ook naar jou publieke verdediging zal mogen komen!

Om af te sluiten nog eens een welgemeende dank u wel voor iedereen die hier vandaag aanwezig is en dus ook op een of andere manier betrokken is geweest bij het tot stand komen van dit doctoraat. Zonder jullie steun had ik hier nu niet gestaan.

Maarten

September 2015, Leuven

Abstract

Tissue engineering has been defined as an interdisciplinary field which aims at developing implants to induce or support the regeneration of tissues and organs in compromised defect environments. Despite significant scientific advances no large scale clinical translation of current concepts has taken place yet. As numerous scientific questions remain unanswered concerning for example mechanisms of action, the current focus of the field is predominantly aimed at the development and validation of novel concepts with potential future clinical applications. Although essential for product development, clinical translation and implementation of these concepts will only be feasible if the production of the resulting products can be accomplished using standardized, automated, controlled, reproducible and safe processes. The translation of lab scale processes to a clinical and industrial relevant environment can, however, have significant implications on the process and resulting product. An integrated approach combining product and process development, thereby taking into account future translational aspects from the conceptual development onwards, can facilitate significant advances towards clinical applications. Within this context the use of various bioreactor systems for cell based product development has already been explored as these systems can provide the required controlled, automated and closed process environment. The integration of essential up- and down-stream process steps such as cell expansion as well as the development of tools for process monitoring and quality control towards integrated bioprocess development is, however, lacking. Consequently, numerous technological challenges essential for successful clinical implementation remain to be addressed. The influence of the *in vitro* micro-environment created to facilitate these up- and down-stream processes on cell viability, identity, purity and potency will, however, determine the final applicability of these bioreactor systems.

In order to assess the potential use of a three dimensional perfusion bioreactor system for the expansion of a progenitor cell population the primary objective of this dissertation was to elucidate the influence of this culture system on the proliferation, differentiation, matrix deposition and post-harvest functionality of the expanded cell

population. To facilitate these observations two additional objectives were defined to enable (i) quantitative monitoring of cell proliferation within the bioreactor system and (ii) to visualize and quantify neo-tissue formation within the three dimensional culture environment.

In the first part of this project a method for monitoring a proliferative cell population in a three dimensional perfusion bioreactor system was developed. A quantitative correlation between cell number and the conversion of a metabolic activity assay was established and the influence of different culture and measurement setups on this correlation was determined indicating mass transport associated limitations. A predictive model was developed establishing a correlation between assay signal, cell number and the different measurement parameters. This enabled not only to determine cell number for a given measurement but also to define an optimal operating window for the measurements.

In the second part of this work, contrast enhanced nanofocus computed X-ray tomography was developed as a technique to visualize and quantify the neo-tissue formation (i.e. cells and extracellular matrix deposition) within the constructs. A first proof of principle study was performed showing the potential for the use of two different contrast agents being Hexabrix® and phosphotungstic acid for the neo-tissue visualization. Using a Design of Experiment approach, the influence of different staining parameters (staining time, concentration and neo-tissue quantity) on the quantitative analysis of the datasets was subsequently determined indicating that an increase in concentration of the staining agents had a positive effect on dataset quality. High concentrations of the phosphotungstic acid, however, resulted in a significant negative influence on the neo-tissue integrity. Hexabrix® on the contrary enabled automated, quantitative analysis of the full neo-tissue developed during the perfusion bioreactor expansion.

Using these novel methodologies, in combination with a number of established techniques, the influence of the *in vitro* micro-environment within which the cells reside during the perfusion bioreactor facilitated expansion process on cellular characteristics was determined. Additionally, to assess cell functionality subsequent to expansion, a method for cell recovery from a three dimensional culture environment was developed using a Design of Experiment approach. Although minor differences were noted no significant induction of an osteogenic or chondrogenic phenotype was observed and post expansion functionality of the cells was maintained based on both *in vitro* and *in vivo* functionality assays.

In conclusion, this dissertation showed that the *in vitro* micro-environment created in a three dimensional perfusion bioreactor can facilitate the expansion of a progenitor cell population without significantly influencing its functional characteristics. In addition, novel methods for on-line monitoring and characterization of the constructs were developed enabling to gain new insights in the bioreactor facilitated processes.

Samenvatting

Weefsel-engineering kan omschreven worden als een interdisciplinair onderzoeksveld gericht op de ontwikkeling van implantaten ten einde de regeneratie van weefsels en organen in gecompromitteerde omgevingen te induceren of ondersteunen. Ondanks de aanzienlijke wetenschappelijke vooruitgang in dit veld blijft de grootschalige klinische translatie van deze concepten momenteel afwezig. Omwille van de complexiteit van de processen in de ontwikkelingsbiologie en weefsel regeneratie blijven veel vragen omtrent onder meer werkingsmechanismen onbeantwoord. De huidige focus van het onderzoeksveld is dan ook gericht op het ontwikkelen van nieuwe concepten die mogelijks kunnen leiden naar toekomstige klinische toepassingen. De nieuwe inzichten die hierdoor zullen verschaft worden zijn essentieel voor de ontwikkeling van nieuwe producten maar hun klinische implementatie zal enkel bereikt kunnen worden mits ze geproduceerd worden in een gecontroleerde, geautomatiseerde en gestandaardiseerde omgeving. De translatie van processen ontwikkeld op labo schaal naar een klinisch en industrieel relevante omgeving kan echter significante invloed hebben op het resulterende proces en product. Er is daarom nood aan een geïntegreerde benadering die vanaf de conceptuele ontwikkeling van een nieuw product toekomstige translationele aspecten in rekening brengt. Het gebruik van geautomatiseerde en gecontroleerde bioreactor systemen wordt in deze context beschouwd als een toegevoegde waarde en verschillende mogelijkheden voor de productie van stamcel gebaseerde inplanten werden reeds geëvalueerd. De integratie van essentiële geassocieerde processen zoals de voorgaande celgroei alsook de ontwikkeling van methodes voor het opvolgen van de processen in de bioreactoren en kwaliteitscontrole van de resulterende producten is echter grotendeels afwezig. Verschillende technische knelpunten verhinderen op dit moment de doorgedreven implementatie van de verschillende ondersteunende proces stappen in een geïntegreerde, gecontroleerde en geautomatiseerde omgeving. Bijkomend zal de invloed die deze artificiële omgeving heeft op het cel gedrag gedurende deze processen beslissend zijn voor hun finale toepasbaarheid.

In deze context was het primaire doel van deze thesis het evalueren van het gebruik van een drie-dimensioneel perfusie bioreactor systeem voor het opgroeien van een voorloper cel populatie in een geautomatiseerde, gecontroleerde en gesloten omgeving. De invloed van deze artificiële omgeving op het cel gedrag werd geanalyseerd op basis van cel proliferatie en differentiatie, matrix depositie en functionaliteit. Ter ondersteuning van deze waarnemingen werden ook twee additionele doelstellingen gedefinieerd zijnde (i) het kwantitatief opvolgen van celgroei in de bioreactor en (ii) het visualiseren en kwantificeren van biologisch weefsel gevormd in de drie dimensionele cel cultuur omgeving.

In het eerste deel van dit project werd een methode voor het opvolgen van celgroei in een drie-dimensionele perfusie bioreactor ontwikkeld. Een kwantitatieve correlatie tussen cel aantal en de conversie van een metabool assay voor het bepalen van cel activiteit werd bepaald alsook de invloed van verschillende cel cultuur methodes en verschillende opstellingen voor het uitvoeren van de metingen. Vervolgens werd een voorspellend model ontwikkeld dat het verband tussen het signaal verkregen met de assay correleert met het cel aantal en de verschillende parameters geassocieerd met de meting. Naast het bepalen van cel aantal op basis van de metabole meting stond dit ook toe om de parameters voor de meting zo te selecteren dat een optimaal operationeel venster kon gedefinieerd worden.

Het tweede deel van dit werk was gefocust op de ontwikkeling van contrast-verbeterde nanofocus X-stralen computer tomografie voor de visualisatie en kwantificatie van biologische weefselvorming in de constructen. Een initiële validatie van het concept gebaseerd op het gebruik van twee verschillende contrast verhogende reagens (Hexabrix® en fosforwolfraamzuur) bevestigde de mogelijkheid van deze nieuwe methodologie voor de visualisatie van het biologisch weefsel. Met behulp van experimenteel ontwerp werd vervolgens de invloed van verschillende methodologische parameters (incubatie tijd, concentratie en volume van het biologisch weefsel) op de kwantitatieve interpretatie van de bekomen beelden bepaald. Het gebruik van een hogere concentratie van beide contrast verhogende reagens resulteerde in een beduidend hogere beeldkwaliteit en contrast. Voor fosforwolfraamzuur resulteerde deze hogere concentraties echter ook degradatie van het biologisch weefsel wat de kwantitatieve interpretatie van de data irrelevant maakte. Het gebruik van Hexabrix® daarentegen stond de geautomatiseerde, kwantitatieve analyse van het biologisch weefsel in de constructen ontwikkeld in de perfusie bioreactor toe.

In combinatie met gevestigde methodes werd deze nieuwe technologie gebruikt om de invloed van de artificiële omgeving in de drie-dimensionele perfusie bioreactor tijdens de celgroei te bepalen op de eigenschappen van de resulterende cel populatie. Om ook de functionaliteit van deze cel populatie te kunnen evalueren werd er een methode ontwikkeld voor de recuperatie van de cellen na het groeiproces op basis van experimenteel ontwerp. Ondanks het vaststellen van enkele verschillen in onder meer gen expressie, geïnduceerd door de perfusie bioreactor cultuur, werd er geen beduidende osteogene of chondrogene differentiatie vastgesteld. Bovendien toonde functionele testen, zowel *in vitro* als *in vivo*, aan dat na het opgroeien en recuperatie de functionele eigenschappen van de cellen bewaard bleef.

In conclusie toonde het werk voorgesteld in dit proefschrift aan dat de artificiële omgeving in de drie-dimensionele perfusie bioreactor de expansie van een voorloper cel populatie ondersteunde zonder een beduidende invloed te hebben op de functionele eigenschappen hiervan. Bijkomend werden vernieuwende methodes ontwikkeld voor het opvolgen van celgroei en voor karakterisatie van de constructen gevormd tijdens het expansie proces ten einde nieuwe inzichten in de bioreactor processen te verkrijgen.

List of Symbols

τ	Shear stress
η	Viscosity
γ	Shear rate
A	Average greyscale difference between the stained neo-tissue and the scaffold
B	Average greyscale difference between the background and the stained neo-tissue
$\dot{C}$	Presto Blue conversion rate
c_{cell}	Cell density
c_R	Spatiotemporal evolution of resazurin
D	Diffusion coefficient resazurin
$\dot{F}$	Flowrate
n	Cell number
Q	Resazurin conversion rate
[R]	Resorufin concentration
SA_{Hex}	Hexabrix® stained neo-tissue surface area
SA_{PTA}	PTA stained neo-tissue surface area
t_d	Time delay between medium entering tubing and reaching scaffold
V	Bioreactor volume
V_T	Tubing volume

List of Abbreviations

2D	Two dimensional
3D	Three dimensional
AB	Alamar Blue®
ATMP	Advanced Therapy Medicinal Product
BMP	Bone Morphogenetic Protein
BSP	Bone Sialoprotein
CD	Cluster of Differentiation
CE-nanoCT	Contrast Enhanced nanofocus Computed Tomography
CFD	Computational Fluid Dynamics
CM	Culture Medium
Col1	Collagen type 1
CT	X-ray Computed Tomography
DMSO	Dimethylsulfoxide
DoE	Design of Experiments
ECM	Extracellular Matrix
EMA	European Medicine Agency
FGF	Fibroblast Growth Factor
FU	Fluorescent Units
GMP	Good Manufacturing Practice
HLA-DR	Human Leukocyte Antigen-D Related
hPDC	human Periosteal Derived Cell
HPRT	Hypoxanthine-Guanine Phophoribosyltransferase
I2KI	Iodine Potassium Iodide
Ihh	Indian Hedgehog
MSC	Mesenchymal Stem Cell
MW	Molecular Weight
OCN	Osteocalcin
OPN	Osteopontin
OSX	Osterix
PAT	Process Analytical Technology

PBS	Phosphate Buffered Saline
PCL	Polycaprolactone
PDGF	Platelet derived growth factor
PGA	Polyglycilic Acid
PLA	Poly-Lactic Acid
PLDL	Poly(L/LD)-Lactide
PLLA	Poly-L-Lactide
PB	Presto Blue®
PTA	Phosphotungstic Acid
PTHrP	Parathyroid Hormone related Protein
PVE	Partial Volume Effect
RT PCR	Real Time Polymerase Chain Reaction
RunX2	Runt-related transcription factor 2
SLM	Selective Laser Melting
SS	Shear Stress
TE	Tissue Engineering
TGF-β1	Transforming Growth Factor β1
Ti	Titanium
Ti6Al4V	Titanium 6-Aluminium 4-Vanadium

Table of Contents

List of Figures

List of Tables

Chapter 1.
General introduction

Tissue engineering (TE) has been defined as an interdisciplinary field which aims at developing implants to induce or support the regeneration of tissues and organs in compromised *in vivo* environments. Despite significant scientific advances and the availability of various proof of concept studies no large scale clinical implementation of these TE concepts has taken place yet. As numerous scientific questions remain unanswered concerning for example mechanisms of action, the current focus of the field concentrates predominantly on the development and validation of novel concepts with potential clinical applications. Although indeed essential for future product development, clinical translation and implementation of these concepts will only be possible if the production of the resulting products can be accomplished using standardized, automated, controlled, reproducible and safe processes. The translation of lab scale processes to such a clinical and industrial relevant environment can, however, have significant implications for the process environment and therefore on the resulting product. An integrated approach combining product and process development, thereby taking into account future translational aspects from the conceptual development onwards, can facilitate significant advances in the field towards clinical applications. Within this context the use of various bioreactor systems for cell based product development has recently gained interest. The implementation of essential up- and down-stream steps correlated with this product development such as cell expansion as well as the development of tools for process monitoring and quality control towards fully integrated bioprocess development is, however, lacking.

The aim of this thesis was therefore to explore the potential of a three dimensional (3D) perfusion bioreactor system for stem cell expansion within the context of the host lab which focusses on skeletal TE applications. In addition, different tools required for monitoring and characterizing the cell behavior in the bioreactor environment were developed. This introductory chapter presents a brief overview of the functions and structure of the skeletal system and the processes involved during skeletal development. The relevance of these pathways in fracture repair and the potential of their application in TE is discussed. Subsequently, an introduction to integrated bioprocess development situates the current state of the art in this field with respect to TE. Finally, a short overview of several aspects essential for the development of a controlled and monitored process such as non-destructive imaging and on-line monitoring is presented.

1.1. Skeletal tissue

1.1.1. Bone structure and composition

The adult human skeleton consists of a total of 206 bones. Although the primary function of this organ is to provide structural support and protection for other fragile organs, it also serves as an important reservoir for minerals and plays an essential role in blood synthesis by hosting the bone marrow. As a living organ, the skeletal system is sensitive to changes in environmental factors such as mechanical loading and is subject to a constant remodeling process. Moreover, it possesses a unique healing capacity enabling it to repair most defects without inducing scar formation.

Depending on shape and function the bones of the skeletal system can be divided into five different categories. The flat bones are present in the skull, ribs and sternum serving mainly to provide extensive protection to the underlying organs as well as providing extensive attachment sites for surrounding muscles, for example in case of the scapula (shoulder blade). The long bones such as the tibia are subjected to the highest loads throughout the body and are essential for mobility. The three other groups of bones (short, irregular and sesamoid bones) consist mainly of smaller bones with a variety of functions ranging from support and stability to protection of vital organs.

Despite this variety of anatomical shapes and functions, most bones have a similar macroscopic structure. The outer layers consist of compact cortical bone which provides the required strength and stiffness. The porous cancellous bone is mainly present in the center of the bones and hosts the bone marrow as well as nerves and blood vessels. Within the bone matrix three different cell types reside: osteoblasts, osteocytes and osteoclasts. The osteoblasts which originate from mesenchymal stem cells (MSCs) are cuboidal mononucleated cells lining the edges of the bone. They deposit a collagen type I (Col1) rich matrix, the osteoid, which subsequently gets mineralized resulting in the entrapment of the cells in the bone matrix. Subsequent differentiation of a fraction of the entrapped osteoblasts will give rise to the star-shaped osteocytes which form an interconnected network through cytoplasmic extensions. Through their mechanosensitivity they can regulate the bone remodeling process by transduction of specific biochemical signals resulting in the recruitment of osteoblasts and osteoclasts. The latter of the two are multinucleated cells originating from the hematopoetic cell

compartment. Through solubilization of the underlying mineralized extracellular matrix (ECM) these cells are responsible for resorption of the bone.

The ECM of the bone provides its functional characteristics and is comprised out of an organic and inorganic fraction. The main constituent of the organic fraction is Col1 which provides the required flexibility and tensile strength to the tissue. Approximately 5% of the organic fraction comprises non-collagenous proteins such as osteocalcin and osteopontin which are associated with the mineral phase of the matrix and correlated with regulation of bone structure and its mechanical characteristics. The inorganic phase of the bone matrix consists mainly of hydroxyapatite crystals providing the required stiffness and strength to the tissue.

1.1.2. Bone development

The fetal development of bone occurs through two different pathways namely intramembranous ossification (direct bone formation) and endochondral ossification (indirect bone formation) (Kronenberg 2003).

In the case of intramembranous ossification condensation of the MSCs present in the connective tissue results in direct differentiation of these cells to osteoblasts. These subsequently initiate the osteoid deposition and matrix maturation towards a functional, mineralized bone matrix. This direct process of bone formation *in vivo* is, however, exceptional and predominantly occurs in the flat bones of the skull (Lenas *et al.* 2011).

In long bone development MSC condensation is followed by the differentiation of these condensations towards chondrocytes resulting in a cartilaginous template. This template will further expand through the proliferation of the chondrocytes and the associated deposition of a collagen type II and aggrecan-rich cartilage matrix (Kronenberg 2003). The cells in the center of the template will subsequently stop proliferating, become hypertrophic and start producing a collagen type X-rich matrix. Through the secretion of multiple biochemical signaling molecules these hypertrophic chondrocytes will attract blood vessels, initialize matrix mineralization, cartilage remodeling and resorption resulting in the formation of the primary ossification center (Lenas *et al.* 2011). Continued proliferation of the surrounding chondrocytes further enlarges the bone template as secondary ossification centers are formed at the epiphyseal ends. Chondrocytes in the cartilaginous zone between primary and secondary ossification centers are spatially organized in a growth plate from resting chondrocytes near to the epiphyseal ends to proliferating, pre-hypertrophic and hypertrophic chondrocytes towards the primary ossification center thereby mediating longitudinal bone growth. For humans, the growth plate will eventually close at the end of adolescence (Mackie *et al.* 2008).

The process of endochondral ossification is tightly regulated by a number of zonal expressed transcription and growth factors as shown in Figure 1.1.A. Briefly, Indian Hedgehog (Ihh), expressed in the pre-hypertrophic zone, inhibits terminal hypertrophic differentiation and cartilage mineralization and stimulates chondrocyte proliferation, both direct and through stimulation of Parathyroid Hormone related Protein (PTHrP) which in turn inhibits Ihh expression through a negative feedback loop (Figure 1.1.B).

Bone Morphogenetic Protein expression (BMP), know to facilitate endochondral ossification when injected subcutaneously, positively influence chondrocyte proliferation and Ihh expression (Figure 1.1.B). Transcription factors Sox9 and RunX2 are essential for the zonal development of the growth plate where Sox9 ensures mesenchymal commitment towards chondrocytes and ensures expression of several critical cartilage matrix genes such as collagen type II and aggrecan. RunX2 on the other hand is essential for terminal hypertrophic differentiation and plays an important role in vascular invasion of the mineralizing cartilage (Kronenberg 2003, Provot *et al.* 2005).

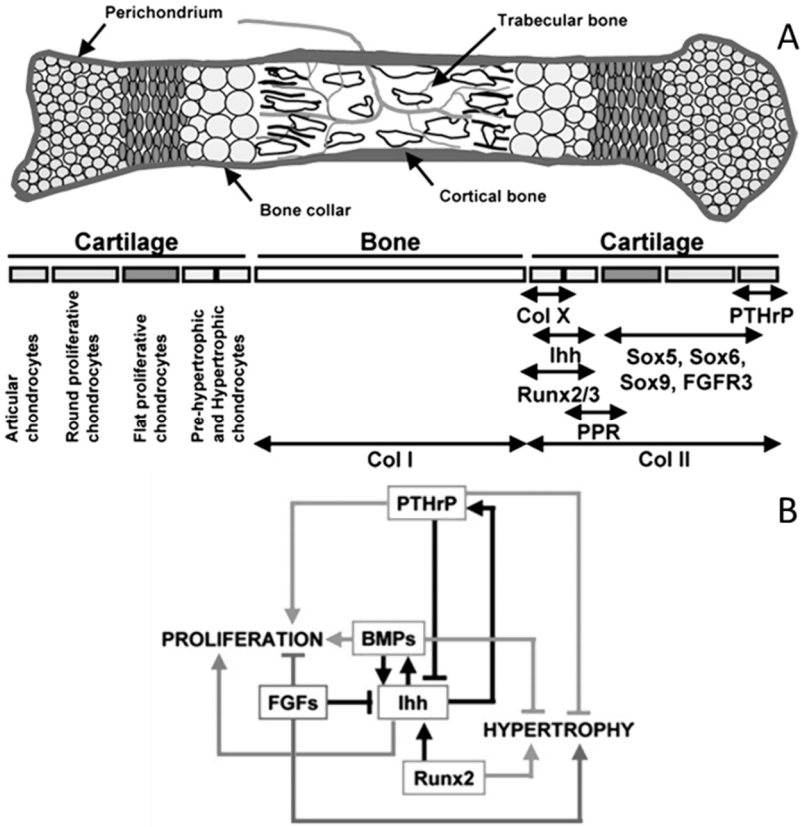

Figure 1.1: Endochondral ossification.
(A) Schematic representation of tibia at late stage of fetal development. Characteristic markers for different zones are indicated. (B) Schematic representation of the growth plate regulation by feedback loops and biological interactions. Indian Hedgehog (Ihh) induces parathyroid hormone related protein (PTHrP), required for chondrocyte proliferation, which in turn inhibits Ihh expression thereby influencing chondrocyte proliferation and differentiation. Ihh also positivly influences Bone morphogenetic proteins (BMP) which, together with Ihh and PTHrP influence chondrocyte proliferation. Fibroblast growth factor (FGF) negativly influences Ihh expression and proliferation and positivly affects terminal differentiation. Finally, RunX2 is a positive modulator of hypertrophy and also upregulates Ihh expression (Provot *et al.* 2005).

1.1.3. Fracture repair

Unlike most adult tissues, bone has the capacity to heal the majority of defects without the formation of scar tissue. The mechanisms governing bone regeneration are closely related to the developmental pathways and are in addition influenced by the mechanical environment of the fracture.

In case of limited stabilization of the defect hematoma formation is induced as a result from the bleeding at the defect site. Subsequent recruitment of inflammatory cells as well as the initiation of cytokine and growth factor production such as transforming growth factor β1 (TGF-β1), platelet derived growth factor (PDGF) and FGF result in recruitment of skeletal progenitor cells from the periosteum, bone marrow and the circulation (Lieberman *et al.* 2002, Papadimitropoulos *et al.* 2014b, Bigham-Sadegh *et al.* 2015). Under the influence of different growth factors among which TGF-β1 and BMPs play a major role these cells will form MSC condensations leading to the development of a cartilaginous callus essential for the mechanical stabilization of the defect (Bigham-Sadegh *et al.* 2015). In parallel with the developmental process of endochondral ossification the cartilaginous callus will mature towards hypertrophy followed by vascular ingrowth and remodeling of the callus leading to the formation of woven bone. Over a period of months this is further remodeled to the more organized, mechanically stronger laminar and cortical bone (Papadimitropoulos *et al.* 2014b). For defects with a rigid stability the formation of a cartilaginous intermediate for stabilization of the defect is not required and intramembranous ossification through the direct differentiation of MSC condensations occurs (Tonnarelli *et al.* 2014).

Critical size bone defects

Despite the remarkable capacity of bone to heal a broad range of defects, provided there is correct realignment and sufficient stabilization of the fracture, between 5 and 10% of the fractures in long bones result in delayed or non-union which remains a significant clinical problem until today (Jakob *et al.* 2012). The preferred treatment for these non-unions is based on the use of autologous graft material obtained from for example the iliac crest of the patient due to the inherent histocompatibility and lack of immunological response associated with the use of this material (Jakob *et al.* 2012, Costa *et al.* 2014). Limited availability of autologous donor material and the significant risk for post-surgical complications, such as donor site morbidity, pain and infection, as well as the extensive surgical procedure are, however, significant drawbacks associated with this methodology (Costa *et al.* 2014). These could be addressed using grafts of allogenic or xenogeneic origin although these are still associated with concerns on pathogen transmission and immunogenicity. Engineered synthetic materials on the other hand often lack osteoinductive and/or osteogenic properties and have shown reduced healing potential in addressing complex and high load bearing fractions. Alternative treatment options circumventing the use of grafting materials are based on distraction osteogenisis. The two ends of the fracture are brought into close proximity of each other using external fixators. Next, they are gradually being moved apart again as the new bone forms. Due to the limited regeneration rate of bone (between 0.5 and 1mm/day) this, however, results in a long healing time associated with a significant risk on clinical complications and pain.

Due to the sub optimal treatment options for these severe bone fractures there is a significant interest and need for the development of novel, efficient methods to address these defects.

1.2. Tissue engineering

TE was defined as an interdisciplinary field that combines the principles of engineering and life sciences towards the development of biological substitutes to restore, maintain or improve tissue function (Langer *et al.* 1993). Through understanding of the complex biology of tissue development and regeneration at the defect site, and by combining knowledge from different scientific disciplines such as material sciences, developmental biology, engineering and computational sciences, 3D constructs with an *in vivo* functionality can be developed *in vitro*.

The original paradigm of TE was based on 3D cell growth and differentiation towards the *in vitro* development of a functional tissue prior to implantation (Lenas *et al.* 2011). Through the combination of cells, a scaffold and different growth factors, followed potentially by the *in vitro* development of this construct, various groups aimed at developing a mineralized construct to facilitate functional repair of the damaged bone (Cartmell *et al.* 2003, Zhao *et al.* 2005, Grayson *et al.* 2010, Grayson *et al.* 2011). Although several of these constructs showed to possess, to a certain extent, an *in vivo* bone forming capacity using ectopic models, reports of successful osteo-integration of these constructs are largely absent (Braccini *et al.* 2005, Janssen *et al.* 2006b, Agata *et al.* 2007, Grayson *et al.* 2007). One of the causes for the shortcomings of this approach was hypothesized to be the lack of relevance of the developed constructs in the *in vivo* bone regeneration process (Ingber *et al.* 2006, Lenas *et al.* 2011).

In order to increase the biological relevance of the TE constructs the paradigm of developmental engineering was introduced which is based on the *in vitro* recapitulation of the *in vivo* processes involved in bone fracture healing (Lenas *et al.* 2011). As discussed earlier the *in vivo* fracture healing process as well as the development of the long bones takes place through endochondral ossification which comprises of consecutive phases of mesenchymal condensation, the development of a cartilaginous template, its subsequent maturation towards hypertrophy and the final remodeling resulting in *in vivo* bone formation. As blood vessel invasion in the developing bones and fracture callus coincides with the remodeling of the hypertrophic cartilage template towards bone and the formation of the primary ossification center the *in vitro* engineered constructs should not be progressed beyond this point to ensure successful incorporation in the host tissue. Different studies already confirmed the feasibility of this approach by inducing *in vivo* bone formation through the implantation of a cartilaginous template (Scotti *et al.* 2010, Weiss *et al.* 2012, Scotti *et al.* 2013, Bourgine *et al.* 2014b, Yang *et al.* 2014b).

1.2.1. Cells

In order to recapitulate the events of the developmental cascade the use of a relevant, suitable cell source is essential. Bone is a complex living tissue comprised of a variety of cell types but, as described earlier, the *in vivo* bone formation is initiated by MSC

condensation towards the development of the cartilaginous intermediate. As the developmental engineering paradigm is based upon the recapitulation of the *in vivo* developmental and fracture repair cascades the use of a potent progenitor cell population involved in the relevant *in vivo* cascades stands to reason.

MSCs were defined by the international society for cellular therapy as a plastic adherent cell population which express CD 105, CD 73 and CD 90 surface markers while lacking the expression of CD 45, CD34, CD 14 or CD 11b, CD 79α or CD 19 and HLA-DR. Additionally, these cells must be able to differentiate *in vitro* towards osteoblasts, adipocytes and chondrocytes (Dominici *et al.* 2006). Based on this definition they can be isolated from a variety of tissues such as the bone marrow, the periosteum and adipose tissue. Although adipose derived MSCs are easily accessible and available in significantly larger numbers than those located in various other tissues some contradictory data on their potency towards the osteogenic and chondrogenic lineage exists (Im *et al.* 2005, Schaffler *et al.* 2007, Ghaemi *et al.* 2013). In addition, when attempting to recapitulate the native process of fracture repair, the use of the *in vivo* contributing cell populations should be aspired. In close proximity to the fracture site two different MSC niches can be found being the bone marrow and the periosteum. Although bone marrow derived MSCs are the cell population of choice for a multitude of research groups the periosteum has been shown to be imperative for fracture repair (Seeman 2003, Malizos *et al.* 2005, Zhang *et al.* 2005, Zhang *et al.* 2008, van Gastel *et al.* 2012a). Additionally, different groups showed their use has several advantages over bone marrow derived MSCs such as a faster *in vitro* proliferative capacity (Eyckmans *et al.* 2006a, Agata *et al.* 2007, Ringe *et al.* 2008) and a higher osteogenic potential (Hutmacher *et al.* 2003, Eyckmans *et al.* 2006a, Becker *et al.* 2010) therefore making them an ideal candidate for bone TE strategies.

1.2.2. *In vitro* cell culture micro-environment

As mentioned, MSCs are an *in vivo* self-sustainable cell population capable of self-renewal, proliferation and differentiation. Their function is tightly controlled by their interaction with the micro-environment within which they reside, often referred to as the stem cell niche (Jiang *et al.* 2013). The influence of this niche on the behavior of the cells is exerted through a variety of components such as soluble factors, the ECM, the biophysical environment and contact with adjacent cells (Scadden 2006, Metallo *et al.* 2007, Ghaemi *et al.* 2013, Tan *et al.* 2013). Within the *in vivo* system this micro-environment is tightly regulated and changes in a variety of critical components will induce a response from the stem cell population residing in that niche. The *in vitro* culture of these cells, and therefore their removal from the native niche, will consequently have a significant influence on their behavior. An in depth understanding of the various interactions of the cells with their native niche is therefore required to enable rigorous control of the *in vitro* behavior of this cell population. Due to the biological complexity of the *in vivo* system its *in vitro* recapitulation has proven to be very challenging. Although recently novel approaches have made significant advances towards engineering an *in vitro* stem cell niche (Gattazzo *et al.* 2014, Papadimitropoulos *et al.* 2014b), most work focusses upon elucidating the influence of isolated parameters. Despite that the relevance of these studies towards the

development of an engineered, biomimetic *in vitro* culture environment might be limited, recapitulation of the most essential aspects might be sufficient to induce the intended cell behavior.

Due to the relative ease of implementation, the use of soluble factors such as growth factors, peptides, single molecules and ions for controlling MSC maintenance and differentiation has already been thoroughly documented (Kolf *et al.* 2007, Ghaemi *et al.* 2013). Although a broad range of these compounds are used in standardized procedures for proliferation and differentiation of MSCs, a lack of in depth understanding of the underlying signaling cascades and interactions is often a limiting factor for their successful application and integration in different setups (Metallo *et al.* 2007). The use of novel, high throughput screening methods and tools for efficient statistical design of experiments has recently enabled to perform more elaborate studies allowing not only the optimization of the intended process but also to study the interactions between different external parameters in an efficient way (Jakobsen *et al.* 2014). These new insights will enable the future development of tailored *in vitro* culture environments.

As MSCs are an adherent cell population the substrate on which they are cultured and its architecture is another essential component of the *in vitro* micro-environment within which they reside. Current standard cell culture procedures use two dimensional (2D) polystyrene surfaces to expand cells in monolayer. Although these methods enable the proliferation of the cell population while maintaining their functional characteristics, the relevance of this *in vitro* culture environment in respect to the *in vivo* cell niche is non-existent. For cell differentiation and construct development, the transition from a 2D to a 3D cell culture environment has been shown to significantly influence signal transduction resulting in for example enhanced differentiation and matrix deposition (Banfi *et al.* 2000, Cukierman *et al.* 2002, Martin *et al.* 2004, Scadden 2006, Wagner *et al.* 2008, Haycock 2011, Tandon *et al.* 2013, Papadimitropoulos *et al.* 2014a). For cell expansion the use of a 3D culture environment has also been suggested to be beneficial due to for example enhanced maintenance of the progenitor phenotype but its use has much less been explored (dos Santos *et al.* 2013).

In order to create this 3D environment the use of various 3D support structures has been evaluated ranging from micro-carriers and hydrogels to porous rigid scaffolds. However, despite significant efforts of the research community, no purpose dependent scaffold specifications have been defined yet although various scaffold related properties have been shown to significantly influence cell behavior (Rezwan *et al.* 2006, O'Brien 2011, Bose *et al.* 2012, Park *et al.* 2013).

Scaffold architecture, both on macro and micro scale, was also shown to influence cell behavior in the *in vitro* engineered niche. While the macro-architecture for example influences nutrient transport and the stresses exerted on the cells in the presence of fluid flow, surface roughness and topology, correlated with the scaffolds micro-architecture, have been shown to influence cell proliferation and differentiation (Melchels *et al.* 2010, McCoy *et al.* 2012, Ghaemi *et al.* 2013). The effects of the scaffolds micro-architecture are, however, often secondary to the influence of the used materials and

the correlated surface chemistry. A wide range of materials has already been applied for research purposes, each correlated with their specific set of advantages and disadvantages. Examining the influence of externally applied stresses or compounds for example requires a biocompatible but preferably inert material while tuned degradability of the scaffold material will be essential for *in vivo* remodeling of a construct. Surface chemistry of these materials can in addition often be altered by specific functionalization in order to for example enhance cell attachment or elicit specific cellular responses (Perez-Sanchez *et al.* 2010, O'Brien 2011, Jiang *et al.* 2013, Custodio *et al.* 2014). The influence of several of these material properties on cell behavior is, however, still poorly understood, often requiring system specific validations of culture setups rather than using a generalized design strategy.

Within the 3D *in vivo* micro-environment the cells are subjected to continuous mechanical loading due to the movement of the body. The intensity of the cyclic compression of the bones has for example been associated with changes in bone mass density while shear stresses (SS) resulting from interstitial fluid flow can also significantly influence cell behavior. Consequently, mechanobiological interactions between cells and their environment can significantly modulate their *in vitro* behavior (Guilak *et al.* 2014). Fluid flow and the associated SS have for example been shown to be potent mediators of cellular differentiation, although commonly applied in combination with chemical inducers and therefore operating as an enhancer rather than inducer (McCoy *et al.* 2010, Fisher *et al.* 2011, Yeatts *et al.* 2013). In addition, next to the presence of growth factors other environmental parameters such as scaffold material and architecture as well as for example oxygen concentration have been shown to influence cellular responses to SS resulting in contradictory results. Other external stimuli such as hydrodynamic pressure, cyclic compression and tension have also been shown to influence MSC differentiation, each again dependent on other aspects of the *in vitro* micro-environment (Guilak *et al.* 2014, Hao *et al.* 2015).

The relevance of engineering a tailored *in vitro* micro-environment for cell expansion and construct development is uncontested and although, as illustrated above, significant advances have been made in understanding the importance of various aspects thereof the compartmentalization of the field and a lack of in depth understanding of the *in vivo* environment still pose significant challenges (Becerra *et al.* 2011).

1.3. Bioprocess development for tissue engineering

Although cells, scaffolds and growth factors are often considered to be the basic components of most TE constructs different publications have discussed the importance of the mechanical environment in the defect as well as the biology present in the host environment introducing respectively the diamond and penta-concept (Giannoudis *et al.* 2007, Lammens *et al.* 2012). An additional aspect which is to be taken into account for the successful development of a TE construct is the actual process used to develop this implant. For the development of a patient specific, autologous construct this multistep process starts with isolation of the primary cells from the patient which are subsequently expanded prior to the development of a functional TE construct. Each of these steps requires dedicated process development ensuring not only efficiency and

efficacy of the employed methodology but also the consideration of different aspects for future clinical and industrial implementation such as reproducibility and automation (Salter *et al.* 2012a). Although current lab scale methodologies have shown significant promise concerning efficiency and efficacy, the manual character of most procedures is a severe limitation for their future translation towards a clinical setting (Loring *et al.* 2014). The development of enabling technologies and tools addressing these, such as bioreactors, has therefore become one of the important focusses of the TE field. Translation of current established manual processes to these automated and controlled systems, however, requires re-validation of the entire process and is often not economically feasible. Therefore, industrial relevant process development should be an inherent part of the product development cycle rather than a final step as is currently often the case.

1.3.1. Bioreactors in bioprocess development for tissue engineering

Bioreactors have been defined as any device in which biological processes progress in an automated environment and in which one or more environmental parameters such as nutrient supply and temperature are closely monitored and controlled. The automation and user independent operation of the system result in a high degree of process standardization essential for future clinical translation (Jakob *et al.* 2012, Loring *et al.* 2014, Nerem 2014).

Within the field of TE and regenerative medicine a variety of bioreactor systems has already been introduced for different applications. The following section will give a brief overview of the different systems used for adherent culture of MSCs, specifically for applications in bone TE.

2D based systems

The current gold standard for cell expansion is still based upon the use of plasma treated 2D polystyrene surfaces in the form of tissue culture flasks despite the associated manual labor, operator dependence and other limitations. The first attempts for automating cell culture were based upon these principles and are in essence automated scale-out versions such as the Cell Factory™ (Nunc) or CellSTACK® (Corning). Due to the relatively simple translation of the established and validated procedures for manual 2D cell culture to these automated environments performance of these systems is close to what is obtained in standard manual cell culture (Liu *et al.* 2013b). Due to space restraints these systems are, however, mainly suited for cell therapy applications with low dosage requirements and/or small patient populations (Kirouac *et al.* 2008). Novel closed process systems such as the Integrity® Xpansion™ muliplate bioreactor system (Pall), the CompacT SelecT (Sartorius) and the Nunc Automatic Cell Factory Manipulator (ThermoFisher Scientific) aim at addressing the shortfalls of the current automated 2D expansion systems such as space efficiency, throughput and a limited possibilities for online system monitoring and control but data on efficacy and efficiency of these systems is currently lacking (Jenkins *et al.* 2015).

Table 1.1: Advantages and disadvantages of different bioreactor systems used in tissue engineering

	Advantages	Disadvantages
2D planar bioreactors	Well characterized environment Optimized procedures	Spontaneous (de)differentiation associated with tissue culture plastic Large surface area Large volumes of media
Micro-carrier bioreactors	Medium to high cell densities Expansion and construct development Easy scale-up Tuning of cell culture surface	Harvest Nutrient gradients through micro-carriers
Hollow fiber bioreactors	Low shear environment Medium to high cell densities Advanced feeding regimes	Scale-up Nutrient gradients
3D bioreactors	Homogenous nutrient distribution Mechanical stimulation 3D micro-environment Spatial organization cells Expansion and construct development High cell densities Tuning of cell culture surface	Harvest No GMP compliant systems available Scale-up

Despite the widespread use of 2D expansion methodologies on tissue culture plastic the artificial culture environment has been shown to influence cell identity and functionality leading to spontaneous (de)differentiation, replication senescence, etc. after prolonged *in vitro* expansion (Banfi *et al.* 2000, Scadden 2006, Wagner *et al.* 2008). Although these cells possess a strong capacity for *in vivo* self-renewal their *in vitro* expansion in these 2D conditions is therefore limited and the development of a more optimized *in vitro* cell culture niche is called for (Sensebe *et al.* 2011)(Table 1.1).

Hollow fiber bioreactors

Hollow fiber bioreactor systems are based on a densely packed bundle of fibers surrounded by a casing. The system can be perfused through the fibers (intra-luminar), the casing surrounding the fibers or both in various setups. In addition, intra- and extra-luminar space can be interconnected depending on the membranes used for the fibers to enable exchange of nutrients, waste products and growth factors.

Using the Quantum cell expansion system (Terumo), a Good Manufacturing Practice (GMP) compliant hollow fiber bioreactor system for cell expansion, different groups reported successful expansion of MSC populations while maintaining original cell

phenotype (Jones *et al.* 2013, Nold *et al.* 2013, Rojewski *et al.* 2013). Due to the versatile setup of the system (intra- versus extra-luminal localization of the cells, the use of different perfusion configurations and advanced feeding regimes) cell behavior in the bioreactor can be optimized towards specific applications (Godara *et al.* 2008, De Napoli *et al.* 2011, Wung *et al.* 2014). Different groups have additionally hypothesized that although the cells cultured in these systems still experience a predominantly 2D environment, the 3D architecture of the system enables to better mimic the native cellular micro-environment which could result in a significantly improved phenotypical stability and post-expansion potency of the cell population (Liu *et al.* 2013b, Wung *et al.* 2014). The major shortfall of this bioreactor system for a multi-step expansion process is the difficulty for up-scaling of the setup (Liu *et al.* 2013b).

Next to the use of these systems for cell expansion different reports discus the application of hollow fiber based perfusion systems for the development of tissue constructs. For these applications cells are often located in the extra-luminal space in which they can proliferate and develop a complex 3D structure, potentially with the support of an additional fibrous matrix or hydrogel, while nutrient supply is ensured by luminal perfusion (Wung *et al.* 2014).

Micro-carrier based systems

Micro-carrier based systems have already frequently been used for the culture of the adherent MSCs (Jakob *et al.* 2012, Jung *et al.* 2012b, Liu *et al.* 2013b). Due to the simplicity and scalability of these systems, together with the versatility of the setup (the availability of different culture vessels and a broad range of micro-carriers) as well as the high surface to volume ratio this technology is often considered as being one of the most potent for industrial scale stem cell expansion (Liu *et al.* 2013b, Tandon *et al.* 2013, Jenkins *et al.* 2015).

Although a variety of systems is available for micro-carrier culture such as stirred tank bioreactors, rotating wall vessels and wave bioreactors all these systems aim at maintaining the micro-carriers in suspension while providing a homogenous external culture environment. The main difference between different systems in how the micro-carriers are maintained in suspension and therefore the applied external forces on the cells. Spinner flasks are for example associated with an inhomogeneous flow profile and local occurrence of turbulence due to the impellers (Liu *et al.* 2013b). These are suggested to be beneficial for preventing aggregation of the micro-carriers and to enhance mass transport to the center of porous micro-carriers but also result in sub-optimal behavior when aiming at the application of a specific range of SS (Chen *et al.* 2006). Despite this, they are the system of choice for micro-carrier facilitated cell expansion and several groups already showed the feasibility of transferring lab based processes towards a more clinically relevant environment (Rafiq *et al.* 2013, Dos Santos *et al.* 2014, Nienow *et al.* 2014). Due to the 3D geometry of the micro-carriers the micro-environment created for cell expansion was also suggested to develop a cell culture niche which is more native to the cells than the standard 2D expansion strategies (Park *et al.* 2013). However, despite the 3D architecture of the micro-carriers, cells expanding on solid carriers such as the Cytodex^{TM} will predominantly experience a 2D

environment as they grow on the surface of the carriers (Martin *et al.* 2011b). Using porous microspheres was shown to both increase the surface to volume ratio and create a more complex 3D microenvironment for cell expansion resulting in significant stronger proliferation although significant nutrient gradients were also shown to be present through the microspheres (Park *et al.* 2013).

More recent the use of micro-carriers for construct development was also explored by inducing differentiation and ECM deposition subsequent to the expansion stage. The resulting micro-tissues could then be used as building blocks for the assembly of a TE construct (Chen *et al.* 2014, Georgi *et al.* 2014).

Perfusion bioreactor systems

A final group of bioreactor systems are perfusion bioreactors in which a fixed 3D support structure, or scaffold, seeded with cells is perfused during culture. The forced perfusion through the scaffold results in a more homogenous distribution of nutrient concentration profiles thereby addressing one of the shortfalls using porous 3D micro-carriers. Additionally, it enables the controlled application of external forces such as fluid exerted SS and hydrodynamic compression (Gardel *et al.* 2014, Li *et al.* 2014). The 3D architecture of the scaffolds can also support the deposition of ECM of which its presence during cell culture has been associated with significant advantages such as enhanced proliferation and differentiation due to the more relevant *in vitro* cell niche (Chen *et al.* 2007, He *et al.* 2009, Lai *et al.* 2010, Li *et al.* 2011, Pei *et al.* 2011, Liu *et al.* 2013a, Tandon *et al.* 2013). As a result of the development of the complex 3D neo-tissue (ECM and cells) the subsequent cell recovery from the expansion system is, however, significantly impaired, thereby putting severe restraints on the use of these systems for cell expansion (Abbasalizadeh *et al.* 2013, dos Santos *et al.* 2013, Gardel *et al.* 2014).

With respect to the development of TE constructs these systems have already been extensively used although the successful implementation of the developmental engineering paradigm is still absent at current. Numerous groups did, however, use the enhanced nutrient supply provided by these systems to develop 3D mineralized constructs (Braccini *et al.* 2005, Grayson *et al.* 2010, Kim *et al.* 2012, Gardel *et al.* 2014) and the influence of the *in vitro* cell niche created in these systems on cell differentiation was extensively studied (Sikavitsas *et al.* 2005, Zhao *et al.* 2009, McCoy *et al.* 2012, Sadr *et al.* 2012, Youssef *et al.* 2012).

1.3.2. Integrated bioprocess development

As discussed earlier the use of bioreactor systems is indispensable for the future clinical implementation of the multi-step TE process. Although the entire bioprocess is centered on the functional construct development a multitude of supporting up- and downstream processes are required. The main process steps which are often discussed for the TE process are the initial cell isolation, the expansion of this cell population towards clinical relevant cell numbers and the final construct development as shown in the black arrows in Figure 1.2. Each of these steps can, however, still be segmented into a series

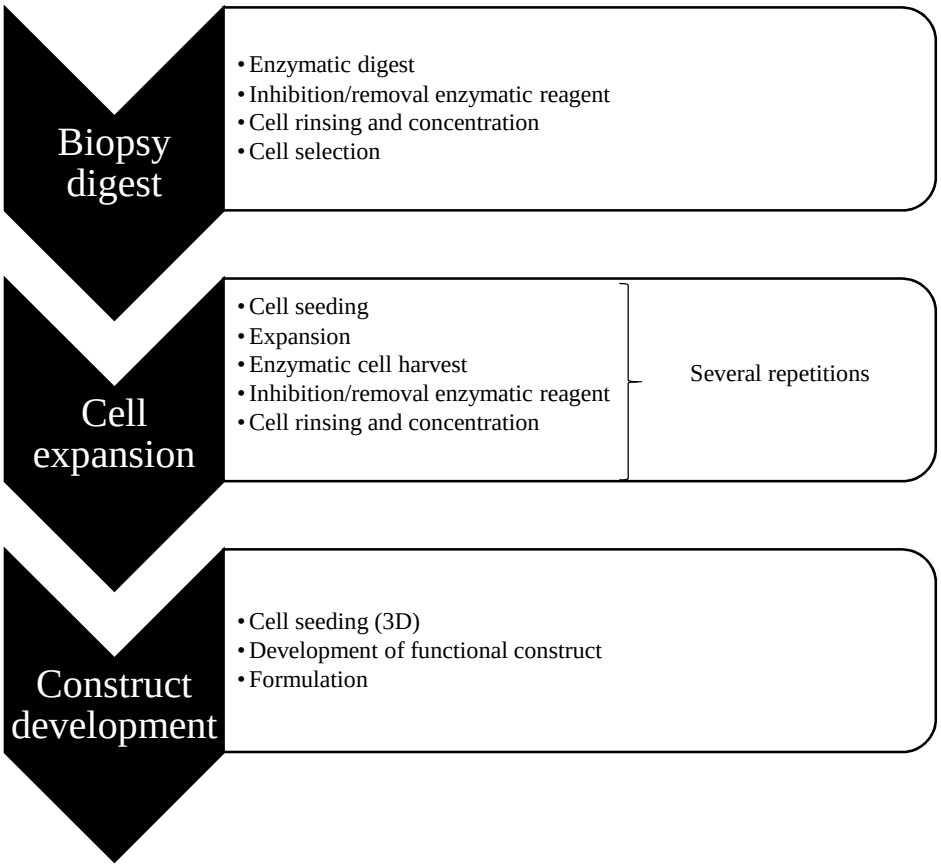

Figure 1.2: Different steps of the TE process

of separate unit operations which all require dedicated process development and integration in the bioprocess flow (Martin *et al.* 2009).

Primary cell isolation

MSCs can be isolated from a variety of tissues ranging from bone marrow and cord blood to adipose tissue and the periosteum. Due to the ease of collection and their relative high frequency in the bone marrow this is the most common source for MSCs (Mosna *et al.* 2010). In order to obtain the mononuclear fraction of the bone marrow which contains the MSCs, density gradient centrifugation is used. Subsequent rinsing steps are applied to wash the collected cell fraction prior to plating the cells out to remove non-adherent cells (Seeger *et al.* 2007, Mosna *et al.* 2010). Similar methods enable the isolation of MSCs from the peripheral or umbilical cord blood circumventing the need for the invasive bone marrow aspiration (Kassis *et al.* 2006, Kern *et al.* 2006). Despite the significant number of clinical trials with MSCs (Fekete *et al.* 2012) the isolation and selection of the MSC fraction from these blood derived sources still contain a significant number of operator dependent, open steps such as the density

gradient centrifugation. In order to address this, various studies have attempted to define a fixed set of surface markers for MSCs which could enable their automated, closed circuit selection based on fluorescent or magnetic activated cell sorting. Although various markers associated with the MSC population have been identified no defining marker set is known yet (Jones *et al.* 2006, Buhring *et al.* 2007, Ghaemi *et al.* 2013, Sivasubramaniyan *et al.* 2013, Lv *et al.* 2014).

Other frequented sources of MSCs can be obtained from a range of different tissues of which the subcutaneous fat and the periosteum are the most clinically relevant sources. In order to isolate the MSC population from these tissues an enzymatic digest is performed after which the adherent cell fraction is selected (Kern *et al.* 2006, Mosna *et al.* 2010). Despite the long standing methodological expertise in enzymatic tissue digests these methodologies have not been implemented in an automated bioreactor environment yet (De Bari *et al.* 2001, Kern *et al.* 2006, Mosna *et al.* 2010, van Gastel *et al.* 2012b, Oseni *et al.* 2013, Centola *et al.* 2014, Lau *et al.* 2014). While no specific technical challenges are correlated with the implementation of the actual enzymatic digest significant efforts still need to be made concerning the required downstream processing steps such as cell selection, concentration, rinsing and volume reduction (Martin *et al.* 2009, Abbasalizadeh *et al.* 2013, dos Santos *et al.* 2013).

A broad range of highly selective, automated methodologies for cell selection such as fluorescent or magnetic activated cell sorting and other antibody or aptamer based systems are available (Abbasalizadeh *et al.* 2013). These molecular or cellular targeting based methods, however, have a limited throughput and often require specific sample preparation making them sub-optimal for large scale integration. Various novel tag-free methods such as field flow fractionation and dielectrophoresis have already shown significant promise for enabling high throughput separation of cell suspensions although further development, certainly concerning scale-up and scale-out approaches will be required (Diogo *et al.* 2012, Abbasalizadeh *et al.* 2013, Fernandes *et al.* 2013). While these methods can also be applied for other downstream processing steps such as volume reduction the high specificity provided by these methodologies is not required. Current GMP-compliant cell expansion systems employ batch centrifugation for cell concentration but the scale-out potential of this methodology is limited (Spanholtz *et al.* 2011, Rojewski *et al.* 2013). The need for these methodological developments was, however, only recognized recently and significant efforts still need to be made towards the development of clinical and industrial relevant processes (Abbasalizadeh *et al.* 2013, dos Santos *et al.* 2013, Sart *et al.* 2014b).

Cell expansion

As clinical relevant cell dosages range between 10^8 and 10^{10} cells/patient and biopsies can yield often only provide up to 10^5 cells a significant phase of *in vitro* cell expansion is required (Liu *et al.* 2013b). Various bioreactor systems which could facilitate this expansion process were already discussed earlier. Although each system is associated with a specific set of technical and process related challenges at current the most limiting step for successful industrial implementation of this process is not the actual cell expansion but the cell recovery subsequent to this expansion (Cierpka *et al.* 2013, Jiang *et al.* 2013, Liu *et al.* 2013b).

The long standing use of enzymatic methods for cell recovery has led to the optimization of cell detachment for various established cell culture systems (Roberts *et al.* 2012, Chen *et al.* 2013, Goh *et al.* 2013, Zhou *et al.* 2013a). The development of 3D culture substrates such as micro-carriers and hollow fiber bioreactors has started to gain more momentum but cell expansion in these setups still predominantly takes place in monolayers. This enables the relatively simple transfer of current 2D, often trypsin or similar proteolytic enzyme based, methods to these 3D culture environments. The use of more complex culture environments in which cells are expanded in a 3D environment and potentially produce their own supportive ECM such as porous micro-carriers or fixed bed perfusion bioreactors, however, offers a new set of currently unaddressed challenges for successful cell recovery (Abbasalizadeh *et al.* 2013, Cierpka *et al.* 2013, dos Santos *et al.* 2013).

The cell expansion process will in most cases consist of a consecutive series of passages. Therefore not only cell recovery but also the associated downstream process steps such as removal of the enzymatic reagent, washing of the recovered cells, volume reduction and inoculating the expansion surface of the subsequent culture need to be carefully considered (Figure 1.2). As each of the consecutive expansion steps will contain a significant higher number of cells the scale-up or scale-out of each of these steps also needs to be taken into account to facilitate successful integrated bioprocess development.

Construct production

Bioreactor systems have already frequently been applied for the final step of the TE process, the functional construct development (Rauh *et al.* 2011, Salter *et al.* 2012a, Gardel *et al.* 2014). In contradiction to the preceding steps significant efforts have already been made towards the integration of associated up- and down-stream processes such as for example cell seeding onto the 3D scaffold (Wendt *et al.* 2003, Griffon *et al.* 2011, Salter *et al.* 2012a).

In order to develop a clinically relevant process the implementation of these different process steps into one integrated process is, however, not the only technical challenge. Next to the need for automation a high degree of reproducibility also needs to be ensured which requires the development of appropriate tools. Stringent process control entails the development of tools for monitoring the *in vitro* expansion and construct development and non-destructive imaging methodologies for characterizing the developing 3D structures.

1.4. On-line monitoring of cell proliferation

In order to receive regulatory approval for the clinical implementation of novel products, ensuring consistent safety and efficacy is indispensable. This requires the in depth characterization and standardization of the product and its production process. Although bioreactors are often considered to be a valuable tool in this regard, at current they are often ‘black box’ systems in which there is no feedback or control of the process (Wendt *et al.* 2009). Next to integrated bioprocess development, bioprocess control, providing real time information on the *in vitro* culture environment as well as

on the cell expansion and construct development, is therefore an essential part of the development of clinically relevant TE processes.

The most direct way of monitoring *in vitro* cell proliferation is measuring the concentration of specific metabolites correlated with cell number. As glucose is the main energy source of cells in *in vitro* culture systems, changes in its concentration and correlated metabolites such as lactate and l-glutamine can be used as an indication for cell number. (Chong *et al.* 2013, Dos Santos *et al.* 2014). Recent advances in technological development have enabled the integration of various techniques such as near infrared spectroscopy in large scale production bioreactors for bacterial culture and Chinese hamster ovary cells but successful, cost efficient implementation of these systems in the small scale TE bioreactors has not been reported yet (Clavaud *et al.* 2013, Alves-Rausch *et al.* 2014). Measuring the consumption of oxygen by the cells as well as production of carbon dioxide is another way of monitoring cell proliferation as both are also involved in the metabolic pathways governing the cells energy regulation. Different authors showed changes in dissolved oxygen concentration could be correlated to cell number (Janssen *et al.* 2006a, Santoro *et al.* 2012). Limitations in sensor sensitivity and the perturbation sensitive setups, however, result in a limited resolution of the measurement, certainly when monitoring relatively low numbers of cells typically present in these TE related setups.

Instead of measuring concentration of cell metabolism correlated compounds such as glucose or oxygen other approaches are based upon the metabolic conversion of non-toxic dyes. The use of resazurin, a non-fluorescent component which is reduced in the cells to form the fluorescent resorufin, already has a long standing use as indicator for cell viability (Gloeckner *et al.* 2001, Cui *et al.* 2007, Mueller *et al.* 2013, Zhou *et al.* 2013b). Recent reports also hint at the quantitative use of this methodology for monitoring cell proliferation but no consistent correlation between cell number and assay conversion has been shown yet (Ng *et al.* 2005, Quent *et al.* 2010).

1.5. Nondestructive imaging in tissue engineering

Characterization of the 3D constructs during expansion and final quality control is imperative for process and product quality assessment. Although histology is currently still the golden standard for analysis of biological structures it is associated with significant disadvantages such as the destructive nature of the technique and the limited 3D resolution. Recent advances in the field of imaging have therefore been moving towards non-destructive characterization of complex 3D structures. The next section will give a brief overview of the frequently applied imaging techniques used for *in vitro* characterization of 3D constructs.

1.5.1. Optical based techniques

Optical, and in particular fluorescence, based imaging techniques have already been applied in the TE field for various applications. Despite its high sensitivity, spatial resolution and specificity it has a limited applicability for the characterization of 3D constructs due to material induced photon scattering, resulting in limited penetration depths of the methodologies (Nam *et al.* 2014). Recent advances such as the use of two-

or multiphoton systems and selective plane illumination microscopy enabled increases in imaging depth up to 500µm but they do not yet enable the visualization of complete TE constructs (Chalal *et al.* 2009, Chen *et al.* 2010, Ntziachristos 2010, Ward *et al.* 2013). The use of probes emitting in the near-infrared spectrum could further enhance this due to the low optical absorption in the tissue although this is also correlated with an increase in optical scattering and therefore a decrease in resolution (Ntziachristos 2010). Optical coherence tomography, another novel technique in the field of optical imaging based upon scattering of the photon beams, can reach a penetration depth up to 3mm and spatial resolutions around 1µm (Mason *et al.* 2004). Different studies already showed the applicability of this technique for characterizing TE constructs but, as is the case for all other optical based techniques, it is still limited to constructs with a relative high optical translucency (Tan *et al.* 2004, Chen *et al.* 2011).

1.5.2. Ultrasound imaging

Ultrasound imaging is based upon the same principles as optical coherence tomography with the difference that sound waves are used instead of light. Depending on the acoustic impedance of the material greyscale images can be generated enabling morphological analysis of the samples. Quantitative analysis of the images enabled to determine overall collagen content of fibrin gels, monitor mineralization or obtain volume averaged data on cell density (Oe *et al.* 2010, Kreitz *et al.* 2011, Gudur *et al.* 2012). Using high frequency transducers higher spatial resolutions (up to approximately 25µm) could be obtained which was, however, associated with a reduced maximal penetration depth to 2mm.

Photoacoustic imaging is considered to be one of the more promising imaging techniques and is based upon the detection of the acoustic waves generated after the thermos-elastic expansion of a sample subsequent to a nanosecond laser pulse irradiation (Ntziachristos 2010, Nam *et al.* 2014). The use of ultrasound significantly increases the penetration depth of the methodology in comparison to optical based methods. In comparison to ultrasound this methodology enables the use of additional contrast agents for obtaining functional and/or molecular information although this is mainly applied for *in vivo* measurements (Luke *et al.* 2012).

1.5.3. Magnetic resonance imaging

Due to its excellent penetration depth and safety magnetic resonance imaging is a frequently applied clinical and preclinical imaging technique based upon the nuclear alignment of the atoms in the presence of a strong magnetic field. Radiofrequency pulses altering the magnetization of the aligned nuclei are applied and the return of the nuclei to the aligned position enables the registration of the transversal and longitudinal relaxation time resulting in greyscale images which depend on proton density of the sample. Although mainly applied for *in vivo* studies the excellent contrast was also applied in a number of *in vitro* studies (Xu *et al.* 2008, Appel *et al.* 2013, Nam *et al.* 2014). In the field of bone TE various studies showed the possibility of monitoring *in vitro* mineralization using this technique (Washburn *et al.* 2004, Xu *et al.* 2006) as well as for evaluating *in vitro* cartilage development (Potter *et al.* 1998, Nieminen *et al.* 2001). The technical complexity of this method and the maximal image resolution,

ranging between 50µm and 500µm, however, limit the broad application of this methodology for *in vitro* analysis of tissue engineered constructs (Xu *et al.* 2008, Appel *et al.* 2013).

1.5.4. X-ray computed tomography

X-ray computed tomography (CT) is based on the material specific attenuation of X-rays enabling the visualization of a broad spectrum of materials at high resolution. 2D projection images are generated while the sample is being rotated enabling subsequent 3D image reconstruction. Depending on the X-ray energy a broad range of materials can be imaged and it is often the technique of choice in bone TE due to the excellent X-ray penetration of the samples (Appel *et al.* 2013, Nam *et al.* 2014). One of the limitations, however, is the limited X-ray contrast induced by soft materials such as ECM. Although low X-ray energies can be employed the attenuation differences between different components of the soft matrix is often insufficient. Additionally, if the materials being imaged are hybrid constructs, containing next to the soft ECM, more dense materials such as a mineralized matrix or a dense scaffold matrix, the X-ray energies required to penetrate the dense materials often do not enable the visualization of the soft tissue. More advanced setups such as phase contrast systems of phase enhanced imaging can enable the visualization of these soft tissues within hybrid constructs (Mastrogiacomo *et al.* 2004, Voronov *et al.* 2012, Olubamiji *et al.* 2014). The availability of these advanced systems is, however, limited and there is a need for more general applicable methodologies for imaging these constructs.

1.6. Conclusion

In this chapter, different aspects of bone and bone development were discussed and their relevance for skeletal TE approaches was elucidated. The need for integrated bioprocess development was introduced and the relevance of bioreactor systems in this context was explained. The current state of the art of bioprocess development for skeletal TE was discussed showing that despite significant efforts several aspects of the skeletal TE bioprocess flow remain unaddressed. In addition, the availability of different tools for bioprocess monitoring and characterization of the 3D constructs were discussed providing a comprehensive overview of the context within which the work discussed in this dissertation was performed.

Chapter 2.
General hypothesis and objectives

2.1. General hypothesis

Despite significant advances in the field of TE, large scale industrial and clinical implementation of established concepts is currently lacking. Bioprocess development, enabling the integration of the entire TE process in a controlled, monitored and automated environment will be essential for the future translation of lab-scale processes to clinically relevant applications. Although this need is recognized within the research field its current focus is mainly on functional construct development while the need for integration of preceding process steps such as cell expansion is often neglected.

The general hypothesis upon which this work is based states that the *in vitro* micro-environment present in a 3D perfusion bioreactor system is supportive for cell proliferation while maintaining its functional characteristics, thereby enabling its use for the automated expansion of a progenitor cell population. The main objective of the research presented in this dissertation was therefore defined as the study of the influence of the *in vitro* cell niche created in a 3D perfusion bioreactor on the behavior of a multipotent progenitor cell population. In addition techniques required for monitoring and characterizing the cell proliferation and neo-tissue formation in the system were developed.

2.2. Methodology

In order to study the formulated hypothesis a specific methodology was defined using a consistent set of materials throughout this dissertation.

- Cell culture system
    - Human Periosteal Derived Cells (hPDCs): As discussed in chapter 1 the multipotent periosteal derived cell population is an ideal candidate for the development of bone TE constructs.
    - Ti6Al4V scaffolds: A porous 3D printed Ti6Al4V scaffold with a repeating unit cell was employed as a 3D cell culture substrate. The regular shape of the scaffold enabled homogenous, reproducible control of the micro-environment created for the cell resulting in consistent application of external stimuli. The Ti6Al4V alloy used for the scaffolds is a clinically approved material with various applications in the orthopedic field. Due to the biocompatibility of this material it provides a suitable culture substrate to study the influence of external stimuli on cell behavior without interfering with the biological processes.
    - Perfusion bioreactor system: To ensure controlled, reproducible and homogenous nutrient supply and waste removal for the cells in the three dimensional scaffold a perfusion bioreactor system was developed.
- Measured outputs
    - Cell number: Cell number was monitored in order to quantify proliferation during the expansion process. DNA measurements and a hemocytometer were used to measure cell number at final time points. On-line monitoring of cell number and proliferation was performed using a non-destructive assay which was quantitatively validated for this purpose within this dissertation.
    - Neo-tissue formation: Expansion of a cell population in standard 2D setups is a space constrained process regulated by the contact inhibition between cells once confluence is reached. As cells proliferate within the 3D environment a neo-tissue containing cells and ECM is formed in the scaffold. Contrast enhanced nano-computed X-ray tomography (CE-nanoCT), a novel technique developed within the context of this dissertation, was used to determine volume filling of the porous scaffolds, thereby monitoring when confluence occurs in the 3D culture system.
    - Cell characteristics: The gene expression profile is an important indicator of cell identity and characteristics. Gene expression analysis of several key marker genes was therefore used as an

indication of the influence of the engineered cell niche on the characteristics of the expanded population.

- Cell functionality: As the final goal of a cell expansion process is to obtain a cell population with an unimpaired functionality, both *in vitro* and *in vivo* functional assays were performed.

2.3. Objectives

Specific research objectives were defined to validate the formulated research hypotheses. The next section summarizes the key objectives for the different chapters which are visually represented in Figure 2.1. The first two objectives concern the development of different methods required for process monitoring and characterization which are subsequently applied to assess the influence of the *in vitro* micro-environment as described in the third objective.

2.3.1. Development of a quantitative method for monitoring cell proliferation in a perfusion bioreactor system

The Presto Blue® metabolic assay (PB) is fluorescent based assay to monitor cell viability in various setups. To enable monitoring cell proliferation in a 3D perfusion bioreactor system a quantitative validation of the assay was required. Therefore the linear operating window of the assay was first determined and the influence of different measurement parameters on the linearity were established using standard 2D cell culture methods. The potential to define quantitative correlations between cell number and conversion of the assay was assessed using standard 2D as well as both static and perfused 3D culture and measurement setups. The quantitative validation of the PB metabolic assay is described in Chapter 3.

2.3.2. Development of Contrast Enhanced nano-computed X-ray tomography as a tool for visualization of soft tissue in metallic scaffolds

CE-nanoCT was developed as a tool to enable soft tissue visualization and quantitative analysis in porous metallic scaffolds. A proof of concept study was first performed to assess the potential of using two different contrast agents to visualize the neo-tissue (cells and ECM) in the metallic scaffolds. The obtained results were compared with established techniques for visualization and quantification of the neo-tissue in an initial attempt to validate the developed techniques. In order to enable quantitative, automated image analysis a design of experiment (DoE) study was subsequently performed to optimize image contrast and quality in function of different staining parameters. A semi-quantitative validation of the different stainings was performed using constructs with a different scaffold material enabling visualization of the neo-tissue without the use of the contrast agents. The results of the proof of concept study are described in chapter 4 while the optimization and validation for quantitative analysis is discussed in chapter 5.

2.3.3. Three dimensional perfusion bioreactor facilitated cell expansion

In order to assess the potential use of a 3D perfusion bioreactor system as a tool for automated cell expansion the influence of the *in vitro* micro-environment on cell characteristics was determined. In addition to a number of established techniques the novel methodologies developed in chapters 3-5 were used to determine the influence of a range of different flowrates on cell proliferation after which a more in-depth assessment was performed for two selected perfusion velocities. Proliferation, matrix deposition and gene expression were assessed over time and compared to cells expanded in a static 3D culture system. To enable functional characterization of the expanded cell population a methodology for cell recovery subsequent to the bioreactor expansion was developed. Therefore different enzymatic reagents were initially screened and a DoE study was performed to optimize the yield of the developed methodology. A series of *in vitro* and *in vivo* assays was subsequently used to determine the potential influence of the expansion and recovery process on cell functionality. The results of these experiments are discussed in chapters 6 and 7.

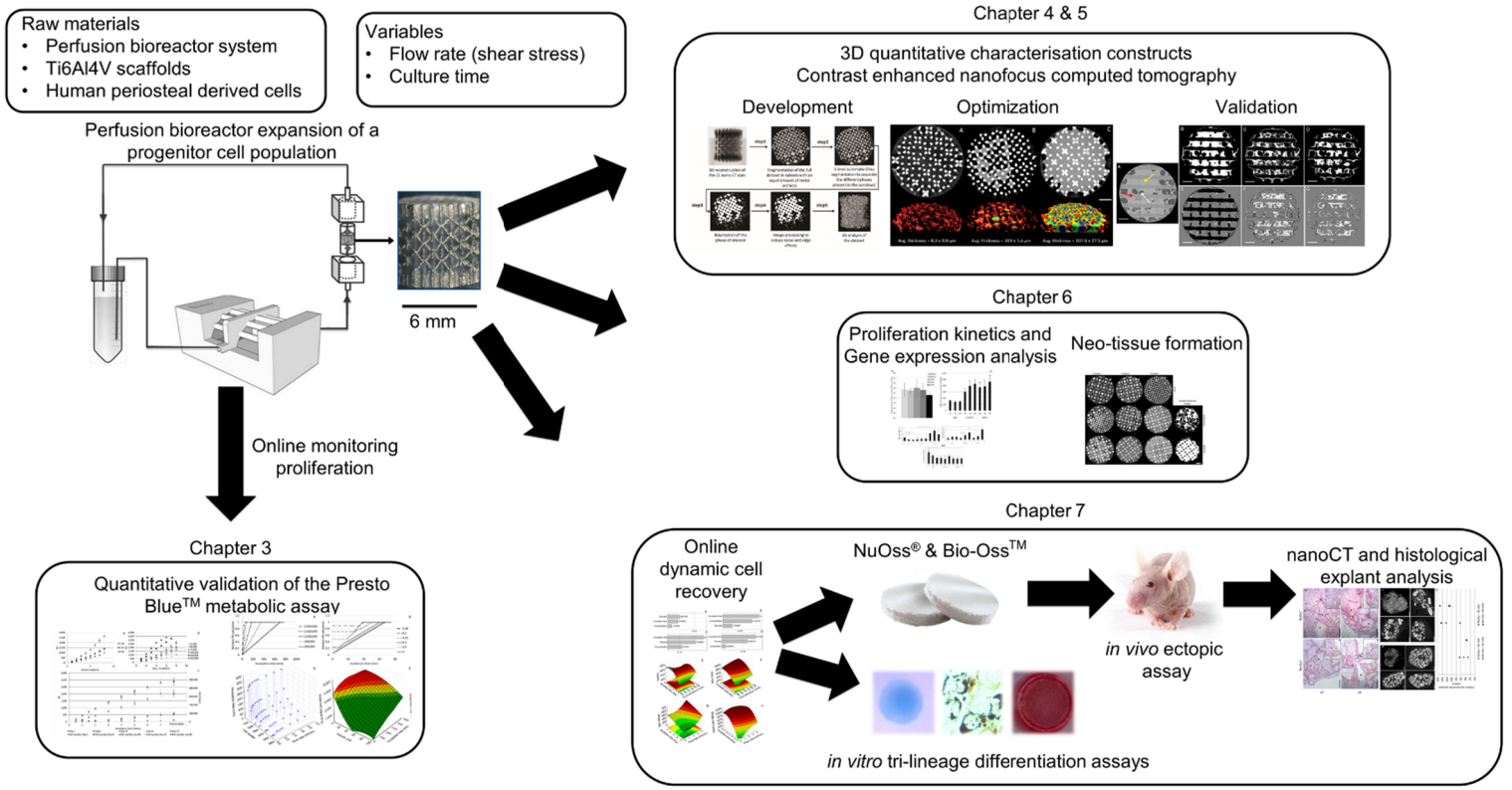

Figure 2.1: Schematic representation of the different aspects of the perfusion bioreactor facilitated expansion process addressed in this dissertation.

Chapter 3.
Quantitative validation of the Presto Blue™ metabolic assay for on-line monitoring of cell proliferation in a 3D perfusion bioreactor system

Sonnaert, M., Papantoniou, I., Luyten, F.P., Schrooten, J.

Published in Tissue Engineering Part C, Methods, 2015 Jun; 21(6):519-529

3.1. Abstract

As the fields of tissue engineering and regenerative medicine mature towards clinical applications the need for on-line monitoring, both for quantitative and qualitative use, becomes essential. Resazurin based metabolic assays are frequently applied for determining cytotoxicity and have shown great potential for monitoring 3D bioreactor facilitated cell culture. However, no quantitative correlation between the metabolic conversion rate of resazurin and cell number has been defined yet. In this work we determined conversion rates of Presto Blue™, a resazurin based metabolic assay, for human periosteal cells during 2D and 3D static and 3D perfusion culture. Our results showed that for the evaluated culture systems there is a quantitative correlation between the Presto Blue™ conversion rate and the cell number during the expansion phase, with no influence of the perfusion related parameters i.e. flow rate and shear stress. The correlation between cell number and Presto Blue™ conversion subsequently enabled the definition of operating windows for optimal signal readouts. In conclusion, our data showed that the conversion of the resazurin based Presto Blue™ metabolic assay can be used as a quantitative read-out for on-line monitoring of cell proliferation in a 3D perfusion bioreactor system although a system specific validation is required.

3.2. Introduction

The development of cell based tissue engineering strategies for the repair or replacement of damaged organs and tissues is a rapidly evolving research field (Martin *et al.* 2011a, Martin *et al.* 2012). As these novel cell-based therapies fall under the definition of the 'Advanced Therapy Medicinal Products' (ATMPs) of the European Medicine's Agency (EMA), the application of the Process Analytical Technology guidelines (PAT) to develop well characterised products by designing and controlling the manufacturing process through timely measurements of critical quality attributes is essential (Chew *et al.* 2010, Rebulla *et al.* 2010, Schneider *et al.* 2010). The integration of bioreactor systems in current lab scale processes therefore holds promise for the translation in a clinical and ultimately commercial setting (Martin *et al.* 2010, Salter *et al.* 2012a). Bioreactors have been employed frequently to provide sufficient nutrient and oxygen transport and removal of waste products (Grayson *et al.* 2004, Martin *et al.* 2004, Haycock 2011, Rodrigues *et al.* 2011, Jakob *et al.* 2012, Salter *et al.* 2012a) while allowing for monitoring and control of physicochemical and biological parameters (Tsao *et al.* 2005, Das *et al.* 2010, Martin *et al.* 2010, Rauh *et al.* 2011, Santoro *et al.* 2012, Zhou *et al.* 2013b) during cell proliferation, differentiation and the development of a cell-carrier constructs. Furthermore these parameters could be used as non-destructive quality indicators of the cells or the developing construct.

Since *in vitro* proliferation is an essential process step for the production of cell based products (Rodrigues *et al.* 2011), on-line measurements of metabolic activity parameters such as glucose, lactate and oxygen concentration, could allow for a non-destructive assessment of the quality of the 3D cell culture (Tsao *et al.* 2005, Das *et al.* 2010, Santoro *et al.* 2012, Frese *et al.* 2014). Although, for example, correlating a decrease in oxygen concentration to cell proliferation has been shown to be a viable strategy to monitor proliferation for high cell numbers (Santoro *et al.* 2012), these

techniques often fall short when lower cell numbers in the order of magnitude 10^4 to 10^6 cells need to be monitored and quantified (Zhou *et al.* 2013b). Limited sensor sensitivity as well as low oxygen and glucose consumption rates per cell hamper the reliability of such measurements (Zhou *et al.* 2013b). Therefore alternate methodologies to monitor cell number, viability and proliferation as well as differentiation in bioreactors are essential, especially for the initial crucial expansion steps (post biopsy expansion) of scarce adult stem cell populations.

Metabolic assays such as the tetrazolium based 3-[4-5-Dimethylthiazol-2-yl]-2-5-diphenyl bromide tetrazolium bromide (MTT) and the resazurin based Alamar Blue® assay (AB) use the redox activity of the cells to qualitatively monitor cell populations based on the generation of an optical or fluorescent detectable component (Nociari *et al.* 1998, Back *et al.* 1999, Quent *et al.* 2010, Uzunoglu *et al.* 2010, Rampersad 2012, Mueller *et al.* 2013). MTT and other tetrazolium based assays are based on the cleavage and reduction of the tetrazolium ring to blue formazan crystals by the mitochondrial dehydrogenases (Nociari *et al.* 1998, Quent *et al.* 2010). These crystals can be solubilised and quantified in the cell lysate as a measure for metabolic cell activity. Despite the frequent use of these assays the fact that this methodology can only be used as an endpoint analysis is a serious disadvantage (Quent *et al.* 2010). The resazurin based AB and Presto Blue® (PB) assays on the other hand use the mitochondrial activity to reduce the non-fluorescent, blue resazurin to the fluorescent, pink resorufin (Nociari *et al.* 1998, O'Brien *et al.* 2000, Quent *et al.* 2010). This non-toxic, water soluble dye enables continuous cell culture monitoring and has been shown to be a powerful tool to assess cell viability and proliferation in both static and dynamic 3D setups (Gloeckner *et al.* 2001, Cui *et al.* 2007, Mueller *et al.* 2013, Zhou *et al.* 2013b). These reports show a clear correlation between the obtained fluorescent signal and the cell number. However, contradictory results showing discrepancies between cell number and the metabolic conversion of the resazurin when using static culture systems are also present, indicating that the performance of these assays is dependent on the cell type, culture and measurement setup (Ng *et al.* 2005, Quent *et al.* 2010).

In order to determine whether the quantitative use of a resazurin based assay in a bioreactor setup is possible, the influence of the cell culture method and measurement setup on the conversion rate of the resazurin and on the metabolic activity of the cells has to be known. The redox activity of a cultured cell population was already shown to be influenced by long term proliferation and the induction of differentiation (Rice *et al.* 2010, Quinn *et al.* 2012). The influence of different culture systems and parameters on the metabolic activity of the cells and the conversion rate of the metabolic assays is, however, not known, which hampers the quantitative use of these methods.

In this work we used the PB metabolic assay to monitor and quantify cell proliferation in a perfusion bioreactor setup up to 21 days. At first, the influence of different culture setups was investigated by measuring the metabolic activity of cells cultured in 2D and in 3D static and 3D perfusion bioreactor setups, and correlating this to DNA content. Subsequently a dynamic monitoring method was developed to overcome diffusion limitations that were observed when 3D scaffolds were measured in a static setup, affecting the conversion rate. Finally, the influence of perfusion flow rate and shear

stress on the conversion of the metabolic assay was determined by using medium with different viscosities. Based on DNA measurements conversion rates for the PB assay in the different setups were found to enable the quantitative monitoring of cell proliferation.

3.3. Materials and Methods

3.3.1. Human Periosteal Derived cells (hPDCs)

hPDCs were isolated from periosteal biopsies obtained from 4 different donors (age 11, 13, 14 and 17, equal distribution of gender) as described previously and pooled for further use (Eyckmans *et al.* 2006a). This procedure was approved by the ethics committee for Human Medical Research (KU Leuven) and performed with patient informed consent. hPDCs were expanded in Dulbecco's modified Eagle's medium with high-glucose (Life Technologies) containing 10% foetal bovine serum (Gibco), 1% sodium pyruvate (Life Technologies) and 1% antibiotic–antimycotic (100 units/mL penicillin, 100mg/mL streptomycin, and 0.25 mg/mL amphotericin B; Life Technologies), further mentioned as culture medium. The cells were seeded at 5,700 cells/cm² and passaged at 80%–90% confluency. Cell expansion and 2D experiments were performed in standard cell culture conditions (relative humidity: 95%, 5%CO_2, 37°C)

3.3.2. Ti6Al4V scaffolds

For 3D cell culture, additive manufactured Ti6Al4V scaffolds (Ø = 6 mm, h = 6 mm) (Van Bael *et al.* 2011, Pyka *et al.* 2012) were used as described before (Papantoniou *et al.* 2014b). The total volume of the scaffolds was 166 ± 3 mm³, the available volume 130 ± 5 mm³ and the available surface 7.5 ± 0.6 cm² as determined with nanoCT (Kerckhofs *et al.* 2013a). Briefly, scaffolds were ultrasonically cleansed prior to use in acetone, ethanol and distilled water for 10 minutes each after which they received an alkaline treatment with 5M sodium hydroxide for 24 hours at 60°C. Subsequently, scaffolds were rinsed with distilled water after which they were sterilised in a steam autoclave. Prior to seeding, the scaffolds were pre-wetted by vacuum impregnation with culture medium for 2 hours in standard cell culture conditions after which they were dried in a non-humidified incubator overnight (Papantoniou *et al.* 2013).

3.3.3. Viscosity measurements culture medium

The viscosity of the culture medium was increased by the addition of dextran (average MW 150,000, Sigma). The viscosity of solutions containing 0, 2.5, 5, 7.5 and 10% dextran was determined using a MCR 501 rheometer (Anton Paar). A C-LTD 180/XL measurement chamber was used to enable shear stress measurements at a constant temperature of 37°C. For each measurement the solution was pre-sheared at a shear rate of 100/s for 30 seconds after which a rate sweep from 100/s to 0.1/s shear rate was performed using a log ramp. Data points corresponding with torques lower than 0.001 mNm were discarded due to inaccuracy of the measurements. Since $\tau=\eta*\gamma$ (with τ: shear stress, η: viscosity and γ: shear rate) the viscosity of the solution could be determined by correlating the applied shear rate to the measured shear stress.

3.3.4. 2D AB and PB measurements

For 2D experiments, cells were seeded at the standard density of 5,700 cells/cm² in 6 well plates and cultured statically in 2 ml of growth medium. For 6 days the metabolic activity of the cells was measured daily using both PB and AB for 3 wells each (both metabolic assays were obtained from Life Technologies). For both reagents a measurement solution containing 1 unit volume of reagent for 10 unit volumes of culture medium was prepared resulting in a 9.09% solution (standard concentration measuring solution unless otherwise mentioned). The medium was removed from the wells and replaced with 2 ml of the PB or AB solution after which the cells were transferred back to the incubator at normal cell culture conditions. At the different incubation times (15, 30, 45, 60, 90 and 120 minutes) a 100 µl sample was taken from every well and transferred to a 96-well plate. The fluorescent signal was measured with an automated microplate fluorometer (SerColab Systems) using an excitation wavelength of 544 nm and an emission wavelength of 590 nm as described earlier (Zhou *et al.* 2013b). The measured fluorescent signal was expressed as arbitrary fluorescent units (FU). For every measurement the background signal of the measurement solution was determined by incubating an identical volume in the absence of cells in the experimental conditions. This blank signal was subsequently subtracted from the signal measured in the presence of cells to obtain the signal induced by the presence of the cells. After the measurement, the PB or AB solution was removed from the wells and replaced by normal culture medium. For the measurement on day 5, 3 ml of the measuring solution was used to allow for a higher number of sampling points. Additional samples were taken after 3, 4, 5 and 6 hours of incubation.

To determine the quantitative correlation between the PB signal and the cell number in a 2D static setting two different approaches were used. 6-well plates were seeded with 100,000 cells each and cells were allowed to attach over night after which the culture medium was removed and 2, 4 or 6 ml of the PB solution was added on triplicate wells. Cells were incubated for 8 hours in total and 100 µl samples were taken every hour and transferred to a 96-well plate for measurement. Alternatively, different amounts of cells were seeded in triplicate in 6-well plates (25,000, 50,000, 75,000, 100,000, 200,000, and 300,000). Cells were incubated overnight to allow cell attachment after which the culture medium was removed and 2ml of PB solution was added. Samples were taken every hour for 8 hours and measured as described before.

3.3.5. 3D static cell culture and PB measurements

For 3D culture experiments cells were drop-seeded onto the scaffolds at a density of 200,000 cells/60 µl as described in previous studies (Papantoniou *et al.* 2013, Zhou *et al.* 2013b, Papantoniou *et al.* 2014b, Sonnaert *et al.* 2014a). 45 minutes after seeding 60 µl culture medium was added and 135 minutes later the medium volume was topped up to 1 ml. Scaffolds were statically incubated overnight in standard culture conditions (37°C, 5% CO_2, 95% relative humidity). Since the seeding process resulted in homogenous and reproducible seeding efficiencies in previous work (~60%) this was not assessed separately in this work (Papantoniou *et al.* 2013, Papantoniou *et al.* 2014b, Sonnaert *et al.* 2014a).

To determine the quantitative correlation between the PB signal and the cell content in a 3D static culturing system, scaffolds were transferred to 12 well plates containing 3 ml of culture medium after seeding. Medium was refreshed every two days and PB measurements were performed at day 1, 6, 10, 15 and 22 by replacing the culture medium with 3 ml of the PB solution and incubating the scaffolds in standard cell culture conditions for 3 hours. The PB signal was measured in triplicate as described before. At each PB time point 3 scaffolds were sacrificed for DNA measurement as described below.

3.3.6. 3D perfusion bioreactor culture and PB measurement

For 3D perfusion bioreactor culture, 3D Ti6Al4V scaffolds were seeded in the bioreactor system using the same methods as described for the static system (Papantoniou *et al.* 2013, Papantoniou *et al.* 2014b, Sonnaert *et al.* 2014a). Scaffolds were subsequently press-fitted in an in-house developed bioreactor chamber (Papantoniou *et al.* 2013, Zhou *et al.* 2013b, Papantoniou *et al.* 2014b, Sonnaert *et al.* 2014a) ensuring forced perfusion through the scaffold and cultured at a flow rate of 1 ml/min in a non-humidified incubator (37°C, 5% CO_2). The total medium volume in each circuit was 10 ml of which 7.2 ml was located in the medium reservoir. Medium was refreshed every second day by attaching a falcon tube containing fresh medium to the system. For PB measurements a falcon tube containing 2.2 ml of a 20.5% PB solution was connected to the circuit resulting in a total volume of 5 ml and a final PB concentration of 9.09% as used for the static measurements. The PB solution was perfused for one hour at 1 ml/min after which the resulting PB signal in the solution was measured. To remove remnants of the PB solution in the bioreactor circuits for continued cell culture two falcon tubes containing 5 ml of culture medium were subsequently connected to the circuits for a perfusion step of 5 minutes each after which a final medium refreshment was performed as described before. After seeding the scaffolds were dynamically cultured for 21 days and PB measurements were performed in triplicate on day 2, 7, 12, 17 and 21. After each PB measurement 3 scaffolds were sacrificed for DNA measurement.

To determine the influence of both culture the measurement setup (static versus bioreactor), 3D cell seeded scaffolds cultured for 14 days in both systems were measured either in the respective culture systems or consecutively both in a static and perfusion bioreactor setup. All conditions were performed and measured in triplicate. In an additional 3 samples cultured in both setups no PB measurements were performed to verify that the performed handlings had no influence on cell number. All samples were used for DNA measurement after the experiment.

To determine the influence of different flow rates during 3D perfusion bioreactor culture on the metabolic activity of cells in the 3D scaffolds, and thereby on the conversion rates of the PB, they were cultured at different flow rates (0.5 ml/min, 1.1 ml/min and 2.2 ml/min) for 21 days after which the metabolic activity of the cells was determined using PB. The flow rates used during the PB measurement were the same as those used during culture for all conditions. The cell content of the scaffolds was

also determined based on DNA measurements. Additionally, two conditions in which the volumetric flow rate was 0.5ml/min but the shear stress was equal to respectively the 1.1 and 2.2 ml/min condition by increasing the viscosity of the medium as described earlier (Section 2.3) using respectively 3.37% and 6.36% dextran (average MW 150,000, Sigma) were evaluated.

3.3.7. DNA measurement

The DNA content was determined using a highly quantitative and selective DNA assay (Quant-iT^{TM} dsDNA HS kit, Life Technologies). The scaffolds were rinsed with PBS and lysed in 350 µl RLT lysis buffer supplemented with 3.5 µl β-mercaptoethanol (Qiagen). The lysed samples were vortexed for 60 seconds and stored at -80°C prior to analysis, thawed at room temperature and spun down for 1 min at 13,000 rpm. 10 µl of the sample was diluted in 90 µl milliQ water after which the DNA content was quantified with a Qubit® Fluorometer (Life Technologies) as described by Chen *et al.*, 2012 (Chen *et al.* 2012)

3.3.8. Mathematical representation of the PB measurement in the perfusion bioreactor system using ordinary differential equations

A schematic representation of the bioreactor system is shown Figure 3.1. The concentration of the resorufin in the medium reservoir could be determined based on a mass balance over the reservoir taking into account the flow rate dependent in and outward fluxes (eq. 1). The outward flux was defined based on the flow rate and the resorufin concentration (eq. 2). The inward flux in the medium reservoir was equal to the outward flux at the scaffold although a flow rate and tubing volume dependent time delay had to be implemented to account for the time the measurement suspension required to be perfused from the scaffold back to the medium reservoir (eq. 3). The flux at the outlet of the scaffold was determined by the ingoing flux and the cell mediated resazurin conversion (eq.4) while the flux at the inlet of the scaffold was defined based on the concentration in the medium reservoir, again implementing the flow rate and tubing volume dependent time delay in order to account for the time required to perfuse the solution from the medium reservoir to the scaffold (eq.5).

At the initial time point the resorufin concentration in the medium reservoir was set at zero while the maximal value was set at 3,500 as these were determined to be the borders of the linear operating window.

$$[R]_{reservoir(t)} = \frac{\left((V - V_T) * [R]_{reservoir(t-\Delta t)} - d[R]_{reservoir,out(t)} + d[R]_{reservoir,in(t)}\right)}{V - V_T} (eq.1)$$

$$\frac{d[R]_{reservoir,out}}{dt} = \dot{F} * [R]_{reservoir} \ (eq.2)$$

$$\frac{d[R]_{reservoir,in}}{dt} = \frac{d[R]_{construct,out\ (t-t_d)}}{dt} = \left([R]_{reservoir\ (t-2*t_d)} * \dot{F} + n * \dot{C}\right)(eq.3)$$

$$\frac{d[R]_{construct,out}}{dt} = \frac{d[R]_{construct,in}}{dt} - n * \dot{C} = [R]_{reservoir\ (t-t_d)} * \dot{F} + n * \dot{C}\ (eq.4)$$

$$\frac{d[R]_{construct,in}}{dt} = [R]_{reservoir\ (t-t_d)} * \dot{F}\ (eq.5)$$

With

$[R] = Resorufin\ concentration\ (\frac{FU}{ml})$

$V_T = Tubing\ volume\ (ml)$

$\dot{F} = flowrate\ (\frac{ml}{s})$

$n = cell\ number$

$\dot{C} = PB\ conversion\ rate\ (\frac{FU}{cell * s})$

$V = Bioreactor\ volume\ (ml)$

t_d(Tubing volume and flow rate dependent time delay) $= \frac{V_T}{2 * \dot{F}}$

$\Delta t = timestep$

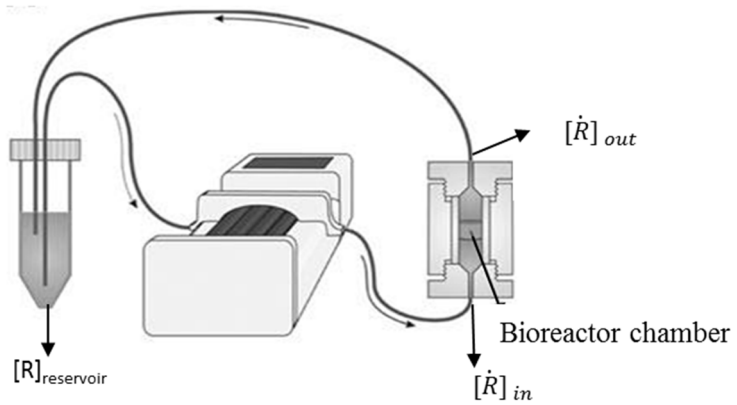

Figure 3.1: Schematic representation of the perfusion bioreactor system. (Adapted from Zhou et al., 2013)

3.3.9. Statistical analysis

One-way Anova was performed to analyse significant differences between groups. A p-value < 0.05 was considered significant.

3.4. Results

Initially the PB metabolic assay was compared with the previously validated AB assay (Zhou *et al.* 2013b) by monitoring for both assays cell proliferation in a static 2D setup for different incubation times (Figure 3.2.A and B). Both metabolic assays showed an increase in metabolic activity in function of culture time in accordance with the expected exponential phase of cell growth. Although the same incubation times and concentrations were used, the PB signal was significantly higher compared to the AB signal for the same incubation time. This was also visible by the stronger increase in signal shown in Figure 3.2.C in which the linear operating window of both assays was determined respectively up to 3,000 FU for the AB assay and 3,500 for the PB assay. The relative standard deviation on the measured signal was also significantly lower for the PB measurement as shown in Figure 3.2.D.

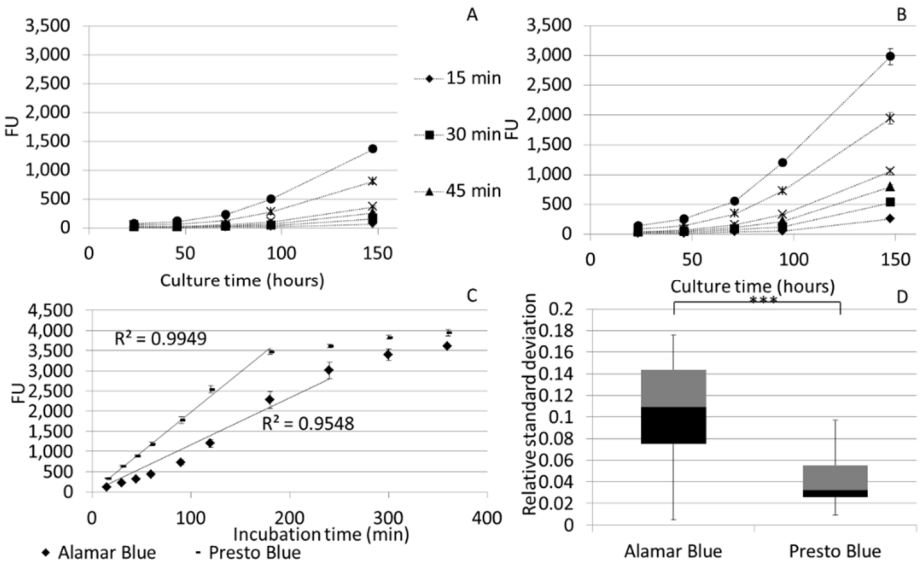

Figure 3.2: Comparison between Presto Blue and Alamar Blue
(A, B) 2D static expansion of hPDCs monitored with Alamar blue and Presto Blue respectively for different incubation times (n=3) (C) Signal saturation determined for Presto Blue and Alamar Blue based on 2D static expansion. The lines indicate the linear operating zone for both assays (R^2 values are shown for a fit forced through 0;0) (n=3) (D) Boxplot of relative standard deviation for 2D static Presto Blue and Alamar Blue measurements (n=60)

Conversion rates for PB were determined in a static setup for both 2D and 3D cell culture systems. For all conditions a time dependent linear increase in the measured signal was observed (Figure 3.3). Linear regression was used to determine the slope coefficients which indicated the increase in FU per hour for all different conditions (Table 3.1). These values were corrected for incubation time, cell number and volume and were then averaged over the different experimental conditions. For the case of 2D cell culture the two different setups used to determine the conversion rate resulted in a similar average value of approximately 616 FU converted per hour for 100,000 cells. For the measurement in the 3D static culture system a linear correlation was again measurement as observed between the PB obtained signal and the cell number based on DNA shown in Figure 3.3.C. The resulting PB conversion rate was, however, significantly lower than the one obtained for the 2D static system (Table 3.1).

Table 3.1: Observed increase in Presto Blue signal per hour for different static culture conditions based on Figure 3.3 and the representative Presto Blue conversion rates.

<table>
<tr><th>Cell number (2D)</th><th>Increase in fluorescent signal/hour</th><th>R^2 Value</th><th colspan="3">FU converted by 100,000 cells in one hour (FU/100,000 cells*hr)</th></tr>
<tr><td>25,000</td><td>107</td><td>0.95</td><td>860</td><td rowspan="6">605 ± 176</td><td rowspan="11">616 ± 141</td></tr>
<tr><td>50,000</td><td>188</td><td>0.94</td><td>750</td></tr>
<tr><td>75,000</td><td>225</td><td>0.93</td><td>601</td></tr>
<tr><td>100,000</td><td>288</td><td>0.95</td><td>575</td></tr>
<tr><td>200,000</td><td>449</td><td>0.99</td><td>449</td></tr>
<tr><td>300,000</td><td>592</td><td>0.98</td><td>395</td></tr>
<tr><td>Volume Presto Blue solution (ml) (2D)</td><td></td><td></td><td></td><td rowspan="4">628 ± 38</td></tr>
<tr><td>2</td><td>295</td><td>0.95</td><td>590</td></tr>
<tr><td>4</td><td>157</td><td>0.95</td><td>629</td></tr>
<tr><td>6</td><td>111</td><td>0.95</td><td>668</td></tr>
<tr><td>Days of culture (3D)</td><td></td><td></td><td></td><td colspan="2" rowspan="6">237± 26</td></tr>
<tr><td>1</td><td>12.5</td><td>0.94</td><td></td></tr>
<tr><td>6</td><td>66.8</td><td>0.93</td><td></td></tr>
<tr><td>10</td><td>275</td><td>0.98</td><td></td></tr>
<tr><td>15</td><td>415</td><td>0.99</td><td></td></tr>
<tr><td>22</td><td>421</td><td>0.99</td><td></td></tr>
</table>

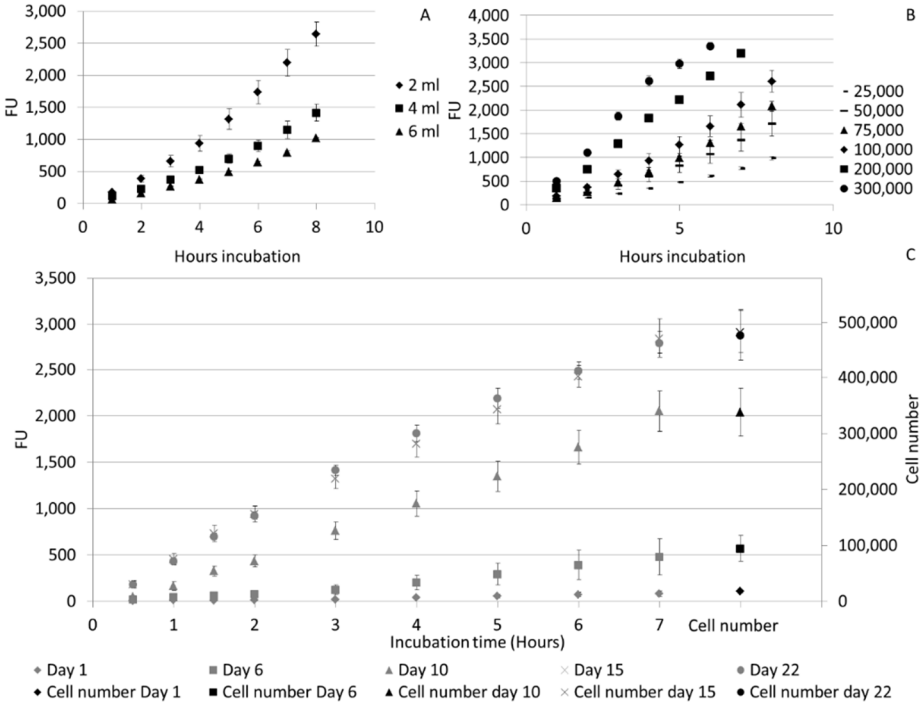

Figure 3.3: Presto Blue and DNA measurement for different culture setups
(A) Fluorescent signal measured for different volumes of Presto Blue solution for 100,000 cells in a 2D static setup (n=3) (B) Fluorescent signal measured for different cell numbers in 2ml Presto Blue solution in a 2D static setup (n=3) (C) Presto Blue signal in function of incubation time for different time points during 3D static culture and corresponding cell number based on DNA measurements (n=3)

As shown for both the 2D and 3D static culture and measurement setups the PB signal and DNA content measured for perfusion bioreactor expanded cells showed no significant differences after fitting the curves as shown in Figure 3.4.A in which both the increase in FU and the increase in cell number are represented on the Y-axis. Normalizing the signal to the volume and cell number resulted in conversion rates which were not significantly different from the earlier determined 2D conversion rates during the proliferative phase (Figure 3.4.B and Table 3.1). As also shown in Figure 3.4.A the metabolic conversion rate of the cells in the scaffold does decrease once confluency is reached as determined with DNA measurements (Figure 3.4.B).

In order to determine the influence of the culture and measurement setup on the PB signal, bioreactor and static measurements of cells expanded in both 3D bioreactor and static setups were performed. Figure 3.5.A shows a significant higher DNA content for all 3D bioreactor expanded cells in comparison to the static 3D expanded cells. No significant difference was observed between the cells expanded under the same

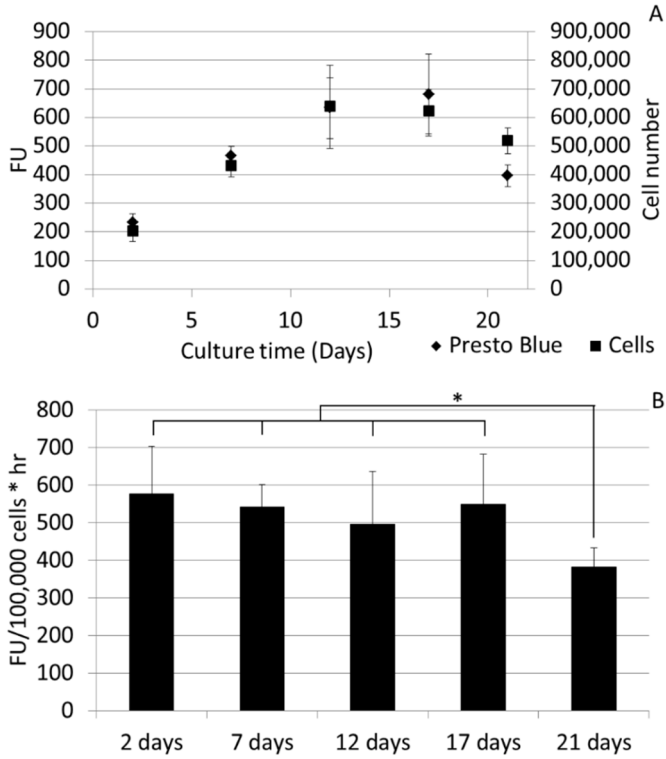

Figure 3.4: Presto Blue and DNA measurements and correlated conversion rates during bioreactor culture.
(A) Cell number and Presto Blue signal during 21 days of 3D perfusion bioreactor culture for different time points (B) Presto Blue conversion rates for different time points during 3D perfusion bioreactor culture. * 0.05>p

conditions indicating that the handlings performed for the measurements did not influence the cell content. Despite the significant differences observed in DNA content no differences in PB signal were observed between the 3D static and bioreactor expanded cells using the static measurement setup (Figure 3.5.C). However the measurements performed in the bioreactor system showed a significant difference between the bioreactor and the statically expanded cells (Figure 3.5.B). Since different incubation times and PB volumes were used for the bioreactor and static measurements the obtained signal was corrected for cell number, time and volume. Figure 3.5.D shows that a similar conversion rate was determined for all bioreactor measured conditions, independently from the culture setup. The conversion rate determined for static measurements were significantly lower in comparison to all bioreactor measured conditions. Additionally, the conversion rate determined for the bioreactor cultured, static measured samples was significantly lower than those for the statically cultured and measured.

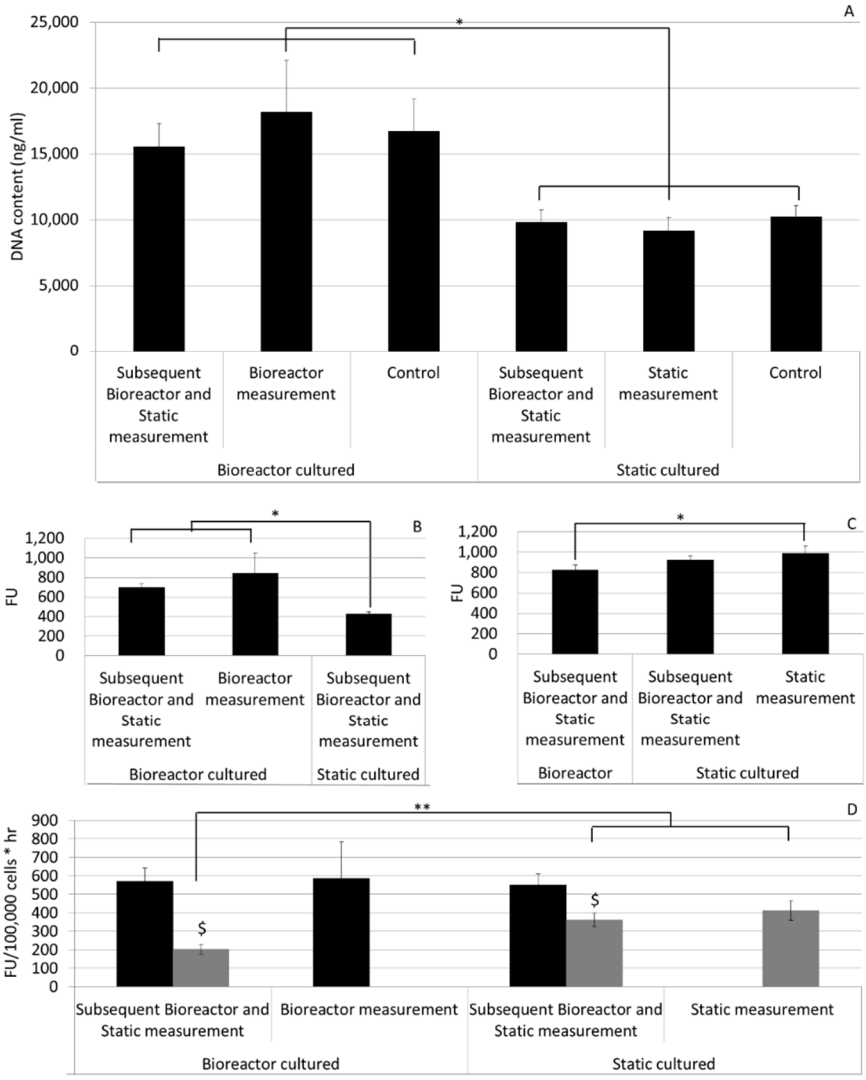

Figure 3.5: Influence of different measurement and culture setups on Presto Blue conversion rates

(A) DNA content (ng/ml) after 3D cell expansion for different culture and measurement setups, as shown on the axis (n=3) (B) Presto Blue signal after either 3D static or perfusion bioreactor cell expansion, measured in the perfusion bioreactor system (n=3) (C) Presto Blue signal after either 3D static or perfusion bioreactor cell expansion, measured in the static system (n=3) (D) Conversion rates for 3D constructs cultured in a bioreactor or static setup determined using a bioreactor (black) or static (grey) measurement setup (n=3). * $0.05>p>0.01$, ** $0.01>p>0.001$, $ indicates significant differences between dynamic and static measurement for the same construct, $p<0.05$

No significant differences in cell proliferation were observed when using different flow rates nor did the increased viscosity and the correlated shear stress for the low volumetric perfusion influence the final cell number (Figure 3.6.A). Additionally, the conversion rates determined for the different conditions were not influenced by the perfusion velocity (Figure 3.6.B) indicating that, next to the proliferation, the PB conversion rates and therefore the metabolic activity of the cell population, was not influenced by flow rate within the examined range corresponding with initial shear stress values between 7E-3 Pa and 3.08E-2 Pa (Sonnaert *et al.* 2014a).

Although flow rate does not influence the conversion rate of the PB assay it should be high enough to prevent local saturation of the assay at the outlet of the scaffold. To determine at which combinations of flow rate and cell number this could influence the readouts, mass balance equations were used to determine the relative saturation of the linear PB operating window in the medium reservoir and at the scaffold in- and outlet in function of flow rate, cell number, measurement volume and incubation time (eq.1-5). The resulting resorufin concentrations at the scaffold outlet obtained from the time dependent mass balances were subsequently converted to relative PB saturation as shown in Figure 3.7.A-C. Although flow rate did not influence the conversion rate of

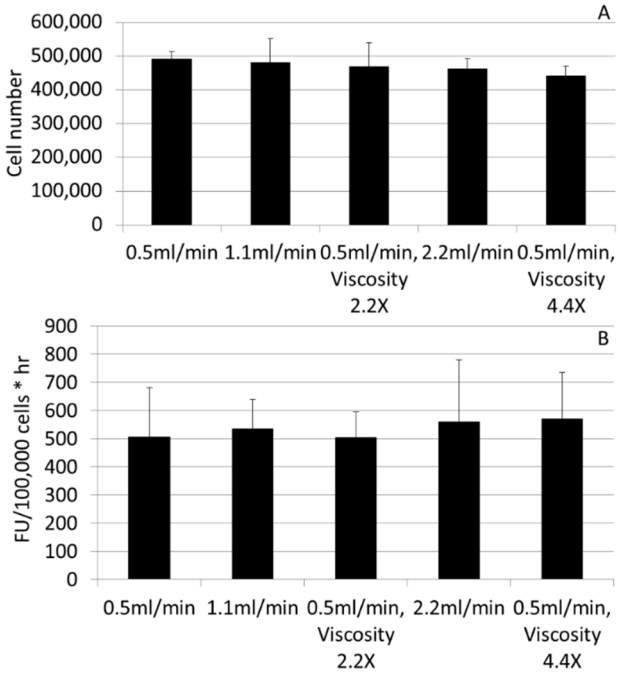

Figure 3.6: Influence of shear stress and volumetric perfusion velocity on Presto Blue conversion rate.
(A) Cell content for 3D constructs cultured in the perfusion bioreactor based on DNA measurement for different flowrates and medium viscosities (n=3) (B) Presto Blue conversion rate for 3D constructs cultured in the perfusion bioreactor with different flowrates and medium viscosities

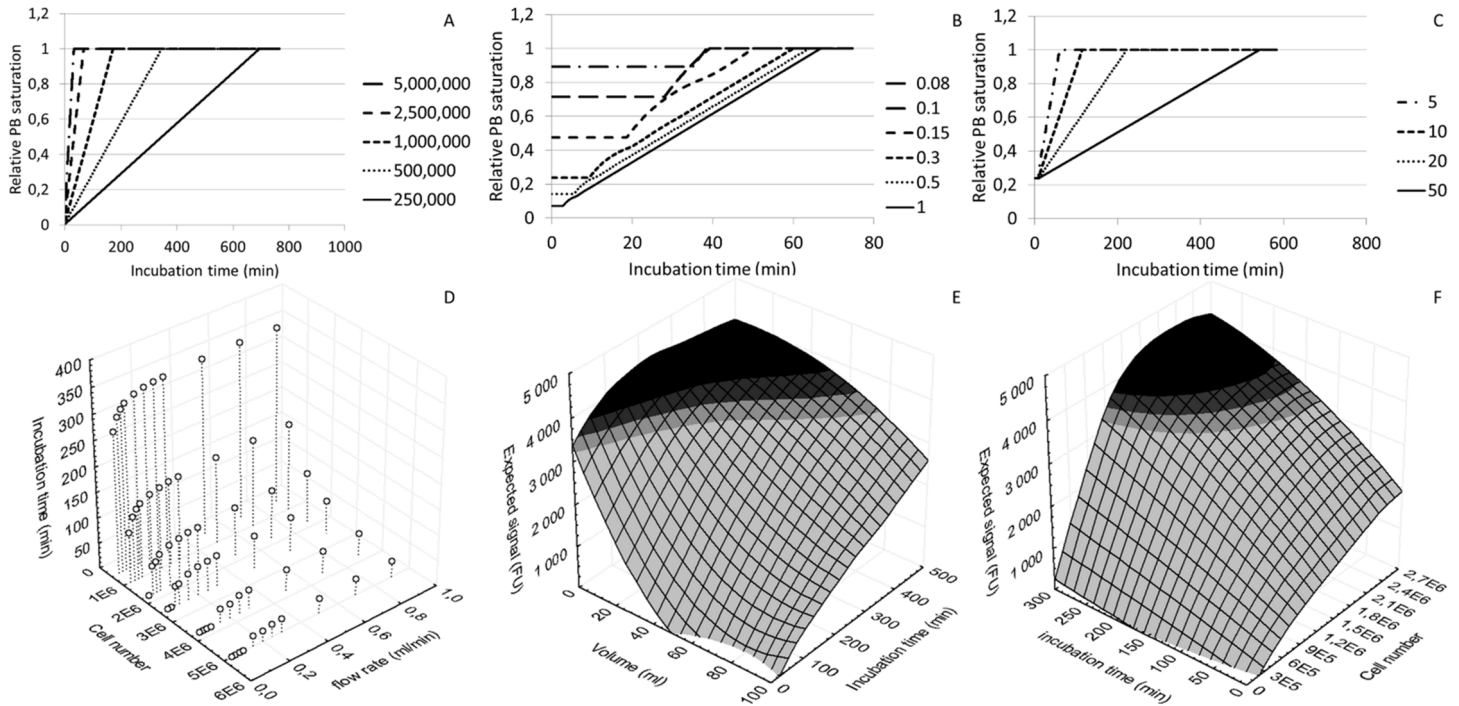

Figure 3.7: Model based estimation of Presto Blue signal.
Presto Blue saturation at the bioreactor chamber outlet determined for (A) different cell numbers (B) different flow rates (ml/min) (C) different measurement volumes (ml) (D) incubation time (min) after which saturation of the Presto Blue assay is reached at the bioreactor chamber outlet for specific combinations of cells and flow rate (ml/min) (E) Operating window for Presto Blue measurement of a bioreactor chamber containing a scaffold with 2,500,000 cells valid for flow rates above 0.4ml/min (F) Operating window for a Presto Blue measurement in a 3D perfusion bioreactor system containing 5ml of measurement solution valid for flow rates above 0.4ml/min. The black area shows the measurement conditions which result in a value outside the linear operating window of the assay.

the assay, flow rate dependent changes in PB saturation were observed (Figure 3.7.B). Figure 3.7.D subsequently shows for which combinations of incubation time, cell number and flow rate saturation at the scaffold outlet is reached, allowing to define an operating window for the measurement.

3.5. Discussion

A number of reports have shown that metabolic assays such as the AB assay can be used to monitor cell proliferation (Mueller *et al.* 2013, Zhou *et al.* 2013b) although no quantitative correlation between the conversion rate of the reagent and the cell number has been defined. To enable a quantitative use of this tool we investigated the influence of three different cell culture methods and correlated measurement set-ups, including bioreactor culture, on the conversion of the resazurin based PB metabolic assay.

Initially, a validated metabolic activity assay, the AB assay (Zhou *et al.* 2013b) was compared with the PB assay for conventional 2D cell expansion. As shown in Figure 3.2.C the maximum signal obtained in the linear operating range was approximately 3,000 FU for the AB assay and 3,500 for the PB assay indicating that the latter has a significantly larger operating window. Additionally, the time dependent increase in signal was significantly higher at each time point for the PB (Figure 3.2.A-C) demonstrating that this assay has a higher sensitivity power which was also confirmed by comparing the relative standard deviations obtained for both assays (Figure 3.2.D).

Table 3.1 shows that a linear correlation between PB signal and cell content exists (R^2=0.87). Due to the increase in cell number, and the correlated decrease in available surface for proliferation, a decreasing trend in PB conversion in function of cell number was, however, present. Nonetheless, no significant differences were observed between the average conversion rates determined using different volumes and cell numbers and a quantitative correlation between cell number and PB signal could be established. Although other groups reported discrepancies between resazurin conversion of the AB assay and cell number (Ng *et al.* 2005, Quent *et al.* 2010) these could probably have been induced by the high cell density in the culture systems used. When performing a similar experiment for static 3D cell culture and monitoring proliferation in function of time a quantitative relation between cell number and PB signal was again observed (Figure 3.3.C) although a significantly lower conversion rate was obtained (Table 3.1). For the perfusion bioreactor 3D cell culture, the PB conversion rate was significantly higher than observed for the static 3D system and no difference was found in relation to the 2D setup (Figure 3.4.B, Table 3.1). Since previous studies already showed that cell growth in 3D scaffolds in a static culture setup is predominantly located at the outer edges of the scaffolds due to limitations in nutrient diffusion (Ishaug *et al.* 1997, Bancroft *et al.* 2002, Sikavitsas *et al.* 2003, Papantoniou *et al.* 2014b, Sonnaert *et al.* 2014a) also the difference in PB conversion rate might be related to limited diffusion.

In order to confirm that the different conversion rates observed between 3D static and perfused culture systems originated from enhanced mass transport in the perfusion bioreactor system, the conversion rate for cells expanded both in the 3D static or bioreactor system were determined using both static and bioreactor measurement setups. As shown in Figure 3.5.A the measurement methods and manipulations did not

influence the final cell content of the scaffolds. Despite the significant differences in DNA content, the PB signal measured in the static setup was not influenced by the culture conditions (Figure 3.5.C). Diffusion limitations possibly influenced the accessibility of the cells in the centre of the densely populated bioreactor cultured scaffolds (Ishaug *et al.* 1997, Bancroft *et al.* 2002, Sikavitsas *et al.* 2003). In order to confirm this hypothesis the maximal diffusion depth of the resazurin in the scaffolds was determined using a partial differential equation describing the spatiotemporal evolution of resazurin (c_R) as discussed by (Demol *et al.* 2011) (eq.6). As no data was available on resazurin diffusion in an engineered neo-tissue the diffusion coefficient (D) of resazurin in aquatic systems was used as an approximation ($2.04*10^{-6}cm^2/s$) (Khazalpour *et al.* 2014). The resazurin conversion rate (Q) was based on the results discussed earlier and cells were assumed to be homogenously distributed in the neo-tissue with a density (c_{cell}) based on previous nano-CT volumetric results (Papantoniou *et al.* 2014b, Sonnaert *et al.* 2014a).

$$\frac{\partial c_R(z,r,t)}{\partial t} = D(z,r,t).\nabla^2 c_R(z,r,t) - Q * c_{cell}(z,r,t) \quad (Eq.6)$$

The steady state solution of the system enabled determining a maximal diffusion depth of 700µm. This results in an active volume of 40% of the total scaffold implying that only the cells present in this volume can contribute to the resazurin conversion. This corresponds to the discrepancy between the apparent conversion rate determined for bioreactor cultured, static measured scaffolds and bioreactor cultured and measured scaffolds in which the resasurin is perfused through the scaffold for which the static determined conversion rate was only 35% of the dynamic based value (Figure 3.5.D). For the bioreactor measured conditions we did observe an influence of the culture system on PB conversion (Figure 3.5.B). To compare conversion rates between the two measurement setups the PB signal was corrected for volume, time and cell number (Figure 3.5.D) which showed that conversion rates measured with the bioreactor setup were not influenced by the culture system used. As the Péclet number was larger than 1, the convective mass transport in this measurement setup ensured a homogeneous distribution of the PB reagent throughout the scaffold independent from the cell distribution and therefore a realistic conversion rate could be determined as opposed to apparent conversion rates obtained in the static, diffusion based setups. Since the used culture systems did not influence the conversion rates, the differences observed between the static and bioreactor measurement setups were not caused by changes in cell metabolic activity but rather by a decreased conversion efficiency caused by diffusion limitations (Ishaug *et al.* 1997, Bancroft *et al.* 2002, Sikavitsas *et al.* 2003). Despite the lower conversion rate in the static setup a correlation between the obtained PB signal and the DNA content still exists as shown in Figure 3.3.C. This indicates that dependent on the measurement system different conversion rates should be used and that quantitative use of the methodology requires a system specific validation of the measurement. This was further validated by generating a correlation plot depicting the cell number based on the PB measurements in function of the cell number based on DNA measurements (Figure 3.8). Taking into account the respective conversion rates for the static cultured/measured and dynamic cultured/measured expansion systems an

R^2 value of 0.9548 was obtained confirming the potential quantitative use of the methodology.

At day 21 of culture, after the proliferative phase as could be observed in Figure 3.4.A, both the increase in cell content, the PB signal and the conversion rate decreased significantly. As suggested for the 2D system (Figure 3.3.B and Table 3.1) the decreased conversion rate of the PB assay for high cell densities might be related to the decrease in cell proliferation. Alternatively, previous work showed a non-linear correlation between the resazurin conversion and the cell number for high density cell cultures which was due to diffusion limitations both in 2D and 3D (Ng *et al.* 2005), although the fluid flow in the bioreactor system should circumvent these problems. Additionally, the high cell density in these constructs has been suggested to result in the further reduction of the fluorescent resorufin in the non-fluorescent, colourless hydroresorufin (O'Brien *et al.* 2000) thereby resulting in a decreased amount of the fluorescent resorufin. However, since multiple groups showed a linear behaviour of the assay within the defined operating conditions (Quent *et al.* 2010, Mueller *et al.* 2013, Zhou *et al.* 2013b), the decrease in cell proliferation remains the most probable explanation for the observed decreased conversion rate of the PB.

In order to determine the applicability of the proposed methodology for a broader range of operating conditions we subsequently also determined the influence of the use of different flow rates and shear stresses (using dextran to increase fluid viscosity) on the metabolic conversion rates of the assay. In a recent publication we showed that the use of range of flow rates (corresponding to initial shear stress values between 5.59E-4 and 5.59E-2Pa) did not induce differentiation of the expanding hPDC cell population

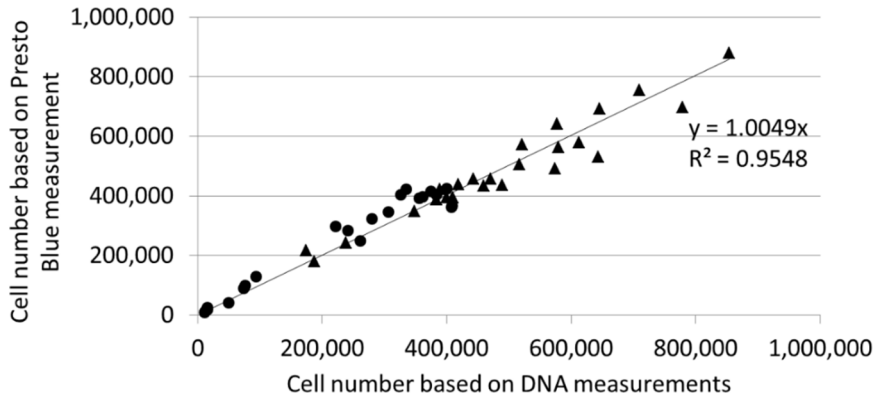

Figure 3.8: Validation of the predictive model.
Correlation between cell number determined on DNA measurement and cell number based on Presto Blue measurement for all 3D static and dynamic cell expansion performed for Figures 2-6 using the respective conversion rates determined for the two culture systems. (▲ 3D dynamic expansion and measurement, ● 3D static expansion and measurement)

(Sonnaert *et al.* 2014a). Furthermore, a functional bone marrow derived MSC population was also expanded in undifferentiated state under flow conditions in a perfusion bioreactor (Papadimitropoulos *et al.* 2014a). In correspondence with these findings, we observed that the metabolic activity of the hPDCs is constant and independent from dextran concentration (affecting shear stress) and volumetric flow rate. Taking into account the determined conversion rates, expected number of cells and the culture and measurement setup these results now allow to define an operating window for each specific setup which will allow a rational selection of operating conditions (Gerontas *et al.* 2009, Papantoniou *et al.* 2013). Figure 3.7.D shows for which combination of cell number, flow rate and incubation time saturation of the assay is reached at the scaffold outlet, thus indicating the minimal flow rate and maximal incubation time required for monitoring an expansion system in function of the expected maximal cell number. It should be noted that, despite the fixed assay volume and therefore the fixed amount of resazurin which can be converted, the maximal incubation time for a certain cell number varies in function of flow rate. Next to the saturation of the assay due to high cell numbers and low flow rates, a significant resazurin concentration gradient will be present in the tubing of the system for high cell numbers and low flow rates. For higher flow rates this concentration gradient will be negligible resulting in a constant, cell dependent maximal incubation time. For these cases the operating window of the assay can be determined based on the total circuit volume, incubation time and expected cell number as shown in Figure 3.7.E and F in which the expected PB signal is shown in function of measurement volume and incubation time (Figure 3.7.E) or incubation time and cell number (Figure 3.7.F). This simplified representation of the system will be valid for flow rates that not significantly influence the maximal incubation time as shown in Figure 3.7.D. Next to using this mathematical representation of the system to define optimal operating conditions, the quantitative correlation between PB conversion and cell number can also be used to determine the cell number in the scaffold at any given time. Additionally, the theoretical boundaries of the window of operation could be determined for the dynamic measurement method i.e. convective perfusion through the constructs. For example, using a flow rate of 1ml/min as employed for measurements in this study, cell numbers as low as 50,000 cells could be detected using 5ml of PB solution although at least 120 minutes incubation time would be required to obtain a quantitative signal. On the other hand, using the same flow rate and 50ml of PB solution, constructs containing up to 25,000,000 cells could be monitored using short incubation times between 15 and 20 minutes. A further increase in PB solution volume would even allow the further broadening of the window of operations, thereby enabling the methodology to effectively cover the entire range of cell densities used for tissue engineering applications for which final cell densities in the engineered constructs were reported between 10^7 and 10^8 cells/cm³ (Bancroft *et al.* 2002, Eyckmans *et al.* 2006a, Haycock 2011, Rodrigues *et al.* 2011, Santoro *et al.* 2012).In conclusion we can state that the PB assay is a promising tool to for on-line monitoring of cell proliferation in a 3D perfusion bioreactor system. Since the conversion of the metabolic assay was shown to be constant in function of time during cell proliferation, and the culture parameters such as flow rate and shear stress did not influence the metabolic activity nor the conversion efficiency, a quantitative correlation between cell number and PB conversion could be

established. This allowed to determine the assay concentration at each location in the setup, thereby enabling to define optimal operating conditions as well as calculating cell number in the scaffold based on the PB concentration.

3.6. Acknowledgements

MS is supported by a Ph.D. grant of the Agency for Innovation by Science and Technology (IWT/ 111457). IP is funded by the ENDEAVOUR project G.0982.11N of the Research Foundation Flanders (FWO Vlaanderen). This work is part of Prometheus, the Leuven Research & Development Division of Skeletal Tissue Engineering of the KU Leuven: www.kuleuven.be/prometheus

Chapter 4.
Three dimensional characterization of tissue-engineered constructs by contrast enhanced nanofocus computed tomography

Ioannis Papantoniou[*], Maarten Sonnaert[*], Liesbet Geris, Frank P. Luyten, Jan Schrooten, Greet Kerckhofs

*These authors have contributed equally and therefore share first authorship

Published in Tissue Engineering Part C, Methods, 2014 March; 20(3): 177-87 doi: 10.1089/ten.TEC.2013.0041. Epub 2013 Oct 19.

4.1. Abstract

In order to successfully implement tissue engineered (TE) constructs as part of a clinical therapy, it is necessary to develop quality control tools that will ensure accurate and consistent TE construct release specifications. Hence advanced methods to monitor TE construct properties need to be further developed. In this study we showed proof of concept for contrast enhanced nanofocus computed tomography (CE-nanoCT) as a 'whole-construct' imaging technique with non-invasive potential that enables 3D visualization and quantification of *in vitro* engineered extracellular matrix (ECM) in TE constructs. In particular we performed a 3D qualitative and quantitative structural and spatial assessment of the *in vitro* engineered ECM, formed during static and perfusion bioreactor cell culture in 3D TE scaffolds, using two contrast agents, namely Hexabrix® and phosphotungstic acid (PTA). To evaluate the potential of CE-nanoCT, a comparison was made to standardly used techniques such as Live/Dead viability/cytotoxicity, picrosirius red staining and to net dry weight measurements of the TE constructs. When using Hexabrix® as contrast agent, the ECM volume fitted linearly with net dry ECM weight independent from the flow rate used, hence suggesting that it stains most of the ECM. When using PTA as contrast agent, comparing to net weight measurements showed that PTA only stains a part of the ECM. This was attributed to the binding specificity of this contrast agent. Also, the PTA-stained CE-nanoCT data showed pronounced distinction between flow conditions when compared to Hexabrix®, indicating culture-specific structural ECM differences. This novel type of information can contribute to optimize bioreactor culture conditions and potentially critical quality characteristics of TE constructs such as ECM quantity and homogeneity, facilitating the gradual transformation of 'TE constructs' in well characterized 'TE products'.

4.2. Introduction

As the field of tissue engineering (TE) matures, the need for novel techniques to characterize engineered constructs (i.e. cells/tissue combined with scaffolds) in a more insightful and quantitative manner becomes imperative. Currently, standard techniques such as histological sectioning and Live/Dead viability/cytotoxicity staining show limited potential as quality controls for TE constructs as these techniques only allow assessment of tissue distribution in two dimensions, with loss of information and with limited depth resolution while being destructive in nature (Hedberg *et al.* 2005, Eniwumide *et al.* 2007, Stephens *et al.* 2007, Smith *et al.* 2010). Techniques such as confocal microscopy may offer a potential for three dimensional (3D) visualization, however, again a limited depth resolution (~300 µm) hinders their performance when larger TE construct need to be analyzed (Georgakoudi *et al.* 2008).

Recent advances in 3D imaging techniques and image analysis strategies have demonstrated the potential of addressing some of the shortfalls of these currently applied methods for accurate TE construct analysis. In particular microCT has been frequently applied as a 3D quantitative imaging technique to assess scaffold structure, (Peyrin *et al.* 2007, van Lenthe *et al.* 2007, Jungreuthmayer *et al.* 2009) as well as bone ingrowth after *in vivo* implantation (Cancedda *et al.* 2007, Jones *et al.* 2007,

Papadimitropoulos *et al.* 2007, van Lenthe *et al.* 2007, Guldberg *et al.* 2008, Jones *et al.* 2009, Chai *et al.* 2012a). Furthermore it has been employed for time-lapsed follow-up of mineralization inside scaffolds during *in vitro* static (Cartmell *et al.* 2004, Hagenmueller *et al.* 2007, Frohlich *et al.* 2010) or bioreactor cultures (Porter *et al.* 2007, Guldberg *et al.* 2008, Hagenmuller *et al.* 2010). In most of these studies polymeric, ceramic, collagen scaffolds or composites were used, in which mineralized extracellular matrix (ECM) could be separated from the scaffold for the purpose of volume calculations and no significant material-dependent artifacts were present. However, when imaging ECM or tissue growth in metallic scaffolds or around implants, additional caution has to be taken during image analysis as metal artifacts (De Man *et al.* 1999, Kerckhofs *et al.* 2008) can significantly influence the accuracy of the quantification of the newly formed ECM or tissue volume (Marechal *et al.* 2005, Stoppie *et al.* 2005).

Several studies have shown that when using phase contrast imaging, in most cases only available by synchrotron radiation, non-mineralized ECM formed *in vitro* in 3D TE constructs can be visualized (Langer *et al.* 2010, Appel *et al.* 2011, Voronov *et al.* 2012). However, routine access to systems allowing phase contrast imaging is limited and there are restrictions on the sample specifications. On the other hand, by using the more routinely available desktop microCT in standard absorption mode, without the use of a contrast agent, it has not been possible yet to visualize *in vitro* produced non-mineralized ECM in 3D scaffolds (Albertini *et al.* 2009, Appel *et al.* 2011). To address this limitation osmium tetroxide, (Hilldore *et al.* 2007) a well-known X-ray opaque staining, has been used to visualize cells in 3D constructs. This stain is, however, toxic to cells, thus cannot be used for non-invasive quality control of ECM growth in the TE construct.

In this study we propose contrast enhanced nanofocus CT (CE-nanoCT) as a 3D imaging technique that combines the high spatial and contrast resolution of nanoCT with the use of contrast agents, to characterize engineered ECM in TE constructs after *in vitro* culture. In particular we performed a 3D quantitative and qualitative structural and spatial assessment of the *in vitro* engineered ECM, formed during static and bioreactor cell culturing in titanium alloy scaffolds. By using metallic scaffolds in this case study we additionally proved the effectiveness of CE-nanoCT, as these scaffold types represent the worst case scenario with regard to material-dependent image artifacts. The two selected tissue-specific contrast agents that were used to stain the TE construct after culture were Hexabrix® and phosphotungstic acid (PTA). The latter is known to bind to connective tissues, and more specifically to collagen and fibrin (Metscher 2009a). The former contains a negatively charged ioxaglate, which will be locally repulsed by the negative fixed charge density of the tissue, thus all tissues which do not contain a negative charge will be stained (Palmer *et al.* 2006, Xie *et al.* 2009). Additionally, Hexabrix® has been used for *in vivo* animal studies (Piscaer *et al.* 2008) and in a clinical setting (Ginai 1987), and thus is a potential candidate for non-invasive TE construct quality assessment. To evaluate the potential of CE-nanoCT for 3D visualization and quantification of *in vitro* engineered ECM by culture of human periosteum derived cells (hPDCS, i.e. a cell type that has been seen to be mulitpotent and to contribute in bone regeneration (De Bari *et al.* 2001, Orwoll 2003)) in 3D

titanium alloy scaffolds, a comparison was made to routine physical measurement techniques, such as Live/Dead viability/cytotoxicity for cell viability, picrosirius red staining for collagen content and ECM weight measurements.

4.3. Materials and Methods

4.3.1. Ti6Al4V scaffolds

3D additive manufactured open porous Ti6Al4V scaffolds (subsequently referred to as Ti scaffolds: Ø = 6 mm, h = 6 mm, porosity = 73 ± 1%, strut diameter = 245 ± 2 µm and pore size = 755 ± 3 µm), produced on an in-house developed selective laser melting (SLM) machine, (Van Bael *et al.* 2011) were used. The design was based on a parametric unit cell (Figure 4.1.A), which consists entirely of identical beams with constant circular cross-section (0.1 mm) and a beam length of 0.9 mm. Figure 4.1.B visualizes a produced open porous Ti scaffold. Prior to cell seeding, all scaffolds were pre-wetted by vacuum impregnation in cell culture medium for 2 h in a humidified incubator at 37°C, and dried overnight in a non-humidified incubator. (Impens *et al.* 2010b)

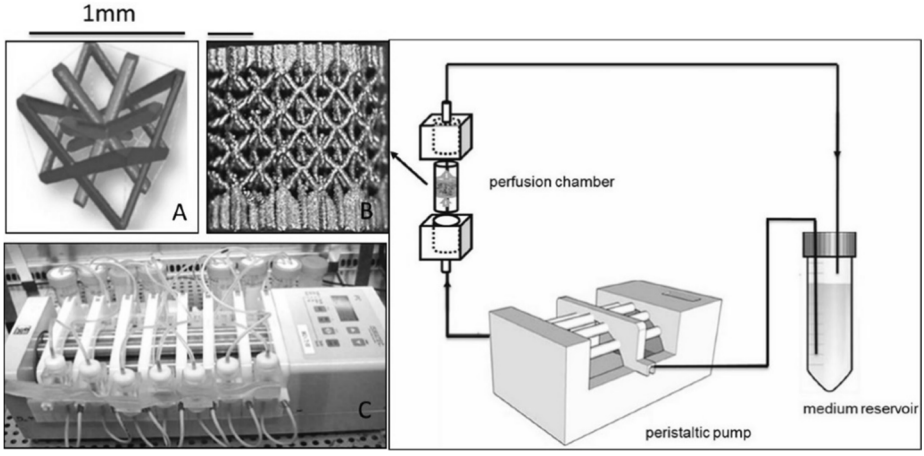

Figure 4.1: Perfusion bioreactor system.
(A) The parametric unit cell of the computer aided design of the porous Ti scaffolds, which consists entirely of identical beams with constant circular cross-section (0.1 mm) and a beam length of 0.9 mm, (B) a typical image of an SLM produced Ti scaffold and (C) an image of the in-house developed perfusion bioreactor equipped with parallel perfusion circuits, (D) Schematic of the bioreactor setup used for 3D dynamic culture, consisting of a medium reservoir containing 10 ml of medium, a peristaltic pump forcing culture medium through the porous scaffold that was positioned in the perfusion chamber.

4.3.2. Standard 2D hPDC Culture

hPDCs were isolated from periosteal biopsies of different donors as described previously (Eyckmans *et al.* 2006a). This procedure was approved by the ethics committee for Human Medical Research (KU Leuven) and with patient informed consent. hPDCs were expanded in Dulbecco's modified Eagle's medium with high-glucose (Invitrogen) containing 10% fetal bovine serum (BioWhittaker) and 1% antibiotic–antimycotic (100 units/mL penicillin, 100mg/mL streptomycin,and 0.25mg/mL amphotericin B; Invitrogen). The seeding density used for the two dimensional (2D) culture dish hPDC expansion was 6000 cells/cm^2. hPDCs were passaged at 80% – 90% confluency. At the time of experiment, cells (with a population doubling number of 15) were trypsinized with Tryple Express (Invitrogen) to be seeded on the scaffolds.

4.3.3. Static & bioreactor TE construct culture

A validated static seeding protocol was used for seeding 2D cultured hPDCs (cell seeding density 30,000 cells/cm^2) onto the preconditioned Ti scaffolds with an average cell seeding efficiency of 60% (Impens *et al.* 2010b). *In* vitro cell culture in the TE constructs lasted for 14, 21 and 28 days under static (n = 7) or dynamic (n = 7) culture conditions. For static culture, TE constructs were positioned in 12-well plates (Greiner Bio One) containing 3ml cell culture medium, and incubated at 37°C in a humidified and CO_2-controlled incubator (relative humidity: 95%, 5% CO_2). For bioreactor culture, TE constructs were cultured in an in-house developed perfusion bioreactor equipped with 7 parallel perfusion circuits (Figure 4.1.C). Each perfusion chamber, holding a single scaffold, was connected to an individual medium reservoir (disposable 50 ml Falcon tubes, BD Biosciences) containing 10 ml of cell culture medium via a Tygon® (Cole Parmer) tubing and via a two-stop tubing (BPT, Cole Parmer) connected to a peristaltic pump (IPC-24, Ismatec SA). Two different perfusion flow rates were used for the bioreactor culture: the low flow rate used was 0.04 ml/min while the high flow rate was 4 ml/min. In both static and bioreactor cultures medium was refreshed every two days for the entire culture duration.

4.3.4. CE-nanoCT

After static or dynamic culture the TE constructs were rinsed with 1ml phosphate buffered saline (PBS) and transferred to a 4% paraformaldehyde solution (Sigma) for 2 hours to fixate the ECM. The TE constructs were stored in PBS prior to analysis. Two contrast agents were used as received, namely Hexabrix® 320 (Guerbet Nederland B.V) and PTA (VWR International). During preliminary experiments (data not shown), for both contrast agents an exposure time of 30 min to consistently stain the entire TE constructs was selected.

Hexabrix® is a radio-opaque injectable solution containing ioxaglate meglumine (39.3 %) and ioxaglate sodium (19.6 %). Ioxalgate is a negatively charged ionic iodinated dimer that is locally repulsed by the negative fixed charge density of the ECM. As a consequence, all tissues with a net negative charge will not be stained, while Hexabrix® will adsorb to the rest. All samples were, before imaging, immersed in a

solution of Hexabrix® 320 (20% in PBS), then wrapped in parafilm and stably positioned in the nanoCT system for imaging.

PTA is a soft tissue contrast agent containing tungsten, which confers strong X-ray contrast when attached to biological tissue, and has a strong binding affinity to fibrin and collagen. Hence PTA is a very useful contrast agent to specifically visualize the collagen and fibrin content in ECM. Similar to Hexabrix®, all samples were, prior to imaging, immersed in a solution of PTA (1.25g/50ml PBS), were then wrapped in parafilm and were stably positioned in the nanoCT system.

The nanoCT system employed in this study was a Phoenix NanoTom S (GE Measurement and Control Solutions) with a 180 kV/15 W high-performance nanofocus X-ray tube. It was equipped with a tungsten target and was operated, for all scans, at a voltage of 90 kV and a current of 170 µA. A 1 mm aluminum and 1 mm copper filter was used to reduce beam hardening and metal artifacts as much as possible. The exposure time was 500 ms and a frame averaging of 1 and image skip of 0 was applied, resulting in a total scanning time of 20 minutes per TE construct. The scanning time was kept low to avoid sample drying during scanning, to allow routine screening and to enable in future more non-invasive use and real-time monitoring. The reconstructed images had an isotropic voxel size of 3.75 µm.

4.3.5. 3D visualization, and image processing and analysis

For 3D visualization of the TE constructs, CTVox (Bruker micro-CT) was used. For image processing and quantification of the ECM volume in the TE constructs we used CTAn (Bruker micro-CT) according to the scheme in Figure 4.2. At first the reconstructed dataset of the entire TE construct was fragmented in different subsets with a similar amount of metallic artifacts (step 1). By using a 3-level automatic Otsu segmentation algorithm (Otsu 1979) on the individual 2D slices, the ECM was separated from both the scaffold and the background, the latter including noise and metal artifacts (step 2). As a result, grey-scale images with distinct grey-scale values for scaffold, ECM and background were generated for the different subsets. A global threshold was then chosen manually to select the ECM (step 3). In order to reduce the errors introduced by the partial volume effect and metallic artifacts for analyzing the ECM volume, the binarized images for the Ti structure were dilatated by 2 voxels and subtracted from the dataset of binarized ECM images (step 4). The noise was minimized by removing black speckle noise smaller than 500 voxels and white speckle noise smaller than 2000 voxels. In order to solidify the resulting structure, a 'closing' operation (~ 2 voxels) was performed on the resulting images (step 4), providing images suitable for the 3D analysis of the ECM volume. Finally, the ECM volume in the TE constructs was analyzed by performing a 3D analysis on the binarized and processed images (step 5).

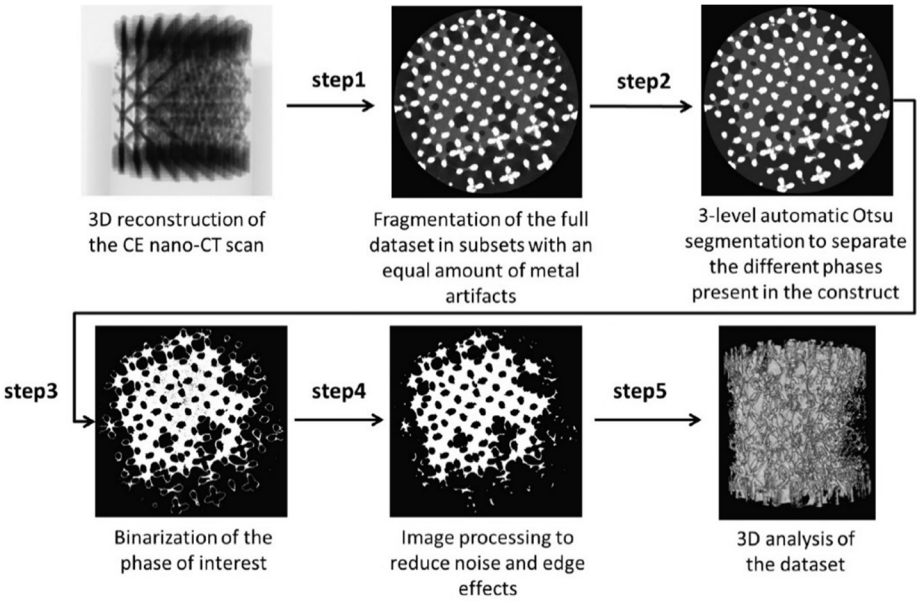

Figure 4.2: Image processing algorithm.
Steps followed for image analysis from the 3D reconstruction of the CE-nanoCT scan to image processing and noise reduction to final 3D quantification and distribution analysis.

4.3.6. Physical characterization of TE constructs for comparison to the CE-nanoCT data

In order to gain further understanding on the properties of the cultured TE constructs, subsequent experimental analyses were performed, as described in this section. They were also used to evaluate the potential of CE-nanoCT and assess the levels of complementarity between established analyses and the suggested imaging technique.

Cell viability by Live/Dead viability/cytotoxicity staining

The cell viability in the TE constructs was evaluated using Live-Dead viability/cytotoxicity staining (Invitrogen, USA). Constructs were rinsed with 1ml PBS, incubated in the staining solution (0.5µl Calcein AM and 2µl Ethidium Homodimer in 1ml PBS) for 20 min under normal cell culture conditions and finally imaged using a Leica M165 FC microscope (Impens *et al.* 2010b).

Collagen content by picrosirius red staining

The collagen-containing ECM production on the TE constructs was characterized by picrosirius red staining (1mg/mL Sirius Red in saturated Picric acid). (Tullberg-Reinert *et al.* 1999). The stained samples were thoroughly washed with distilled water to remove unbound dye and dried at 37°C before qualitative analysis by stereomicroscopy. For quantitative analysis, the picrosirius red dye was dissolved in 0.2M

NaOH/Methanol (1:1 ratio) with mild shaking overnight, and the optical density was measured at 492nm using a microplate reader (TECAN) for 1 ml triplicate samples for each condition.

ECM weight measurement

The liquid in the TE constructs was carefully removed using vacuum after which they were dried overnight in 37ºC and subsequently weighed on a high accuracy balance (Sartorius CPA225D). Ti scaffolds were cleansed ultrasonically, immersed for 10 min in acetone, 10 min in ethanol 70%, and 10 min in distilled water, subsequently an alkali treatment was applied for 24 h at 60°C in a 5 M sodium hydroxide (Sigma-Aldrich) solution, samples were rinsed with distilled water, and finally sterilized in a steam autoclave. The weight of the cleansed Ti scaffold was subtracted from the total weight, resulting in the net ECM weight.

4.4. Results

4.4.1. CE-nanoCT allows 3D visualization of ECM in TE constructs

As a first step in this study TE constructs were scanned with nanoCT without the use of contrast agents. It allowed a visual inspection of 3D hPDC-driven ECM formation in the TE constructs after static or dynamic *in vitro* culture. However the reconstructed 2D slices (Figure 4.3.A) were of low image quality (i.e. low contrast between ECM and background) making accurate qualitative evaluation and further 3D quantification impossible. When using Hexabrix® and PTA, both contrast agents respectively infiltrated and bonded to the ECM, resulting in an increase in 3D grey-scale intensity of the ECM for static (Figure 4.3.B) as well as for both (low and high flow rate) bioreactor culture derived TE constructs (Figure 4.3.C and D). Black arrows in the image indicate ECM boundaries within the TE construct. The high contrast difference between ECM, background and Ti scaffold allowed further processing of the raw CE-nanoCT images.

Live/dead viability/cytotoxicity staining was employed as a benchmark analysis of cell viability and distribution on the different TE constructs. The fluorescent images showed that cells were distributed over the entire outer TE construct surface, indicating similar results for all 3 culture conditions (Figure 4.4.A). However, CE-nanoCT images of the same TE constructs showed that for static culture, ECM was only formed at the scaffold periphery, resulting in only partially ECM filled TE constructs, while in the bioreactor cultured TE constructs ECM was also found back throughout the internal TE construct volume (Figure 4.4.B).

The cross-sectional CE-nanoCT images were subsequently binarized and processed as described in Figure 4.2 to quantify the volume of the ECM formed. Figure 4.4.C shows representative binarized images for all culture conditions, visualizing the ECM in white and background plus Ti scaffold in black. In the case of static culture only thin strands of ECM were present at the periphery of the TE construct, resulting in a loss of representation after binarization and correction for metallic artifacts (i.e. step 4 in

Figure 4.2), making the 3D quantification and visualization of the ECM in statically cultured TE constructs inaccurate. Qualitative assessment of the spatial ECM distribution in 3D in these samples was nevertheless possible throughout the entire TE construct

4.4.2. CE-nanoCT allows 3D quantification of ECM volume in TE constructs

Image analysis of the binarized CE-nanoCT slices for the different contrast agents allowed to quantify the total amount of stained ECM formed within the available void volume (i.e. total TE construct volume excluding the volume of Ti scaffold) for the bioreactor perfusion culture conditions, which was not possible for statically cultured TE constructs as the amount of ECM formed was too small to be quantified. In order to comprehend the CE-nanoCT-based ECM characterization in the TE constructs, a comparison was made to two established methods for ECM assessment, namely picrosirius red staining to measure the collagen content and ECM dry weight measurement (Figure 4.5 and Figure 4.6). TE constructs giving increased values of picrosirius red values (absorption at 492nm, Figure 4.5.A) also showed increased values of ECM when measured via Hexabrix® and PTA stained CE-nanoCT (Figure 4.5.B). Overall, Hexabrix® stained CE-nanoCT values were seen to follow the picrosirius red

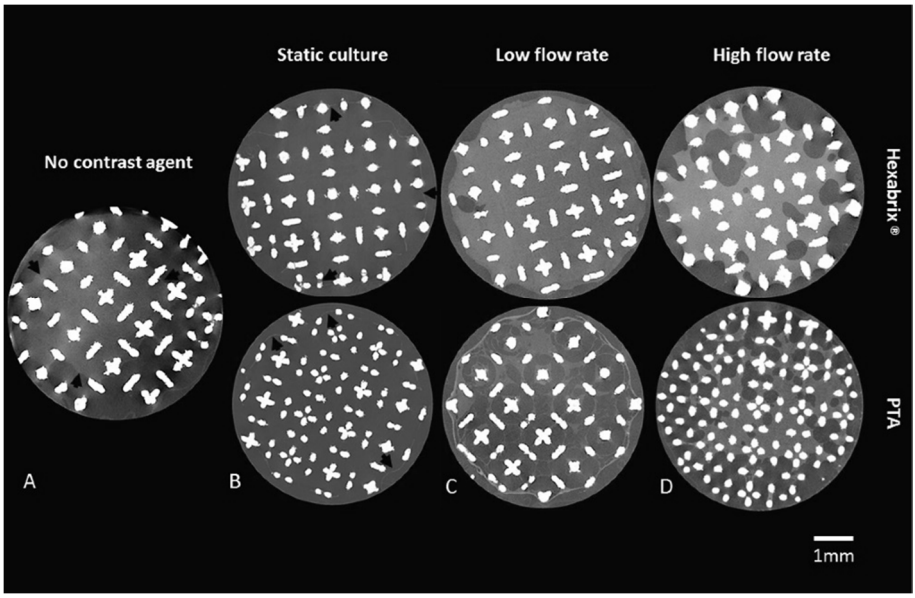

Figure 4.3: Representative 2D CE-nanoCT cross-sections of different constructs (A) scanned without contrast agent, after bioreactor perfusion high flow rate (B) scanned after static culture with both Hexabrix® and PTA, (C) after bioreactor perfusion (low flowrate) culture with both Hexabrix® and PTA and (D) after bioreactor perfusion (high flowrate) culture with both Hexabrix® and PTA. Black arrows indicate boundaries of the ECM in the constructs.

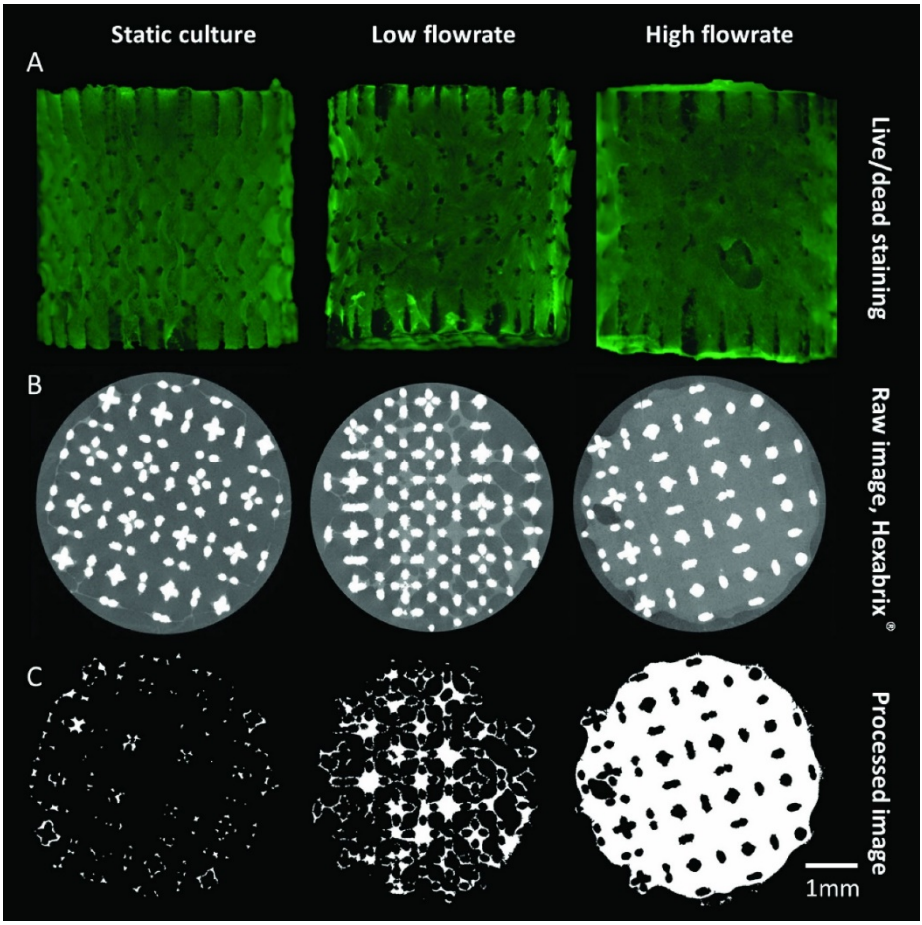

Figure 4.4: Live/dead and CE-nanoCT images constructs.
(A) Live/dead viability/cytotoxicity staining of constructs cultured in different conditions, (B) typical 2D grey-scale CE-nanoCT cross-sections using Hexabrix® and (C) the corresponding binarized and processed cross-sections serving as input for the analysis of the ECM volume.

absorption values more closely than the PTA stained ones with a stronger dependency on the flow rate used for TE construct culture. The ECM volume after Hexabrix® staining was seen to fit linearly with net dry weight values independent from the flow rate used (Figure 4.6.A). While for TE constructs cultured at high flow rate, only a small difference in ECM volume was observed between the Hexabrix® and PTA staining, for those TE constructs cultured at a low flow rate, Hexabrix® staining resulted in significantly higher ECM volumes than those obtained via PTA staining (Figure 4.5.B) because of the binding specificity of PTA to proteins and collagen. Indeed, both Figure 4.5.B and Figure 4.6.B show that a part of the ECM was not stained by PTA,

and that this part was more pronounced for the lower ECM content conditions (seen for the low flow rate).

4.4.3. CE-nanoCT allows spatial visualization and quantification of the ECM in TE constructs

Figure 4.7.B and C show typical 3D renderings of the CE-nanoCT images (both for Hexabrix® and PTA staining respectively) for a bioreactor perfusion cultured TE construct at high flow rate, together with the corresponding Live/Dead viability/cytotoxicity staining (Figure 4.7.A) and picrosirius red staining (Figure 4.7.D). The 3D image obtained with Hexabrix® staining, visualizing all the ECM

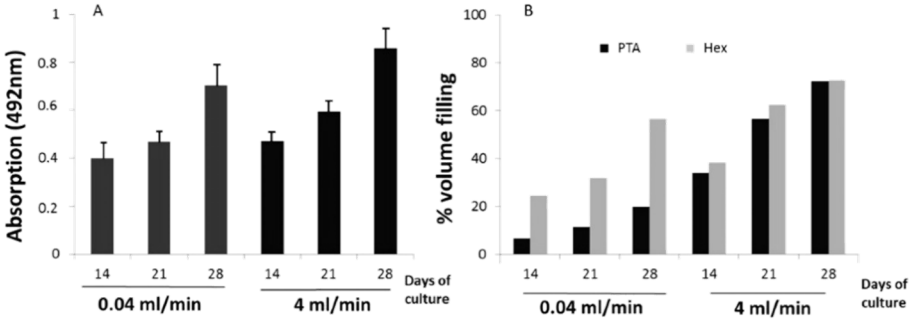

Figure 4.5: Comparison Picrosirius red and CE-nanoCT.
(A) ECM content quantification via picrosirius red for both flow rates over culture. (B) Relative ECM volume filling as function of the total TE construct internal void volume calculated based on CE-nanoCT using respectively Hexabrix® and PTA.

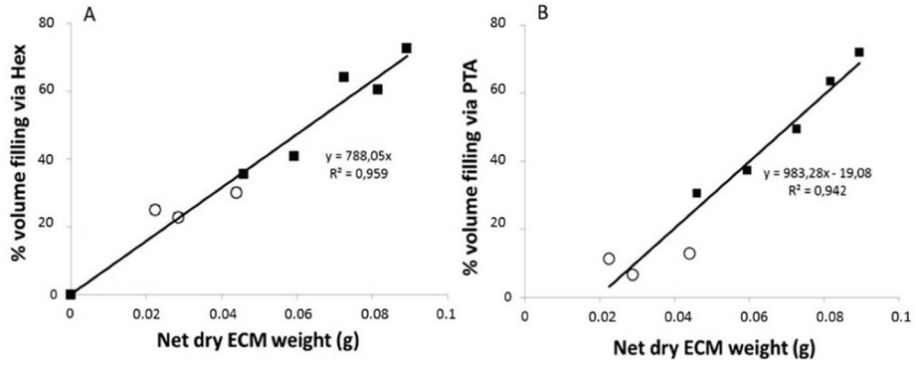

Figure 4.6: Validation CE-nanoCT based on ECM weight measurements.
Relative ECM volume filling as function of the total TE construct internal void volume calculated based on CE-nanoCT using respectively Hexabrix® (A) and PTA (B) in function of net dry weight. TE constructs were cultured under: (○) Low flow rate condition (0.04 ml/min); (■) High flow rate condition (4ml/min).

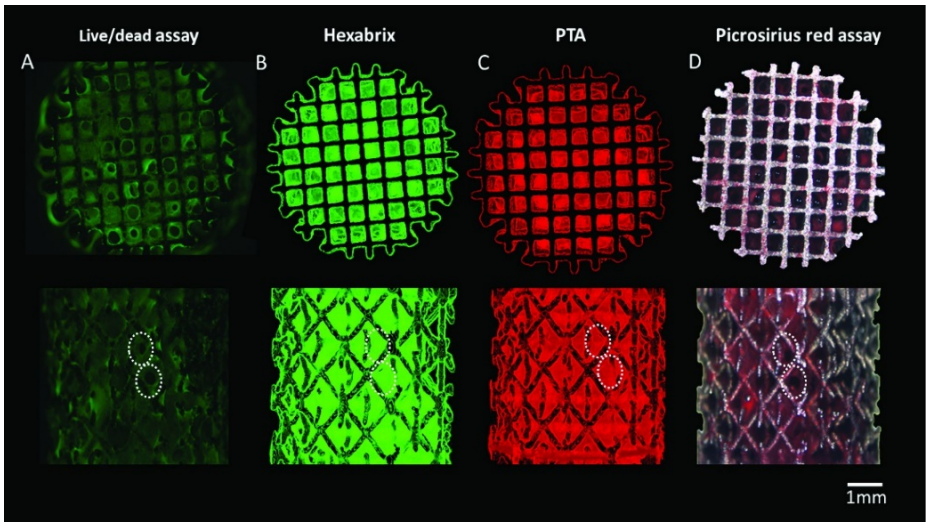

Figure 4.7: Visual comparison of Live/dead and Picrosirius red staining with CE-nanoCT
Top and side view of the (A) live/dead staining of a perfusion bioreactor cultured construct at a flow rate of 4 ml/min, (B) 3D rendering of the CE-nanoCT images with Hexabrix® staining, (C) 3D rendering of the CE-nanoCT images with PTA staining and (D) Brightfield image of scaffold stained with Picro-sirius red. White dashed lines indicate identical geometric features of the ECM in microscopic images and reconstructed images

present in the construct in green, showed a comparable ECM distribution as the Live/Dead viability/cytotoxicity staining for the outer TE construct surface (indicated by the white arrows). The PTA stained 3D images, showing the collagen and fibrin containing ECM in red, had a comparable ECM distribution as the picrosirius red staining for the outer TE construct surfaces. Moreover, the 3D rendered CE-nanoCT images of both the Hexabrix® and PTA staining allowed a full 3D visualization of the ECM distribution throughout the entire TE construct (supplementary videos may be seen in the appendix). A volumetric ECM distribution histogram over the TE construct height was plotted both for the Hexabrix® and PTA staining (Figure 4.8), giving an indicative example of the 3D qualitative (distribution) and quantitative (volume of ECM) information obtainable with CE-nanoCT. Although a homogeneous ECM distribution over the TE construct height could be expected, both stainings showed that a larger amount of ECM was formed at the bottom of the TE construct.

4.5. Discussion

In order to successfully implement TE constructs as part of a clinical therapy, it is necessary to develop quality control tools that will ensure accurate and consistent TE construct release specifications (Schneider *et al.* 2010). In general a substantial amount of routine lab techniques currently used in TE were initially developed and optimized for 2D analysis of cell growth, distribution and matrix secretion in culture flasks and

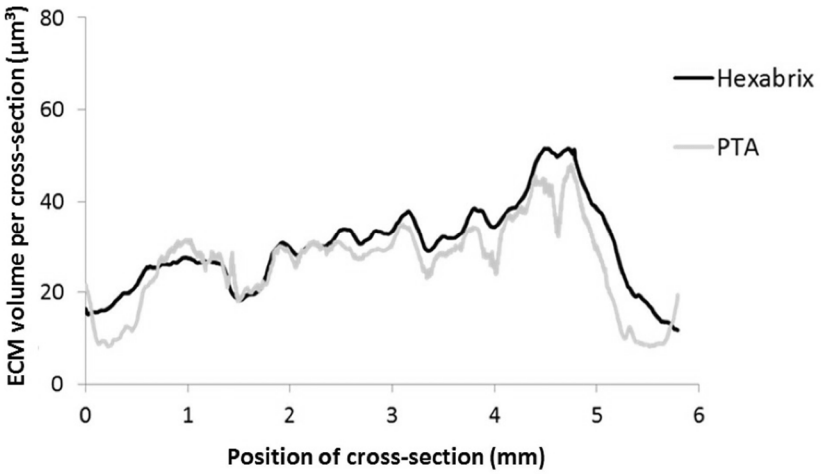

Figure 4.8: CE-nanoCT based ECM distribution in TE construct.
Representative longitudinal ECM distribution throughout the full TE construct i.e. volume of ECM per cross section, where the height of the section is 3.75 µm equal to the voxel size used for the analysis, in function of the scaffold height. Distributions obtained via Hexabrix® and PTA staining for a scaffold that was cultured for 21 days under a flow rate of 0.04 ml/min.

not for use in a 3D setting such as TE constructs (Table 4.1). For example the information obtained by destructive scanning electron microscopy (SEM) remains 2D and rather elusive even when multiple sample slices are analyzed (Peyrin *et al.* 2007, Albertini *et al.* 2009, Voronov *et al.* 2012). Thus one has to be careful when using 2D validated techniques to draw 3D conclusions. Proper validation under 3D conditions and/or complementary use of additional real 3D information requires substantial additional research, but it is a much safer route to obtain reliable information of 3D cell and tissue behavior. Hence advanced 3D methods to, preferably non-invasively, monitor TE construct properties need to be further developed.

Routine Techniques	Specificity	Depth analysis	Scale	Ref.
Live/dead stain	cells	2D: limited depth	µm-mm	(Du *et al.* 2009)
Picro-sirius red stain	collagen	2D: limited depth	µm-mm	(Paletta *et al.* 2011)
SEM and optical microscopy	cells, collagen, mineral phase	2D	~ µm	(Peyrin *et al.* 2007)
Alizarin red stain	Mineral phase	2D: limited depth	µm-mm	(Frohlich *et al.* 2010)

Table 4.1: Categorization of bench imaging techniques that have been routinely employed for the visualization and analysis of 3D engineered tissues (related to bone TE).

X-ray micro and nanoCT offer a potential solution because of their non-destructive 3D character. However, the value of X-ray CT-based information for TE will ultimately be a trade-off of factors such as physicochemical, morphological and dimensional TE construct properties, contrast enhanced agent and equipment limitations (Table 4.2). According to specific study objectives, a customized strategy will be required to extract the necessary information in a robust way, ranging from (i) accurate and detailed (100s of µm scale) identification and quantification of different TE construct components limited to small TE construct samples and using phase contrast imaging, (Voronov *et al.* 2012) to (ii) using standard desktop micro- or nanoCT as a routine 3D imaging technique for whole TE construct analysis (mm to cm scale) and quantification of mineralization after *in vivo* implantation (Jones *et al.* 2007, Guldberg *et al.* 2008). The latter approach, without the use of a contrast agent, has also been used for static or bioreactor *in vitro* cultures, (Cartmell *et al.* 2004, Porter *et al.* 2007, Hagenmuller *et al.* 2010) showing distinct contrast differences between mineralized matrix and scaffold. Phase contrast imaging (Langer *et al.* 2010, Appel *et al.* 2011, Voronov *et al.* 2012) or microCT combined with osmium tetroxide as a contrast agent (Hilldore *et al.* 2007) have shown their potential to assess non-mineralized ECM in an *in vitro* engineered TE construct. However, the limited availability of synchrotron radiation or CT systems allowing phase contrast imaging, the toxicity of osmium tetroxide and the high cost associated with its disposal, all hamper their use as routine quality control for TE constructs.

Both contrast agents used in this work (Hexabrix® and PTA) increased the grey-scale intensity difference between the different phases in the TE constructs as seen in Figure 4.3. In the static culture case, ECM was only found around the periphery of the Ti scaffold in contrast with ECM the bioreactor cultured TE constructs (Porter *et al.* 2007). also reported peripheral deposition of mineralized matrix on statically cultured TE constructs in respect to a more dense and spatially homogeneous distribution of mineralized matrix in bioreactor cultured TE constructs based on microCT analysis. Additionally they also reported that mineralized matrix formation was initiated at the scaffold periphery and progressed towards the scaffold center over a period of 44 days. These dynamics may be attributed to fluid flow and convective nutrient and oxygen transport throughout the TE construct volume during culture (Bancroft *et al.* 2002, Grayson *et al.* 2011, Papantoniou *et al.* 2013). In this study CE-nanoCT revealed a dramatic increase of ECM content for bioreactor cultured TE constructs (up to 75% of void volume) with respect to the statically cultured ones (less than 4% of void volume). The low ECM quantity in the static culture case was below the CE-nanoCT threshold for ECM quantification, which in this study was determined to be an ECM volume lower than 4% of the total Ti scaffold void volume (Figure 4.4). This lower quantification limit was directly related to the artifacts introduced by the metallic scaffolds used in this work (Stradiotti *et al.* 2009). For other scaffold materials however, it is anticipated that the lower quantification threshold of CE-nanoCT will further decrease, since material-dependent artifacts will be reduced compared to the worst case scenario described here.

	Specificity	Size Range	Resolution	Scaffold material	Imaging modality
CE-nanoCT	ECM and mineral phase	Whole construct (6 mm)	µm	Ti6Al4V	Absorption - nanoCT
(Voronov *et al.* 2012)	cells, ECM, mineral phase	Localized region in the samples (~500 µm)	Sub-µm	PLA	Phase Contrast – micro-CT
(Porter *et al.* 2007)	mineral phase	Whole construct (3 - 9 mm)	µm	PCL	Absorption - micro-CT
(Hilldore *et al.* 2007)	ECM	Localized region in the sample	µm	Hydroxy-apatite	Absorption - micro-CT
(Albertini *et al.* 2009)	ECM	Localized region in the samples	Sub-µm	PLLA/PGA	Phase contrast - synchrotron
(Cartmell *et al.* 2004)	Mineral phase	Whole construct (6mm)	µm	PLDL & Demineralized trabecular bone matrix scaffolds	Absorption - micro-CT
(Langer *et al.* 2010)	Mineral phase, ECM	Localized region in the samples	µm	bone graft substitute	Phase contrast - synchrotron
(Hagenmueller et al. 2007)	Mineral phase	Whole construct	µm	Silkworm fibroin	Absorption - micro-CT

Table 4.2: Categorization and evaluation of X-ray tomography techniques employed for the visualization of features of *in vitro* 3D engineered tissues (related to bone TE).

CE-nanoCT results were then compared to known physical ECM characterization methods, such as dry net weight as a global ECM related parameter and picrosirius red staining as a collagen specific assay, to comprehend the CE-nanoCT data and hence evaluate the potential of CE-nanoCT for 3D ECM quantification in TE constructs. In Figure 4.6.A, the relative ECM void volume filling obtained via Hexabrix® staining (an equilibrium contrast agent, thus it does not bind to the ECM) was correlated to the net dry weight, resulting in a linear correlation for both flow rates, suggesting that Hexabrix® stains most of the ECM in a quantitative manner. However when using the more tissue-specific contrast agent PTA, which is known to bind to various proteins and connective tissue, (Hanker *et al.* 1983, Blewitt 1984) a difference with Hexabrix® staining was found (Figure 4.5.B), while when comparing to the net dry weight, it was shown that PTA only stained a fraction of the ECM (Figure 4.6.B).

Figure 4.5 shows a qualitative relationship between experimental values obtained via the collagen specific picrosirius red staining and CE-nanoCT values demonstrating both increasing trends over time. Additionally, a clear flow rate dependence was seen (Figure 4.5.B) for both PTA and Hexabrix® stains. It can be observed that TE constructs cultured under high flow rate showed a larger fraction of the ECM stained by PTA, which could be explained as an ECM richer in protein components (on which PTA may specifically bind). Fluid flow is known to enhance matrix synthesis within TE constructs during perfusion culture (Bancroft *et al.* 2002, Du *et al.* 2009, Hagenmuller *et al.* 2010). Furthermore differences in fibrillar collagen organization of the ECM, which are flow dependent, (Pedersen *et al.* 2010) could also explain the ECM differences that were observed by PTA staining as the ECM morphology could influence the binding mechanism of PTA to the ECM proteins. In Figure 4.5, it may also be observed that the difference in collagen content, as determined by picrosirius red staining, for the different flow rates is less pronounced than the one observed with the PTA staining. However one has to keep in mind that the picrosirius red staining was used without any customization and validation for the specifics of the 3D environment under investigation, which could underestimate actual collagen content (Papantoniou *et al.* 2013). Certainly, for more dense TE constructs, like the ones obtained from high flow rate culture, this issue becomes more relevant due to increased inter-construct mass transport limitations that would affect the performance of the assay.

CE-nanoCT-based imaging and quantification clearly show that by using this technique information that could not be previously generated by standard experimental techniques such as microscopy of TE constructs stained with Live/Dead viability/cytotoxicity or collagen-specific picrosirius red staining which are line-of-sight techniques lacking a 3D internal visualization potential may now be obtained. Hence, a direct validation of CE-nanoCT using these techniques is irrelevant. Images obtained by standard experimental techniques are mainly limited to surface restricted TE construct characterization as they are line-of-sight techniques and only provide limited depth information (Du *et al.* 2009, Paletta *et al.* 2011). Not taking into account the latter limitation may result in the misinterpretation of statically cultured TE constructs as being full of ECM while in reality only an outer layer of ECM exists, as confirmed by CE-nanoCT (Figure 4.4). A potential validation technique could be histological

sectioning. However, the use of Ti scaffolds in this work does not allow the sectioning of the produced TE constructs, and thus will also not present full 3D data.

To conclude, for the combination of factors used in this work, i.e. scaffold size and material type, type of CT device and scanning mode (Table 4.2), and its objective, CE-nanoCT has shown potential as a cost effective TE construct quality control methodology, by providing volumetric and distribution measurements throughout the entire TE construct (Figure 4.7 and Figure 4.8). Although there are preliminary indications for ECM composition analysis via this method which need to be further investigated, the novel information that CE-nanoCT generates will assist to increase our insight in the ECM characteristics within *in vitro* manufactured TE constructs. In this study we showed proof of concept for CE-nanoCT as a 'whole-construct' imaging technique with non-invasive potential that enables 3D visualization and quantification of *in vitro* engineered ECM in TE constructs. The development of robust tools and methodologies such as CE-nanoCT to assess important and potentially critical quality characteristics of TE constructs such as ECM quantity and homogeneity, can facilitate the gradual transformation of 'TE constructs' to well characterized 'TE products'.

4.6. Acknowledgements

IP is funded by the ENDEAVOUR project G.0982.11N of the Research Foundation Flanders (FWO Vlaanderen). MS is supported by a Ph.D. grant of the Agency for Innovation by Science and Technology (IWT/ 111457). GK and LG acknowledge support by the European Research Council under the European Union's Seventh Framework Program (FP7/2007-2013)/ERC grant agreement n°279100. This work is part of Prometheus, the Leuven Research & Development Division of Skeletal Tissue Engineering of the KU Leuven: www.kuleuven.be/prometheus.

Chapter 5.
Multifactorial optimization of contrast-enhanced nanofocus computed tomography for quantitative analysis of neo-tissue formation in tissue engineering constructs

Maarten Sonnaert[*], Greet Kerckhofs[*], Ioannis Papantoniou, Sandra Van Vlierberghe, Veerle Boterberg, Peter Dubruel, Frank P. Luyten, Jan Schrooten[$], Liesbet Geris[$]

*These authors have contributed equally and share first authorship

[$] These authors share senior authorship

Published in. PLoS ONE 10(6): e0130227. doi: 10.1371/journal.pone.0130227

5.1. Abstract

To progress the fields of tissue engineering and regenerative medicine, development of quantitative methods for non-invasive three dimensional characterization of engineered constructs (i.e. cells/tissue combined with scaffolds) becomes essential. In this study, we optimized contrast-enhanced nanofocus computed tomography for three dimensional visualization and quantitative analysis of in vitro engineered neo-tissue (i.e. extracellular matrix containing cells) in perfusion bioreactor-developed constructs. A fractional factorial 'design of experiments' approach was used to elucidate the influence of the staining time and concentration of two contrast agents (Hexabrix® and phosphotungstic acid) and the neo-tissue volume on the image contrast and dataset quality. Additionally, the neo-tissue shrinkage that was induced by phosphotungstic acid staining was quantified to determine the operating window within which this contrast agent can be accurately applied. For Hexabrix® the staining concentration was the main parameter influencing image contrast and dataset quality. Using phosphotungstic acid the staining concentration had a significant influence on the image contrast while both staining concentration and neo-tissue volume had an influence on the dataset quality. The use of high concentrations of phosphotungstic acid did, however, introduce significant shrinkage of the neo-tissue indicating that, despite sub-optimal image contrast, low concentrations of this staining agent should be used to enable quantitative analysis. To conclude, using design of experiments we have optimized contrast-enhanced nanofocus computed tomography for routine screening of neo-tissue formation in constructs, transforming it into a robust three dimensional quality control methodology.

5.2. Introduction

The field of tissue engineering (TE) is evolving towards the development of complex, three-dimensional (3D) constructs (i.e. cells/tissue combined with scaffold) to mediate the repair of severe defects. In order to facilitate the successful clinical implementation of these constructs an in-depth understanding of how they develop as well as the optimization of the developed procedures and the availability of robust 3D quality assessment tools becomes essential.

Currently, the standard technique for evaluating tissue formation is histological sectioning. It has a high discriminative power, both on tissue and cellular level. However, it shows limited potential for quantifying 3D tissue formation as it is destructive and costly in terms of time and resources. Most importantly, in standard settings it only allows assessment of tissue distribution in 2D, with loss of information due to a restricted sectioning orientation and with limited depth resolution (Hedberg *et al.* 2005, Eniwumide *et al.* 2007, Smith *et al.* 2010). Other standard techniques to assess the quality of a construct are Live/Dead, DNA content (providing cell number estimation), histology and weight measurements. Although Live/Dead staining gives additional important information concerning cell state, it has limitations for internal, 3D visualization of tissue formation in a construct. Both DNA content and weight measurements are bulk measurement techniques not providing spatial information. Techniques such as confocal or multiphoton microscopy offer a potential for 3D

visualization of cells and tissues. However, limited depth resolution (~300µm) and limited options for detailed quantification hinders their performance when clinically relevant sized or opaque samples are to be analyzed. Ultrasound and magnetic resonance imaging could obtain significantly higher imaging depths, but limitations in the spatial resolution result in significant restrictions for quantitative 3D analysis. Therefore, there is a need for more advanced, quantitative 3D imaging techniques (Nam *et al.* 2014).

Recent advances in 3D imaging techniques and image analysis have demonstrated the potential of the currently applied methods and their limitations for accurate analysis. In particular X-ray micro and nanofocus computed tomography (micro and nanoCT) have been frequently applied as 3D quantitative imaging techniques to assess mineralized skeletal tissues (Jones *et al.* 2007, van Lenthe *et al.* 2007). However, because of their low X-ray attenuation, soft tissue contrast is inherently poor in absorption mode imaging. Phase contrast imaging could be a solution (Davis *et al.* 1995, Wilkins *et al.* 2014). Due to the electromagnetic properties of the X-rays, a phase shift of the waves can be induced as a result of differences in the refractive index of different materials while passing through an object. Taking this phase shift into account, the contrast sensitivity will be increased, which is especially for low absorbing materials an important benefit. As this technology requires sophisticated X-ray optics and preferably monochromatic X-rays, it is mostly available using synchrotron radiation (Langer *et al.* 2010), although recently also desktop CT devices allowing phase contrast imaging have become available (Appel *et al.* 2011, Voronov *et al.* 2012).

A recent shift in micro- and nanoCT imaging focuses on the use of X-ray opaque contrast agents for visualizing soft tissues, such as cartilage (Xie *et al.* 2010, Kerckhofs *et al.* 2013b, Lakin *et al.* 2013, Kerckhofs *et al.* 2014), blood vessels (Granton *et al.* 2008, Fei *et al.* 2010, Lusic *et al.* 2013) and connective tissues (Metscher 2009b, Wong *et al.* 2012). Specifically in the case of neo-tissues (cells and extracellular matrix), we have shown proof-of-concept of contrast-enhanced nanoCT (CE-nanoCT) for the 3D visualization and quantification of neo-tissue within constructs formed in bioreactor cultures (Papantoniou *et al.* 2014b). Two tissue-specific contrast agents were used to stain the neo-tissue, i.e. Hexabrix® and phosphotungstic acid (PTA). As opposed to the standard techniques mentioned earlier, it was shown that CE-nanoCT could allow 3D qualitative and quantitative structural and spatial assessment of the *in vitro* engineered neo-tissue, created during static and bioreactor cell culturing in titanium alloy scaffolds, revealing 3D neo-tissue distribution.

Although this study indicated the potential of CE-nanoCT, the staining conditions, which were based on preliminary internal experiments (Kerckhofs *et al.* 2013b, Kerckhofs *et al.* 2014), resulted in datasets with sub-optimal image quality. This was due to limited contrast in combination with scaffold-induced imaging artifacts, such as beam hardening and streaks. Although extensive image processing enabled quantitative interpretation of the datasets, no automated image analysis was possible yet; this posed considerable limitations to the proposed methodology. A recent publication that assessed several contrast agents for CE-CT indicated the necessity to optimize the staining parameters for obtaining quantitative datasets. It was demonstrated that for the

same staining conditions each contrast agent displayed agent-specific contrast enhancement levels and penetration depth, while the sample size further affected its performance (Pauwels *et al.* 2013).

An additional concern for the use of contrast agents is their potential to influence the integrity of the stained tissue. Iodine potassium iodide (I2KI) was shown to cause substantial soft tissue shrinkage dependent on the concentration, staining time and tissue structure/composition (Vickerton *et al.* 2013). Also PTA was shown to introduce shrinkage of brain and muscle tissue, although in a lesser extent than I2KI (Buytaert *et al.* 2013). For some studies, the compositional information of the soft tissues in the sample, only obtainable by the staining, was most important (Metscher 2009a, Jeffery *et al.* 2011, Schulz-Mirbach *et al.* 2013), although structural tissue alterations due to dehydration or staining were noticed (Schulz-Mirbach *et al.* 2013). However, when aiming at using the CE-CT data for morphometric and volumetric analyses, the degree of specimen shrinkage, and potential deformation, is an important consideration.

In the current study, we applied a 'Design of Experiments' (DoE) approach, a statistical method for planning experiments, for a multiparametric investigation of the influence of staining parameters (staining time and concentration) and neo-tissue volume on (i) image quality (i.e. image contrast), (ii) dataset quality (i.e. potential for quantitative interpretation of the obtained datasets) and (iii) tissue integrity (only for PTA). Based on the DoE outcome, optimum staining conditions for both contrast agents were selected. For these staining conditions, we were able to develop an automated, user-independent and highly quantitative image processing and analysis procedure for morphometric analysis of neo-tissue within the constructs. As a result, CE-nanoCT was optimized for routine screening of the neo-tissue formation in TE constructs transforming it to a robust quality control methodology.

5.3. Materials and Methods

5.3.1. TE constructs

Ti6Al4V based constructs

To evaluate the influence of the staining parameters of the contrast agents (staining time and concentration) and neo-tissue volume on the image quality, dataset quality and tissue integrity, selective laser melted porous cylindrical 3D Ti6Al4V scaffolds with a height of 6mm and a diameter of 6mm were used. The design and production of the Ti6Al4V scaffolds is described in detail in Ref. (Van Bael *et al.* 2011). Human periosteal derived cells (hPDCs) (De Bari *et al.* 2006) were seeded as described before using a static drop-seeding protocol (Sonnaert *et al.* 2014a).

In order to generate constructs with different amounts of neo-tissue they were subsequently cultured in a static setup for 3 weeks (low volumes of neo-tissue) or in an in-house developed perfusion bioreactor system for 1 to 3 weeks (respectively medium and high volumes of neo-tissue) as described earlier (Papantoniou *et al.* 2014b, Sonnaert *et al.* 2014a). For all conditions the constructs were cultured in growth medium (Dulbecco's modified Eagle's medium with high-glucose (Life Technologies)

containing 10% foetal bovine serum (FBS, Gibco), 1% sodium pyruvate (Life Technologies) and 1% antibiotic–antimycotic (100 units/mL penicillin, 100 mg/mL streptomycin, and 0.25 mg/mL amphotericin B; Life Technologies)), which was refreshed every two days. For the perfusion bioreactor system a flow rate of 1 ml/min was used.

PCL based constructs

To assess the effect of the different contrast agents on the tissue integrity, we used porous cylindrical polycaprolactone (PCL) scaffolds with a height of 3 mm and a diameter of 6 mm. PCL scaffolds were produced using the BioscaffolderVR device (Sys-Eng, Germany). The pressure was maintained at 5 bars and the temperature was set to 120°C. The selected overlay pattern was 0-90°, the anticipated strut diameter was 100 µm and the anticipated pore size 200 µm. The scaffolds were designed in Inventor while PrimCam (Sys-Eng, Germany) was used to create the final structure (Desmet *et al.* 2010, Berneel *et al.* 2012a, Berneel *et al.* 2012b). Also the PCL scaffolds were seeded with hPDCs using a static drop-seeding protocol. The PCL based constructs were cultured using the same operating conditions in the perfusion bioreactor system as for the Ti6Al4V based constructs, but for a period of 2 weeks.

5.3.2. Contrast-enhanced nanofocus CT (CE-nanoCT)

After static or dynamic culture, the TE constructs were rinsed with 1 ml phosphate buffered saline (PBS) and transferred to a 4% paraformaldehyde solution (Sigma) for 2 hours to fixate the neo-tissue. The TE constructs were stored in PBS prior to CE-nanoCT scanning. Two contrast agents were used, namely Hexabrix® 320 (Guerbet Nederland B.V) and phosphotungstic acid (PTA - VWR International). Hexabrix®, containing the negatively charged ioxaglate, is an equilibrium contrast agent staining all non-negatively charged tissues. PTA on the other hand is known to specifically bind to various components of the connective tissue such as collagen and fibrin (Papantoniou *et al.* 2014b). The nanoCT system used was a Phoenix NanoTom S (GE Measurement and Control Solutions).

Ti6Al4V constructs

For the Ti6Al4V constructs, different concentrations and staining times of both contrast agents were used according to a 3-level 3-parameter fractional factorial design as shown in Table 5.1. TE constructs were initially stained and scanned with Hexabrix®, after which they were rinsed 3 times in PBS overnight to remove all Hexabrix® traces prior to subsequent staining. The same constructs were then stained with PTA and scanned again. As after removal from the liquid prior to scanning, remnants of the staining solution could be present at locations where there is no neo-tissue, and thus could influence the visualization of the neo-tissue, samples were dried for 15 minutes on a paper tissue at room temperature for both contrast agents (Papantoniou *et al.* 2014b).

For scanning the Ti6Al4V-based TE constructs, the nanoCT was equipped with a tungsten target, and was operated at a voltage of 90 kV and a current of 170 µA. A 1 mm filter of aluminum and 1 mm of copper was used to reduce beam hardening and metal artifacts as much as possible during scanning. The exposure time was 500 ms and

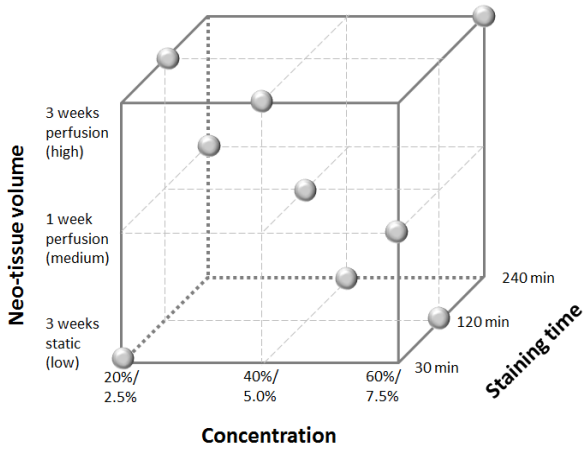

Figure 5.1: Design space for the DoE, showing the three levels of the three parameters. For the concentration, the top value is for Hexabrix® staining and the bottom value for PTA staining. The grey dots indicate the experimental conditions for the fractional factorial design (n=3).

Table 5.1: The experimental conditions to be evaluated for the 3-level, 3-parameter fractional factorial design.

Neo-tissue volume	staining time	Concentration
3 weeks static (Low)	120 min	60% Hex -- 7.5% PTA
3 weeks static (Low)	240 min	40% Hex -- 5% PTA
3 weeks static (Low)	30 min	20% Hex -- 2.5% PTA
1 week perfusion (Mid)	120 min	40% Hex -- 5% PTA
1 week perfusion (Mid)	240 min	20% Hex -- 2.5% PTA
1 week perfusion (Mid)	30 min	60% Hex -- 7.5% PTA
3 weeks perfusion (High)	120 min	20% Hex -- 2.5% PTA
3 weeks perfusion (High)	240 min	60% Hex -- 7.5% PTA
3 weeks perfusion (High)	30 min	40% Hex -- 5% PTA

2400 radiographic images were acquired in fast scan mode (frame averaging of 1 and image skip of 0) resulting in a scanning time of 20 minutes per sample. The scanning time was kept low to allow routine screening and eliminate sample movement during scanning. The reconstructed images had an isotropic voxel size of 3.75 µm. A beam hardening correction of 9 and a Gaussian filter of 6 was applied during reconstruction [Datos|x, GE Measurement and Control Solutions, Germany].

PCL based constructs

To determine the effect of the contrast agents on the neo-tissue integrity, a comparison between the datasets of constructs with and without staining was made. Therefore, the PCL based TE constructs were consecutively scanned (1) without contrast agent, (2) with Hexabrix®, (3) with PTA, (4) again with Hexabrix® and finally (5) without contrast agent.

For scanning the PCL-based TE constructs, a 1 mm aluminum filter was used and the tungsten target was operated at a voltage of 60 kV and 220 µA. All other scanning as well as the reconstruction parameters were similar to what was used for the Ti6Al4V based constructs.

5.3.3. DoE analysis

To determine the influence of the concentration and staining time of the contrast agents as well as the neo-tissue volume (further referred to as DoE parameters) on the image quality, dataset quality and tissue integrity, a DoE approach was used. This statistical method for planning experiments enables to study the influence of various parameters with minimal required experimental input but resulting in the required objective conclusions (Kreutz *et al.* 2009). Figure 5.1 and Table 5.1 show the different combinations of the DoE parameters, selected in a randomized manner by the statistics software JMP (SAS, Cary, USA), that were evaluated according to a 3-level, 3-factor fractional factorial design. Based on previous experiments (Papantoniou *et al.* 2014b) and a preliminary range screening, the three levels were selected for each parameter. Ti6Al4V based TE constructs cultured for 3 weeks in the static system represented the low neo-tissue volume level, 1 week in the perfusion bioreactor system the mid-level and 3 weeks in the perfusion bioreactor the high level (Papantoniou *et al.* 2014b, Sonnaert *et al.* 2014a). For each condition, 3 samples were evaluated.

DoE was applied to obtain statistically sound and objective conclusions on the magnitude and the importance of the main effects of the investigated factors (i.e. volume of neo-tissue, contrast agent concentration and staining time) on (i) the normalized contrast of the stained neo-tissue (i.e. contrast of the stained neo-tissue compared to the background and scaffold), (ii) the dataset quality (i.e. the amount of slices with a mismatch between the stained and the binarized neo-tissue fraction) and (iii) the tissue integrity (i.e. difference between the Hexabrix® and PTA stained neo-tissue). The Pareto charts display the absolute values of the standardized effects and have a reference line for $p = 0.05$. Any effect that extends beyond this reference line is a significant effect. The more the effect extends the reference line, the more important the effect is.

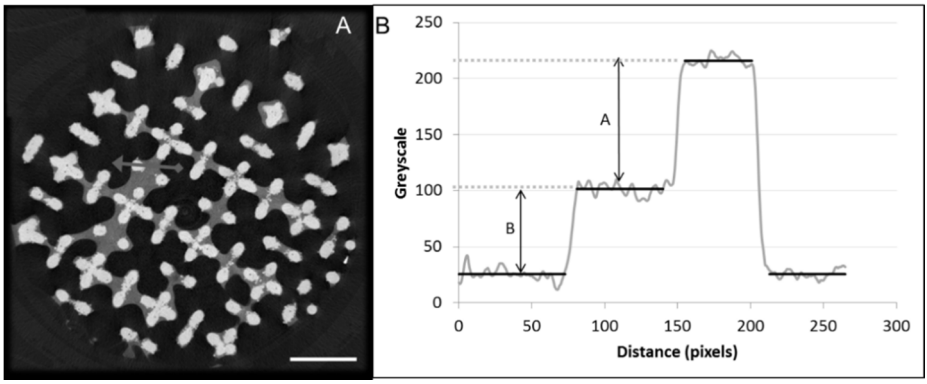

Figure 5.2: Normalized image contrast quantification of the stained neo-tissue compared to the background and scaffold.
(A) A representative transaxial cross-section of a Hexabrix® (60%) stained construct with a mid-level of neo-tissue volume. Scale bar is 1 mm. (B) The greyscale histogram through the grey arrow indicated in (A), used to quantify the contrast of the stained neo-tissue compared to the background and scaffold. 'A' is the average greyscale difference between the stained neo-tissue and the scaffold, and 'B' is the average greyscale difference between the background and the stained neo-tissue.

Influence of the DoE parameters on the image contrast

To quantify the contrast of the stained neo-tissue compared to the background and scaffold, a greyscale histogram was plotted along an arbitrary line through the background, neo-tissue and scaffold (Figure 5.2.A) using DataViewer (Bruker MicroCT, Belgium). The normalized contrast was then calculated according to eq. 1 (Figure 5.2.B).

$$\frac{B}{(A+B)} = normalized\ contrast \qquad (eq\ 1.)$$

where A is the average greyscale difference between the stained neo-tissue and the scaffold, and B is the average greyscale difference between the background and the stained neo-tissue. A + B is thus the average greyscale difference between the background and the scaffold. The calculated averages did not take into account the transition grey-scale values between the different phases. We only considered the grey-scale values within the range that did not deviate too much from the average value (i.e. plateau region). The thresholds to define the range for which the average was determined, were set at the grey-scale values that decreased below (or increased above) the lowest/highest value within the plateau region.

Influence of the DoE parameters on the dataset quality

The fraction of images containing a mismatch between the stained and binarized neo-tissue fraction, being a measure for the potential for quantitative interpretation or the dataset quality, was determined as a second input for the DoE. To obtain the binarized

neo-tissue fraction multi-level Otsu segmentation was applied. This algorithm, which is a histogram-based methodology that maximizes the variance between the different classes in the greyscale image (Otsu 1979), was performed on each individual 2D slice using CTAn (Bruker micro-CT, Belgium). Segmentation classes corresponding to the neo-tissue were subsequently binarized. The number of levels for the Otsu segmentation had a strong influence on the mismatch, because depending on the neo-tissue volume and/or contrast, the background noise and artifacts could be assigned to different segmentation classes. Therefore, the optimal number of Otsu-levels was determined for each contrast agent based on the datasets obtained with low, mid and high levels for each DoE parameter. The optimized number of Otsu levels per contrast agent was then used on the datasets of all the DoE conditions to determine the dataset quality.

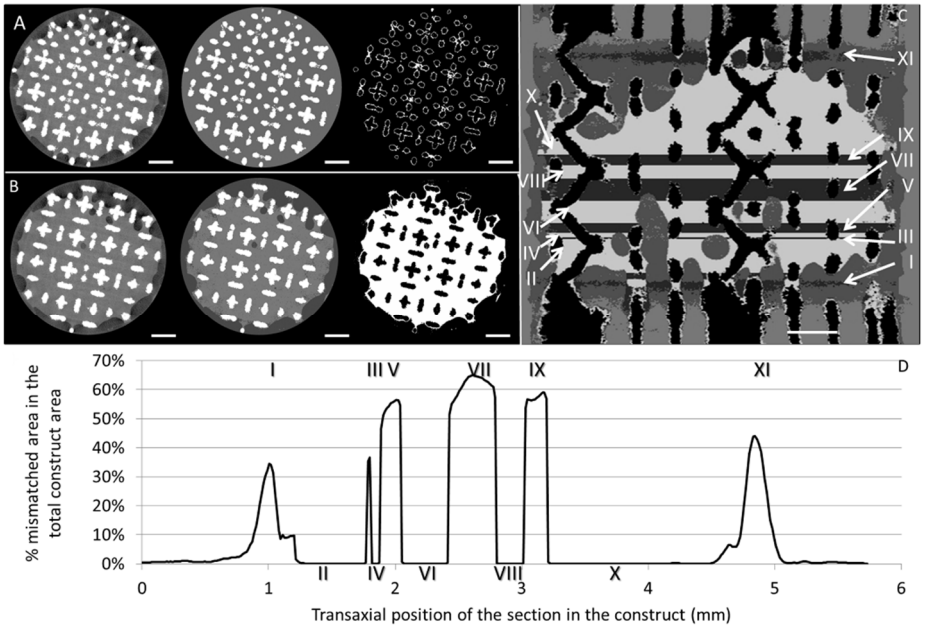

Figure 5.3: Mismatch between the stained and binarized neo-tissue fraction as a measure for the dataset quality.
(A, B) A raw (left), 2-level segmented (middle) and binarized image (right) cross-section of a TE construct with a high level of neo-tissue volume after 120 min staining with 20% Hexabrix® located in the middle of zone V (A) and zone VI (B). Zoning depicted in (C) – green numbers indicates zones without mismatch and red numbers indicate zones with a mismatch larger than the 1% threshold. (C) Differential overlay (coronal view) of the raw image and the binarized neo-tissue with indication of the zones (green) without mismatch between the raw and the binarized images and (red) where the 2-level segmentation resulted in a mismatch between the raw and the binarized images. (D) The histogram showing the mismatched area between the raw and the binarized images as indicated in (C). The grey striped line indicates the 1% threshold above which a mismatch was considered. Scale bars are 1 mm.

To calculate the mismatch between the stained neo-tissue and the binarized neo-tissue fraction (Figure 5.3.A and B), a differential overlay of both was made (Figure 5.3.C). Binarized differential overlays were subsequently analyzed for the 'mismatched neo-tissue' fraction and histograms that show the area of the mismatched fraction were generated (Figure 5.3.D). Based on these histograms, the fraction of mismatched images was determined. In order to omit the influence of background noise on the analysis, slides with a mismatch lower than 1% of the total slide surface were excluded from the analysis.

Influence of the DoE parameters for PTA staining on the neo-tissue integrity

To first evaluate the influence of both contrast agents on the neo-tissue integrity, a comparison between the datasets of constructs with and without staining was made. For the Ti6Al4V-based TE constructs, visualization of the neo-tissue without contrast agent was not possible as the scanning energies required to obtain sufficient transmission through the metal scaffold resulted in greyscale values for the neo-tissue that could not be segmented from the background noise and streaks. Therefore, PCL based TE constructs were used, as the lower X-ray opacity of PCL enabled the visualization of the neo-tissue without the presence of a contrast agent. Differential overlays of the datasets of TE constructs consecutively scanned (1) without contrast agent, (2) with Hexabrix®, (3) with PTA, (4) again with Hexabrix® and finally (5) without contrast agent were generated. The mismatch between the binarized neo-tissue for the different scans was determined to evaluate the influence of the contrast agent on the tissue integrity, and the potential staining-induced tissue shrinkage.

Then, as final DoE read-out, the influence of the PTA staining on the tissue integrity was determined. This was quantified as the difference between the Hexabrix® (Figure 5.4.A) and PTA (Figure 5.4.B) stained neo-tissue surface area relative to the Hexabrix® stained neo-tissue surface area in the corresponding CE-nanoCT slices. Hereto, the Hexabrix® and PTA stained datasets of the same sample were registered in 3D using DataViewer (Bruker MicroCT, Belgium). To avoid the evaluation of mismatched slices, three transaxial slices per dataset, distributed over the height of the TE construct, were selected. Using the optimal segmentation procedure for the different contrast agents as described earlier, the neo-tissue was binarized applying CTAn (Bruker MicroCT, Belgium). To reduce the errors introduced by the partial volume effect (PVE) and metallic artifacts for analyzing the neo-tissue surface area, the binarized images for the scaffold structure were dilated by 2 voxels and subtracted from the dataset of the binarized neo-tissue. The noise in the binarized neo-tissue images was minimized by removing black and white speckle noise smaller than 200 voxels. In order to solidify the resulting structure, a 'closing' operation of 2 voxels was performed. Finally, the surface area of the binarized neo-tissue was quantified and the degree of tissue shrinkage (i.e. inverse of the tissue integrity) was determined relative to the Hexabrix® stained neo-tissue using eq. 2. The average neo-tissue thickness was calculated on every CT slice using the 2D thickness analysis algorithm from CTAn (Bruker MicroCT). Based on the 3D thickness analysis ona subsection without mismatch of the datasets,

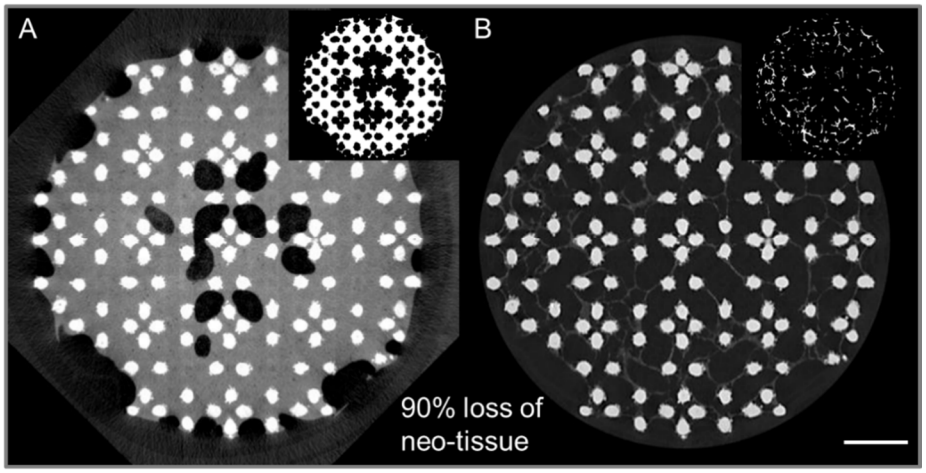

Figure 5.4: Representative transaxial cross-sections
(A) a Hexabrix® (60%, 240 min) stained TE construct and (B) the same TE construct stained with PTA (7.5%, 240 min). The insets show the binarized images of the neo-tissue in the cross-section, based on which the surface area of neo-tissue was calculated. Scale bar is 1 mm.

3D color-coded rendering showing the neo-tissue thickness distribution were generated using CTVox (Bruker MicroCT).

$$\frac{SA_{Hex} - SA_{PTA}}{SA_{Hex}} = degree\ of\ tissue\ shrinkage \quad (eq\ 2.)$$

where SA_{Hex} is the Hexabrix® stained neo-tissue surface area and SA_{PTA} is the PTA stained neo-tissue surface area in the corresponding CE-nanoCT slice.

5.4. Results and discussion

5.4.1. Contrast quantification

As a DoE analysis read-out, the normalized contrast of the stained neo-tissue compared to the background and scaffold was determined for each experimental condition. For both contrast agents, the concentration was the most influencing parameter (Figure 5.5.B and C). This could also be observed from the raw data (Figure 5.5.A), which showed a concentration-dependent increase in relative contrast, independent of the staining time or neo-tissue volume.

Staining time did not significantly influence the normalized contrast, indicating that both contrast agents had infiltrated the neo-tissue within 30 minutes, even for the largest neo-tissue volume (Figure 5.5.B and C). Although limitations in staining homogeneity and intensity due to diffusion limitations of the contrast agent have been reported (Pauwels *et al.* 2013), these were not observed in our experiments. Non-mineralized

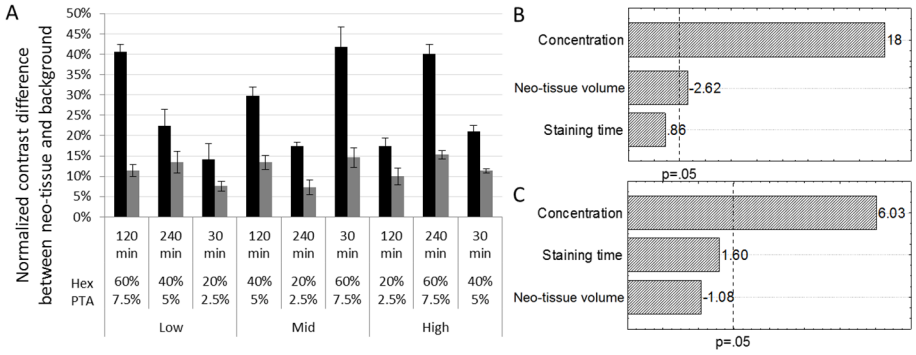

Figure 5.5: Contrast quantification and DoE analysis
(A) Normalized contrast difference between neo-tissue and background as shown in eq. 1 for Hexabrix® (black) and PTA (grey) for all conditions of the DoE. Pareto charts for (B) Hexabrix® and (C) PTA stained TE constructs, showing the ranking of the influence of all staining parameters on normalized contrast. The dotted line indicates a significance level of p = 0.05.

neo-tissue developed in a perfusion bioreactor system, such as the neo-tissue in this study, was reported to have an approximate cell density of $6 * 10^6$ cells/cm³ (Sonnaert *et al.* 2014a, Sonnaert *et al.* 2014b), while the density of native tissue, in which diffusion limitations were previously reported, can on average be between 10^8 and 10^9 cells/cm³. Since no influence of the staining time was observed within the operating window of our experiments, the lower cell density of the engineered neo-tissues will enable both contrast agents to fully infiltrate within the minimal staining time of 30 min.

For Hexabrix® (Figure 5.5.B), the normalized neo-tissue contrast was negatively influenced by the neo-tissue volume. As shown in earlier work, the neo-tissue has a fibrous structure (Papantoniou *et al.* 2013). Due to the limited spatial image resolution and the dense packing of the individual fibers (i.e. inter-fiber distances below the spatial image resolution), they cannot be discriminated in the CE-nanoCT images. Moreover, since Hexabrix® is an equilibrium contrast agent, the staining solution might be entrapped between neo-tissue fibers during infiltration. For the high level of neo-tissue volume, the neo-tissue fibers might be more densely packed and we could hypothesize that less volume is available within the porous neo-tissue for the Hexabrix® solution to be entrapped. As a result, the greyscale of the bulk neo-tissue will be lower compared to the less packed neo-tissue for the low- and mid-level of neo-tissue volume. Consequently, the normalized contrast of the neo-tissue is lower, as depicted in the pareto chart.

5.4.2. Dataset quality

Optimization of the image segmentation procedure

To quantitatively and objectively evaluate which segmentation procedure was optimal for each contrast agent, the fraction of images containing a mismatch between the stained and the binarized neo-tissue fraction was determined for datasets with low, mid and high levels of each DoE factor. Figure 5.6 indicates that both for the Hexabrix® and PTA stained 'low-level' constructs (low values of all 3 parameters), binarization of the neo-tissue could not be done correctly, hence excluding automated analysis of the neo-tissue volume for these conditions. Both for the Hexabrix®-stained TE constructs with a mid- and high-level parameter set, the 2-level Otsu segmentation enabled binarization of the neo-tissue with a minor mismatch (Figure 5.6.A), and was therefore further used for the evaluation of the Hexabrix® stained TE constructs. For the PTA stained TE

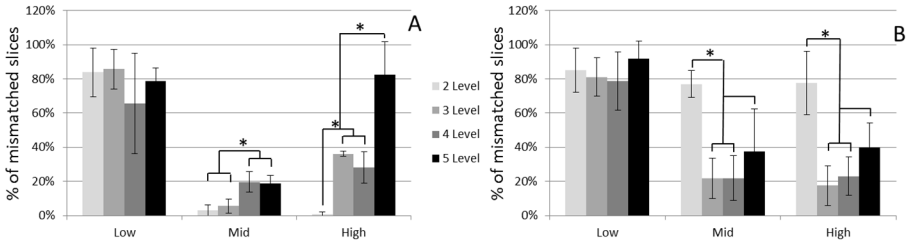

Figure 5.6: Mismatch between stained and binarized neo-tissue
Percentage of slices of the full dataset showing a mismatch between the stained and binarized neo-tissue for different Otsu segmentation levels and different value sets for all three DoE parameters (neo-tissue volume, staining time and concentration) for (A) Hexabrix® and (B) PTA stained TE constructs. *p < 0.05

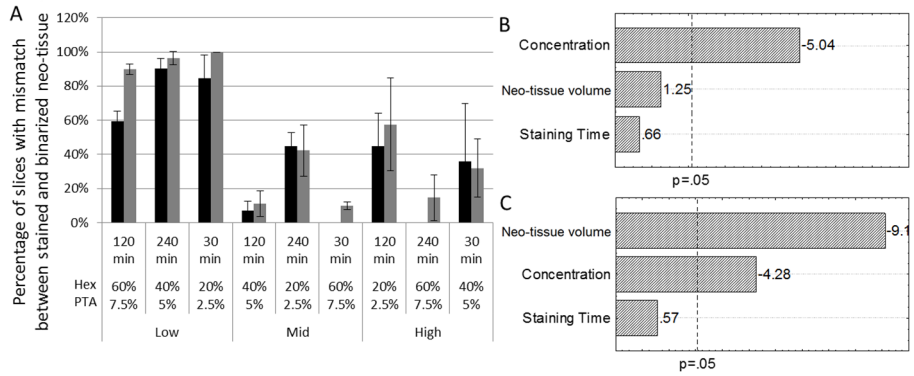

Figure 5.7: Mismatched slices and DoE analysis
(A) The percentage of slices with a mismatch between the stained and binarized neo-tissue for Hexabrix® (black) and PTA (grey) for all conditions of the DoE. (B, C) Pareto charts for Hexabrix® (B) and PTA (C) stained TE constructs respectively, showing the influence of the different staining parameters on the mismatch. The dotted line indicates a significance level of p = 0.05.

constructs with a mid- and high-level neo-tissue volume, all segmentation levels resulted in a high mismatch between the stained and binarized neo-tissue fraction. No significant differences were observed between the 3, 4 and 5-level segmented images (Figure 5.6.B). However, the more levels that needed to be segmented, the larger the processing time that was required to generate the segmented images. Therefore a 3-level Otsu segmentation was used for further analysis of the PTA-stained TE constructs.

Influence of DoE parameters on the dataset quality

To determine the influence of the DoE parameters on the dataset quality, the fraction of slices with a mismatch between the stained and binarized neo-tissue was evaluated using the optimized segmentation settings as described above. For both contrast agents, their concentration significantly influenced the fraction of mismatched slices (Figure 5.7.B and C). As the normalized contrast of neo-tissue increased with increasing concentration, it could be more easily separated from the scaffold-dependent image artifacts, and thus the amount of mismatched slices decreased significantly (Figure 5.7.A).

Both contrast agents showed a high mismatch for low volumes of neo-tissue (Figure 5.7.A). This confirmed the findings from our previous study, where we determined the CE-nanoCT threshold for neo-tissue quantification to be a neo-tissue volume lower than 4% of the total TE construct void volume (Papantoniou *et al.* 2014b). This lower quantification limit was directly related to the artifacts introduced by the metallic scaffolds. The DoE analysis showed, however,that only in the case of PTA the neo-tissue volume had a significant effect on the dataset quality, as an increase in neo-tissue volume resulted in a significant decrease in mismatched slices (Figure 5.7.C). This is mainly caused by the neo-tissue structure, which for the low neo-tissue volume is on average much thinner compared to the other levels of neo-tissue volume (Figure 5.8). When compared to the Hexabrix® stained neo-tissue (Figure 5.8), the PTA stained neo-tissue showed for all experimental conditions a more fibrous structure. Moreover its thickness could approach the spatial resolution of the images (i.e. 7.5 µm – 11.5 µm). Consequently, the PVE reduces the contrast of the neo-tissue, making it no longer separable from the scaffold-dependent image artifacts. Additionally, when the volume fraction of the bulk neo-tissue became too small, as was the case for the low neo-tissue volume, its peak in the cross-section greyscale histogram could no longer be segmented from the other phases in the images. The combination of the above mentioned factors all contributed to the mismatch quantified in Figure 5.7.

5.4.3. Tissue integrity

Influence of the contrast agents on the neo-tissue integrity

As mentioned earlier, the use of PTA as a contrast agent can cause tissue shrinkage (Buytaert *et al.* 2013). For Hexabrix®, as this is a clinically approved contrast agent that does not chemically bind to the tissue, no effect on the tissue integrity was expected. To the best of our knowledge, there are no studies in the literature that have reported an effect of Hexabrix® staining on the tissue integrity. Using PCL-based TE constructs

without and with Hexabrix® staining (Figure 5.9.A and B respectively), we could confirm this, as the PCL scaffolds allow us to visualize the neo-tissue without the use

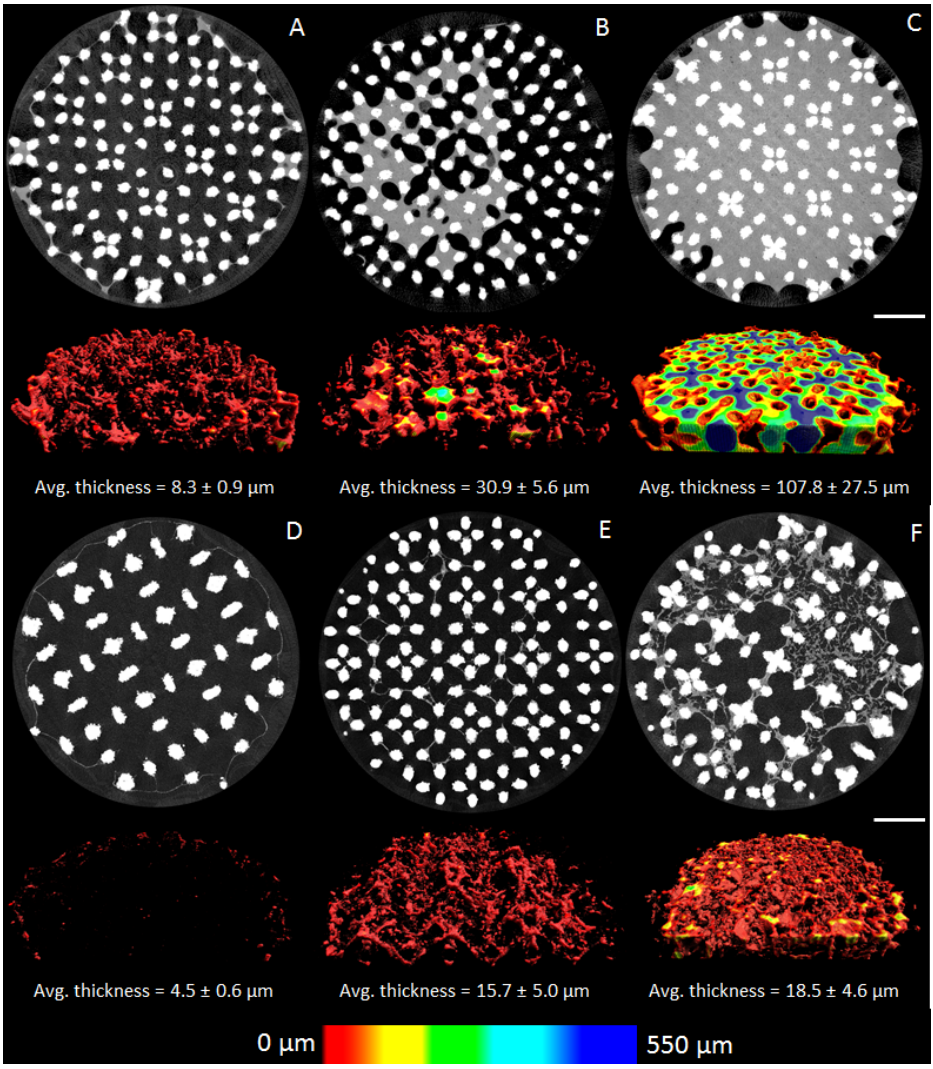

Figure 5.8: Morphology and thickness of the neo-tissue for different DoE conditions. (A-C) Representative cross-sectional images and 3D color-coded renderings for TE constructs with (from left to right) low, medium and high levels of neo-tissue volume, stained with 60% Hexabrix®. (D-F) Representative cross-sectional images and 3D color-coded renderings for TE constructs with (from left to right) low, medium and high levels of neo-tissue volume, stained with 7.5% PTA. Scale bar is 1 mm. For each condition, the average neo-tissue thickness is included (n = 3).

of a contrast agent. When overlaying both datasets (Figure 5.9.E), the largest difference (indicated in black) was the scaffold itself, since this could not be segmented from the neo-tissue in the images without contrast agent. Some small differences (indicated in white) were found in the small pores, where the Hexabrix® solution might have been not removed during the short drying step prior to scanning (on average 4.81 ± 3.95 % of the total neo-tissue volume, n = 3). The viscosity of the Hexabrix® solution is higher than that of the PBS itself, causing a more difficult removal of the liquid from the pores during the drying step. We could therefore conclude that the Hexabrix® staining does not influence the neo-tissue structure.

Subsequent to the Hexabrix® staining and an overnight rinsing step in PBS solution to remove the Hexabrix®, TE constructs were stained with PTA and imaged again. A strong influence on the neo-tissue integrity was appreciated (Figure 5.9.C), and a clear difference with the Hexabrix® stained dataset was seen (Figure 5.9.F). To confirm that this difference was due to the PTA staining, the TE construct was once again stained with Hexabrix® after overnight rinsing in PBS and scanned (Figure 5.9.D). Although the small pores were again filled with the Hexabrix® solution as mentioned earlier, a significant difference was seen compared to the first Hexabrix® stained dataset (up to 29 ± 17.5 % of the total neo-tissue volume), indicating that the PTA staining indeed caused tissue shrinkage.

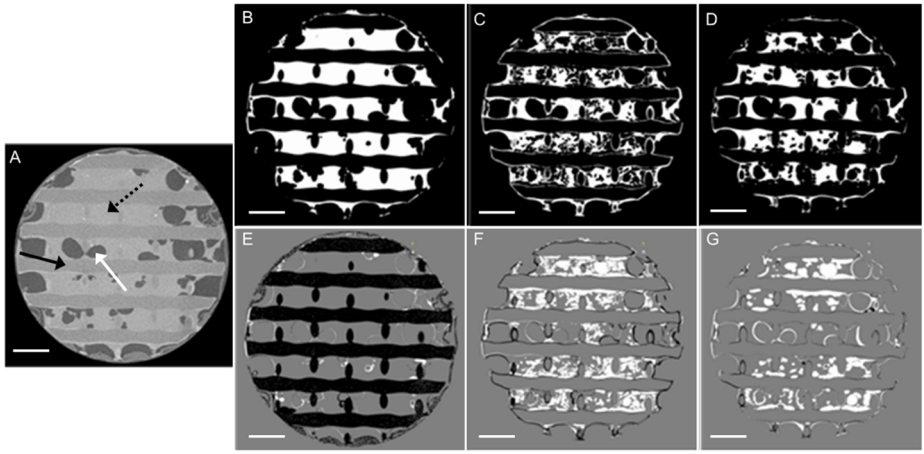

Figure 5.9: Influence of the different contrast agents on the neo-tissue integrity.
(A) A typical transaxial cross-section through a PCL-based TE construct without a contrast agent. The black arrow indicates the PCL scaffold; the dashed arrow indicates the neo-tissue; the white arrow indicates the air space. The corresponding binarized images for neo-tissue of the (B) Hexabrix® (60 %) stained dataset, (C) PTA (7.5 %) stained dataset after Hexabrix® staining and (D) Hexabrix® (60 %) stained dataset after the consecutive Hexabrix and PTA staining. (E) The differential overlay image of (A) and (B); (F) the differential overlay image of (B) and (C); and (G) differential overlay image of (B) and (D). The black voxels in the overlay images represent the voxels present in the first dataset, but not in the second; the white voxels represent the voxels present in the second dataset, but not in the first. Scale bars are1 mm.

Influence of the DoE parameters for PTA staining on the neo-tissue integrity

The degree of tissue shrinkage due to PTA staining was quantified as the difference between the Hexabrix® and PTA stained neo-tissue surface area in the corresponding CE-nanoCT slices relative to the Hexabrix® stained neo-tissue surface area. In agreement with other studies (Buytaert *et al.* 2013, Vickerton *et al.* 2013), the DoE showed that the concentration of the contrast agents has the strongest effect on the tissue shrinkage (Figure 5.10). Although an increase in the concentration caused a significant increase in the normalized neo-tissue contrast (Figure 5.5.C), as well as a significant decrease in the amount of mismatched images (Figure 5.7.C), it did introduce a significant tissue shrinkage. Hence, when accurate neo-tissue morphometric analyses should be performed, the concentration should be kept as low as possible. Additionally, also an increase in neo-tissue volume was shown to result in a significant increase in tissue shrinkage, which could be expected as more neo-tissue is available for the PTA to affect.

As the chemistry of the staining is not fully defined yet (Vickerton *et al.* 2013), we cannot give a clear explanation for the tissue shrinkage. It has, however, been shown that tissue shrinkage because of the contrast agents is strongly dependent on the tissue composition and structure, since a different degree of shrinkage was found for different soft and mineralized tissue types (Buytaert *et al.* 2013, Vickerton *et al.* 2013, Papantoniou *et al.* 2014b). As we currently have no quantitative data on the composition or fibrous structure of the neo-tissue for the different levels of neo-tissue volume, we cannot claim that this could influence the tissue shrinkage. We did, however, show that the bulk neo-tissue structure for the low-level neo-tissue volume was much thinner than for the mid- and high-level neo-tissue volume. As a result, the segmentation and binarization of the neo-tissue was less accurate (Figure 5.7). Because of this, and due to the influence of the PVE, the calculation of the degree of tissue shrinkage for the low-level of the neo-tissue volume might be inaccurate and should be evaluated with care.

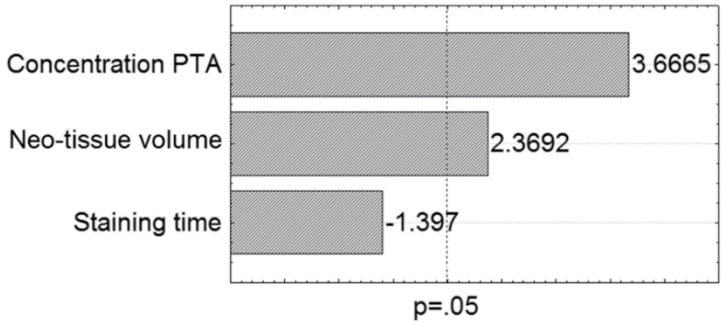

Figure 5.10: Influence of the DoE parameters for PTA staining on the neo-tissue integrity.
Pareto chart for the PTA-stained TE constructs when evaluating the degree of tissue shrinkage. The dotted line indicates a significance level of p = 0.05

5.5. Conclusions

Using a DoE approach, we were able to optimize a 3D imaging protocol by quantifying and ranking in statistical importance the factors that influence the CE-nanoCT staining procedure using Hexabrix® and PTA. These factors were contrast agent concentration, staining time and the presence of neo-tissue (volume). Their effect on image quality, dataset quality and tissue integrity was investigated.

For Hexabrix® staining of the neo-tissue in Ti alloy scaffolds, in this study the optimal staining conditions were (i) a concentration of 60% (vol% in PBS) and (ii) a staining time of 30 minutes. These were sufficient to allow accurate and fully automated quantification of the neo-tissue formed. When the neo-tissue volume fraction was, however, less than 4% of the open space, in this study represented by the low-level neo-tissue volume, quantitative analysis of the datasets was not possible.

For PTA staining, the DoE showed that in this study a high concentration was necessary for sufficient image contrast and accurate, automated 2D/3D image analysis, although significant tissue shrinkage was introduced. Hence, based on the results from the DoE, for this study we concluded using only 2.5% (weight% in PBS) of PTA. As the staining time did not have any significant influence, this was kept as low as possible (in this case 30 minutes).

As a result of this study, and by using a DoE approach to optimize the staining conditions, we have converted CE-nanoCT into an optimized, quantitative and 3D measuring tool to evaluate neo-tissue formation in TE constructs and its spatial distribution.

5.6. Acknowledgements

MS is supported by a Ph.D. grant of the Agency for Innovation by Science and Technology (IWT/ 111457). GK is currently financed by a postdoctoral grant of the Research Foundation - Flanders (FWO/12R4315N). GK and LG acknowledge support by the European Research Council under the European Union's Seventh Framework Program (FP7/2007-2013)/ERC grant agreement n°279100. IP was supported by the European Research Council under the European Union's Seventh Framework Program (FP7/2007-2013)/ERC grant agreement REJOIND n°294191. The CE-nanoCT images have been generated on the X-ray computed tomography facilities of the Department of Materials Engineering of the KU Leuven, financed by the Hercules Foundation (project AKUL 09/001: Micro-and nano-CT for the hierarchical analysis of materials). SVV would like to acknowledge the Research Foundation-Flanders (FWO, Belgium) for financial support under the form of a post-doctoral fellowship and a Research Grant ('Development of the ideal tissue engineering scaffold by merging state-of-the-art processing techniques', FWO Krediet aan Navorsers). This work is part of Prometheus, the Leuven Research & Development Division of Skeletal Tissue Engineering of the KU Leuven: www.kuleuven.be/prometheus

Chapter 6.
Human periosteal derived cell expansion in a perfusion bioreactor system: Proliferation, differentiation and extracellular matrix formation

Sonnaert, M., Papantoniou, I., Bloemen, V., Kerckhofs, G., Luyten, F.P., Schrooten, J.

Published in Journal of tissue engineering and regenerative medicine, 2014 doi: 10.1002/term.1951. [Epub ahead of print]

6.1. Abstract

Perfusion bioreactor systems have shown to be a valuable tool for the *in vitro* development of 3D cell-carrier constructs. Their use for cell expansion is, however, much less explored. Since maintenance of the initial cell phenotype is essential in this process, it is imperative to get an insight in the bioreactor-related variables determining cell fate. Therefore, this study investigated the influence of fluid flow induced shear stress on the proliferation, differentiation and matrix deposition of human periosteal derived cells in the absence of additional differentiation inducing stimuli. 120 000 cells were seeded on additive manufactured 3D Ti6Al4V scaffolds and cultured up to 28 days at different flow rates ranging between 0.04 and 6 ml/min. DNA measurements showed on average a threefold increase in cell content for all perfused conditions in comparison to static controls whereas the magnitude of the flow rate did not have an influence. Contrast-enhanced nanofocus X-ray computed tomography showed substantial formation of an engineered neo-tissue in all perfused conditions, resulting in a filling up to 70% of the total internal void volume and no flow-rate dependent differences were observed. The expression of key osteogenic markers such as RunX2, OCN, OPN and Col1 did not show any significant changes in comparison to static controls after 28 days of culture, with the exception of Osx at high flow rates. We therefore concluded that, in the absence of additional osteogenic stimuli, the investigated perfusion conditions increased cell proliferation but did not significantly enhance osteogenic differentiation thus allowing for this process to be used for cell expansion.

6.2. Introduction

The development of cell-based regenerative therapies to treat defects in the body is rapidly evolving (Martin *et al.* 2011a, Martin *et al.* 2012). However, the translation of these techniques to a clinical setting still remains a major challenge due to suboptimal cell culture strategies leading to low yields of progenitor cells (Rodrigues *et al.* 2011). To address this, the development of robust processes using three dimensional (3D) bioreactor culture systems is a promising prospective (Grayson *et al.* 2004, Martin *et al.* 2004, Haycock 2011, Rodrigues *et al.* 2011, Jakob *et al.* 2012, Salter *et al.* 2012a). Bioreactors play a crucial role in establishing and maintaining 3D cell culture, controlling and monitoring physicochemical parameters in the system as well as automating manual procedures (Martin *et al.* 2010). Next to this, these systems allow to exert controlled mechanical stimuli such as hydrostatic pressure and shear stress (SS) on the developing construct (i.e. combination of a 3D carrier and cells/extracellular matrix (ECM)), which can be used to guide cell behavior (McCoy *et al.* 2010, Salter *et al.* 2012a).

Bioreactor facilitated stem cell expansion has already been achieved using multiple systems ranging from multi-layered cell factories to micro-carriers in stirred tank bioreactors (Jung *et al.* 2012b). Different groups have already shown that the stem cell phenotype can be maintained in these systems despite the external hydrodynamic stresses applied on the cells by fluid flow during culture (Hewitt *et al.* 2011, Chang *et al.* 2012, Jung *et al.* 2012b). However, despite the 3D shape of the carriers used in these

systems, cells predominantly grow in a monolayer which does not reproduce the native environment of the cells (Haycock 2011). Additionally, the use of these systems does not stimulate ECM formation although its presence in a 3D architecture has been shown to restrain spontaneous differentiation and preserve differentiation potential (Chen *et al.* 2007). The shortfalls of these 3D culture systems can be addressed using a 3D perfusion bioreactor system.

Next to enhancing the mass transport in the culture system, the combination of a 3D carrier and volumetrically controlled mass transport through perfusion has the potential to guide cell fate in function of culture conditions applied. In a range between 10^{-4} Pa and 10^{-1} Pa the SS exerted by the fluid flow on the developing construct has already been shown to have an enhancing effect on both osteogenic differentiation and mineralized matrix deposition, when the fluid flow is used as an additional stimuli combined with osteogenic inductive medium (Goldstein *et al.* 2001, Bancroft *et al.* 2002, Cartmell *et al.* 2003, Gomes *et al.* 2003, Sikavitsas *et al.* 2003, Hosseinkhani *et al.* 2005, Grayson *et al.* 2008, Grayson *et al.* 2010, McCoy *et al.* 2010, Fisher *et al.* 2011, Grayson *et al.* 2011, Liu *et al.* 2012, McCoy *et al.* 2012, Salter *et al.* 2012a). However, when the bioreactor system is intended to be used for a cell population expansion rather than the development of TE constructs containing differentiated cells, the maintenance of the progenitor phenotype is essential. Although the use of different perfusion regimes such as the use of intermittent shear stress in normal growth medium affects the behavior of bone marrow derived Mesenchymal stem cells (MSCs) (Kim *et al.* 2012), the expansion of a Mesenchymal progenitor cell population in the presence of SS with maintenance of its phenotype has proven to be possible (Scherberich *et al.* 2007). Also substrate specific interactions have the potential to trigger specific cell responses to external stimuli (Grayson *et al.* 2011), explaining the large variation in specific cell responses to SS reported in literature (McCoy *et al.* 2010, Fisher *et al.* 2011). Therefore, it is required to determine the effect of a bioreactor culture on the proliferation and differentiation of a targeted cell population for specific combinations of SS and carrier material and structure.

Human periosteal derived cells (hPDCs) obtained from periost biopsies contain osteochondro-progenitor cell populations (De Bari *et al.* 2006, Eyckmans *et al.* 2006a, Marolt *et al.* 2010). Their multi-lineage differentiation potential, phenotypical stability, high proliferation and accessibility make these cells a suitable cell source for bone tissue engineering (Hutmacher *et al.* 2003, De Bari *et al.* 2006, Eyckmans *et al.* 2006a, Agata *et al.* 2007, Ringe *et al.* 2008, Marolt *et al.* 2010). Several studies have already demonstrated the osteoinductive potential of these cells when implanted *in vivo* (Agata *et al.* 2007, Marechal *et al.* 2008, Roberts *et al.* 2011), and they are further being used for the development of tissue engineered bone products (Chai *et al.* 2012c, van Gastel *et al.* 2012a, van Gastel *et al.* 2012b). The use of hPDCs in bioreactor systems and concomitantly the effect of such a system on the osteogenic differentiation of this cell population, is still very limited (Matziolis *et al.* 2006, Papantoniou *et al.* 2013).

In order to determine the potential of using a perfusion bioreactor system for the expansion of this progenitor cell population, the goal of this study was to determine the influence of perfusion on the *in vitro* proliferation, differentiation and matrix formation

of hPDCs in the absence of differentiation inducing medium. hPDCs were cultured on inert Ti6Al4V porous scaffolds at different flow rates corresponding to the range of SS values used in literature and proliferation was evaluated in function of the applied SS based on DNA content. Thereafter the influence of two levels of SS, reported to respectively have a proliferation enhancing or osteogenic inductive effect, on the cell behavior was determined and compared with static 3D culture. Real time PCR (RT-PCR) was employed to analyze gene expression in combination with the analysis of the proliferation. Contrast enhanced nanofocus X-ray computed tomography (CE-nanoCT) was employed in combination with Live/Dead staining to visualize and quantify the 3D dynamics of cell growth and extracellular matrix deposition.

6.3. Materials and methods

6.3.1. Ti6Al4V Scaffolds

Regular, 3D additive manufactured Ti6Al4V scaffolds (Ø = 6 mm, h = 6 mm) were produced in-house using selective laser melting based on a diamond shaped unit cell (Van Bael *et al.* 2011, Pyka *et al.* 2012) (Figure 6.1.A). The total volume of the scaffolds was 166 ± 3 mm³, the available volume 130 ± 5 mm³ and the available surface 7.5 ± 0.6 cm² as determined with nanoCT (Kerckhofs *et al.* 2013a). Prior to use, scaffolds were ultrasonically cleaned for 10 min consecutively with acetone, ethanol and distilled water. Subsequently they received an alkali treatment with 5M sodium hydroxide (Sigma-Aldrich) at 60°C for 24 hours, were rinsed with distilled water, and finally sterilized in a steam autoclave. Prior to cell seeding, all scaffolds were pre-wetted by vacuum impregnation in cell culture medium for 2 h in a humidified incubator at 37°C, and dried overnight in a non-humidified incubator (Impens *et al.* 2010a, Papantoniou *et al.* 2013, Zhou *et al.* 2013b, Papantoniou *et al.* 2014b).

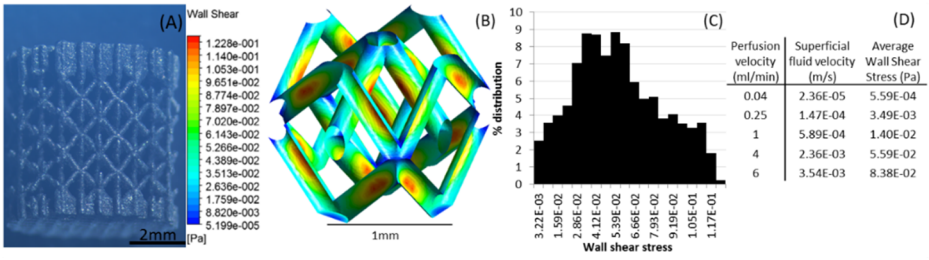

Figure 6.1: CFD based shear stress distribution in Ti6Al4V scaffold
(A) Bright field image of a Ti6Al4V scaffold, (B) SS distribution on a scaffold unit cell for a perfusion velocity of 4 ml/min, (C) relative distribution of the SS on the scaffold unit cell for a perfusion velocity of 4 ml/min and (D) interstitial fluid velocity and average SS corresponding with the applied perfusion velocities. All calculations were performed on an empty scaffold, thus representing the initial SS present after cell attachment and prior to construct culturing.

6.3.2. Fluid flow modelling

In order to determine the SS correlated with the volumetric perfusion velocity and hence select a relevant range of flow rates, fluid flow modelling using computational fluid dynamics (CFD) was used as described by Truscello *et al.*, 2012. Due to the symmetrical design of the scaffold the calculations were limited to one geometrical unit cell. A 3D geometrical model of a scaffold unit cell was created and meshed in the ACIS-based solid modeller Gambit 2.2 (Fluent). The mesh was refined until the solution was stable (mesh independent) and contained 750 000 elements which were sized to 30 μm^3. To determine velocity fields and the related SS in the scaffold the finite volume code Fluent 6.3 (Fluent) was used. The culture medium was considered to be an incompressible and homogeneous Newtonian fluid with properties equal to water (viscosity: 10^{-3} Pa s, density: 10^3 kg/m^3, temperature: 37 °C). Since the Reynolds number was lower than 1 the correlation between the flow rate and the SS was linear. Therefore the correlation between the flow rate and the SS was determined for one flow rate and thereafter extrapolated to the range of interest. A constant velocity of 2.36 mm/s was assigned to the inlet, corresponding to a volumetric flow rate of 4 ml/min. No-slip conditions were applied to the walls of the scaffolds, symmetry conditions to the lateral surfaces and a zero gauge pressure was set at the outlet. The flow problem was described with steady-state Navier-Stokes equations.

6.3.3. hPDC culture

hPDCs were isolated from periosteal biopsies of different donors as described previously (Eyckmans *et al.* 2006a). This procedure was approved by the ethics committee for Human Medical Research (KU Leuven) and with patient informed consent. hPDCs were expanded in Dulbecco's modified Eagle's medium with high-glucose (Invitrogen) containing 10% foetal bovine serum (Gibco), 1% sodium pyruvate (Invitrogen) and 1% antibiotic–antimycotic (100 units/mL penicillin, 100 mg/mL streptomycin, and 0.25mg/mL amphotericin B; Invitrogen). The cells were seeded at 5 700 cells/cm^2 and passaged at 80 % – 90 % confluence. Prior to the 3D culture experiments cells were harvested using Triple Express (Invitrogen) and drop-seeded by a single drop onto the scaffolds at a density of 200 000 cells per 60µl drop as performed in earlier studies (Papantoniou *et al.* 2013, Zhou *et al.* 2013b, Papantoniou *et al.* 2014b). 45 min after seeding 60 µl culture medium was added and 135 min later the medium volume was topped up to 1 ml. Scaffold-cell constructs (further mentioned as constructs) were incubated overnight in standard culture conditions (37°C, 5% CO_2, 95% relative humidity). Since the seeding process resulted in homogenous and reproducible seeding efficiencies in earlier experiments (~60%) this was not assessed separately in this work (Papantoniou *et al.* 2013, Papantoniou *et al.* 2014b). This seeding procedure resulted in an initial cell density of 17 100 cells/cm^2 or $7*10^5$ cells/cm^3.

For the initial flow rate screening 5 different values (0.04, 0.25, 1, 4 and 6 ml/min) were applied, corresponding with a SS range of $5.6*10^{-4}$ Pa to $8.4*10^{-2}$ Pa, thereby covering the range of SS reported in literature (McCoy *et al.* 2010). 30 scaffolds were seeded as described before (5 scaffolds per flow rate and 5 as static control). After the overnight

static incubation, the constructs were transferred to a 12 well plate containing 3ml culture medium/well for static culture or to an in-house developed bioreactor system. This system contained in total 13 ml of culture medium for perfusion culture of which 3 ml was located in the circuit and the remaining 10 ml in the medium reservoir. Medium was refreshed every two days either by attaching a new medium reservoir containing 10 ml of fresh culture medium or by manually replacing the 3 ml of culture medium for the static constructs. Continuous perfusion was applied for a total duration of 21 days.(Papantoniou *et al.* 2013, Zhou *et al.* 2013b, Papantoniou *et al.* 2014b).

For the time point experiment 54 scaffolds were seeded and afterwards divided in 3 groups for static culture and perfusion at low and high flow rate (0.04 ml/min and 4 ml/min) corresponding with SS values reported to have a proliferation of differentiation enhancing effect in different systems (McCoy *et al.* 2010). Samples were taken at 14, 21 and 28 days. Time points were chosen to allow for the different stages of possible osteogenic differentiation and matrix deposition to occur.

As a positive control for mineralization constructs were cultured for 21 days at the high flow rate using a bio-instructive medium based on normal growth medium with the addition of 6 mM Ca^{2+}, 4 mM P_i and 0.05 ng/ml ascorbic acid (Chai *et al.* 2012d, Papantoniou *et al.* 2013).

6.3.4. DNA measurement

The DNA content was determined using a highly quantitative and selective DNA assay (Quant-iT^{TM} dsDNA HS kit, Invitrogen). The methods used were developed and optimised for combined DNA measurement and RNA extraction from 3D constructs (Chai *et al.* 2012c, Chen *et al.* 2012, Papantoniou *et al.* 2013). The constructs were rinsed with PBS and lysed in 350 µl RLT lysis buffer (Qiagen) supplemented with 3.5 µl β-mercaptoethanol after which the lysed samples were vortexed for 60 s and stored at -80°C. Prior to analysis, the samples were thawed at room temperature and spun down for 1 min at 13 000 rpm. 10 µl of the sample was diluted in 90 µl milliQ water after which the DNA content was quantified with a Qubit® Fluorometer (Invitrogen) as described by Chen *et al.*, 2012.

6.3.5. Quantitative PCR

For the time point experiment, RNA was extracted from 4 random, representative constructs for each culturing condition and time point using the RNeasy mini kit (Qiagen) and quantified using a Nanodrop ND-1000 spectrophotometer (Thermo Scientific). Complementary DNA was synthesized using the RevertAid H Minus First Strand complementary DNA synthesis kit (Fermentas). Sybr green quantitative polymerase chain reaction was performed for different key osteogenic and chondrogenic markers (Sox9, Col1, RunX2, OCN, OPN, OSX and BSP (Chai *et al.* 2012c)) and compared to HPRT (HPRT-F, 5'-TGAGGATTTGGAAAGGGTGT-3'; HPRT-R, 5'-GAGCACACAGAGGGCTACAA-3'). The PCR reaction was cycled in a Rotor-Gene sequence detector (Qiagen) as follows: 95 °C for 3 min, 40 cycles of 95 °C for 3 s and 60 °C for 60 s. Differences in gene expression were determined relatively in comparison to HPRT and shown as $2^{-\Delta CT}$.

For the constructs cultured with or without bioinstructive mineralisation medium for 21 days the expression of Sox9, OCN, OPN and OSX was determined. Differences in gene expression were shown relative to HPRT expression and to the static control ($2^{-\Delta\Delta CT}$).

6.3.6. Contrast-enhanced nanofocus computed tomography (CE-nanoCT)

CE-nanoCT was performed on two random, representative constructs for each time point and culture condition as described earlier (Papantoniou *et al.* 2014b). The constructs were fixed in 4% paraformaldehyde (Sigma) for two hours and stored in PBS prior to analysis. Hexabrix® 320 (Guerbet) was used as a contrast agent to visualize the neo-tissue formed in the construct (Papantoniou *et al.* 2014b). As the Hexabrix® is an equilibrium contrast agent it will equally infiltrate all non-negatively charged tissues and thereby enable the visualization of the radio-transparent neo-tissue in the opaque Ti6Al4V structure.

A Phoenix NanoTom S (GE Measurement and Control Solutions) with a 180 kV/15 W high-performance nanofocus X-ray tube was used to perform the CE-nanoCT. A tungsten target was operated at a voltage of 90 kV and a current of 170 µA. An aluminum and copper filter, both 1 mm thick, were used to reduce beam hardening and metal artefacts. The exposure time was 500 ms, a frame averaging of 1 and image skip of 0 were applied, resulting in a scanning time of 20 min. The reconstructed images had an isotropic voxel size of 3.75 µm.

6.3.7. 3D visualization, image processing and analysis

CTAn (Bruker micro-CT) was used for image processing as described by Papantoniou *et al*., 2013b. Briefly, the neo-tissue was separated from the background noise and the scaffold using a 2-level Otsu thresholding method (Otsu 1979), resulting in a greyscale image containing 3 fractions, respectively background, neo-tissue and scaffold material. To analyze the volume of the Ti6Al4V scaffolds the resulting greyscale dataset was thresholded to obtain binary images representing the scaffold. In order to subsequently reduce the influence of the partial volume effect, edge effects and metallic artefacts introduced by the presence of the Ti6Al4V scaffold while analyzing the neo-tissue volume, the binarised images for the scaffold were dilatated by two voxels and subtracted from the region of interest for further analysis. The neo-tissue fraction within the new region of interest was then binarised and the noise was removed by removing black speckles smaller than 500 voxels and white speckles smaller than 2 000 voxels. To solidify the resulting structure, a 'closing' operation (~ 2 voxels) was performed on the resulting images, providing the images used for the 3D analysis of the neo-tissue volume.

6.3.8. Live/Dead assay

A Live/Dead viability/cytotoxicity kit (Invitrogen) was used to evaluate qualitatively cell viability and cell distribution by optical microscopy. For each culture condition two random, representative constructs were imaged of which one was subsequently used for CE-nanoCT and one for DNA measurement and RNA extraction. Constructs were

rinsed with 1 ml PBS after which they were incubated in the staining solution (0.5 µl of a 4mM Calcein AM in anhydrous DMSO solution and 2 µl of a 2mM Ethidium Homodimer in DMSO/H_20 (1:4, v:v) in 1 ml PBS) for 20 min in normal cell culture conditions. The constructs were imaged using a Leica M165 FC microscope.

6.3.9. Alizarin red staining

Constructs cultured for 21 days with normal growth medium or bio-instructive medium were fixed in 4% paraformaldehyde and stored in PBS prior to staining. Staining was performed with a 2% Alizarin Red S (Sigma) solution in water (pH 4.2) for 1 hour at room temperature during continuous gentle agitation. Samples were subsequently rinsed with demineralized water until no additional staining was removed from the constructs after which they were imaged using a stereo microscope (Leica M165 FC).

6.3.10. Statistical analysis

Student t-test was performed to analyze significant differences between groups using Statistica 7 (Statsoft). A p-value < 0.05 was considered significant.

6.4. Results

6.4.1. Shear stress range

CFD was used to determine the initial SS which the fluid exerted on the constructs in order to compare our results with other reports (Grayson *et al.* 2011, Kim *et al.* 2012). Since the scaffold design consists of a repetition of a regularly shaped diamond unit cell (Figure 6.1.A), the calculations were performed for only one unit cell (Truscello *et al.* 2012). Figure 6.1.B-C show a 3D visualization of the SS on a scaffold unit cell and the corresponding histogram of the relative SS distribution within the unit cell. Figure 6.1.D shows the initial average CFD-calculated SS based on the experimentally used flow rates. The obtained distribution could be extrapolated for the other flow rates used since fluid flow remained laminar in the used range.

6.4.2. Proliferation

The use of different flow rates did not significantly influence the DNA content of the constructs after 21 days of dynamic culture in growth medium (Figure 6.2.A). However, analysis of all perfused constructs cultured for 21 days at different flow rates showed that the DNA content of the constructs cultured in perfusion was on average 2.75 ± 0.27 fold increased in comparison with the static control. To get a better understanding of the time-dependent influence on hPDC proliferation of a constant volumetric flow rate in combination with a morphological changing matrix, which resulted in a time dependent increase in SS, the 0.04 ml/min and 4 ml/min flow rate conditions were selected and compared to the static culture for 14, 21 and 28 days. For all time-points the perfused conditions showed a significant increased DNA content in comparison to the static control. However, the static control as well as the perfused conditions did not

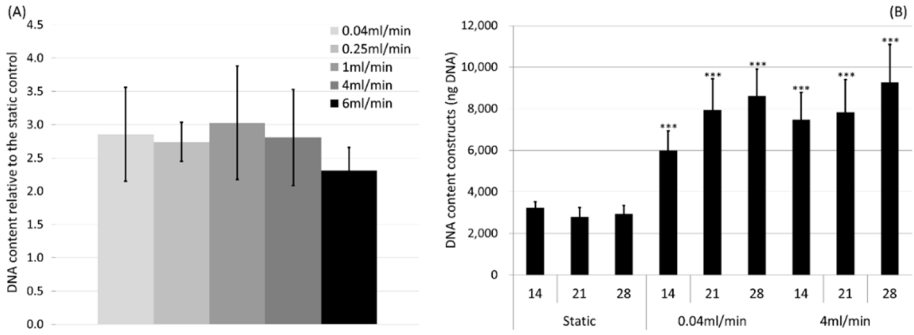

Figure 6.2: DNA content for constructs cultured at different flow rates
(A) DNA content of the constructs relative to the static control after 3 weeks of dynamic culture (n=4 to 6), (B) DNA content of the constructs after 14, 21 or 28 days of culture in a static or perfused (0.04 ml/min and 4 ml/min) system (n=4, ***p<0.001, black bars show standard deviations of the mean).

show any significant time dependent changes from 14 up to 28 days (Figure 6.2.B), although an increasing trend was still observed for the perfused constructs.

Based on our in-house 2D hPDC expansion database an average cell expansion of 2.9 ± 0.65 was determined in comparison to the initial cell density for a 7 day expansion period or 8.4 ± 2.6 in 14 day when cells are replated according to standardized cell expansion protocols (n=20).

6.4.3. Live/Dead staining

Cell distribution at the periphery of the constructs was visualized using the Live-Dead viability/cytotoxicity kit (Figure 6.3). For both the statically cultured and the 0.04 ml/min perfused samples the construct was fully covered with cells after 21 days of culture. For the high flow rate (4 ml/min) the cell coverage of the outer surfaces did not seem to increase over time for the imaged time points. A clearly less dense coverage of the surface was observed in comparison with the two previously described conditions. There were no significant amounts of dead cells observed in any of the examined conditions.

6.4.4. 3D matrix image analysis by CE-nanoCT

CE-nanoCT using Hexabrix® as contrast agents was used to visualize and quantify in 3D the neo-tissue formed in the constructs. Figure 6.4 shows axial 2D cross-sections representative for the entire construct for 0.04 and 4 ml/min as well as the static control for different time points. In the raw images (left 3 columns) the white zones represent the scaffold structure, while the delineated grey features represent the neo-tissue in the constructs. The binarised images (right) show the quantified neo-tissue fraction in white. In correspondence with the Live/Dead staining shown in Figure 6.3, the outer

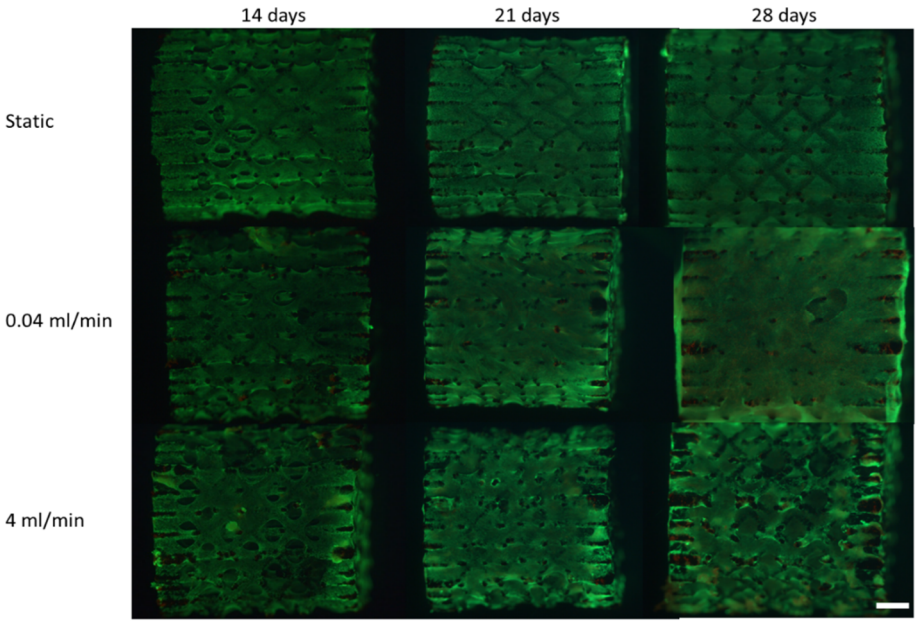

Figure 6.3: Live/dead stainings for constructs cultured at different flow rates
Live/Dead staining of constructs for different culture regimes and durations. The green fluorescent dye shows all the living cells while the red dye visualises the nuclei of the dead cells. Scale bar is 1mm

surface of the statically cultured constructs was nearly completely covered with cell-matrix after 14 days, which is visible as a thin line with a lighter shade of grey on the images in Figure 6.4 as indicated with the arrows. Increasing the static culture duration did not result in a significant increase in cell-matrix volume for these constructs. The perfusion cultured constructs showed that the morphology of the cell-matrix formed was influenced by the culture condition. Instead of forming a cell sheet on the outer edges of the construct as was the case for the static control, cell-matrix was formed throughout the entire scaffold resulting in a much denser and more filled construct as was also observed by DNA analysis (Figure 6.2.B). In both the 0.04 ml/min and 4 ml/min perfused culture the Hexabrix® based images showed that the cell-matrix was gradually filling up the available space in the construct.

As reported earlier, the amount of cell-matrix present in the statically cultured constructs was too low to be quantified (Papantoniou *et al.* 2014b). As shown in Figure 6.4 the neo-tissue developed in these constructs was fibrous in appearance and was only located in thin strands (average diameter of about 5 µm as determined with DataViewer, Bruker MicroCT) at the outer edges of the constructs. Although most of these structures can be visually discriminated in the CE-nanoCT images, the limited contrast difference between the stained neo-tissue and the background did not allow to accurately segment both from each other, resulting in an erroneous quantification of the neo-tissue volume. Therefore, quantitative analysis of the cell-matrix volume was performed only on the

perfused constructs. In Figure 6.5, the relative filling volume, determined using Hexabrix® as a contrast agent, was normalized to DNA content. For the high flow rate, a stronger increase after 21 days of culture was observed compared to the low flow rate where this increase was only observed after 28 days indicating a difference in matrix deposition kinetics. At the final time-point however, no differences in deposited matrix per cell was present.

6.4.5. Gene expression analysis

Finally gene expression analysis was performed to assess the influence of the different culture conditions on cell differentiation (Figure 6.6). For the statically cultured constructs a significant down regulation of the Col1 expression was observed in function of time. The 14 and 21 day expression of Col1 in the perfused conditions was

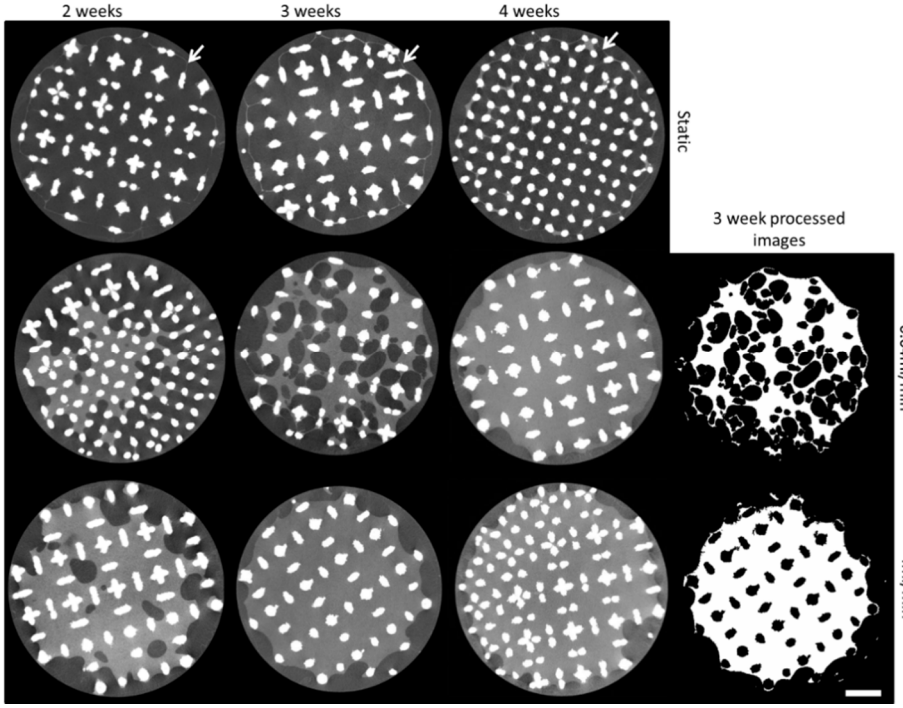

Figure 6.4: 2D CE-nanoCT based slices of constructs cultured under different conditions
Representative 2D CE-nanoCT cross-sectional images stained with Hexabrix® of the constructs cultured at different conditions and their corresponding processed images for 3 weeks of perfusion culturing. White arrows indicate cell-matrix in the static conditions. Scale bar is 1mm.

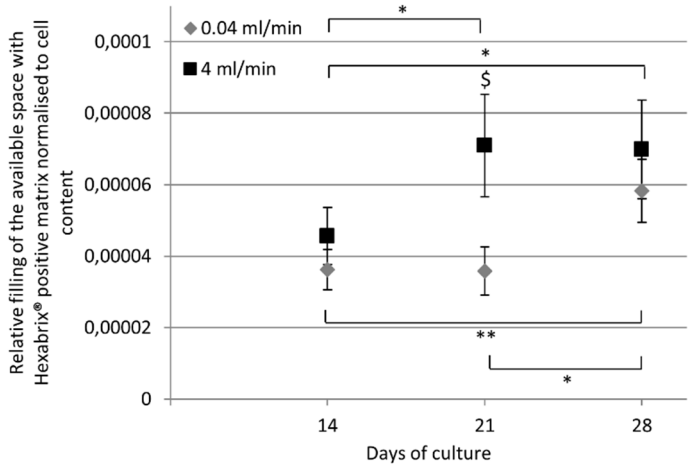

Figure 6.5: CE-nanoCT based filling of the constructs.
Relative filling of the scaffold determined with Hexabrix® normalized to cell content, $ indicates a significant difference between the two flow rates ($p<0.05$), *: $0.05>p>0.01$, **: $0.01>p>0.001$

also down-regulated in comparison to the static constructs but this difference was no longer present at the 28 day time point. For RunX2 the expression remained stable in function of time for the static constructs and no differences were observed between the static and perfused conditions. For the low flow rate a significant increase was observed between day 14 and 28. For the high flow rate this increase was observed at the 21 day time point, although it was no longer present at the final day 28 time point. In the case of OCN no significant differences were observed between the static controls and both perfused conditions. At day 14 a higher expression was observed for the low flow rate in comparison to the high flow rate but this difference was no longer observed at later time points. Except for the low flow rate at day 14 no differences were observed in OPN expression between the static control and the perfused conditions. Although a time dependent increase was observed for the low flow rate, OPN expression was significantly higher for the high flow rate in comparison to the low flow rate. BSP showed a time-dependent increase in both perfused conditions resulting in a significantly higher expression in comparison to the static control at day 28. No significant differences between the perfused conditions were observed. Sox9 expression decreased significantly over time in the static control. In both perfused conditions Sox9 expression was significantly lower at day 14 and 21 but this difference was no longer observed at day 28. OSX expression showed a time dependent decrease in the static control. Except at day 14 no differences were present between the static control and the low flow rate condition. The high flow rate showed a significantly higher expression in comparison to the low flow rate (all time points) and to the static control (after 21 and 28 days).

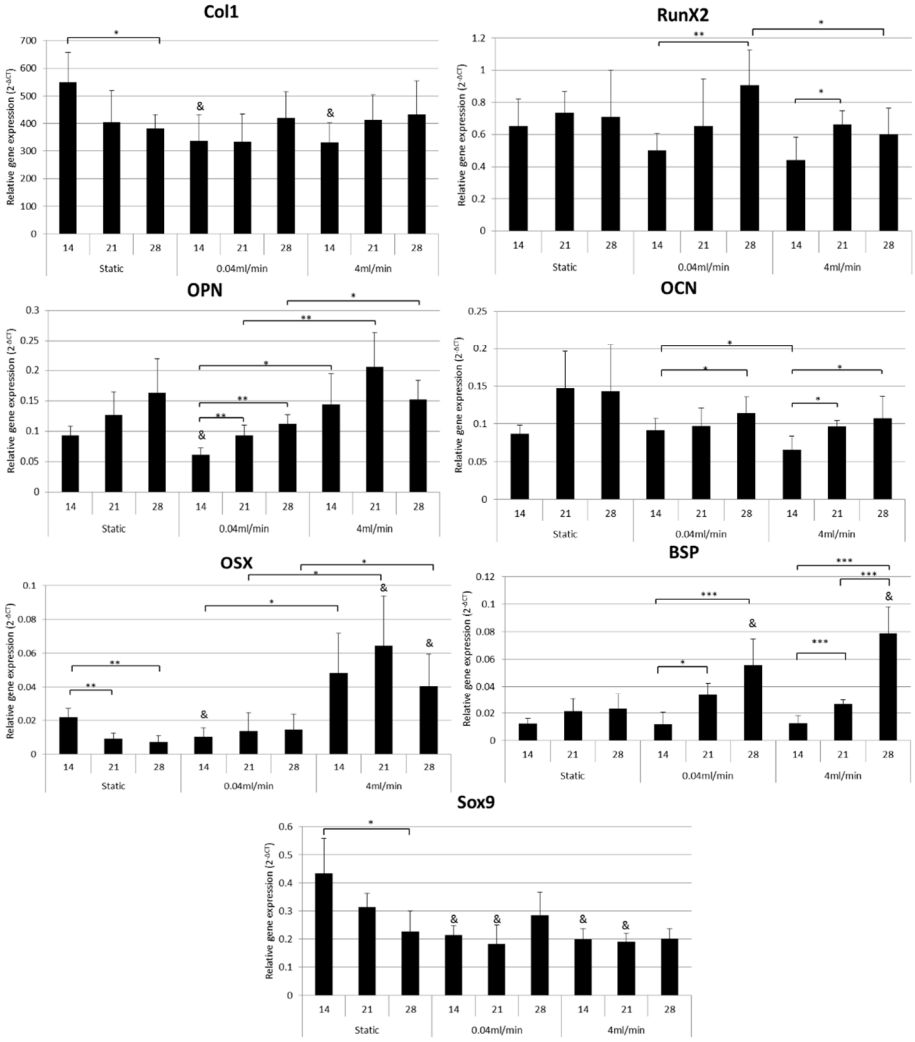

Figure 6.6: Gene expression profile for constructs cultured at different conditions. Gene expression of the cultured constructs by means of RT PCR for Col1, RunX2, OPN, OCN, BSP, Sox9 and OSX relative to HPRT. & indicates a significant difference with the corresponding time point of the static control ($p<0.05$, *; $0.05>p>0.01$, **; $0.01>p>0.001$, ***) (n=4).

6.5. Discussion

Perfusion bioreactor systems show great promise as a tool for automated 3D cell expansion and their use will be essential for the clinical implementation of current tissue engineering and regenerative medicine strategies (Martin *et al.* 2010, Fisher *et al.* 2011, Salter *et al.* 2012a). Therefore, it is imperative to understand the influence of the process environment on the behavior and properties of the cell populations expanded in these systems and define suitable operating conditions which support cell expansion while maintaining a progenitor cell phenotype. The present study used hPDCs seeded on a Ti6Al4V scaffold in a perfusion bioreactor system to determine its potential for cell expansion by evaluating the influence of flow-induced SS on the proliferation, differentiation and extracellular cell-matrix deposition in the absence of additional differentiation-inducing stimuli such as osteogenic inductive medium.

3D perfusion bioreactor culture has been extensively used for the production of bone TE constructs and has shown to significantly increase proliferation, differentiation and mineralised matrix deposition in comparison to static controls (McCoy *et al.* 2010, Fisher *et al.* 2011). Additionaly, SS dependent increases in proliferation and mineralisation have been reported for MSCs in combination with osteogenic medium (Bancroft *et al.* 2002, Cartmell *et al.* 2003, Sikavitsas *et al.* 2003, McCoy *et al.* 2010). Additionally, the use of intermittent SS exerted on the a construct developing in normal growth medium resulted in the significant induction of an osteogenic phenotype in comparison to the continuous shear conditions, although no comparison with a static control was made here (Liu *et al.* 2012). In correspondence with this literature data, our work showed that perfusion significantly increased the cell number on the Ti6Al4V scaffolds in comparison to the static control (Figure 6.2.A), as both dynamic conditions resulted in a significant increase in DNA content in comparison to the static control for all time points. The enhanced mass transport present in a perfusion setup in comparison to the static setup will provide an optimal nutrient supply to the entire construct, thereby enabling all the cells in the construct to proliferate under more optimal conditions. This was confirmed with the CE-nanoCT which shows that the developed neo-tissue is only present at the outer edges of the statically cultured constructs while in both perfused conditions the neo-tissue is deposited uniformly throughout the entire construct. As the use of a higher flow rate did not significantly improve the nutrient supply to the developing constructs, the absence of correlated changes in proliferation could be explained, as also reported earlier for similar systems using osteogenic medium supplements (Sikavitsas *et al.* 2003, Dai *et al.* 2009, Grayson *et al.* 2011).

An average cell density increase of 3.6 ± 0.6 times, with respect to the static constructs or an 8.4 ± 1.7 fold increase in relation to the initial cell density were observed after 28 days (Figure 6.2.B). These expansion rates were not significantly different from those observed in the standard 2D culture at the 14 day time point for the high flow rate (8.4 ± 2.6 for 2D vs 7 ± 1.2 in the perfusion system), without the need for replating. For later time points the proliferation rate, based on the DNA measurement, in the 3D perfusion bioreactor setup decreased, due to the gradual filling and closing of the open spaces in the construct as shown in Figure 6.4 In 2D culture systems a decrease in proliferation is also observed when cells are not replated prior to confluence, but for

2D static culture systems this phenomenon already occurs after 8 to 10 days resulting in an average cell expansion of 4 to 5 times. This shows that the perfusion bioreactor system performs at least as efficient as a standard 2D sub-culture system with regard to cell expansion, but not requiring manual intermediate trypsinisation and replating steps.

Besides conventional, manual, 2D cell expansion, the use of micro carriers is often mentioned to be a promising technique for automated cell expansion despite the absence of a real 3D environment (dos Santos *et al.* 2011b, Hewitt *et al.* 2011, Goh *et al.* 2013). In these systems 7 to 20 fold increases in cell number have been reported after already 7 days of cell expansion resulting in significantly higher expansion rates in comparison to the 3D perfusion bioreactor system used for this work. However, the maximal cell density that could be obtained in micro-carrier based expansion systems is on average between $2*10^5$ and $8*10^5$ cells/cm³ (dos Santos *et al.* 2011b, Hewitt *et al.* 2011, Goh *et al.* 2013) while, based on the DNA content and assuming an average of 8.9 pg DNA/cell as reported earlier (Zhou *et al.* 2013), the 3D perfusion system used in this work reached a cell density of 5 to $6*10^6$ cells/cm³. This demonstrates that a higher cell number per volume unit can be obtained, thereby indicating their high cell expansion potential per volumetric unit. Additionally, current protocols for the 3D perfusion bioreactor system have not been optimised yet for cell expansion. Reducing the initial cell seeding density in the system from $7*10^5$ cells/cm³ or 17 100 cells/cm² to the densities which are currently used for micro carrier expansion (10 to 20 fold lower (Hewitt *et al.* 2011)) could further increase the yield of the 3D perfusion bioreactor culture.

Live/dead staining of the constructs showed that the flow rate had no significant influence on the cell viability in the outer layers of the formed neo-tissue (Figure 6.3). The differences in DNA content between static and dynamically cultured constructs could not be visually confirmed. However, microscope-based live/dead staining is a line-of-sight visualization technique, allowing only observation of the peripheral part of the scaffold, hence a novel imaging technique, CE-nanoCT was used in order to monitor cell growth and provide quantitative volumetric information regarding cell and extracellular matrix distribution throughout the entire volume of the scaffold (Figure 5.4)(Papantoniou *et al.* 2014b). CE-nanoCT images showed a time dependent 3D filling of the scaffold void volume. For the static constructs cell-matrix was only situated on the outer edges of the construct as reported by other groups using destructive 2D based techniques such as histology (Ishaug *et al.* 1997, Bancroft *et al.* 2002, Sikavitsas *et al.* 2003). In function of time not only was more cell-matrix deposited but also the amount of cell-matrix deposited per cell, as calculated based on the CE-nanoCT based images and the measured DNA content, increased for both flow rates as observed by the Hexabrix® based images (Figure 6.4, Figure 6.5). As higher SS has been reported to result in increased matrix deposition (Jaasma *et al.* 2008, Grayson *et al.* 2011), the increase in SS present in the developing constructs due to the filling of the available volume could explain the observed increase in matrix deposition per cell. Despite the difference in matrix deposition kinetics no differences in matrix deposition were observed for the different flow rates at the final time-point.

In this work initial SS values exerted on the developing constructs, as determined by CFD, ranged between $5.59*10^{-4}$ and $8.38*10^{-2}$ Pa. Although in this range, enhanced osteogenic differentiation and collagen production has been previously reported for MSCs in combination with osteogenic medium (McCoy *et al.* 2010) its influence in normal growth medium is not known. The SS values determined using CFD were based on the empty Ti6Al4V scaffold geometry. However, as observed by the experimental data, cell and matrix growth gradually filled up the internal volume of the Ti6Al4V scaffold, thereby significantly altering the flow environment. The increase in cell-matrix volume will reduce the volume available for the fluid to flow through, thereby increasing the flow rate of the medium and the correlated SS. Calculated SS values will therefore more closely represent those SS values that hPDCs will experience during the initial period of the bioreactor culture and serve mainly as a reference for comparison with literature data in which a similar approach was used (Bancroft *et al.* 2002, Sikavitsas *et al.* 2003, Kim *et al.* 2012, Liu *et al.* 2012). In future work the neo-tissue filling determined via CE-nanoCT as function of culture duration may be used as input for CFD modeling to obtain dynamic SS information to which the cells are actually exposed during the expansion process.

To further assess the influence of flow rate on the hPDCs the expression of a range of genes was analyzed to determine cell commitment towards a specific lineage (Figure 6.6). Results showed that Sox9 was significantly down-regulated for both perfusion conditions at day 14 and 21 in comparison to the static control, but that this was no longer the case at day 28 due to the gradual decrease observed in the static control. Sox9 expression was already shown to be increased in a perfusion system in chondrogenic medium (Tigli *et al.* 2011) but, in correspondence with our findings, there were no reports of increased chondrogenic differentiation in the absence of biochemical inducers in a perfusion system. Therefore no additional chondrogenic markers were evaluated in this work. Different osteogenic markers, such as Col1, RunX2, OPN and OCN, showed limited time-dependent changes in expression. In accordance to previously reported data (Bjerre *et al.* 2008, Kim *et al.* 2012), certain flow-rate-dependent changes in expression were observed, but perfusion as such did not have a significant influence on the expression of these key osteogenic markers as no differences between the static control and the perfused conditions were present (Figure 6.6). Additionally, the limited observed time dependent changes in expression of these markers are negligible in comparison to what was reported earlier for induced osteogenic differentiation for this cell type (Chai *et al.* 2011). Despite that no significant changes were observed in the expression of ECM related genes such as Col1 and OCN significant differences in the ECM deposition per cell were observed between the different conditions. The culture of cells under SS has earlier been shown to potentially induce changes in posttranscriptional regulation of certain ECM proteins (Bjerre et al. 2008) and differences in the incorporation of secreted matrix proteins (Grayson et al. 2011). This indicates that SS can significantly influence the composition of the deposited neo-tissue in a 3D culture system without influencing gene expression, thus potentially explaining the differences in neo-tissue volume deposited in static versus the perfused conditions.

BSP on the other hand showed, compared to the static control, an 8-fold time-dependent increase in expression in both perfused conditions. However, as shown by Grayson *et al*, 2011 the combination of perfusion and osteogenic medium can result in a 100-fold increase in BSP expression after one week and even a 1 000-fold increase after 5 weeks of perfusion culture using MSCs (Grayson *et al.* 2011), indicating that the increase observed in our study is limited for both perfused conditions. For OSX, an important early osteogenic transcription factor (Kim *et al.* 2012), a flow rate dependent increase in expression was observed. In the normal osteogenic differentiation cascade of events this increase would be preceded by an increase in RunX2, of which OCN is a downstream target, and followed by an increased expression of BSP and OCN (Lian *et al.* 2006, Franceschi *et al.* 2007, Kim *et al.* 2012). This cascade of events was, however, not observed in the studied system. Although the expected initial increase of RunX2 in osteogenic differentiation could have occurred at an earlier time point and a subsequent increase in BSP expression was present no differences in OCN expression were detected. In the absence of the OCN increase, the increased OSX expression could be explained by cell lineage commitment rather than to full osteogenic differentiation.

This was confirmed by comparing the expression of Sox9, OCN, OPN and OSX for constructs cultured for 21 days using normal growth medium and bio-instructive mineralization medium (Figure 6.7.A). Although a significant lower Sox9 expression was detected in the normal constructs after 21 days, a 100-fold stronger decrease in expression was present in the induced constructs. For the OCN, OPN and OSX expression respectively a 12-, 90- and 6-fold increase in expression was detected for the induced constructs in comparison with the growth medium cultured. Alizarin red

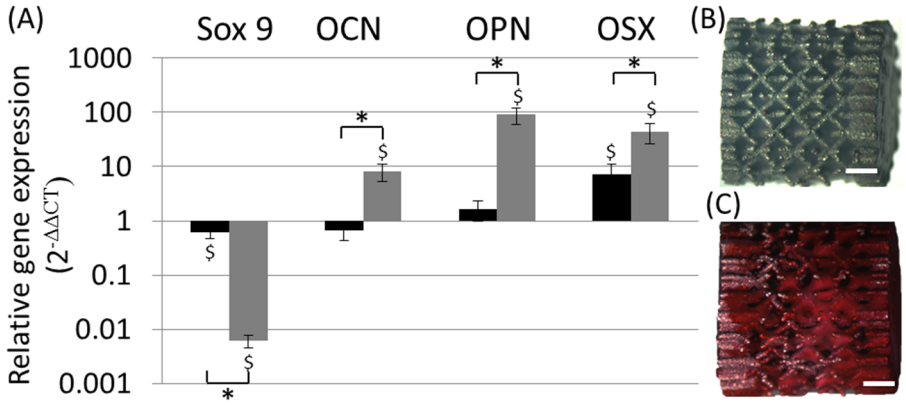

Figure 6.7: Comparison bioreactor cultured constructs in normal and osteogenic medium.
(A) Gene expression of perfusion bioreactor cultured constructs with normal growth medium (Black) and mineralization medium (Grey) for 21 days relative to HPRT and to the static control (ΔΔCT) by means of RT PCR for Sox9, OCN, OPN and OSX. $ shows relative to the static control. $P<0.05$, $n=3$ (B and C) Alizarin red staining of respectively normal growth medium and mineralization medium cultured constructs after 21 days of culture. Scale bars are 1 mm

staining visually confirmed the presence of a mineralized matrix in the induced constructs (Figure 6.7.C), while this was not detected in the growth medium constructs (Figure 6.7.B). This further confirmed that expansion of the MSC like hPDC cell population in a perfusion bioreactor system does not result in significant osteogenic differentiation nor in an associated mineralized matrix deposition although there are indications of osteogenic lineage commitment as shown by the increased OSX and BSP expression. In conclusion, we can state that, for our experimental set-up, perfusion bioreactor culture resulted in expansion rates similar to those obtained in different validated cell expansion systems. Additionally, the system did not induce significant changes in the expression pattern of the osteogenic and chondrogenic markers analyzed. Although small differences in the expression of certain markers were observed between different flow rates, these were limited in comparison to the reported increases in expression when using osteo- or chondro-inductive media in both static and perfused conditions as well as to changes in gene expression in the constructs cultured with bio-instructive mineralization medium. Perfusion did, however, significantly increase cell proliferation and resulted in flow rate-dependent changes in matrix deposition kinetics. These results indicate the potential of perfusion bioreactor facilitated stem cell expansion.

6.6. Acknowledgements

MS is supported by a Ph.D. grant of the Agency for Innovation by Science and Technology (IWT/ 111457). IP is funded by the ENDEAVOUR project G.0982.11N of the Research Foundation Flanders (FWO Vlaanderen). GK acknowledges support by the European Research Council under the European Union's Seventh Framework Program (FP7/2007-2013)/ERC grant agreement n°279100. The X-ray computed tomography images have been generated on the X-ray computed tomography facilities of the Department MTM of the KU Leuven, financed by the Hercules Foundation (project AKUL 09/001: Micro-and nano-CT for the hierarchical analysis of materials) This work is part of Prometheus, the Leuven Research & Development Division of Skeletal Tissue Engineering of the KU Leuven: www.kuleuven.be/prometheus

Chapter 7.
Bioreactor-based online recovery of human progenitor cells with uncompromised regenerative potential: a bone tissue engineering perspective

Maarten Sonnaert, Frank P. Luyten, Jan Schrooten*, Ioannis Papantoniou*

* Shared senior authorship

Resubmitted after minor revisions

7.1. Abstract

The use of a 3D perfusion culture environment for stem cell expansion has been shown to be beneficial for maintenance of the original cell functionality but due to several system inherent characteristics such as the presence of extracellular matrix, the continued development and implementation of 3D perfusion bioreactor technologies is hampered. Therefore, this study developed a methodology for harvesting a progenitor cell population from a 3D open porous culture surface after expansion in a perfusion bioreactor and performed a functional characterization of the expanded cells. An initial screening showed collagenase to be the most interesting reagent to release the cells from the 3D culture surface as it resulted in high yields without compromising cell viability. Subsequently a Design of Experiment approach was used to obtain optimized 3D harvest conditions by assessing the interplay of flow rate, collagenase concentration and incubation time on the harvest efficiency, viability and single cell fraction. Cells that were recovered with the optimized harvest protocol, by perfusing a 880 U/ml collagenase solution for 7 hours at a flow rate of 4 ml/min, were thereafter functionally analyzed for their characteristics as expanded progenitor cell population. As both the in vitro tri-lineage differentiation capacity and the in vivo bone forming potential were maintained after 3D perfusion bioreactor expansion we concluded that the developed seeding, culture and harvest processes did not significantly compromise the viability and potency of the cells and can contribute to the future development of integrated bioprocesses for stem cell expansion.

7.2. Introduction

As the field of tissue engineering evolves towards clinical applications, the development of well characterized bioprocesses to provide consistent production of tissue engineered (TE) advanced therapy medicinal products (ATMPs) becomes imperative. However, at current, the production of such ATMPs consists of a series of discrete manual unit operations ranging from progenitor cell isolation from donor biopsies, to cell expansion and differentiation to achieve those numbers needed for therapy and functional TE construct development. Although preliminary studies using these manual methodologies have demonstrated the potential of TE ATMPs for in vivo tissue regeneration (Roberts *et al.* 2011, Chai *et al.* 2012b), closed and integrated bioprocesses should be developed to reduce the dependence on operator expertise and minimizing risk of contamination. The use of bioreactors is considered to be essential for the successful clinical introduction of novel ATMPs in these aspects (Schneider *et al.* 2010, Salter *et al.* 2012b). Next to contributing to the development of automated, controlled and monitored processes, bioreactors also enable the use of 3D cell culture substrates which were hypothesized to have beneficial effects on the characteristics of the expanding cell population such as enhanced maintenance of the original cell phenotype (Banfi et al. 2000, Martin et al. 2004, Scadden 2006, Wagner et al. 2008, Haycock 2011).

The use of perfusion bioreactors, incorporating 3D open porous inert and rigid scaffolds as 3D culture substrate for cell expansion, has been associated with significant advantages concerning the identity and potency of the resulting cell population

(Papadimitropoulos *et al.* 2014a). In previous studies the ability of cells to grow into the third dimension leading to 3D culture surface with filled pores, has been demonstrated (Sonnaert et al. 2014a). During 3D growth, cells secrete extracellular matrix (ECM) depending, amongst others, on the flow rate employed for cell culture (Papantoniou et al. 2014b, Sonnaert et al. 2014a). Even though the presence of a supportive ECM has been shown to possess significant advantages concerning maintenance of the potency of the expanded cells (Chen et al. 2007, He et al. 2009, Li et al. 2011, Pei et al. 2011), cell recovery is significantly impaired, requiring dedicated process development and optimization.

Detachment or dissociation of cells from the culture surface with subsequent retention of cell quality is therefore equally important as cell attachment and proliferation, given that the product of interest in cell therapy applications is the cell itself (Abbasalizadeh et al. 2013, dos Santos et al. 2013). Despite reports of adverse effects on cell characteristics (Wersinger et al. 2004, Mitalipova et al. 2005, Brown et al. 2007), trypsin is one of the most widely used reagents for cell recovery and was already used for the recovery of cells from microcarrier based expansion systems (dos Santos et al. 2011b, Rafiq et al. 2013, Nienow et al. 2014) as well as for the digest of primary tissues, although often in combination with other enzymes which specifically target the collagen containing fraction of the ECM (Jakob *et al.* 2003, Papadimitropoulos *et al.* 2014a). Additionally, various optimization studies for collagenase-based digestion of primary tissues such as cartilage are available indicating the feasibility of a trypsin free approach although no detailed reports are available regarding the recovery of cells from 3D culture surfaces (Oseni et al. 2013, Centola et al. 2014, Lau et al. 2014).

Functional characterization of the expanded and recovered cell population is imperative to assess the relevance of the developed processes. Current approaches focus mainly on the in vitro characterization which enables the potential classification of the expanded population as being an adult mesenchymal stromal stem cell population (Eibes *et al.* 2010, Bianco *et al.* 2013, Rafiq *et al.* 2013, Zhou *et al.* 2013a, Nienow *et al.* 2014, Papadimitropoulos *et al.* 2014a, Sonnaert *et al.* 2014a). However, the final goal of these expansion processes is to obtain a progenitor cell population which can contribute to the development of an in vivo functional tissue. Therefore not only the post expansion characterization but also the functional *in vivo* assessment of the expanded cell population is critical (Bianco *et al.* 2013).

In this work we expanded human periosteum derived cells (hPDCs) in a 3D flow-through perfusion bioreactor (Sonnaert *et al.* 2014a) and monitored their growth non-destructively using the Presto Blue metabolic assay (Sonnaert *et al.* 2014b). Upon confluence, as was confirmed by contrast enhanced X-ray nano-computed tomography (CE-nanoCT), a range of cell recovery reagents was assessed. Subsequently the most efficient harvest reagent was selected and for the harvest protocol was further optimized for the reagent concentration, flow rate used for detachment and harvest time leading to maximal cell viability and harvested single cell yield based on a Design of Experiment (DoE) approach. Finally, the functionality of the expanded progenitor cell population was defined using a combination of *in vitro* and *in vivo* proliferation, differentiation and bone forming assays.

7.3. Materials and Methods

7.3.1. Human periosteum-derived cells

hPDCs were isolated from periosteal biopsies obtained from 4 different donors (age 11, 13, 14 and 17, equal distribution of gender) as described previously and pooled for further use (Eyckmans et al. 2006a). This procedure was approved by the ethics committee for Human Medical Research KU Leuven (ML7861). Patient informed written consent was provided by the legal guardian. hPDCs were expanded in Dulbecco's modified Eagle's medium with high-glucose (Life Technologies) containing 10% fetal bovine serum (FBS, Gibco), 1% sodium pyruvate (Life Technologies) and 1% antibiotic–antimycotic (100 units/mL penicillin, 100 mg/mL streptomycin, and 0.25 mg/mL amphotericin B; Life Technologies), further mentioned as culture medium (CM). The cells were seeded at 5,700 cells/cm² and passaged at 80%–90% confluency. Cell expansion was performed in standard cell culture conditions (relative humidity: 95%, 5% CO2, 37°C).

7.3.2. Ti6Al4V scaffolds

For 3D perfusion bioreactor cell expansion, additive manufactured Ti6Al4V scaffolds (Ø = 6 mm, h = 6 mm) (Van Bael *et al.* 2011, Pyka *et al.* 2012) were used as described before (Papantoniou *et al.* 2014a, Papantoniou *et al.* 2014b, Sonnaert *et al.* 2014a, Sonnaert *et al.* 2014b). The total volume of the scaffolds was 166 ± 3 mm³, the available volume 130 ± 5 mm³ and the available surface 7.5 ± 0.6 mm² as determined with µCT (Kerckhofs *et al.* 2013a). Scaffolds were cleaned and prepared for experiments as described before (Papantoniou *et al.* 2014a, Papantoniou *et al.* 2014b, Sonnaert *et al.* 2014a, Sonnaert *et al.* 2014b).

7.3.3. Scaffold seeding and culture

Prior to the 3D culture experiments cells were harvested at passage 6 using Triple Express (Life Technologies) and drop-seeded onto the scaffolds at a final density of 120,000 cells per scaffold (Papantoniou et al. 2014a, Papantoniou et al. 2014b, Sonnaert et al. 2014a, Sonnaert et al. 2014b). Scaffold-cell constructs were incubated overnight in standard culture conditions resulting in an initial cell density of 17,100 cells/cm² or 700,000 cells/cm³.

For cell expansion, seeded constructs were inserted in an in-house developed perfusion bioreactor system consisting of an interconnected bioreactor chamber and a medium reservoir (Papantoniou et al. 2014a, Papantoniou et al. 2014b, Sonnaert et al. 2014a, Sonnaert et al. 2014b). A total volume of 10 ml CM was perfused at a constant flow rate of 1 ml/min. CM was refreshed every two days by attaching a new medium reservoir containing 10 ml fresh CM.

7.3.4. Presto Blue measurement

To monitor cell growth, a Presto Blue (PB, Life Technologies) measurement was performed every second day on quadruplicate samples as described earlier for a period of 17 days (Sonnaert *et al.* 2014b). 5 ml of a 9% solution was perfused for 2 hours at

1 ml/min after which three 100 µl samples were taken from each unit and the fluorescent signal was measured with a Synergy HT Multi-Mode Microplate Reader (Biotek) using an excitation wavelength of 544 nm and an emission wavelength of 590 nm (Sonnaert *et al.* 2014b). The measured fluorescent signal was expressed as arbitrary fluorescent units (FU).

7.3.5. Calcein Acetoxymethyl staining

A Calcein acetoxymethyl (AM) staining was used to qualitatively visualize the distribution of live cells by optical fluorescent microscopy. At day 3, 8 and 15, representative cell loaded scaffolds (based on PB measurements) were imaged. Constructs were rinsed with 1 ml phosphate buffered saline (PBS) after which they were incubated in the staining solution (0.5 µl of a 4 mM Calcein AM in anhydrous dimethylsulfoxide solution, Life technologies) for 20 min in normal cell culture conditions. The constructs were imaged using a Leica M165 FC microscope.

7.3.6. Contrast enhanced nano computed X-ray tomography of cell expansion constructs

Cell - ECM structure developed during the expansion (further mentioned as neo-tissue) was visualized using contrast enhanced CE-nanoCT (Kerckhofs *et al.* 2013b, Papantoniou *et al.* 2014b, Sonnaert *et al.* 2014a). Prior to staining constructs were fixed in a 4% paraformaldehyde solution (Sigma) for 2 hours. To enable visualization of the neo-tissue, constructs were stained with a 60% Hexabrix® 320 solution (Guerbet) for 20 min (Papantoniou *et al.* 2014b, Sonnaert *et al.* 2014a). A Phoenix NanoTom S (GE Measurement and Control Solutions) with a 180 kV/15 W high-performance nanofocus X-ray tube was used with a tungsten target, which was operated at a voltage of 90 kV and a current of 170 µA. An aluminum and copper filter, both 1 mm thick, were used to reduce beam hardening and metal artefacts. The exposure time was 500 ms, a frame averaging of 1 and image skip of 0 were applied, resulting in a scanning time of 20 min. The obtained radiographic images were reconstructed using Phoenix Datos|X (GE Measurement and Control Solutions). The reconstructed images had an isotropic voxel size of 3.75 µm (Papantoniou *et al.* 2014b, Sonnaert *et al.* 2014a).

7.3.7. Cell harvest

For the use of the StemPro® Accutase® Cell Dissociation Reagent (Life Technologies) or 0.05% Trypsin – ethylenediaminetetraacetic acid (EDTA) solution (Life Technologies) the bioreactor circuits were first rinsed with Phosphate buffered saline (PBS, Life Technologies) to remove all FBS remnants. Cell harvest using the Accutase® solution was performed at a flow rate of 1ml/min up to one hour at 37°C or up to 6 hours at room temperature (incubation times and temperatures according to the manufacturer's instructions for cell recovery and tissue dissociation). The trypsin solution was applied up to 40 min at 37°C at 1ml/min. For the collagenase IV solution (Life Technologies) a 440U/ml solution in CM was perfused at 1ml/min up to 13 hours at 37°C as was also performed for the initial digest of the periosteum (Eyckmans *et al.* 2006b). Harvest efficiency was determined based on DNA measurements on the scaffolds after harvest and on the resulting cell suspension as described further.

Table 7.1: Experimental conditions used for optimization of Collagenase IV harvest of the expanded cells according to a 3-parameter, 3-level fractional factorial design.

Concentration (U/ml)	Incubation time (hrs)	Flow rate (ml/min)
440	3	0.04
880	5	0.04
660	7	0.04
880	3	0.4
660	5	0.4
440	7	0.4
660	3	4
440	5	4
880	7	4

Scaffolds that did not receive any harvest treatment were used as a control. All conditions were performed in triplicate on constructs expanded for 13 days.

A DoE approach was used to further optimize the cell harvest procedure using the Collagenase IV solution. In order to determine the influence of incubation time, concentration and flow rate on the cell yield and the viability of the harvested cell population a 3-level, 3-parameter fractional factorial design was used resulting in 9 combinations of the aforementioned parameters as shown in Table 7.1. The assessed range of flow rates was selected based upon pervious work where we showed that no significant influence of the fluid flow could be observed on cell proliferation between 0.04ml/min and 4ml/min (Sonnaert *et al.* 2014a). As the preliminary screening experiment for Collagenase IV showed no significant increase in cell yield after 7 hours this was selected as the maximal incubation time. Additionally, no negative influence of the used setup was observed on cell viability. Therefore, the assessed preliminary concentration was selected as the low value for the DoE to achieve potential higher yields using shorter incubation times using higher concentrations. Harvest efficiency was determined both based on DNA measurements and by using a hemocytometer in combination with trypan blue staining, thereby enabling to determine the viability of the resulting cell suspension. Each measurement was performed on triplicate samples obtained from 13 day cultured constructs.

For the functional characterization of the expanded cell population the optimal harvest condition as determined by the DoE was used. A total of 20 expansion constructs was cultured for 13 days and resulting cell suspensions were pooled for functional characterization of the harvested cells.

7.3.8. DNA measurement

The DNA content of samples was determined using a highly quantitative and selective DNA assay (Quant-iT^{TM} dsDNA HS kit, Life Technologies). The constructs were

rinsed with PBS and lysed in 350 µl RLT lysis buffer (Qiagen) supplemented with 3.5 µl β-mercaptoethanol after which the lysed samples were vortexed for 60 s and stored at -80°C. Prior to analysis, the samples were thawed at room temperature and spun down for 1 min at 13,000 rpm. 10 µl of the sample was diluted in 90 µl milliQ water after which the DNA content was quantified with a Qubit® Fluorometer (Life Technologies) (Chen *et al.* 2012). For measurement of DNA content of the cell suspensions resulting from the harvest procedure the cells were rinsed with PBS and re-suspended in 350 µl RLT lysis buffer supplemented with 3.5 µl β-mercaptoethanol. Further processing for the DNA measurements was identical as described for the constructs.

7.3.9. Proliferation assay

In order to determine the proliferative capacity of cells expanded in the 3D perfusion bioreactor cells were seeded at a density of 10,000 cells/well in a standard 24-well cell culture plate (Nunc) and cultured for 6 days in CM (n=4). Proliferation was monitored daily using the Presto Blue metabolic assay by replacing the growth medium with 0.5ml of a 9% Presto Blue solution and incubating for 2 hours. The resulting fluorescent signal was subsequently measured as described before. 2D expanded cells were used as control.

7.3.10. Osteogenic differentiation assay

Both 2D and 3D expanded cells were seeded at 4,500 cells/cm² in quadruplicate wells and were allowed to proliferate for 2 days prior to adding osteogenic inductive medium (CM supplemented with 100 nM Dexamethasone, 50 µg/ml ascorbic acid and 10 mM β-glycerolphosphate (All from Sigma)) which was subsequently refreshed every two days for 21 days (Roberts *et al.* 2014). Cultures were subsequently rinsed with PBS, fixed with 4% formaldehyde and rinsed with distilled water prior to staining with alizarin red solution (pH 4.2) for 60 min. Non-specific staining was removed by extensive rinsing with distilled water after which the calcium deposits were quantified by dissolving the bound dye with 10% cetylpyridinium chloride (in distilled water) for 60 min and measuring the absorbance of the resulting solution at 570 nm.

7.3.11. Chondrogenic differentiation assay

The chondrogenic differentiation capacity of the 3D and 2D expanded hPDCs was determined based on a micromass assay as described earlier (Roberts *et al.* 2014). Briefly, quadruplicate 10 µl micro-masses containing 200,000 cells each were made in 24-well plates for both 2D and 3D expanded cells and incubated overnight in CM. Subsequently the medium was replaced by chondrogenic inductive medium based on DMEM-F12 (Life Technologies) supplemented with 2% FBS, 1% antibiotic–antimycotic, 1X insulin, transferrin, selenous acid (ITS+) Premix universal Culture Supplement (Corning), 100 nM Dexamethasone, 10 µM Y27632 (Axonmedchem), 50 µg/ml Ascorbic Acid, 40 µg/ml Proline (Sigma) and 10 ng/ml transforming growth factor beta 1 (TGFβ1) (Peprotech) (Roberts *et al.* 2014). Chondrogenic medium was refreshed every 2 days for 7 days after which the micro-masses were rinsed with PBS and fixed with ice cold methanol for 1 hour at 4°C. Subsequent rinsing steps with PBS

and MiliQ water were followed by staining for 1 hour with a 0.1% Alcian Blue solution (in 0.1 M HCl). Non-specific dye was thereafter removed and a 6M guanidine hydrochloride solution was added overnight to dissolve the dye bound to the glycosaminoglycans present and quantification was performed by measuring the resulting absorbance at 620nm.

7.3.12. Adipogenic differentiation assay

2D and 3D expanded cells were seeded at a density of 10,000 cells/cm² in 24-well plates in quadruplicate and incubated overnight in CM. Subsequently medium was replaced by adipogenic inductive medium based on αMEM (Life technologies) supplemented with 10% FBS, 1% antibiotic–antimycotic, 1µ M Dexamethasone, 10 µg/ml human insulin, 100 µM indomethacin and 25 µM 3-Isobutyl-1-methylcanthine (all from Sigma) (Roberts *et al.* 2014). Medium was refreshed every 2 days for a total duration of 14 days after which the cultures were rinsed with PBS and fixed with a 10% formaldehyde solution for 30 min. Plates were subsequently rinsed twice with PBS and dried at room temperature prior to adding the Oil red O staining solution (0.2% Oil Red O in a 60% Isopropanol solution). Samples were stained for 1 hour after which the staining solution was removed, rinsed with PBS to remove non-specific staining and destained for quantification at 492 nm with pure isopropanol.

7.3.13. *In vivo* ectopic implantation

In vivo bone forming capacity was evaluated using an ectopic implantation model (Roberts *et al.* 2011). NuOss™, a porous bone mineral matrix material (ACE surgical Sypply CO), and Bio-Oss®, a bone substitute for regenerative dentistry (Geistlich), were used as a scaffold material. Cylindrical scaffolds with a diameter and height of 3 mm were punched out of the raw material and drop seeded with 1,000,000 2D or 3D expanded cells in a volume of 25 µl (n=3 or 4 respectively for the Bio-Oss® and NuOss™ scaffolds). Scaffolds were incubated overnight at 37°C in 3 ml of CM to allow cell attachment after which they were implanted ectopically in the back at the cervical region and the lower back of female NMRI-nu/nu mice as described previously [2]. Empty scaffolds were implanted as negative control. The total of 21 scaffolds were randomly distributed between the 6 experimental animals and grouped per scaffold type. The implants were collected after 8 weeks of implantation and fixed in 4% paraformaldehyde. The animals were sacrificed using cervical dislocation. The volume of mineralized tissue in the explants was quantified using nanoCT as described further on, after which they were decalcified in EDTA/PBS (pH 7.5) for 14 days, embedded in paraffin and processed for haematoxylin and eosin (H&E) as well as Masson's Trichrome staining. All procedures on animal experiments were approved by the local ethical committee for Animal Research, KU Leuven (P171-2011). The animals were housed according to the guidelines of the Animalium Leuven (KU Leuven).

7.3.14. nanoCT based quantification of mineralized tissue volume

For visualization and quantification of the mineralized tissue volume the same system was used as for the neo-tissue visualization in the perfusion bioreactor expanded

constructs but the tungsten target was operated at a voltage of 60 kV and a current of 210 µA. A 1 mm thick aluminum filter was used to reduce beam hardening and the isentropic voxel size was 3µm.

The resulting transaxial images were analyzed by CTAn (Skyscan NV). Images were segmented into three distinct phases (background, mineralized tissue and scaffold grains) using a 2-Level, 3D multilevel Otsu algorithm generating grayscale images with distinct grayscale values for each fraction. A global threshold was applied to select the scaffold fraction upon which a closing of 1 voxel was applied in combination with a despeckling operation of 200 voxels (black and white) to remove image noise prior to analysis of the scaffold volume. In order to prevent edge effects and the correlated partial volume effect from influencing quantification of the bone volume the selected scaffold fraction was subsequently dilatated with 1 voxel and subsequently subtracted from the original grayscale images. The grayscales corresponding with the newly formed bone were selected and image noise was removed as performed for the scaffold fraction prior to volumetric analysis.

7.3.15. Statistical analysis

Student t-test was performed to analyse significant differences between individual conditions for data not analysed in the DoE using Statistica 7 (Statsoft). A p-value < 0.05 was considered significant.

7.4. Results

7.4.1. Perfusion bioreactor facilitated cell expansion

The Presto Blue metabolic assay was used to monitor hPDC population proliferation during bioreactor expansion in correspondence with earlier published work (Sonnaert *et al.* 2014b). A strong increase in metabolic activity was observed during the first 10 days of culture which thereafter levelled off at day 13 to subsequently decreased towards day 17 as shown in Figure 7.1. Both Calcein AM staining and CE-nanoCT showed that 3D cell growth and ECM deposition gradually filled the voids on the 3D culture substrate, resulting in filled pores towards day 15. Based on the Presto Blue, a 10 fold expansion of the initial cell population was obtained at day 13 with an average cell density of 9,200 cells/mm³ or 1,200,000 cells/construct.

7.4.2. Reagent screening for cell harvest

DNA measurements on the scaffolds after harvest showed a significant decrease of cells attached to the 3D culture substrate in function of time for all 3 harvest reagents (Figure 7.2). Despite the significant, time dependent, decrease in cells remaining on the scaffolds, DNA measurement on the harvested cell suspension did not showed a significant recovery of cells using trypsin (Figure 7.2.A). Accutase® enabled the recovery of approximately 23% of cells after 15 minutes of incubation but no time-dependent increase in yield was observed at 37°C. Subsequent testing for longer incubation times at room temperature resulted in significant cell loss (Figure 7.2.B). Using collagenase IV a significant increase in cell recovery up to 76% was observed up to 7 hours of incubation. Prolonged incubation did not result in further significant

increases of cell yield and no cell loss was either observed (Figure 7.2.C). Therefore collagenase IV was chosen as reagent for harvest optimization.

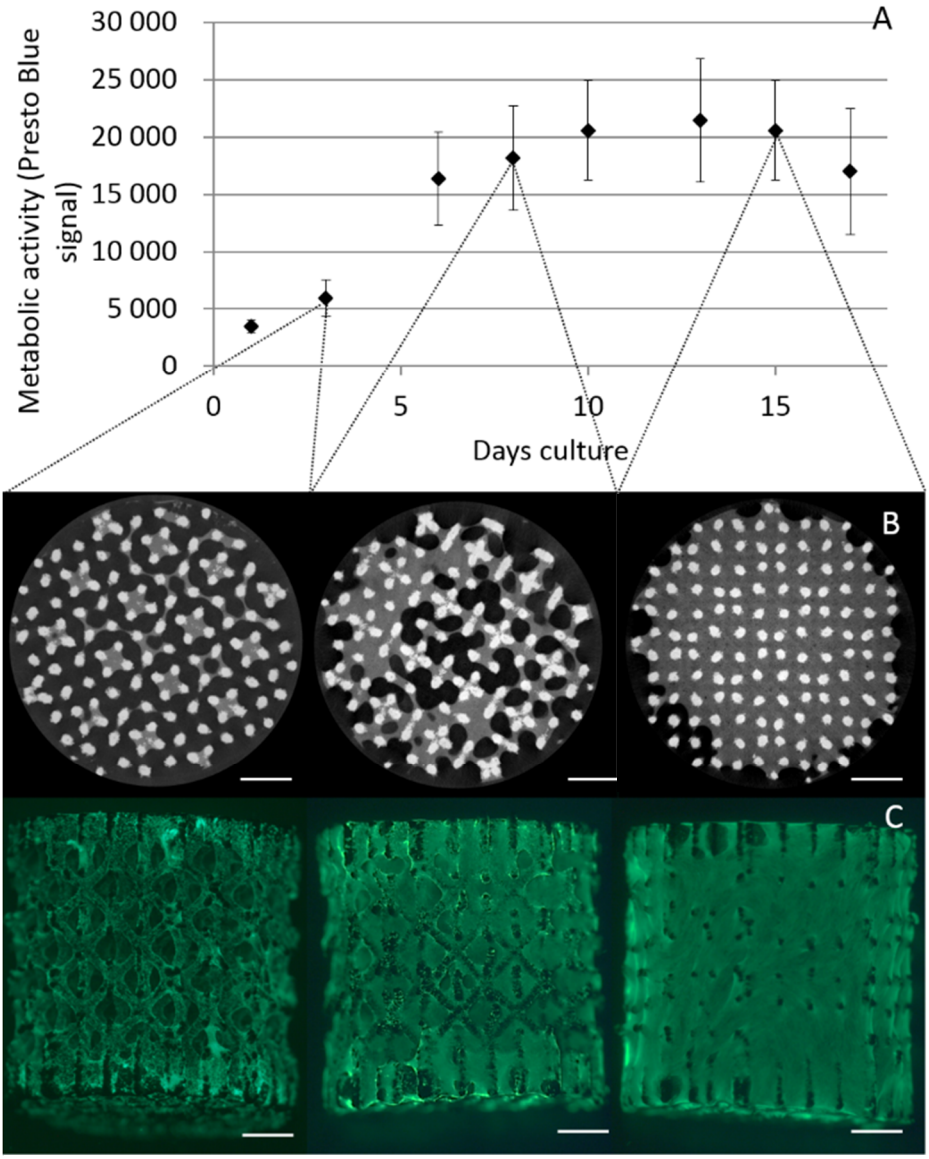

Figure 7.1: Perfusion bioreactor facilitated expansion.
(A) Presto Blue based metabolic activity of perfusion bioreactor expanded constructs (n=4). (B) Contrast Enhanced nano-Computed X-ray Tomography images of constructs at day 3, 8 and 15. Scale bar is 1 mm (C) Calcein AM staining of perfusion bioreactor expanded constructs at day 3, 8 and 15. Scale bar is 1mm.

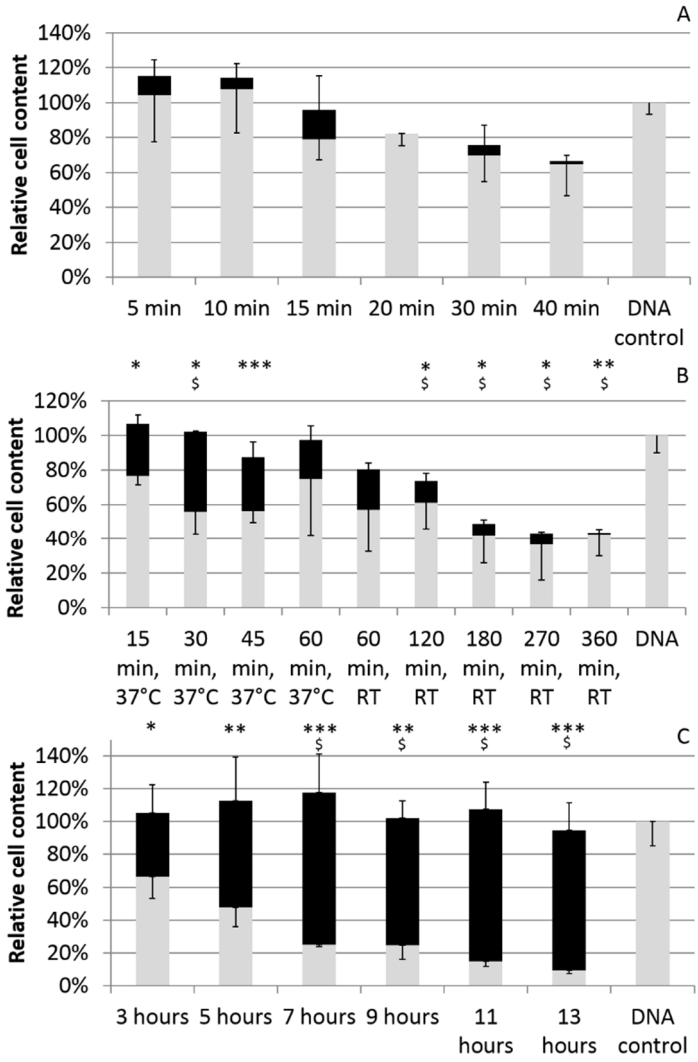

Figure 7.2: Harvest efficiency for different treatment protocols.
Harvest efficiency for different treatment protocols as determined by DNA measurements and shown relative in comparison to non-treated constructs (DNA control). Grey bars depict fraction of the cells remaining on the scaffold, black bars the recovered cell fraction. (A) 0.05% Trypsin - EDTA treatment (B) Accutase treatment at 37°C or room temperature (RT) (C) 440 U/ml Collagenase IV treatment. Significant differences in DNA content of the constructs after treatment in comparison to the DNA control are depicted with *(0.05>p>0.01), ** (0.01>p>0.001) and ***(0.001>p). Significant differences in DNA content of the recovered cell fraction in comparison to what was obtained at the first time point for each treatment are depicted with $. n=4 for all measurements.

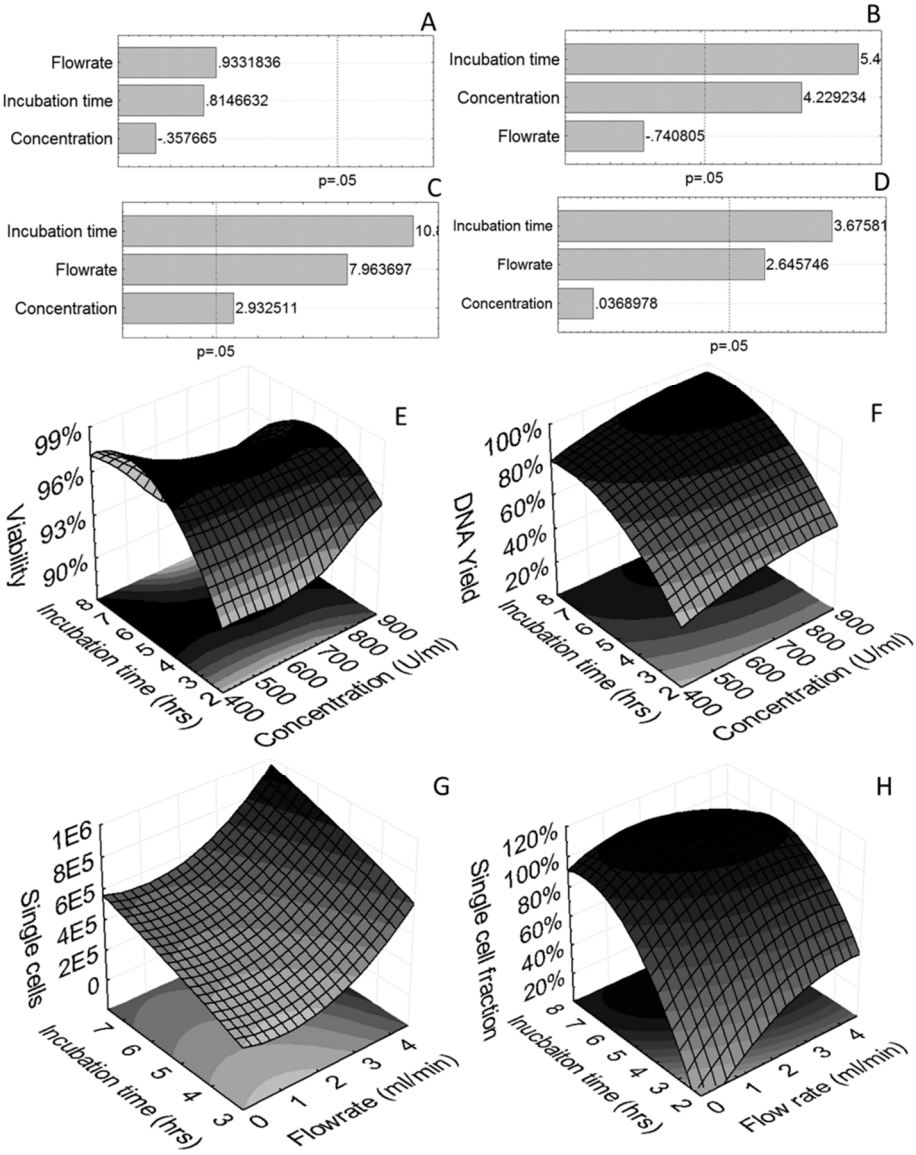

Figure 7.3: DoE analysis of harvest optimisation study using collagenase IV.
(A-D) Pareto chart of standardised effects and (E-H) 3D surface plots for respectively (left to right) Cell viability, Harvest yield as determined with DNA measurements, Single cell yield determined by hemocytometer, Single cell content of the recovered cell suspension.

7.4.3. Dynamic harvest optimization

A 3-level, 3-parameter fractional factorial design (Table 7.1) was employed to study the (i) influence of incubation time, (ii) flow rate and (iii) concentration of collagenase IV on 3D dynamic harvest efficiency. The incubation time did not influence the viability of the harvested cells (Figure 7.3.A and E). Additionally, neither collagenase concentration, nor shear stress due to fluid flow were shown to have an influence on the viability of the harvested cell population which was on average 96 ± 2 %. Both incubation time and collagenase concentration significantly increased cell recovery as determined by DNA measurements (Figure 7.3.B and F). Flow rate was not shown to influence the overall harvest efficiency within the examined range. Incubation time, flow rate and concentration (ranked in order of importance) did however have a significantly positive effect on the single cell yield as determined by manual cell counting (using a hemocytometer) (Figure 7.3.C and G). As for certain conditions the presence of cell aggregates was observed in the recovered cell fraction the single cell fraction was also quantified and shown to be positively influenced by an increase in incubation time and flow rate (Figure 7.3.D and H).

7.4.4. *In vitro* functional assessment of the harvested hPDC population

Harvested cells were seeded in well plates to investigate their proliferative potential. The Presto Blue assay was used to monitor cell growth over time showing a significantly lower metabolic activity in the proliferation assay for the 3D expanded cells (Figure 7.4). The profile of the growth curves was however similar for the duration of the proliferation assay.

Post-harvest tri-lineage differentiation assays showed that the dynamically 3D expanded and harvested cells maintained their *in vitro* differentiation capacity as shown in Figure 7.5. For the osteogenic differentiation assay a significantly higher amount of

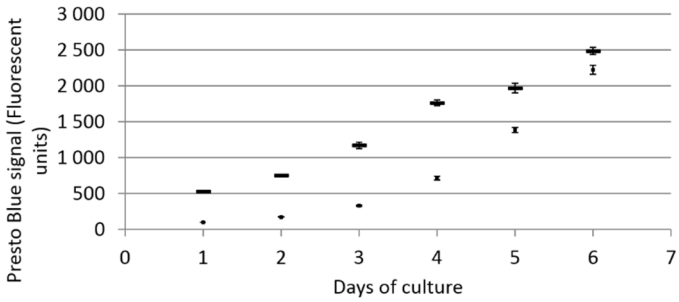

Figure 7.4: *in vitro* proliferation assay
Metabolic activity during 2D proliferation assay of 2D and 3D expanded cells as measured with the Presto Blue®. n=4

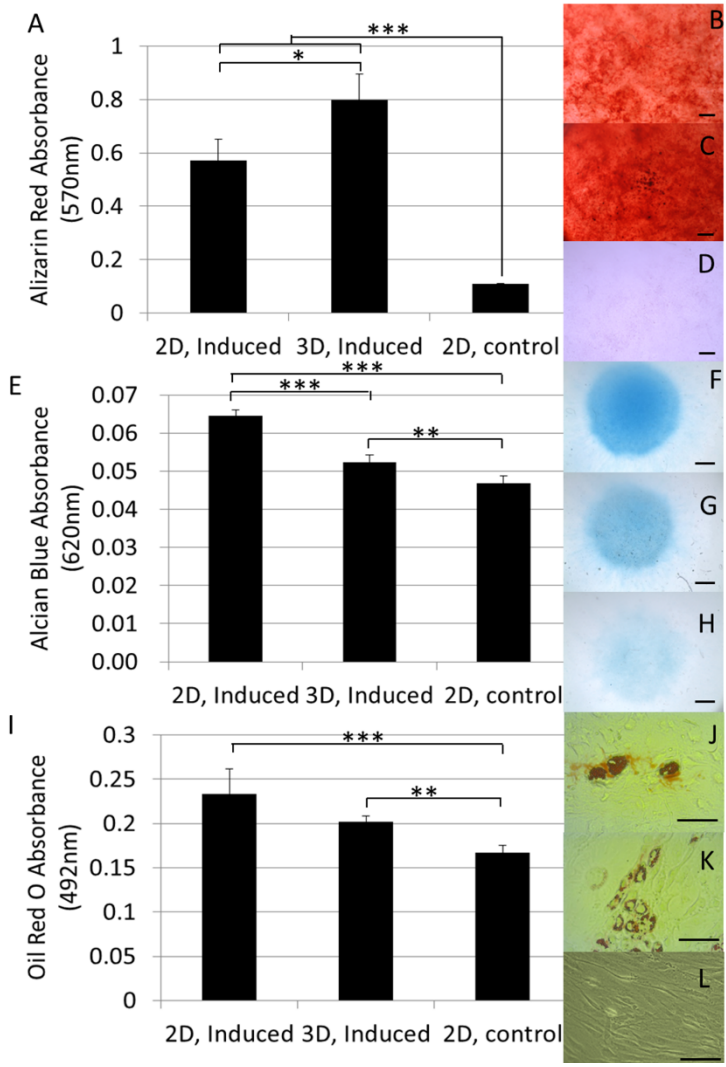

Figure 7.5: *In vitro* functional assessment of the harvested cells
(A) Quantification of the calcium depositions in the osteogenic differentiation assay using Alizarin red absorbance at 570nm. (B-D) Alizarin red staining of osteogenic induced hPDCs subsequent to (B) 2D expansion or (C) 3D expansion and (D) non-induced control from 2D expanded cells. (E) Quantification of the glycosaminoglycan deposition in the micromass based chondrogenic differentiation assay using Alcian blue absorbance at 620nm. (F-H) Alcian Blue staining of chondrogenic induced hPDC micromass systems subsequent to (F) 2D expansion or (G) 3D expansion and (H) non induced control from 2D expanded cells. (I) Quantification of the lipid globules formed in the adipogenic differentiation assay using Oil Red O absorbance at 492nm. (J-L) Oil Red-O staining of adipogenic induced hPDCs subsequent to (J) 2D expansion or (K) 3D expansion and (L) non induced control from 2D expanded cells. 3D expanded cells were recovered using a 880U/ml collagenase IV solution for 7 hours at a flow rate of 4ml/min. n=4 for all samples. Scale bar is 100µm.

mineral deposits was observed in comparison to the 2D expanded cells as well as to the negative control as shown after quantification of the alizarin red staining (Figure 7.5.A). Gycosaminoglycan accumulation induced by chondrogenic differentiation in the micromass system was lower than what was observed for the 2D expanded cells though still significantly higher than for the negative control (Figure 7.5.E). Both 2D and 3D expanded cells also showed a significant capacity for adipogenic differentiation as shown by the lipid globule deposition visualized by Oil Red-O staining and no significant differences were observed between both culture conditions (Figure 7.5.I).

7.4.5. *In vivo* functional assessment

The *in vivo* bone forming functionality of the expanded hPDC population was evaluated in an established ectopic bone formation model using calcium phosphate – collagen based scaffolds (Roberts *et al.* 2011). Both in Bio-Oss® and NuOss™ significant bone formation was observed as determined with H&E and Masson's Trichrome staining (Figure 7.6). Quantification of the bone volume was performed based on nanoCT analysis (Figure 7.7.A and B) and showed no significant differences between 2D and 3D expanded cells for both scaffold types. Respectively 4.25% and 12.1 % of the available volume were filled with bone in the Bio-Oss® and NuOss™ scaffolds (Figure 7.7.C). No significant bone formation could be observed in the non-cell seeded controls for both materials as can be observed in the histological sections (Figure 7.6). CT-based quantification of the mineralized tissue could therefore also not be performed on these samples.

7.5. Discussion

Despite the need for the development of methods for cell recovery from 3D cell culture substrates this still remains a largely unexplored field (Abbasalizadeh *et al.* 2013, dos Santos *et al.* 2013). Although recently the use of microcarrier based expansion systems has started to receive more attention, differences between these and other culture setups hamper the translation of existing harvest techniques across setups (Abbasalizadeh *et al.* 2013). We therefore developed and optimized a dynamic methodology that enabled the recovery of cells from a 3D culture substrate after which the functional characteristics of the expanded cell population was assessed and compared to established 2D cultured cells.

Using metabolic activity measurements, which are directly correlated with the total cell number (Sonnaert *et al.* 2014b), the time-point for cell recovery was set at 13 days to ensure maximum cell expansion and prevent over-confluence (Figure 7.1). Both the Calcein AM staining and the CE-nanoCT showed that the 3D culture environment was gradually being filled by cells and ECM resulting in 3D confluency by day 15 where no further hPDC expansion was expected (Papantoniou *et al.* 2014b, Sonnaert *et al.* 2014a). The decrease of metabolic activity measurements at subsequent time points further indicated that cell growth ceased at this time point.

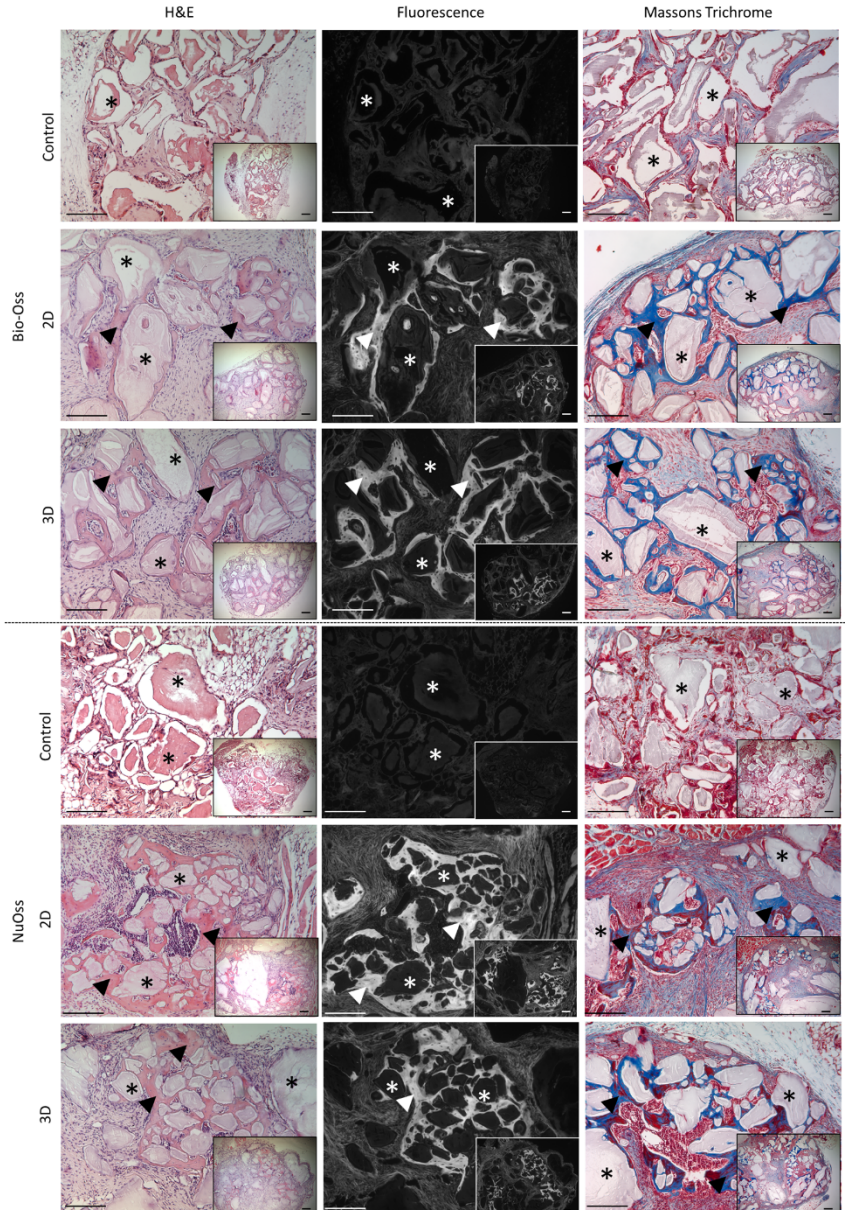

Figure 7.6: Histological analysis of explants obtained after the in vivo functional assessment of harvested cells.
Histological sections (H&E, H&E autofluorescence and Masson's Trichrome) from Bio-Oss and NuOss constructs seeded with 2D and perfusion bioreactor expanded hPDCs respectively as well as the non-cell seeded controls after 8 weeks of in vivo. Asterisks indicate remaining Calcium Phosphate grains, arrow heads indicate newly formed bone with embedded osteocytes. Scale bar is 100 µm.

In order to choose the most suitable harvest reagent for cell recovery the use of Trypsin/EDTA, Accutase® and collagenase IV was evaluated (Figure 7.2). Trypsin and Accutase® are commonly used reagents for cell recovery from 2D cell culture substrates on which cells grow predominantly in a monolayer such as standard 2D cell expansion

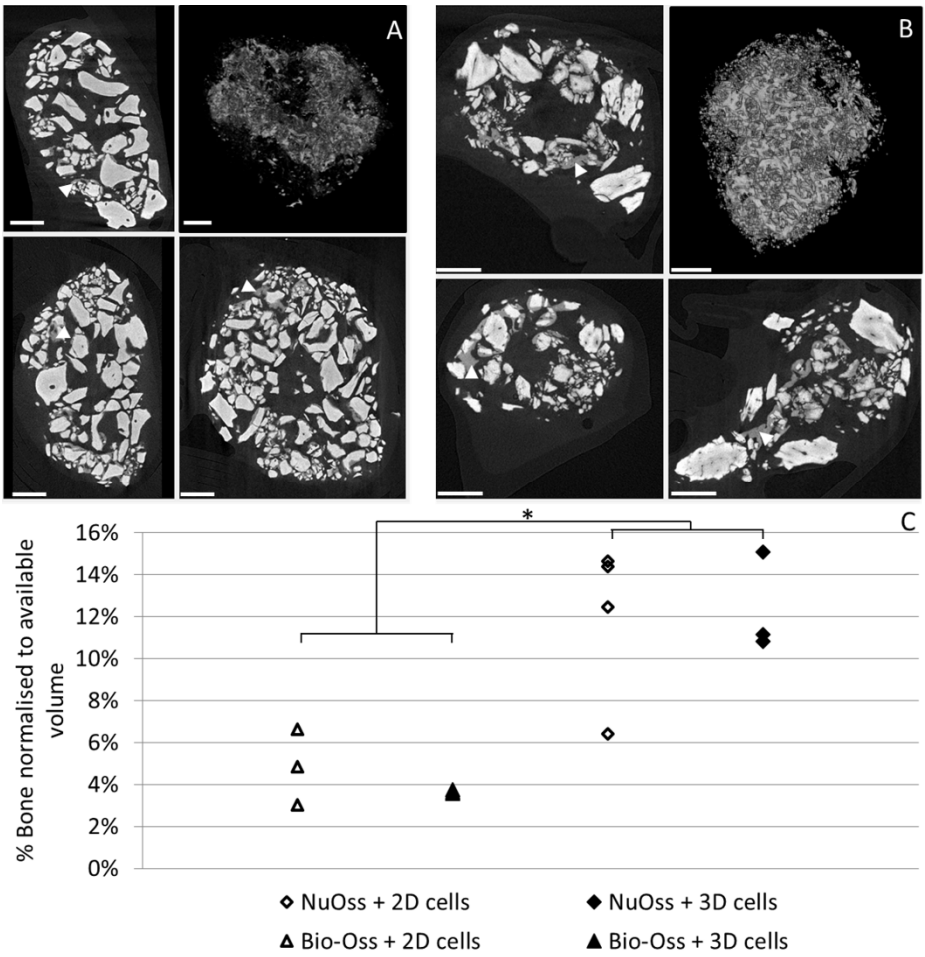

Figure 7.7: Bone volume analysis using µCT.
(A and B) sagittal, transaxial and coronal 2D µCT based section of respectively Bio-Oss (A) and NuOss (B) explant showing CaP grains of the scaffold material (light grey) and newly formed bone (dark grey, indicated with white arrow) combined with 3D visualization of the processed images showing the newly formed bone (right top). Scale bar is 500µm. (C) µCT based quantification of bone formed in the explants after the respective implantation periods normalized to the available volume in the scaffold. 3D expanded cells were recovered using a 880 U/ml collagenase IV solution for 7 hours at a flow rate of 4 ml/min. Scale bar is 100 µm. n=3 for Bio-Oss constructs, n=4 for NuOss constructs. * $p<0,05$

systems or microcarriers (Frauenschuh *et al.* 2007, Eibes *et al.* 2010, dos Santos *et al.* 2011a, Hewitt *et al.* 2011, Rafiq *et al.* 2013). The loss of cells observed using trypsin and Accutase® (respectively up to 35% and 57%) could be explained by the mechanism by which they act. Both agents are known to specifically cleave peptide chains at the carboxyl site of lysine or arginine. They will therefore cleave extracellular proteins as well as trans-membrane associated structures leading to the time dependent increase in cell loss observed for both solutions. Most setups (always 2D) therefore use a maximal incubation time of 10 to 15 minutes (Wersinger *et al.* 2004, Mitalipova *et al.* 2005, Brown *et al.* 2007). Additionally, trypsin it is known to be unable to cleave the helical structures of the collagen fibers, hence limiting its capacity to degrade the *in vitro* deposited collagen. As this is a major constituent of the ECM its application for cell recovery from a 3D cell culture environment within which abundant ECM is present is therefore suboptimal. Prolonging the incubation with trypsin in our system did consequently not result in an increased release of the cells from the deposited ECM but, as shown in Figure 7.2, only resulted in progressive damage to the expanded cell population. The use of a pure collagenolytic solution was expected to prevent this proteolytic related cell degradation as these enzymes specifically target the peptide bounds in collagen. As this is a major constituent of the ECM but is not present in the cell membranes it was successfully used previously for the recovery of primary cells from various tissues (De Bari *et al.* 2001, van Gastel *et al.* 2012b, Oseni *et al.* 2013) and application in our system resulted in a successful recovery with an overall cell recovery efficiency of up to 92% (Figure 7.2.C).

Expanding further on the successful application of the collagenase IV solution for the recovery of single cells from the 3D culture substrate a DoE approach was employed to optimize its use. Prolonged exposure to collagenase (between 10 and 24 hrs) was previously shown to affect cell viability for the digest of primary tissues (Yonenaga et al. 2010, Oseni et al. 2013), and as the strongest increase in yield was observed during the first 7 hours in the screening experiments (Figure 7.2.C), this was chosen as the maximal incubation time for the DoE study. None of the studied parameters showed a linear influence on the viability of the recovered cell population within the examined operating window which was on average 96% (Figure 7.3.A and E). Concentration and incubation time were shown to have a significant effect on both overall harvest efficiency and single cell yield while flow rate only had a significant positive effect on the single cell yield (Figure 7.3.B, C, F and G). The single cell fraction was positively influenced by a high incubation time and flow rate resulting in a continued dissociation of the aggregates into a single cell suspension as was shown earlier for different stem cell aggregate systems (Figure 7.3.D and H)(Papantoniou et al. 2011). No adverse effects related to shear stress on cell viability were observed in accordance with previous studies for comparable flow regimes as the maximal shear stress experienced by the cells in the tubing was approximately 2 mPa (Zoro et al. 2009, Mulhall et al. 2011). This was evidenced by unaffected single cell viability while the cumulative DNA content of the cells remaining on the 3D culture substrate and in the harvested suspension was equal to that of the post expansion, pre-harvest culture environment (as also shown in Figure 7.2.C).

Despite the fact that no adverse effects of the applied procedure on the cell viability were detected the metabolic activity of the hPDCs was significantly decreased after replating in comparison to standard 2D expanded cells (Figure 7.4.). Adverse effects of prolonged use of a collagenase solution between 10 and 24 hours were reported for the digest of primary tissues which could result in a decrease of the metabolic activity of the harvested cell population (Yonenaga et al. 2010, Oseni et al. 2013). Recent work also showed cells to possess a "mechanical memory" which can influence their behavior depending on the previous physical environments used for culture (Yang *et al.* 2014a). The switch from the complex, ECM containing 3D culture environment in the perfusion bioreactor system to the standard tissue culture plastic might therefore also influence the metabolic activity of the recovered hPDC cell population and might result in an initial lower metabolic activity.

Maintenance of the in vitro differentiation potential of a progenitor cell population expanded in bioreactor systems has been reported for several MSC cell sources and was also observed in our system (Figure 7.5)(Rafiq *et al.* 2013, Dos Santos *et al.* 2014, Papadimitropoulos *et al.* 2014a). The observed increase in calcium depositions and decrease in GAG accumulation suggest an osteogenic priming of the expanded cell population (Figure 7.5). In previously published work we already hypothesized that the shear stress exerted on the cells during expansion might result in osteogenic priming of the expanded cell population based on the up regulation of certain gene markers associated with osteogenic differentiation which is further substantiated by this data (Sonnaert et al. 2014a). Although the 3D perfusion bioreactor expansion of primary MSCs was previously shown to result in enhanced in vitro osteo-, chondro- and adipogenic differentiation potential as well as an enhanced clonogenicity of freshly isolated primary MSCs (Papadimitropoulos *et al.* 2014a), we only observed an increase in osteogenic differentiation (Figure 7.5.A). The cells used for this study were however pre-expanded for multiple passages using standard cell culture methodologies, including the use of plasma treated polystyrene. This has been correlated with the progressive loss of the progenitor cell phenotype and commitment to the osteogenic lineage indicating that the differences in post expansion differentiation potential for primary cells might originate from an enhanced maintenance of the progenitor cell phenotype (Banfi et al. 2000, Scadden 2006, Wagner et al. 2008). The initial 2D expansion of the hPDC population used for this work could therefore explain the absence of a significant difference in differentiation potential between 2D and 3D expanded cells in this culture setup.

Post expansion cell characterization is currently focused on cell identity as established by in vitro assays (Rafiq *et al.* 2013, Dos Santos *et al.* 2014, Papadimitropoulos *et al.* 2014a) while their functionality as evidenced by their performance in both in vitro and in vivo models is largely subsided. Furthermore the lack of such data hinders the development of correlations that will eventually allow to link in vitro and in vivo cell behavior (Bianco et al. 2013). To the best of our knowledge no reports exist assessing the in vivo potency of a progenitor cell population after expansion and recovery in a 3D bioreactor system despite the need for adequate in vivo controls for the validation of these processes (Bianco et al. 2013). We therefore assessed the in vivo bone forming capacity of the 3D expanded and recovered cells in a standard ectopic bone formation

assay (Roberts et al. 2011). Histological staining showed the clear presence of bone spicules in all cell seeded conditions (Figure 7.6). In addition, the presence of bone marrow lacunae and blood vessels was unimpaired in comparison to their 2D control indicating the unaffected in vivo differentiation capacity of the 3D expanded cells. This was further confirmed and quantified by nanoCT analysis where no differences between 2D and 3D expanded cells were apparent (Figure 7.7.C) and observed volumes of newly formed bone were comparable to what was shown earlier (Roberts et al. 2011).

In conclusion, we optimized a closed bioprocess enabling the expansion and recovery of a viable cell population. The produced cell population showed minor differences in its in vitro differentiation potential as compared to the 2D standard while it showed an uncompromised bone forming potential upon ectopic implantation. The development of this multi-unit integrated bioprocess shows the potential for integrated bioprocess development and sets the scene for the continued integrated optimization of current manual tissue engineering strategies to a clinical relevant setting.

7.6. Acknowledgements

MS is supported by a Ph.D. grant of the Agency for Innovation by Science and Technology (IWT/111457). IP is funded by the ERC advanced grant 'REJOIND'. The X-ray computed tomography images have been generated on the X-ray computed tomography facilities of the Department MTM of the KU Leuven, financed by the Hercules Foundation (project AKUL 09/001). We would like to acknowledge Dr. Greet Kerckhofs and Carla Geeroms for the development of the image analysis protocol of the explants. This work is part of Prometheus, the Leuven Research & Development Division of Skeletal Tissue Engineering, www.kuleuven.be/prometheus

Chapter 8.
General discussion and future perspectives

8.1. Summary

The development of cost-effective, scalable and robust processes for stem cell expansion will be imperative for the successful translation of current lab-scale TE approaches to clinical applications. Integrated bioprocess development, combining multiple unit operations in a continuous, closed and controlled culturing strategy, thereby negating the need for manual, labor intensive methodologies and circumventing various process bottlenecks, is considered to be essential for this clinical translation. Within this context bioreactor systems are a powerful enabling technology as these permit a high degree of scalability, control and automation. As discussed in the introduction of this dissertation a variety of bioreactor systems, each demonstrating specific advantages and shortfalls both on the technological and biological aspects of the process, are currently under investigation. Although technological advances will be essential for successful industrialization, the influence of the *in vitro* micro-environment within which the cells reside on their functional characteristics and identity will determine the final applicability of the different systems. In order to assess the potential use of a 3D perfusion bioreactor system for the expansion of a progenitor cell population the primary objective of this dissertation was therefore to elucidate the influence of this culture system on the proliferation, differentiation, matrix deposition and post-harvest functionality of the expanded cell population. In order to facilitate these observations two additional objectives were defined; (i) to enable the quantitative monitoring of the cell proliferation within the bioreactor system and (ii) to visualize and quantify the neo-tissue formation within the 3D culture environment. A schematic representation of the different aspects addressed in this dissertation is shown in Figure 8.1 and the main findings discussed in the different chapters are concisely summarized in the next sections.

In order to characterize the influence of a range of culture parameters on cell proliferation in bioreactor systems the development of quantitative methods for monitoring cell number is essential. As non-destructive, direct measurements of cell number during the expansion process are largely limited to 2D culture systems, indirect methods need to be developed. In this context the use of metabolic assays has been suggested as an interesting candidate, although contradicting reports exist regarding its quantitative application. Therefore, a quantitative validation of the PB metabolic assay was performed showing that indeed a correlation existed between the metabolic conversion of the resazurin and the number of cells present in the culture system (chapter 3). Depending on the cell culture but also on the measurement setup different conversion rates were obtained. Further validation showed these to be correlated to differences in the measurement setup rather than to the changes in the *in vitro* culture environment as measurement of samples cultured under different conditions using the same measurement setup yielded similar conversion rates. This indicated that changes in culture setup (2D to 3D culture and static vs perfusion culture) did not induce significant changes in the metabolic activity of the cell population and therefore also did not significantly influence cell behavior. This hypothesis was further supported by the absence of significant changes in gene expression comparing the 3D static and perfusion culture system (chapter 6) as well as the post expansion functionality of cells expanded in both culture systems (chapter 7). The established correlations subsequently enabled estimating the cell number during the exponential growth phase of the cells based on the metabolic measurements within the linear operating window of the system.

Visualization and quantitative analysis of neo-tissue formation (the combination of cells and the deposited ECM) in Ti6Al4V alloy scaffolds was enabled through the development of CE-nanoCT. A first proof of concept study (chapter 4) showed the potential of visualizing the neo-tissue using two different contrast agents, Hexabrix®

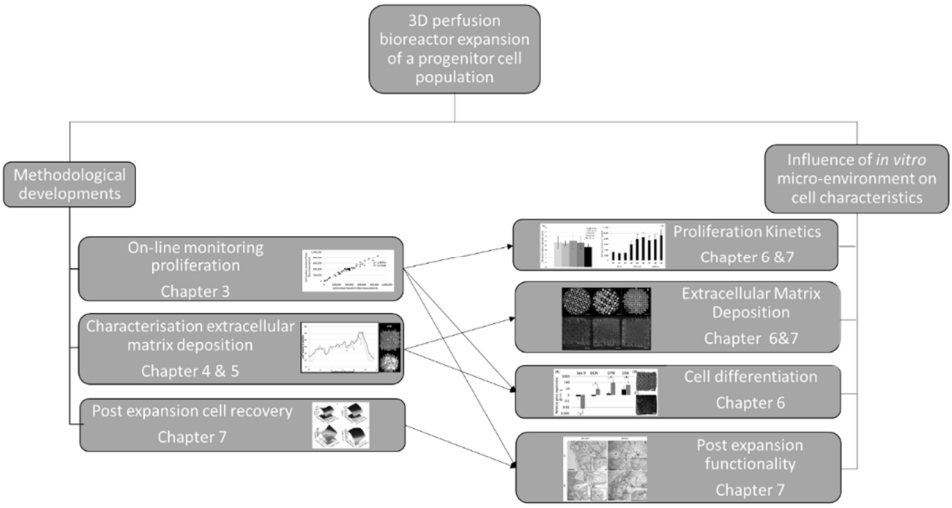

Figure 8.1: Schematic overview of the various aspects of the 3D perfusion bioreactor expansion process addressed in this dissertation.

and PTA. Using Hexabrix® a linear correlation between neo-tissue volume and net dry weight of the neo-tissue was established suggesting that it enables visualization and quantification the full neo-tissue in the scaffold. This was visually confirmed comparing the obtained images with established optical techniques such as life/dead and picrosirius red staining. Using PTA the comparison between stained neo-tissue volume and dry weight suggested that only a fraction of the neo-tissue was visualized using this contrast agent. In addition, distinct differences in PTA stained neo-tissue for the different experimental conditions hinted that this staining enabled the visualization of a specific sub-fraction of the neo-tissue. As intensive manual image processing was required for quantitative analysis of the datasets in this proof of concept study a follow up study was conducted aimed at the optimization of the staining procedure as well as a further validation of both staining agents (chapter 5). Using a DoE approach the influence of staining parameters (i.e. incubation time, concentration of the staining agent and neo-tissue volume) on image contrast and dataset quality (i.e. the mismatch between raw and processed images) was determined. Both for Hexabrix® as well as for PTA an increase in concentration of the staining agent resulted in a positive influence on the image contrast and consequently also on the image dataset quality. In addition, for PTA an increase in neo-tissue volume was also shown to result in an increased dataset quality. Using a different scaffold material, Hexabrix® was confirmed to stain the entire neo-tissue present in the scaffolds. PTA staining on the other hand was shown to result in a concentration dependent degradation of the neo-tissue rather than being a staining with a higher specificity as hypothesized based upon the results obtained in the proof of concept study discussed in chapter 4. Although the DoE showed high concentrations resulted in higher image contrast and dataset quality, PTA should be used at low concentrations to prevent significant tissue shrinkage and enable quantitative interpretation of the data. No such restrictions are present when using Hexabrix® for visualizing the full neo-tissue and based upon the DoE optimal staining conditions for quantitative data analysis could be determined.

In order to determine the influence of the micro-environment created in the 3D perfusion bioreactor system a first study elucidating its effects on the proliferation, differentiation and ECM formation was conducted (chapter 6). Proliferation was shown not to be influenced within the examined range of flow rates but was significantly increased in comparison to the 3D static controls. Live/dead staining showed a similar neo-tissue distribution at the outside of the scaffolds for both perfused and static culture conditions. However, CE-nanoCT enabled the visualization and quantitative analysis of the complete neo-tissue and showed that while static cultured constructs mainly contained neo-tissue at the outer layers of the scaffolds the perfused conditions resulted in densely filled scaffolds which was potentially caused by the enhanced nutrient transport in the perfused conditions. Total neo-tissue volume after 4 weeks of culture was shown not to be influenced by the flow rate although the neo-tissue deposition kinetics were different. Gene expression analysis showed minor differences in the expression profile of several osteogenic and chondrogenic marker genes. Comparison with the gene expression profile obtained from chemically induced osteogenic differentiation in the same bioreactor setups showed that the observed changes in the gene expression profile were significantly lower (between 2 and 100 fold) than for the

chemically induced conditions indicating that the perfusion bioreactor culture does not induce full osteogenic differentiation though it might result in an osteogenic priming of the cell population.

To further characterize the influence of the perfusion bioreactor expansion on the cell characteristics, post expansion functionality of the progenitor cell population was evaluated (chapter 7). Therefore, a method for cell recovery from 3D scaffold based cultures was developed and optimized using a DoE approach. An initial screening of different reagents showed collagenase to be the most efficient in the recovery of a viable cell population which was then used for the optimization study using DoE. This showed that the high levels off all three process parameters (i.e. flow rate, concentration and incubation time) were beneficial for cell recovery as well as the single cell fraction in the recovered cell suspension. In order to determine the time point at which maximal expansion was obtained the previously validated PB assay was used to monitor cell proliferation while CE-nanoCT was employed to assess the degree of filling and provide an estimate on volumetric 'confluence'. Subsequent functional assessment of the recovered cells showed that both the *in vitro* tri-lineage differentiation potential as well as the *in vivo* bone forming capacity of the cells was maintained post expansion and harvest confirming the potential of this system to be used as a tool for cell expansion. This was the first systematic investigation of 3D cell harvest from scaffold based cultures. Moreover it builds further on the recently expanding field of integrated bioprocessing for regenerative medicine, adopting a whole bioprocessing approach from 'vial to patient'.

8.2. Critical reflections on perfusion bioreactor development for tissue engineering

The results discussed in this dissertation and summarized in the previous section present a proof of concept for the use of a 3D perfusion bioreactor system as a tool for the expansion of a progenitor cell population. The next section provides some critical reflections upon the presented results towards the continued progression of the field to clinical relevant processes.

8.2.1. Development of methods for bioprocess monitoring and characterization

The use of metabolic assays for monitoring cell proliferation has already been suggested as an interesting approach for monitoring cell proliferation in bioreactor systems but contradicting results prevented their quantitative use to date. We hypothesized that one of the constraints in earlier published studies was the presence of mass transport limitations induced by the high cell densities used (up to 750.000 cells/cm²) resulting in the reported non-linear behavior (Ng *et al.* 2005, Quent *et al.* 2010). Our results confirmed that indeed diffusion limitations can influence the performance of the assay as depending on the mass transport characteristics of the measurement setup, changes in the conversion efficiency of the assay were detected. A quantitative correlation between assay conversion and cell number could, however, be

established given that the measurement setup ensured adequate and homogenous supply of the assay to the entire construct.

Another important aspect to enable the quantitative use of the methodology is the homogeneity of the cell population with respect to phenotypic state, both in function of time as well as on a given time point. Proliferation of a MSC like population is associated with glucose consumption through the glycolytic pathways supporting a high degree of nutrient incorporation into the biomass and resulting in high lactate production rates. Upon differentiation these cells will switch their metabolism towards oxidative phosphorylation requiring higher levels of oxygen but resulting in higher energy yields for each processed glucose molecule (Sart *et al.* 2014a). Detailed assessment of cell energy metabolism showed that mitochondrial ATP production through oxidative phosphorylation only contributed up to 30% in the total ATP generation during cell proliferation while this fraction increased up to 48% during osteogenic differentiation and only contributed 13% during chondrogenesis (Pattappa *et al.* 2011). Although the exact mechanism of action for the metabolic conversion of the resazurin is not yet clear most authors concur that the reduction to the fluorescent resorufin is facilitated by the mitochondrial activity (Nociari *et al.* 1998, O'Brien *et al.* 2000, Quent *et al.* 2010). As changes in the cellular metabolism impact upon mitochondrial activity, this will therefore influence the conversion of the metabolic assay. This could also be observed in our results as a decrease in proliferation, and therefore a decrease in cellular activity, resulted in a decreased conversion of the assay. This prevents a broader application of the developed methodology towards for example the monitoring of the maturation of an *in vitro* developing neo-tissue but, as shown, does not impair its use for monitoring cellular proliferation in systems such as the ones used in this work which enable the expansion of a cell population without significantly influencing its phenotype.

This thesis presents a significant contribution to the field as no validated methods for online monitoring of proliferation in systems with a similar setup were available. In addition, it provides a valuable tool for *in vitro* models and assays for e.g. drug compound screening. As at current, however, no clinical approved version of the assay is available its potential for application in clinically relevant systems is limited. The implementation of methods used for monitoring large scale fermenters such as oxygen, glucose and lactate measurements provide an interesting alternative. Until recently however, limited sensitivity of the sensors, required for monitoring the relative low number of cells present in systems such as used in this study, considerably restricted their application. Advances in sensor technology combined with the development of novel monitoring strategies, however, started to address these limitations. This was shown for example in a proof of concept study correlating changes in oxygen concentration with cell number and PB signal (Lambrechts *et al.* 2014). Indisputably, these methods have the advantage of being in- or on-line and present significant advances towards the development of clinically relevant systems. However, they often require a significant investment both in equipment as in the implementation in the bioreactor systems which on a research scale might be a significant limitation in comparison to the use of the PB assay. Moreover, monitoring the concentration of a single metabolite focuses on one specific aspect of the energy metabolism of the cells

and is associated with the same limitations as the PB metabolic assay concerning monitoring of a cell population throughout different stages of proliferation and differentiation. Due to the complexity of the pathways involved in the energy metabolism no single metabolite can be defined that would enable to monitor cell number through various *in vitro* stages of neo-tissue development. Simultaneous monitoring of a number of key metabolites and nutrients such as lactate, glucose, glutamate, ammonia, oxygen and carbon dioxide could enable to obtain significant insight in the energy metabolism of the cell population and correlate this with cell number and differentiation stage. Detailed understanding of the influence of the various processes involved in cellular differentiation could enable to use this information to define cell state but quantitative definition thereof would require compiling a more elaborate metabolic profile of the cell population including not only components involved in the energy metabolism but also several key metabolites or molecular markers associated with cellular differentiation (Kell *et al.* 2005, McNamara *et al.* 2012). The information obtained from these advanced techniques could significantly improve the understanding of the various processes taking place in the bioreactor system and their integration in clinical relevant systems might be required in order to ensure process compliance with the operating window approved by the regulatory agencies. However, large scale implementation of these techniques in research scale bioreactors might not be feasible due to economic considerations.

As discussed, the PB metabolic assay is an interesting candidate as it can provide quantitative information on the proliferation of the expanding cell population. During this expansion in the 3D system cells will start secreting a supportive ECM. The composition of this *in vitro* developed neo-tissue as well as the kinetics of the matrix deposition can provide valuable additional information on the cell population in the bioreactor system.

As mentioned in the introduction of this dissertation different techniques which enable 3D visualization of the neo-tissue such as confocal tomography, micro-magnetic resonance imaging and optical coherence tomography are available (Appel *et al.* 2013, Nam *et al.* 2014). Restriction on spatial resolution and penetration depth as well as limited throughput, however, put significant restraints on the application of these techniques as a tool for online monitoring (Georgakoudi *et al.* 2008, Appel *et al.* 2013, Nam *et al.* 2014). In this respect the development of the CE-nanoCT provides a significant addition to the field of non-destructive 3D imaging as the combined high penetration depth and resolution enable quantitative analysis on the *in vitro* developed neo-tissue. In addition to volumetric analysis, the use of contrast agents with composition dependent staining specificity could also enable their use for compositional analysis towards the development of non-destructive 3D histology (Pauwels *et al.* 2013, Gignac *et al.* 2014, Kerckhofs *et al.* 2014). As the tissue specific binding mechanism of several of these contrast agents is, however, still unknown, extensive experimental validation of these techniques is still required. In addition, the influence of the staining procedure and contrast agent on the neo-tissue integrity needs to be assessed in detail as we for example showed that PTA, a contrast agent frequently reported in literature in the context of the staining of embryos (Pauwels *et al.* 2013), can significantly influence the integrity of the stained neo-tissue.

The use of this technique for the characterization of the *in vitro* developed neo-tissue will enable to obtain a better understanding of the cellular processes progressing during 3D *in vitro* cell expansion and construct development. At the same time it also addresses a significant need in the regenerative medicine field for non-destructive tools for quality control of engineered tissues. Regulatory requirements for clinical applications will entail to show process and product consistency within a clearly defined operating window in order to meet the final release criteria for the product. The availablility of non-destructive, quantitative methods for 3D characterization of these products such as CE-nanoCT will therefore be imperative. In this respect, enabling online monitoring of neo-tissue formation and construct development could even further improve the applicability of the methodology as it would enable early fault detection. In addition, it could enhance the understanding of the cellular processes during expansion in the bioreactor and create new opportunities for further optimization of the methodology. Depending on the contrast agents used this could not only provide information on the kinetics of the neo-tissue formation but potentially also on tissue composition which could, in combination with results obtained from the PB metabolic assay, be used as an indication of tissue maturation and cell differentiation. Although X-ray toxicity due to prolonged or repeated exposure is a significant concern for the in- and on-line application of this methodology, various studies on *in vivo* and *in vitro* monitoring of mineralization confirm the feasibility (Porter *et al.* 2007, van Lenthe *et al.* 2007, Hagenmuller *et al.* 2010, Laperre *et al.* 2011, Beck *et al.* 2013, Appel *et al.* 2015)

8.2.2. Engineering a supportive in vitro micro-environment for progenitor cell expansion

The above mentioned novel techniques were, in combination with a range of established methods, subsequently used to characterize the influence of the perfusion bioreactor facilitated cell expansion on cell behavior and potency. Our results indicated that within the used operating window the *in vitro* micro-environment to which the cells were exposed did not significantly influence the functionality of the expanding cell population. Despite the hypothesized advantages of a 3D culture system on the maintenance of progenitor cell potency only limited differences were observed in comparison to standard 2D cell expansion. The cells used for this work were, however, already pre-expanded for multiple passages using standard cell culture methodologies which probably already resulted in the progressive loss of progenitor cell phenotype and potency as discussed earlier in this dissertation (Banfi *et al.* 2000, Scadden 2006, Wagner *et al.* 2008).

Secondly, the rationale behind the use of a 3D environment for progenitor cell expansion was to create a micro-environment which more closely resembles the native cell niche and therefore better supports the maintenance of cell phenotype. Although the use of a Ti6Al4V based 3D scaffold enabled us to study the influence of the fluid flow induced SS on the cell behavior during and after expansion the relevance of this scaffold system in respect to the native cell niche is limited. Additionally, the use of artificial substrates for cell culture has been shown to influence cell identity and functionality potentially resulting in spontaneous (de)differentiation, replication senescence,… (Banfi *et al.* 2000, Scadden 2006, Wagner *et al.* 2008). In an attempt to

prevent or limit these *in vitro* culture induced artefacts different strategies for engineering an *in vitro* cell niche in which the combination of different active components such as fibronectin and collagen could result in a more supportive cell culture environment have been assessed (Chen *et al.* 2007, Abraham *et al.* 2010, Sadr *et al.* 2012). Due to the complex nature of the native environment of the cells successes using these approaches have been limited. Rather than isolating a defined set of active components, a decellularized version of the native ECM in which the cells reside is hypothesized to be another interesting candidate to enable maintenance of the original cell characteristics (Scadden 2006). As these materials are, however, difficult to obtain, engineering strategies in which a cell deposited ECM was used as cell culture substrate are being evaluated (He *et al.* 2009, Seib *et al.* 2009, Lai *et al.* 2010, Thibault *et al.* 2010, Pei *et al.* 2011, Prewitz *et al.* 2013). Different successes reporting enhanced proliferation (Chen *et al.* 2007, He *et al.* 2009, Li *et al.* 2011, Pei *et al.* 2011, Pattabhi *et al.* 2014), differentiation (Chen *et al.* 2007, He *et al.* 2009, Lai *et al.* 2010, Li *et al.* 2011, Pei *et al.* 2011) and construct development (Pham *et al.* 2008, Thibault *et al.* 2010, Sadr *et al.* 2012) show the potential of this strategy. Further exploration of this approach for the development of functional constructs is ongoing (Papadimitropoulos *et al.* 2014b) but the use of these decellularized, ECM based materials for cell expansion is less explored and could result in significant changes in cell behavior.

Next to cell culture surface a range of other parameters associated with standard cell expansion methodologies result in a micro-environment which is significantly different from the native niche. The ambient air currently used for cell culture is for example significantly different from the oxygen concentrations present in the MSC niche which ranges between 2 and 8% (Mohyeldin *et al.* 2010). Hypoxic culturing conditions (oxygen concentrations under 2%) have been shown to result in significant decreases in proliferation and differentiation of MSCs while normoxic culture (oxygen concentrations between 2 and 8%) was shown to enhance proliferation and maintenance of stemness as well as influence the differentiation towards the different MSC lineages (Mohyeldin *et al.* 2010, Sheehy *et al.* 2012). Next to the oxygen concentration used during cell culture another important aspect of the extracellular micro-environment during *in vitro* culture is the medium composition. At current irradiated fetal bovine serum is a standard supplement for the culture of human derived cells. Although its use is still accepted by the European medicine agency, the large inter-batch variability can result in significant changes in cellular behavior and, combined with the associated risk for zoonosis, limits its applicability in clinically relevant processes (Heathman *et al.* 2015). Recent advances have shown human platelet lysate to be a valuable alternative to the use of animal derived products although also here the inter-batch variability remains a limiting factor (Schallmoser *et al.* 2007, Bieback *et al.* 2009, Hofbauer *et al.* 2014). The development of standardized, chemically defined media is therefore still a priority (Mannello *et al.* 2007, Jung *et al.* 2012a, Bieback 2013).

8.2.3. Integrated bioprocess development

Although the optimization of the expansion micro-environment, and thereby the expansion process, is essential for the performance of this process step, its

implementation within 'whole' bioprocess schemes will be imperative for its future industrial applicability.

To date, most methods for large scale cell expansion are based upon systems with a high surface to volume ratio such as hollow fiber bioreactor systems or micro-carrier based setups. Due to the predominant 2D cell growth in these systems, enzymatic methods for cell recovery subsequent to the expansion are closely related to the procedures used in the standard 2D expansion setups and require only limited optimization. The added complexity in 3D culture systems within which significant amounts of ECM is secreted during the expansion requires significant alterations to the procedure such as for example the reagents used for cell recovery. Although our work showed that this could be achieved without impairment to the cell functionality, additional optimization will still be needed as for example long holding times can significantly influence cell characteristics (Delahaye *et al.* 2015). Further optimization of this procedure towards economic feasibility in terms of cost of goods and time will be a significant contributor to the potential industrial implementation of this expansion methodology (Heathman *et al.* 2015).

In addition to cell recovery, a number of other challenges for post-processing in the bioreactor field remain to enable successful implementation of automated expansion methodologies. The enzymatic harvest procedures result in large volumes of cell suspensions which require considerable volume reduction and washing steps. Current lab scale processes use dead end centrifugation as standard tool for cell concentration and several clinical scale expansion systems such as the Quantum cell expansion system (Terumo BTC) and the Xpansion multiplate bioreactor system (Pall) still rely on this manual procedure in the absence of other acceptable alternatives. While this method cannot be translated to a fully automated and closed unit operation, it provides a standard operational procedure applicable over a wide range of systems (Delahaye *et al.* 2015). The potential for scale-up or scale-out and full automation and integration of this batch process is, however, limited. Various other systems for automated, on-line cell separation already exist within the biopharmaceutical world with the production of vaccines as an example. The main goal of these processes is, however, to remove the cells from the solution as they are merely a byproduct rather than retaining them for future applications. Recent advances showed, however, that optimization of these methods, such as tangential flow filtration, do enable the successful retention of a significant fraction of the cells without altering their viability or potency indicating the potential of these techniques (Cunha *et al.* 2015a, Cunha *et al.* 2015b).

8.3. Future perspectives for perfusion bioreactors in tissue engineering

Substantial progress in the development of automated cell expansion has been made using various systems which each have considerable operational advantages over the 3D culture system. Despite often mentioned, the hypothesis that a biomimetic 3D environment would be beneficial for stem cell maintenance during expansion in comparison to other, predominantly 2D based setups, has not been confirmed yet (Prewitz *et al.* 2013, Gattazzo *et al.* 2014, Papadimitropoulos *et al.* 2014b). The absence

of suitable methodologies for cell expansion, recovery and online monitoring of the proliferation and neo-tissue formation have been important restrictions in this respect which we attempted to address within the framework of this dissertation. Within the next section we will discuss some future perspectives required for the continued development of perfusion bioreactor systems in the field of TE based upon the general discussion formulated in the previous section.

8.3.1. Micro environment

The rationale behind the use of a 3D perfusion bioreactor system is the hypothesized relevance of the 3D culture environment in respect to the development of a supportive *in vitro* micro-environment resembling the *in vivo* stem cell niche (Tan *et al.* 2013). In order to assess this hypothesis and thereby harness the full potential of 3D perfusion bioreactor systems the development of suitable scaffolds should be a priority. As detailed above, the use of decellularized ECM based materials provides interesting perspectives in this context and should be pursued further. Firstly, the influence of various types of this ECM on cell behavior should be elucidated. Although a biomimetic approach, attempting to recreate the native *in vivo* environment of the hPDCs, could be interesting as this *in vivo* niche is supportive for the maintenance of the progenitor cell phenotype, its potential to support substantial proliferation is unknown. An *in vivo* environment which is supportive of periosteal cell proliferation is the fracture callus within which the first steps of endochondral ossification take place being mesenchymal cell proliferation and condensation. As recapitulating the different aspects of the *in vivo* stem cell niche in an *in vitro* engineered environment will be a considerable challenge requiring new insights on the *in vivo* micro-environment and its interaction with the cells, this will be a time consuming approach without a guarantee of success. Based upon the same principles the use of different types of ECM deposited by the same cell type that will subsequently be expanded on the decellularized ECM could be evaluated. Proof of concept of this methodology is already present for some time but these principles have mainly been applied for the development of decellularized constructs as implants rather than as *in vitro* scaffold system (He *et al.* 2009, Seib *et al.* 2009, Lai *et al.* 2010, Thibault *et al.* 2010, Pei *et al.* 2011, Prewitz *et al.* 2013, Bourgine *et al.* 2014b, Papadimitropoulos *et al.* 2014b).

Independent from the applied strategy, the development of a scaffold based upon decellularized ECM will entail the availability of a stable cell line needed to guarantee consistent production. Various cell lines are already available and of special interest in this context is an immortalized MSC line with an integrated inducible apoptotic mechanism (Bourgine *et al.* 2014a, Bourgine *et al.* 2014b). Although the tri-lineage differentiation potential of these cells after genetic engineering was maintained the reported use of the cell line is at current limited to the development of a cartilaginous ECM indicating that further work is required. Induced pluripotent stem cells are a different promising cell source in this context. The pluripotent differentiation potential of these cells, combined with their unlimited capacity for self-renewal make them an interesting candidate for cell therapy products and various reports of their use for skeletal applications illustrate the potential of this novel cell source for tissue engineering strategies (Park *et al.* 2014). The availability of such a cell line which could

be cultured under different conditions resulting in either a neutral, osteogenic or chondrogenic induced ECM could result in a wide range of off the shelf available scaffolds which could be used either as a substrate for cell expansion but also as a template for further construct development and tissue regeneration.

8.3.2. Integrated bioprocess development

A number of systems for automated cell expansion are already available on the market and efforts are being made towards the development of fully automated processes integrating up- and down-stream process steps. Due to cost of goods, equipment and process time, cell expansion, however, remains an expensive process step, thereby significantly influencing the price of ATMPs for which these cells are needed. Limiting the required cell expansion by optimizing process performance but also post expansion cell potency should therefore be a priority. Multi-passage *in vitro* expansion of a cell population has been shown to result in reduced proliferative and differentiation potential (Banfi *et al.* 2000, Scadden 2006, Wagner *et al.* 2008). The use of a supportive *in vitro* micro-environment, potentially based upon an ECM derived culture substrate but also including optimized media compositions and oxygen concentrations, could allow the cells to better maintain their original potency.

Also in construct development further tailoring of for example the supportive matrix or added growth factors as well as optimizing the delivery methods ensuring optimal implant survival could further decrease the need for an extensive cell expansion phase. Within skeletal TE the application of the developmental engineering paradigm aims for the *in vitro* development of a cartilaginous template to facilitate the *in vivo* bone formation (Lenas *et al.* 2011). As this process is initiated by MSC proliferation and condensation the final cell expansion step can be integrated with the initiation of the construct development circumventing the need for cell recovery, rinsing, volume reduction and seeding between these steps. Overall elimination of these particular down-stream process steps by using a one-step expansion and construct development process would be ideal to advance towards a streamlined, lean bioprocess. Due to the limited availability of autologous cells a number of expansion steps preceding the construct development will, however, be inevitable for most approaches. The use of a potent cell population which is readily available in larger numbers, such as MSCs isolated from the bone marrow or adipose tissue, could, however, significantly reduce the number of passages required form 6-8 for hPDCs to 2-3 for bone marrow derived MSCs (Robey *et al.* 2015) and potentially even less for adipose derived MSCs (Baer *et al.* 2012).

Finally, as mentioned before, the development of closed, automated processes will be imperative for the successful industrial implementation of current TE and regenerative medicine concepts in a clinically relevant setting. Rather than transferring the often manual lab scale processes to such an automated environment the intended production process should be considered from the conceptual phase onwards. Ideally, containment of the different optimized process steps within one system, such as the Cocoon bioreactor developed by Octane, should be aimed for (Martin *et al.* 2009). This modular, GMP compliant bioreactor is, to the best of our knowledge, the first system

combining the three main steps of the TE process (biopsy digest, cell expansion and construct development) in one integrated system. Despite the availability of this regulatory compliant system its application for the development of novel strategies is limited due to the associated costs. A better integration between research and product development through industrial collaborations, evolving towards research for development, will therefore be required to bring current TE concepts to the market.

Bibliography

Abbasalizadeh, S. and H. Baharvand (2013). "Technological progress and challenges towards cGMP manufacturing of human pluripotent stem cells based therapeutic products for allogeneic and autologous cell therapies." Biotechnology Advances **31**(8): 1600-1623.

Abraham, S., M. J. Riggs, K. Nelson, V. Lee and R. R. Rao (2010). "Characterization of human fibroblast-derived extracellular matrix components for human pluripotent stem cell propagation." Acta Biomater **6**(12): 4622-4633.

Agata, H., I. Asahina, Y. Yamazaki, M. Uchida, Y. Shinohara, *et al.* (2007). "Effective bone engineering with periosteum-derived cells." Journal of Dental Research **86**(1): 79-83.

Albertini, G., A. Giuliani, V. Komlev, F. Moroncini, A. Pugnaloni, *et al.* (2009). "Organization of extracellular matrix fibers within polyglycolic acid-polylactic acid scaffolds analyzed using X-ray synchrotron-radiation phase-contrast micro computed tomography." Tissue Eng Part C Methods **15**(3): 403-411.

Alves-Rausch, J., R. Bienert, C. Grimm and D. Bergmaier (2014). "Real time in-line monitoring of large scale Bacillus fermentations with near-infrared spectroscopy." J Biotechnol **189**: 120-128.

Appel, A., M. A. Anastasio and E. M. Brey (2011). "Potential for imaging engineered tissues with X-ray phase contrast." Tissue Eng Part B Rev **17**(5): 321-330.

Appel, A. A., M. A. Anastasio, J. C. Larson and E. M. Brey (2013). "Imaging challenges in biomaterials and tissue engineering." Biomaterials **34**(28): 6615-6630.

Appel, A. A., J. C. Larson, A. B. Garson, H. F. Guan, Z. Zhong, *et al.* (2015). "X-ray Phase Contrast Imaging of Calcified Tissue and Biomaterial Structure in Bioreactor Engineered Tissues." Biotechnology and Bioengineering **112**(3): 612-620.

Back, S. A., R. Khan, X. Gan, P. A. Rosenberg and J. J. Volpe (1999). "A new Alamar Blue viability assay to rapidly quantify oligodendrocyte death." J Neurosci Methods **91**(1-2): 47-54.

Baer, P. C. and H. Geiger (2012). "Adipose-Derived Mesenchymal Stromal/Stem Cells: Tissue Localization, Characterization, and Heterogeneity." Stem Cells International.

Bancroft, G. N., V. I. Sikavitsas, J. van den Dolder, T. L. Sheffield, C. G. Ambrose, *et al.* (2002). "Fluid flow increases mineralized matrix deposition in 3D perfusion culture of marrow stromal osteoblasts in a dose-dependent manner." Proc Natl Acad Sci U S A **99**(20): 12600-12605.

Banfi, A., A. Muraglia, B. Dozin, M. Mastrogiacomo, R. Cancedda, *et al.* (2000). "Proliferation kinetics and differentiation potential of ex vivo expanded human bone marrow stromal cells: Implications for their use in cell therapy." Exp Hematol **28**(6): 707-715.

Becerra, J., L. Santos-Ruiz, J. A. Andrades and M. Mari-Beffa (2011). "The Stem Cell Niche Should be a Key Issue for Cell Therapy in Regenerative Medicine." Stem Cell Reviews and Reports **7**(2): 248-255.

Beck, A., S. Woods, J. L. Lansdowne and D. Arens (2013). "The effects of multiple high-resolution peripheral quantitative computed tomography scans on bone healing in a rabbit radial bone defect model." Bone **56**(2): 312-319.

Becker, S. T., T. Douglas, Y. Acil, H. Seitz, S. Sivananthan, *et al.* (2010). "Biocompatibility of individually designed scaffolds with human periosteum for use in tissue engineering." Journal of Materials Science-Materials in Medicine **21**(4): 1255-1262.

Berneel, E., T. Desmet, H. Declercq, P. Dubruel and M. Cornelissen (2012a). "Double protein-coated poly-epsilon-caprolactone scaffolds: Successful 2D to 3D transfer." Journal of Biomedical Materials Research Part A **100A**(7): 1783-1791.
Berneel, E. M., T. Desmet, H. Declercq, P. Dubruel and R. Cornelissen (2012b). "Biological evaluation of a successful transferred double protein coating from 2D PCL coatings to 3D scaffolds." Journal of Tissue Engineering and Regenerative Medicine **6**: 372-372.
Bianco, P., X. Cao, P. S. Frenette, J. J. Mao, P. G. Robey, *et al.* (2013). "The meaning, the sense and the significance: translating the science of mesenchymal stem cells into medicine." Nature Medicine **19**(1): 35-42.
Bieback, K. (2013). "Platelet lysate as replacement for fetal bovine serum in mesenchymal stromal cell cultures." Transfus Med Hemother **40**(5): 326-335.
Bieback, K., A. Hecker, A. Kocaomer, H. Lannert, K. Schallmoser, *et al.* (2009). "Human alternatives to fetal bovine serum for the expansion of mesenchymal stromal cells from bone marrow." Stem Cells **27**(9): 2331-2341.
Bigham-Sadegh, A. and A. Oryan (2015). "Basic concepts regarding fracture healing and the current options and future directions in managing bone fractures." International Wound Journal **12**(3): 238-247.
Bjerre, L., C. E. Bunger, M. Kassem and T. Mygind (2008). "Flow perfusion culture of human mesenchymal stem cells on silicate-substituted tricalcium phosphate scaffolds." Biomaterials **29**(17): 2616-2627.
Blewitt, P. W. (1984). "Histological and Histochemical Methods - Kiernan,Ja." Biochemical Education **12**(1): 46-46.
Bose, S., M. Roy and A. Bandyopadhyay (2012). "Recent advances in bone tissue engineering scaffolds." Trends Biotechnol **30**(10): 546-554.
Bourgine, P., C. Le Magnen, S. Pigeot, J. Geurts, A. Scherberich, *et al.* (2014a). "Combination of immortalization and inducible death strategies to generate a human mesenchymal stromal cell line with controlled survival." Stem Cell Res **12**(2): 584-598.
Bourgine, P. E., C. Scotti, S. Pigeot, L. A. Tchang, A. Todorov, *et al.* (2014b). "Osteoinductivity of engineered cartilaginous templates devitalized by inducible apoptosis." Proc Natl Acad Sci U S A.
Braccini, A., D. Wendt, C. Jaquiery, M. Jakob, M. Heberer, *et al.* (2005). "Three-dimensional perfusion culture of human bone marrow cells and generation of osteoinductive grafts." Stem Cells **23**(8): 1066-1072.
Brown, M. A., C. S. Wallace, C. C. Anamelechi, E. Clermont, W. M. Reichert, *et al.* (2007). "The use of mild trypsinization conditions in the detachment of endothelial cells to promote subsequent endothelialization on synthetic surfaces." Biomaterials **28**(27): 3928-3935.
Buhring, H. J., V. L. Battula, S. Treml, B. Schewe, L. Kanz, *et al.* (2007). "Novel markers for the prospective isolation of human MSC." Hematopoietic Stem Cells Vi **1106**: 262-271.
Buytaert, J. A. N., S. B. Johnson, M. Dierick, W. H. M. Salih and P. A. Santi (2013). "MicroCT versus sTSLIM 3D Imaging of the Mouse Cochlea." Journal of Histochemistry & Cytochemistry **61**(5): 382-395.
Cancedda, R., A. Cedola, A. Giuliani, V. Komlev, S. Lagomarsino, *et al.* (2007). "Bulk and interface investigations of scaffolds and tissue-engineered bones by X-ray microtomography and X-ray microdiffraction." Biomaterials **28**(15): 2505-2524.
Cartmell, S., K. Huynh, A. Lin, S. Nagaraja and R. Guldberg (2004). "Quantitative microcomputed tomography analysis of mineralization within three-dimensional scaffolds in vitro." Journal of Biomedical Materials Research Part A **69A**(1): 97-104.
Cartmell, S. H., B. D. Porter, A. J. Garcia and R. E. Guldberg (2003). "Effects of medium perfusion rate on cell-seeded three-dimensional bone constructs in vitro." Tissue Eng **9**(6): 1197-1203.
Centola, M., B. Tonnarelli, J. Hendriks, M. Van den Doel, W. De Jong, *et al.* (2014). "An improved cartilage digestion method for research and clinical applications." Journal of Tissue Engineering and Regenerative Medicine **8**: 148-149.
Chai, Y. C., G. Kerckhofs, S. J. Roberts, S. Van Bael, E. Schepers, *et al.* (2012a). "Ectopic bone formation by 3D porous calcium phosphate-Ti6Al4V hybrids produced by perfusion electrodeposition." Biomaterials **33**(16): 4044-4058.
Chai, Y. C., S. J. Roberts, E. Desmet, G. Kerckhofs, N. van Gastel, *et al.* (2012b). "Mechanisms of ectopic bone formation by human osteoprogenitor cells on CaP biomaterial carriers." Biomaterials **33**(11): 3127-3142.
Chai, Y. C., S. J. Roberts, E. Desmet, G. Kerckhofs, N. van Gastel, *et al.* (2012c). "Mechanisms of ectopic bone formation by human osteoprogenitor cells on CaP biomaterial carriers." Biomaterials **33**(11): 3127-3142.
Chai, Y. C., S. J. Roberts, J. Schrooten and F. P. Luyten (2011). "Probing the osteoinductive effect of calcium phosphate by using an in vitro biomimetic model." Tissue Eng Part A **17**(7-8): 1083-1097.

Chai, Y. C., S. J. Roberts, S. Van Bael, Y. Chen, F. P. Luyten, *et al.* (2012d). "Multi-Level Factorial Analysis of Ca2+/P-i Supplementation as Bio-Instructive Media for In Vitro Biomimetic Engineering of Three-Dimensional Osteogenic Hybrids." Tissue Engineering Part C-Methods **18**(2): 90-103.
Chalal, M., F. Ehrburger-Dolle, I. Morfin, J. C. Vial, M. R. A. de Armas, *et al.* (2009). "Imaging the Structure of Macroporous Hydrogels by Two-Photon Fluorescence Microscopy." Macromolecules **42**(7): 2749-2755.
Chang, J., H. Lei, Q. Liu, S. Qin, K. Ma, *et al.* (2012). "Optimization of culture of mesenchymal stem cells: a comparison of conventional plate and microcarrier cultures." Cell Prolif **45**(5): 430-437.
Chen, A. K., S. Reuveny and S. K. Oh (2013). "Application of human mesenchymal and pluripotent stem cell microcarrier cultures in cellular therapy: achievements and future direction." Biotechnology Advances **31**(7): 1032-1046.
Chen, C. W., M. W. Betz, J. P. Fisher, A. Paek and Y. Chen (2011). "Macroporous hydrogel scaffolds and their characterization by optical coherence tomography." Tissue Eng Part C Methods **17**(1): 101-112.
Chen, H. C. and Y. C. Hu (2006). "Bioreactors for tissue Engineering." Biotechnology Letters **28**(18): 1415-1423.
Chen, M. Q., M. Zhou, Z. Y. Ye, Y. Zhou and W. S. Tan (2014). "Ectopic Osteogenesis of Macroscopic Tissue Constructs Assembled from Human Mesenchymal Stem Cell-Laden Microcarriers through In Vitro Perfusion Culture." Plos One **9**(10).
Chen, W. L., C. H. Huang, L. L. Chiou, T. H. Chen, Y. Y. Huang, *et al.* (2010). "Multiphoton imaging and quantitative analysis of collagen production by chondrogenic human mesenchymal stem cells cultured in chitosan scaffold." Tissue Eng Part C Methods **16**(5): 913-920.
Chen, X. D., V. Dusevich, J. Q. Feng, S. C. Manolagas and R. L. Jilka (2007). "Extracellular matrix made by bone marrow cells facilitates expansion of marrow-derived mesenchymal progenitor cells and prevents their differentiation into osteoblasts." Journal of Bone and Mineral Research **22**(12): 1943-1956.
Chen, Y. T., M. Sonnaert, S. J. Roberts, F. P. Luyten and J. Schrooten (2012). "Validation of a PicoGreen-Based DNA Quantification Integrated in an RNA Extraction Method for Two-Dimensional and Three-Dimensional Cell Cultures." Tissue Engineering Part C-Methods **18**(6): 444-452.
Chew, W. and P. Sharratt (2010). "Trends in process analytical technology." Analytical Methods **2**(10): 1412-1438.
Chong, L., M. Saghafi, C. Knappe, S. Steigmiller, C. Matanguihan, *et al.* (2013). "Robust on-line sampling and analysis during long-term perfusion cultivation of mammalian cells." J Biotechnol **165**(2): 133-137.
Cierpka, K., C. L. Elseberg, K. Niss, M. Kassem, D. Salzig, *et al.* (2013). "hMSC Production in Disposable Bioreactors with Regards to GMP and PAT." Chemie Ingenieur Technik **85**(1-2): 67-75.
Clavaud, M., Y. Roggo, R. Von Daeniken, A. Liebler and J. O. Schwabe (2013). "Chemometrics and in-line near infrared spectroscopic monitoring of a biopharmaceutical Chinese hamster ovary cell culture: prediction of multiple cultivation variables." Talanta **111**: 28-38.
Costa, P. F., A. Martins, N. M. Neves, M. E. Gomes and R. L. Reis (2014). "Automating the Processing Steps for Obtaining Bone Tissue-Engineered Substitutes: From Imaging Tools to Bioreactors." Tissue Engineering Part B-Reviews **20**(6): 567-577.
Cui, Z. F., X. Xu, N. Trainor, J. T. Triffitt, J. P. Urban, *et al.* (2007). "Application of multiple parallel perfused microbioreactors and three-dimensional stem cell culture for toxicity testing." Toxicol In Vitro **21**(7): 1318-1324.
Cukierman, E., R. Pankov and K. M. Yamada (2002). "Cell interactions with three-dimensional matrices." Curr Opin Cell Biol **14**(5): 633-639.
Cunha, B., T. Aguiar, M. M. Silva, R. J. Silva, M. F. Sousa, *et al.* (2015a). "Exploring continuous and integrated strategies for the up- and downstream processing of human mesenchymal stem cells." J Biotechnol.
Cunha, B., C. Peixoto, M. M. Silva, M. J. Carrondo, M. Serra, *et al.* (2015b). "Filtration methodologies for the clarification and concentration of human mesenchymal stem cells." Journal of Membrane Science **478**: 117-129.
Custodio, C. A., R. L. Reis and J. F. Mano (2014). "Engineering biomolecular microenvironments for cell instructive biomaterials." Adv Healthc Mater **3**(6): 797-810.
Dai, K. R., D. Q. Li, T. T. Tang and J. X. Lu (2009). "Effects of Flow Shear Stress and Mass Transport on the Construction of a Large-Scale Tissue-Engineered Bone in a Perfusion Bioreactor." Tissue Engineering Part A **15**(10): 2773-2783.
Das, R. H., G. J. van Osch, M. Kreukniet, J. Oostra, H. Weinans, *et al.* (2010). "Effects of individual control of pH and hypoxia in chondrocyte culture." J Orthop Res **28**(4): 537-545.
Davis, T. J., D. Gao, T. E. Gureyev, A. W. Stevenson and S. W. Wilkins (1995). "Phase-Contrast Imaging of Weakly Absorbing Materials Using Hard X-Rays." Nature **373**(6515): 595-598.

De Bari, C., F. Dell'Accio and F. P. Luyten (2001). "Human periosteum-derived cells maintain phenotypic stability and chondrogenic potential throughout expansion regardless of donor age." Arthritis and Rheumatism **44**(1): 85-95.
De Bari, C., F. Dell'Accio, J. Vanlauwe, J. Eyckmans, I. M. Khan, *et al.* (2006). "Mesenchymal multipotency of adult human periosteal cells demonstrated by single-cell lineage analysis." Arthritis and Rheumatism **54**(4): 1209-1221.
De Man, B., J. Nuyts, P. Dupont, G. Marchal and P. Suetens (1999). "Metal streak artifacts in X-ray computed tomography: A simulation study." Ieee Transactions on Nuclear Science **46**(3): 691-696.
De Napoli, I. E., S. Scaglione, P. Giannoni, R. Quarto and G. Catapano (2011). "Mesenchymal stem cell culture in convection-enhanced hollow fibre membrane bioreactors for bone tissue engineering." Journal of Membrane Science **379**(1-2): 341-352.
Delahaye, M., K. Lawrence, S. J. Ward and M. Hoare (2015). "An ultra scale-down analysis of the recovery by dead-end centrifugation of human cells for therapy." Biotechnol Bioeng **112**(5): 997-1011.
Demol, J., D. Lambrechts, L. Geris, J. Schrooten and H. Van Oosterwyck (2011). "Towards a quantitative understanding of oxygen tension and cell density evolution in fibrin hydrogels." Biomaterials **32**(1): 107-118.
Desmet, T., T. Billiet, E. Berneel, R. Cornelissen, D. Schaubroeck, *et al.* (2010). "Post-Plasma Grafting of AEMA as a Versatile Tool to Biofunctionalise Polyesters for Tissue Engineering." Macromolecular Bioscience **10**(12): 1484-1494.
Diogo, M. M., C. L. da Silva and J. M. Cabral (2012). "Separation technologies for stem cell bioprocessing." Biotechnol Bioeng **109**(11): 2699-2709.
Dominici, M., K. Le Blanc, I. Mueller, I. Slaper-Cortenbach, F. C. Marini, *et al.* (2006). "Minimal criteria for defining multipotent mesenchymal stromal cells. The International Society for Cellular Therapy position statement." Cytotherapy **8**(4): 315-317.
dos Santos, F., P. Z. Andrade, M. M. Abecasis, J. M. Gimble, L. G. Chase, *et al.* (2011a). "Toward a Clinical-Grade Expansion of Mesenchymal Stem Cells from Human Sources: A Microcarrier-Based Culture System Under Xeno-Free Conditions." Tissue Engineering Part C-Methods **17**(12): 1201-1210.
dos Santos, F., P. Z. Andrade, G. Eibes, C. L. da Silva and J. M. Cabral (2011b). "Ex vivo expansion of human mesenchymal stem cells on microcarriers." Methods Mol Biol **698**: 189-198.
Dos Santos, F., A. Campbell, A. Fernandes-Platzgummer, P. Z. Andrade, J. M. Gimble, *et al.* (2014). "A xenogeneic-free bioreactor system for the clinical-scale expansion of human mesenchymal stem/stromal cells." Biotechnol Bioeng **111**(6): 1116-1127.
dos Santos, F. F., P. Z. Andrade, C. L. da Silva and J. M. S. Cabral (2013). "Bioreactor design for clinical-grade expansion of stem cells." Biotechnology Journal **8**(6): 644-654.
Du, D. J., K. S. Furukawa and T. Ushida (2009). "3D Culture of Osteoblast-Like Cells by Unidirectional or Oscillatory Flow for Bone Tissue Engineering." Biotechnology and Bioengineering **102**(6): 1670-1678.
Eibes, G., F. dos Santos, P. Z. Andrade, J. S. Boura, M. M. Abecasis, *et al.* (2010). "Maximizing the ex vivo expansion of human mesenchymal stem cells using a microcarrier-based stirred culture system." J Biotechnol **146**(4): 194-197.
Eniwumide, J. O., H. Yuan, S. H. Cartmell, G. J. Meijer and J. D. de Bruijn (2007). "Ectopic bone formation in bone marrow stem cell seeded calcium phosphate scaffolds as compared to autograft and (cell seeded) allograft." Eur Cell Mater **14**: 30-38; discussion 39.
Eyckmans, J. and F. P. Luyten (2006a). "Species specificity of ectopic bone formation using periosteum-derived mesenchymal progenitor cells." Tissue Eng **12**(8): 2203-2213.
Eyckmans, J. and F. P. Luyten (2006b). "Species specificity of ectopic bone formation using periosteum-derived mesenchymal progenitor cells." Tissue Engineering **12**(8): 2203-2213.
Fei, J., F. Peyrin, L. Malaval, L. Vico and M. H. Lafage-Proust (2010). "Imaging and quantitative assessment of long bone vascularization in the adult rat using microcomputed tomography." Anat Rec (Hoboken) **293**(2): 215-224.
Fekete, N., M. T. Rojewski, D. Furst, L. Kreja, A. Ignatius, *et al.* (2012). "GMP-Compliant Isolation and Large-Scale Expansion of Bone Marrow-Derived MSC." Plos One **7**(8).
Fernandes, T. G., C. A. V. Rodrigues, M. M. Diogo and J. M. S. Cabral (2013). "Stem cell bioprocessing for regenerative medicine." Journal of Chemical Technology and Biotechnology **89**: 34-47.
Fisher, J. P. and A. B. Yeatts (2011). "Bone tissue engineering bioreactors: Dynamic culture and the influence of shear stress." Bone **48**(2): 171-181.
Franceschi, R. T., C. X. Ge, G. Z. Xiao, H. Roca and D. Jiang (2007). "Transcriptional regulation of osteoblasts." Skeletal Biology and Medicine, Pt A **1116**: 196-207.

Frauenschuh, S., E. Reichmann, Y. Ibold, P. M. Goetz, M. Sittinger, *et al.* (2007). "A microcarrier-based cultivation system for expansion of primary mesenchymal stem cells." Biotechnology Progress **23**(1): 187-193.
Frese, J., A. Morgenroth, M. E. Mertens, S. Koch, L. Rongen, *et al.* (2014). "Nondestructive monitoring of tissue-engineered constructs." Biomed Tech (Berl) **59**(2): 165-175.
Frohlich, M., W. L. Grayson, D. Marolt, J. M. Gimble, N. Kregar-Velikonja, *et al.* (2010). "Bone Grafts Engineered from Human Adipose-Derived Stem Cells in Perfusion Bioreactor Culture." Tissue Engineering Part A **16**(1): 179-189.
Gardel, L. S., L. A. Serra, R. L. Reis and M. E. Gomes (2014). "Use of Perfusion Bioreactors and Large Animal Models for Long Bone Tissue Engineering." Tissue Engineering Part B-Reviews **20**(2): 126-146.
Gattazzo, F., A. Urciuolo and P. Bonaldo (2014). "Extracellular matrix: a dynamic microenvironment for stem cell niche." Biochim Biophys Acta **1840**(8): 2506-2519.
Georgakoudi, I., W. L. Rice, M. Hronik-Tupaj and D. L. Kaplan (2008). "Optical Spectroscopy and Imaging for the Noninvasive Evaluation of Engineered Tissues." Tissue Engineering Part B-Reviews **14**(4): 321-340.
Georgi, N., C. van Blitterswijk and M. Karperien (2014). "Mesenchymal Stromal/Stem Cell- or Chondrocyte-Seeded Microcarriers as Building Blocks for Cartilage Tissue Engineering." Tissue Engineering Part A **20**(17-18): 2513-2523.
Gerontas, S., S. S. Farid and M. Hoare (2009). "Windows of Operation for Bioreactor Design for the Controlled Formation of Tissue-Engineered Arteries." Biotechnology Progress **25**(3): 842-853.
Ghaemi, S. R., F. J. Harding, B. Delalat, S. Gronthos and N. H. Voelcker (2013). "Exploring the mesenchymal stem cell niche using high throughput screening." Biomaterials **34**(31): 7601-7615.
Giannoudis, P. V., T. A. Einhorn and D. Marsh (2007). "Fracture healing: the diamond concept." Injury **38 Suppl 4**: S3-6.
Gignac, P. M. and N. J. Kley (2014). "Iodine-enhanced micro-CT imaging: methodological refinements for the study of the soft-tissue anatomy of post-embryonic vertebrates." J Exp Zool B Mol Dev Evol **322**(3): 166-176.
Ginai, A. Z. (1987). "Clinical Use of Hexabrix for Radiological Evaluation of Leakage from the Upper Gastrointestinal-Tract Based on Experimental-Study." British Journal of Radiology **60**(712): 343-346.
Gloeckner, H., T. Jonuleit and H. D. Lemke (2001). "Monitoring of cell viability and cell growth in a hollow-fiber bioreactor by use of the dye Alamar Blue." J Immunol Methods **252**(1-2): 131-138.
Godara, P., C. D. McFarland and R. E. Nordon (2008). "Design of bioreactors for mesenchymal stem cell tissue engineering." Journal of Chemical Technology and Biotechnology **83**(4): 408-420.
Goh, T. K., Z. Y. Zhang, A. K. Chen, S. Reuveny, M. Choolani, *et al.* (2013). "Microcarrier culture for efficient expansion and osteogenic differentiation of human fetal mesenchymal stem cells." Biores Open Access **2**(2): 84-97.
Goldstein, A. S., T. M. Juarez, C. D. Helmke, M. C. Gustin and A. G. Mikos (2001). "Effect of convection on osteoblastic cell growth and function in biodegradable polymer foam scaffolds." Biomaterials **22**(11): 1279-1288.
Gomes, M. E., V. I. Sikavitsas, E. Behravesh, R. L. Reis and A. G. Mikos (2003). "Effect of flow perfusion on the osteogenic differentiation of bone marrow stromal cells cultured on starch-based three-dimensional scaffolds." Journal of Biomedical Materials Research Part A **67A**(1): 87-95.
Granton, P. V., S. I. Pollmann, N. L. Ford, M. Drangova and D. W. Holdsworth (2008). "Implementation of dual- and triple-energy cone-beam micro-CT for postreconstruction material decomposition." Med Phys **35**(11): 5030-5042.
Grayson, W. L., S. Bhumiratana, C. Cannizzaro, P. H. Chao, D. P. Lennon, *et al.* (2008). "Effects of initial seeding density and fluid perfusion rate on formation of tissue-engineered bone." Tissue Eng Part A **14**(11): 1809-1820.
Grayson, W. L., M. Frohlich, K. Yeager, S. Bhumiratana, M. E. Chan, *et al.* (2010). "Engineering anatomically shaped human bone grafts." Proceedings of the National Academy of Sciences of the United States of America **107**(8): 3299-3304.
Grayson, W. L., T. Ma and B. Bunnell (2004). "Human mesenchymal stem cells tissue development in 3D PET matrices." Biotechnol Prog **20**(3): 905-912.
Grayson, W. L., D. Marolt, S. Bhumiratana, M. Frohlich, X. E. Guo, *et al.* (2011). "Optimizing the Medium Perfusion Rate in Bone Tissue Engineering Bioreactors." Biotechnology and Bioengineering **108**(5): 1159-1170.
Grayson, W. L., F. Zhao, B. Bunnell and T. Ma (2007). "Hypoxia enhances proliferation and tissue formation of human mesenchymal stem cells." Biochemical and Biophysical Research Communications **358**(3): 948-953.

Griffon, D. J., J. P. Abulencia, G. R. Ragetly, L. P. Fredericks and S. Chaieb (2011). "A comparative study of seeding techniques and three-dimensional matrices for mesenchymal cell attachment." Journal of Tissue Engineering and Regenerative Medicine **5**(3): 169-179.
Gudur, M., R. R. Rao, Y. S. Hsiao, A. W. Peterson, C. X. Deng, *et al.* (2012). "Noninvasive, quantitative, spatiotemporal characterization of mineralization in three-dimensional collagen hydrogels using high-resolution spectral ultrasound imaging." Tissue Eng Part C Methods **18**(12): 935-946.
Guilak, F., D. L. Butler, S. A. Goldstein and F. P. Baaijens (2014). "Biomechanics and mechanobiology in functional tissue engineering." J Biomech **47**(9): 1933-1940.
Guldberg, R. E., C. L. Duvall, A. Peister, M. E. Oest, A. S. P. Lin, *et al.* (2008). "3D imaging of tissue integration with porous biomaterials." Biomaterials **29**(28): 3757-3761.
Hagenmueller, H., S. Hofmann, T. Kohler, H. P. Merkle, D. L. Kaplan, *et al.* (2007). "Non-invasive time-lapsed monitoring and quantification of engineered bone-like tissue." Annals of Biomedical Engineering **35**(10): 1657-1667.
Hagenmuller, H., M. Hitz, H. P. Merkle, L. Meinel and R. Muller (2010). "Design and validation of a novel bioreactor principle to combine online micro-computed tomography monitoring and mechanical loading in bone tissue engineering." Rev Sci Instrum **81**(1): 014303.
Hanker, J. S. and B. I. Giammara (1983). "Principles and Techniques of Electron-Microscopy, Biological Applications, Vol 1, 2nd Edition - Hayat,Ma." Stain Technology **58**(3): 184-184.
Hao, J., Y. Zhang, D. Jing, Y. Shen, G. Tang, *et al.* (2015). "Mechanobiology of mesenchymal stem cells: Perspective into mechanical induction of MSC fate." Acta Biomater **20**: 1-9.
Haycock, J. W. (2011). "3D cell culture: a review of current approaches and techniques." Methods Mol Biol **695**: 1-15.
He, F., X. Chen and M. Pei (2009). "Reconstruction of an in vitro tissue-specific microenvironment to rejuvenate synovium-derived stem cells for cartilage tissue engineering." Tissue Eng Part A **15**(12): 3809-3821.
Heathman, T. R., V. A. Glyn, A. Picken, Q. A. Rafiq, K. Coopman, *et al.* (2015). "Expansion, harvest and cryopreservation of human mesenchymal stem cells in a serum-free microcarrier process." Biotechnol Bioeng.
Hedberg, E. L., H. C. Kroese-Deutman, C. K. Shih, J. J. Lemoine, M. A. K. Liebschner, *et al.* (2005). "Methods: A comparative analysis of radiography, microcomputed tomography, and histology for bone tissue engineering." Tissue Engineering **11**(9-10): 1356-1367.
Hewitt, C. J., K. Lee, A. W. Nienow, R. J. Thomas, M. Smith, *et al.* (2011). "Expansion of human mesenchymal stem cells on microcarriers." Biotechnology Letters **33**(11): 2325-2335.
Hilldore, A., A. Wojtowicz and A. W. Johnson (2007). "Micro-CT based quantification of non-mineralized tissue on cultured hydroxyapatite scaffolds." Journal of Biomedical Materials Research Part A **82A**(4): 1012-1021.
Hofbauer, P., S. Riedl, K. Witzeneder, F. Hildner, S. Wolbank, *et al.* (2014). "Human platelet lysate is a feasible candidate to replace fetal calf serum as medium supplement for blood vascular and lymphatic endothelial cells." Cytotherapy **16**(9): 1238-1244.
Hosseinkhani, H., Y. Inatsugu, Y. Hiraoka, S. Inoue and Y. Tabata (2005). "Perfusion culture enhances osteogenic differentiation of rat mesenchymal stem cells in collagen sponge reinforced with poly(glycolic acid) fiber." Tissue Engineering **11**(9-10): 1476-1488.
Hutmacher, D. W. and M. Sittinger (2003). "Periosteal cells in bone tissue engineering." Tissue Engineering **9**: S45-S64.
Im, G. I., Y. W. Shin and K. B. Lee (2005). "Do adipose tissue-derived mesenchymal stem cells have the same osteogenic and chondrogenic potential as bone marrow-derived cells?" Osteoarthritis and Cartilage **13**(10): 845-853.
Impens, S., Y. Chen, S. Mullens, F. Luyten and J. Schrooten (2010a). "Controlled Cell-Seeding Methodologies: A First Step Toward Clinically Relevant Bone Tissue Engineering Strategies." Tissue Eng Part C Methods **16**(6): 1575-1583.
Impens, S., Y. T. Chen, S. Mullens, F. Luyten and J. Schrooten (2010b). "Controlled Cell-Seeding Methodologies: A First Step Toward Clinically Relevant Bone Tissue Engineering Strategies." Tissue Engineering Part C-Methods **16**(6): 1575-1583.
Ingber, D. E., V. C. Mow, D. Butler, L. Niklason, J. Huard, *et al.* (2006). "Tissue engineering and developmental biology: going biomimetic." Tissue Eng **12**(12): 3265-3283.
Ishaug, S. L., G. M. Crane, M. J. Miller, A. W. Yasko, M. J. Yaszemski, *et al.* (1997). "Bone formation by three-dimensional stromal osteoblast culture in biodegradable polymer scaffolds." J Biomed Mater Res **36**(1): 17-28.

Jaasma, M. J., N. A. Plunkett and F. J. O'Brien (2008). "Design and validation of a dynamic flow perfusion bioreactor for use with compliant tissue engineering scaffolds." Journal of Biotechnology **133**(4): 490-496.
Jakob, M., O. Demarteau, D. Schafer, M. Stumm, M. Heberer, *et al.* (2003). "Enzymatic digestion of adult human articular cartilage yields a small fraction of the total available cells." Connect Tissue Res **44**(3-4): 173-180.
Jakob, M., F. Saxer, C. Scotti, S. Schreiner, P. Studer, *et al.* (2012). "Perspective on the Evolution of Cell-Based Bone Tissue Engineering Strategies." European Surgical Research **49**(1): 1-7.
Jakobsen, R. B., E. Ostrup, X. Zhang, T. S. Mikkelsen and J. E. Brinchmann (2014). "Analysis of the effects of five factors relevant to in vitro chondrogenesis of human mesenchymal stem cells using factorial design and high throughput mRNA-profiling." PLoS One **9**(5): e96615.
Janssen, F. W., I. Hofland, A. van Oorschot, J. Oostra, H. Peters, *et al.* (2006a). "Online measurement of oxygen consumption by goat bone marrow stromal cells in a combined cell-seeding and proliferation perfusion bioreactor." J Biomed Mater Res A **79**(2): 338-348.
Janssen, F. W., J. Oostra, A. Oorschot and C. A. van Blitterswijk (2006b). "A perfusion bioreactor system capable of producing clinically relevant volumes of tissue-engineered bone: in vivo bone formation showing proof of concept." Biomaterials **27**(3): 315-323.
Jeffery, N. S., R. S. Stephenson, J. A. Gallagher, J. C. Jarvis and P. G. Cox (2011). "Micro-computed tomography with iodine staining resolves the arrangement of muscle fibres." Journal of Biomechanics **44**(1): 189-192.
Jenkins, M. J. and S. S. Farid (2015). "Human pluripotent stem cell-derived products: advances towards robust, scalable and cost-effective manufacturing strategies." Biotechnol J **10**(1): 83-95.
Jiang, J. and E. T. Papoutsakis (2013). "Stem-cell niche based comparative analysis of chemical and nano-mechanical material properties impacting ex vivo expansion and differentiation of hematopoietic and mesenchymal stem cells." Adv Healthc Mater **2**(1): 25-42.
Jones, A. C., C. H. Arns, D. W. Hutmacher, B. K. Milthorpe, A. P. Sheppard, *et al.* (2009). "The correlation of pore morphology, interconnectivity and physical properties of 3D ceramic scaffolds with bone ingrowth." Biomaterials **30**(7): 1440-1451.
Jones, A. C., C. H. Arns, A. P. Sheppard, D. W. Hutmacher, B. K. Milthorpe, *et al.* (2007). "Assessment of bone ingrowth into porous biomaterials using MICRO-CT." Biomaterials **28**(15): 2491-2504.
Jones, E. A., A. English, S. E. Kinsey, L. Straszynski, P. Emery, *et al.* (2006). "Optimization of a flow cytometry-based protocol for detection and phenotypic characterization of multipotent mesenchymal stromal cells from human bone marrow." Cytometry Part B-Clinical Cytometry **70B**(6): 391-399.
Jones, M., M. Varella-Garcia, M. Skokan, S. Bryce, J. Schowinsky, *et al.* (2013). "Genetic stability of bone marrow-derived human mesenchymal stromal cells in the Quantum System." Cytotherapy **15**(11): 1323-1339.
Jung, S., K. M. Panchalingam, L. Rosenberg and L. A. Behei (2012a). "Ex Vivo Expansion of Human Mesenchymal Stem Cells in Defined Serum-Free Media." Stem Cells International **2012**: 21.
Jung, S., K. M. Panchalingam, R. D. Wuerth, L. Rosenberg and L. A. Behie (2012b). "Large-scale production of human mesenchymal stem cells for clinical applications." Biotechnol Appl Biochem **59**(2): 106-120.
Jungreuthmayer, C., S. W. Donahue, M. J. Jaasma, A. A. Al-Munajjed, J. Zanghellini, *et al.* (2009). "A Comparative Study of Shear Stresses in Collagen-Glycosaminoglycan and Calcium Phosphate Scaffolds in Bone Tissue-Engineering Bioreactors." Tissue Engineering Part A **15**(5): 1141-1149.
Kassis, I., L. Zangi, R. Rivkin, L. Levdansky, S. Samuel, *et al.* (2006). "Isolation of mesenchymal stem cells from G-CSF-mobilized human peripheral blood using fibrin microbeads." Bone Marrow Transplantation **37**(10): 967-976.
Kell, D. B., M. Brown, H. M. Davey, W. B. Dunn, I. Spasic, *et al.* (2005). "Metabolic footprinting and systems biology: The medium is the message." Nature Reviews Microbiology **3**(7): 557-565.
Kerckhofs, G., G. Pyka, M. Moesen, S. Van Bael, J. Schrooten, *et al.* (2013a). "High-Resolution Microfocus X-Ray Computed Tomography for 3D Surface Roughness Measurements of Additive Manufactured Porous Materials." Advanced Engineering Materials **15**(3): 153-158.
Kerckhofs, G., J. Sainz, M. Maréchal, M. Wevers, T. Van de Putte, *et al.* (2014). "Contrast-Enhanced Nanofocus X-Ray Computed Tomography Allows Virtual Three-Dimensional Histopathology and Morphometric Analysis of Osteoarthritis in Small Animal Models." Cartilage **5**(1): 55-65.
Kerckhofs, G., J. Sainz, M. Wevers, T. Van de Putte and J. Schrooten (2013b). "Contrast-enhanced nanofocus computed tomography images the cartilage subtissue architecture in three dimensions." Eur Cell Mater **25**: 179-189.

Kerckhofs, G., J. Schrooten, T. Van Cleynenbreugel, S. V. Lomov and M. Wevers (2008). "Validation of x-ray microfocus computed tomography as an imaging tool for porous structures." Review of Scientific Instruments **79**(1): 1-9.
Kern, S., H. Eichler, J. Stoeve, H. Kluter and K. Bieback (2006). "Comparative analysis of mesenchymal stem cells from bone marrow, umbilical cord blood, or adipose tissue." Stem Cells **24**(5): 1294-1301.
Khazalpour, S. and D. Nematollahi (2014). "Electrochemical study of Alamar Blue (resazurin) in aqueous solutions and room-temperature ionic liquid 1-butyl-3-methylimidazolium tetrafluoroborate at a glassy carbon electrode." Rsc Advances **4**(17): 8431-8438.
Kim, J. and T. Ma (2012). "Perfusion regulation of hMSC microenvironment and osteogenic differentiation in 3D scaffold." Biotechnol Bioeng **109**(1): 252-261.
Kirouac, D. C. and P. W. Zandstra (2008). "The Systematic Production of Cells for Cell Therapies." Cell Stem Cell **3**(4): 369-381.
Kolf, C. M., E. Cho and R. S. Tuan (2007). "Mesenchymal stromal cells. Biology of adult mesenchymal stem cells: regulation of niche, self-renewal and differentiation." Arthritis Res Ther **9**(1): 204.
Kreitz, S., G. Dohmen, S. Hasken, T. Schmitz-Rode, P. Mela, *et al.* (2011). "Nondestructive method to evaluate the collagen content of fibrin-based tissue engineered structures via ultrasound." Tissue Eng Part C Methods **17**(10): 1021-1026.
Kreutz, C. and J. Timmer (2009). "Systems biology: experimental design." Febs Journal **276**(4): 923-942.
Kronenberg, H. M. (2003). "Developmental regulation of the growth plate." Nature **423**(6937): 332-336.
Lai, Y., Y. Sun, C. M. Skinner, E. L. Son, Z. Lu, *et al.* (2010). "Reconstitution of marrow-derived extracellular matrix ex vivo: a robust culture system for expanding large-scale highly functional human mesenchymal stem cells." Stem Cells Dev **19**(7): 1095-1107.
Lakin, B. A., D. J. Grasso, S. S. Shah, R. C. Stewart, P. N. Bansal, *et al.* (2013). "Cationic agent contrast-enhanced computed tomography imaging of cartilage correlates with the compressive modulus and coefficient of friction." Osteoarthritis Cartilage **21**(1): 60-68.
Lambrechts, T., I. Papantoniou, M. Sonnaert, J. Schrooten and J. M. Aerts (2014). "Model-Based Cell Number Quantification Using Online Single-Oxygen Sensor Data for Tissue Engineering Perfusion Bioreactors." Biotechnology and Bioengineering **111**(10): 1982-1992.
Lammens, J., A. Laumen, H. Delport and J. Vanlauwe (2012). "The Pentaconcept in skeletal tissue engineering. A combined approach for the repair of bone defects." Acta Orthop Belg **78**(5): 569-573.
Langer, M., Y. Liu, F. Tortelli, P. Cloetens, R. Cancedda, *et al.* (2010). "Regularized phase tomography enables study of mineralized and unmineralized tissue in porous bone scaffold." J Microsc **238**(3): 230-239.
Langer, R. and J. P. Vacanti (1993). "Tissue Engineering." Science **260**(5110): 920-926.
Laperre, K., M. Depypere, N. van Gastel, S. Torrekens, K. Moermans, *et al.* (2011). "Development of micro-CT protocols for in vivo follow-up of mouse bone architecture without major radiation side effects." Bone **49**(4): 613-622.
Lau, T. T., Y. Peck, W. Huang and D. A. Wang (2014). "Optimization of Chondrocyte Isolation and Phenotype Characterization for Cartilage Tissue Engineering." Tissue Eng Part C Methods.
Lenas, P. and F. P. Luyten (2011). "An Emerging Paradigm in Tissue Engineering: From Chemical Engineering to Developmental Engineering for Bioartificial Tissue Formation through a Series of Unit Operations that Simulate the In Vivo Successive Developmental Stages." Industrial & Engineering Chemistry Research **50**(2): 482-522.
Li, J. and M. Pei (2011). "Optimization of an in vitro three-dimensional microenvironment to reprogram synovium-derived stem cells for cartilage tissue engineering." Tissue Eng Part A **17**(5-6): 703-712.
Li, Z. and Z. Cui (2014). "Three-dimensional perfused cell culture." Biotechnol Adv **32**(2): 243-254.
Lian, J. B., G. S. Stein, A. Javed, A. J. van Wijnen, J. L. Stein, *et al.* (2006). "Networks and hubs for the transcriptional control of osteoblastogenesis." Reviews in Endocrine & Metabolic Disorders **7**(1-2): 1-16.
Lieberman, J. R., A. Daluiski and T. A. Einhorn (2002). "The role of growth factors in the repair of bone. Biology and clinical applications." J Bone Joint Surg Am **84-A**(6): 1032-1044.
Liu, L., B. Yu, J. Chen, Z. Tang, C. Zong, *et al.* (2012). "Different effects of intermittent and continuous fluid shear stresses on osteogenic differentiation of human mesenchymal stem cells." Biomech Model Mechanobiol **11**(3-4): 391-401.
Liu, M., N. Liu, R. Zang, Y. Li and S. T. Yang (2013a). "Engineering stem cell niches in bioreactors." World J Stem Cells **5**(4): 124-135.
Liu, N., R. Zang, S. T. Yang and Y. Li (2013b). "Stem cell engineering in bioreactors for large-scale bioprocessing." Engineering in Life Sciences **14**: 4-15.
Loring, J. F., T. C. McDevitt, S. P. Palecek, D. V. Schaffer, P. W. Zandstra, *et al.* (2014). "A global assessment of stem cell engineering." Tissue Eng Part A **20**(19-20): 2575-2589.

Luke, G. P., D. Yeager and S. Y. Emelianov (2012). "Biomedical applications of photoacoustic imaging with exogenous contrast agents." Ann Biomed Eng **40**(2): 422-437.
Lusic, H. and M. W. Grinstaff (2013). "X-ray-computed tomography contrast agents." Chem Rev **113**(3): 1641-1666.
Lv, F. J., R. S. Tuan, K. M. C. Cheung and V. Y. L. Leung (2014). "Concise Review: The Surface Markers and Identity of Human Mesenchymal Stem Cells." Stem Cells **32**(6): 1408-1419.
Mackie, E. J., Y. A. Ahmed, L. Tatarczuch, K. S. Chen and M. Mirams (2008). "Endochondral ossification: How cartilage is converted into bone in the developing skeleton." International Journal of Biochemistry & Cell Biology **40**(1): 46-62.
Malizos, K. N. and L. K. Papatheodorou (2005). "The healing potential of the periosteum molecular aspects." Injury **36 Suppl 3**: S13-19.
Mannello, F. and G. A. Tonti (2007). "Concise review: no breakthroughs for human mesenchymal and embryonic stem cell culture: conditioned medium, feeder layer, or feeder-free; medium with fetal calf serum, human serum, or enriched plasma; serum-free, serum replacement nonconditioned medium, or ad hoc formula? All that glitters is not gold!" Stem Cells **25**(7): 1603-1609.
Marechal, M., J. Eyckmans, J. Schrooten, E. Schepers, F. P. Luyten, *et al.* (2008). "Bone augmentation with autologous periosteal cells and two different calcium phosphate scaffolds under an occlusive titanium barrier: An experimental study in rabbits." Journal of Periodontology **79**(5): 896-904.
Marechal, M., F. Luyten, J. Nijs, A. Postnov, E. Schepers, *et al.* (2005). "Histomorphometry and micro-computed tomography of bone augmentation under a titanium membrane." Clinical Oral Implants Research **16**(6): 708-714.
Marolt, D., M. Knezevic and G. V. Novakovic (2010). "Bone tissue engineering with human stem cells." Stem Cell Research & Therapy **1**(2): 1-10.
Martin, I., H. Baldomero, C. Bocelli-Tyndall, J. Passweg, D. Saris, *et al.* (2012). "The Survey on Cellular and Engineered Tissue Therapies in Europe in 2010." Tissue Engineering Part A **18**(21-22): 2268-2279.
Martin, I., H. Baldomero, C. Bocelli-Tyndall, I. Slaper-Cortenbach, J. Passweg, *et al.* (2011a). "The survey on cellular and engineered tissue therapies in europe in 2009." Tissue Eng Part A **17**(17-18): 2221-2230.
Martin, I., S. A. Riboldi and D. Wendt (2010). Bioreactor Systems in Regenerative Medicine. Advances in Regenerative Medicine: Role of Nanotechnology, and Engineering Principles. Dordrecht, The Netherlands, Springer Science+Business Media**:** 95-113.
Martin, I., T. Smith and D. Wendt (2009). "Bioreactor-based roadmap for the translation of tissue engineering strategies into clinical products." Trends in Biotechnology **27**(9): 495-502.
Martin, I., D. Wendt and M. Heberer (2004). "The role of bioreactors in tissue engineering." Trends in Biotechnology **22**(2): 80-86.
Martin, Y., M. Eldardiri, D. J. Lawrence-Watt and J. R. Sharpe (2011b). "Microcarriers and Their Potential in Tissue Regeneration." Tissue Engineering Part B-Reviews **17**(1): 71-80.
Mason, C., J. F. Markusen, M. A. Town, P. Dunnill and R. K. Wang (2004). "The potential of optical coherence tomography in the engineering of living tissue." Phys Med Biol **49**(7): 1097-1115.
Mastrogiacomo, M., V. S. Komlev, M. Hausard, F. Peyrin, F. Turquier, *et al.* (2004). "Synchrotron radiation microtomography of bone engineered from bone marrow stromal cells." Tissue Eng **10**(11-12): 1767-1774.
Matziolis, G., J. Tuischer, G. Kasper, M. Thompson, B. Bartmeyer, *et al.* (2006). "Simulation of cell differentiation in fracture healing: Mechanically loaded composite scaffolds in a novel bioreactor system." Tissue Engineering **12**(1): 201-208.
McCoy, R. J., C. Jungreuthmayer and F. J. O'Brien (2012). "Influence of flow rate and scaffold pore size on cell behavior during mechanical stimulation in a flow perfusion bioreactor." Biotechnol Bioeng **109**(6): 1583-1594.
McCoy, R. J. and F. J. O'Brien (2010). "Influence of shear stress in perfusion bioreactor cultures for the development of three-dimensional bone tissue constructs: a review." Tissue Eng Part B Rev **16**(6): 587-601.
McNamara, L. E., T. Sjostrom, R. M. D. Meek, R. O. C. Oreffo, B. Su, *et al.* (2012). "Metabolomics: a valuable tool for stem cell monitoring in regenerative medicine." Journal of the Royal Society Interface **9**(73): 1713-1724.
Melchels, F. P., A. M. Barradas, C. A. van Blitterswijk, J. de Boer, J. Feijen, *et al.* (2010). "Effects of the architecture of tissue engineering scaffolds on cell seeding and culturing." Acta Biomater **6**(11): 4208-4217.
Metallo, C. M., J. C. Mohr, C. J. Detzel, J. J. de Pablo, B. J. Van Wie, *et al.* (2007). "Engineering the stem cell microenvironment." Biotechnology Progress **23**(1): 18-23.
Metscher, B. D. (2009a). "MicroCT for comparative morphology: simple staining methods allow high-contrast 3D imaging of diverse non-mineralized animal tissues." BMC Physiol **9**: 11.

Metscher, B. D. (2009b). "MicroCT for developmental biology: a versatile tool for high-contrast 3D imaging at histological resolutions." Dev Dyn **238**(3): 632-640.
Mitalipova, M. M., R. R. Rao, D. M. Hoyer, J. A. Johnson, L. F. Meisner, *et al.* (2005). "Preserving the genetic integrity of human embryonic stem cells." Nature Biotechnology **23**(1): 19-20.
Mohyeldin, A., T. Garzon-Muvdi and A. Quinones-Hinojosa (2010). "Oxygen in stem cell biology: a critical component of the stem cell niche." Cell Stem Cell **7**(2): 150-161.
Mosna, F., L. Sensebe and M. Krampera (2010). "Human Bone Marrow and Adipose Tissue Mesenchymal Stem Cells: A User's Guide." Stem Cells and Development **19**(10): 1449-1470.
Mueller, D., G. Tascher, G. Damm, A. K. Nussler, E. Heinzle, *et al.* (2013). "Real-time in situ viability assessment in a 3D bioreactor with liver cells using resazurin assay." Cytotechnology **65**(2): 297-305.
Mulhall, H., M. Patel, K. Alqahtani, C. Mason, M. P. Lewis, *et al.* (2011). "Effect of capillary shear stress on recovery and osteogenic differentiation of muscle-derived precursor cell populations." Journal of Tissue Engineering and Regenerative Medicine **5**(8): 629-635.
Nam, S. Y., L. M. Ricles, L. J. Suggs and S. Y. Emelianov (2014). "Imaging Strategies for Tissue Engineering Applications." Tissue Eng Part B Rev.
Nerem, R. M. (2014). "Stem cell engineering." Tissue Eng Part A **20**(5-6): 893-894.
Ng, K. W., D. T. W. Leong and D. W. Hutmacher (2005). "The challenge to measure cell proliferation in two and three dimensions." Tissue Engineering **11**(1-2): 182-191.
Nieminen, M. T., J. Rieppo, J. Toyras, J. M. Hakumaki, J. Silvennoinen, *et al.* (2001). "T-2 relaxation reveals spatial collagen architecture in articular cartilage: A comparative quantitative MRI and polarized light microscopic study." Magnetic Resonance in Medicine **46**(3): 487-493.
Nienow, A. W., Q. A. Rafiq, K. Coopman and C. J. Hewitt (2014). "A potentially scalable method for the harvesting of hMSCs from microcarriers." Biochemical Engineering Journal **85**: 79-88.
Nociari, M. M., A. Shalev, P. Benias and C. Russo (1998). "A novel one-step, highly sensitive fluorometric assay to evaluate cell-mediated cytotoxicity." J Immunol Methods **213**(2): 157-167.
Nold, P., C. Brendel, A. Neubauer, G. Bein and H. Hackstein (2013). "Good manufacturing practice-compliant animal-free expansion of human bone marrow derived mesenchymal stroma cells in a closed hollow-fiber-based bioreactor." Biochem Biophys Res Commun **430**(1): 325-330.
Ntziachristos, V. (2010). "Going deeper than microscopy: the optical imaging frontier in biology." Nat Methods **7**(8): 603-614.
O'Brien, F. J. (2011). "Biomaterials & scaffolds for tissue engineering." Materials Today **14**(3): 88-95.
O'Brien, J., I. Wilson, T. Orton and F. Pognan (2000). "Investigation of the Alamar Blue (resazurin) fluorescent dye for the assessment of mammalian cell cytotoxicity." Eur J Biochem **267**(17): 5421-5426.
Oe, K., M. Miwa, K. Nagamune, Y. Sakai, S. Y. Lee, *et al.* (2010). "Nondestructive evaluation of cell numbers in bone marrow stromal cell/beta-tricalcium phosphate composites using ultrasound." Tissue Eng Part C Methods **16**(3): 347-353.
Olubamiji, A. D., Z. Izadifar and D. X. Chen (2014). "Synchrotron Imaging Techniques for Bone and Cartilage Tissue Engineering: Potential, Current Trends, and Future Directions." Tissue Engineering Part B-Reviews **20**(5): 503-522.
Orwoll, E. S. (2003). "Toward an expanded understanding of the role of the periosteum in skeletal health." J Bone Miner Res **18**(6): 949-954.
Oseni, A. O., P. E. Butler and A. M. Seifalian (2013). "Optimization of chondrocyte isolation and characterization for large-scale cartilage tissue engineering." J Surg Res **181**(1): 41-48.
Otsu, N. (1979). "Threshold Selection Method from Gray-Level Histograms." Ieee Transactions on Systems Man and Cybernetics **9**(1): 62-66.
Paletta, J. R. J., F. Mack, H. Schenderlein, C. Theisen, J. Schmitt, *et al.* (2011). "Incorporation of Osteoblasts (Mg63) into 3d Nanofibre Matrices by Simultaneous Electrospinning and Spraying in Bone Tissue Engineering." European Cells & Materials **21**.
Palmer, A. W., R. E. Guldberg and M. E. Levenston (2006). "Analysis of cartilage matrix fixed charge density and three-dimensional morphology via contrast-enhanced microcomputed tomography." Proceedings of the National Academy of Sciences of the United States of America **103**(51): 19255-19260.
Papadimitropoulos, A., M. Mastrogiacomo, F. Peyrin, E. Molinari, V. S. Komlev, *et al.* (2007). "Kinetics of in vivo bone deposition by bone marrow stromal cells within a resorbable porous calcium phosphate scaffold: An X-ray computed microtomography study." Biotechnology and Bioengineering **98**(1): 271-281.
Papadimitropoulos, A., E. Piccinini, S. Brachat, A. Braccini, D. Wendt, *et al.* (2014a). "Expansion of Human Mesenchymal Stromal Cells from Fresh Bone Marrow in a 3D Scaffold-Based System under Direct Perfusion." PLoS One **9**(7).

Papadimitropoulos, A., C. Scotti, P. Bourgine, A. Scherberich and I. Martin (2014b). "Engineered decellularized matrices to instruct bone regeneration processes." Bone.
Papantoniou, I., Y. C. Chai, F. P. Luyten and J. Schrooten (2013). "Process quality engineering for bioreactor-driven manufacturing of tissue engineered constructs for bone regeneration." Tissue Eng Part C Methods **19**(8): 596-609.
Papantoniou, I., Y. Guyot, M. Sonnaert, G. Kerckhofs, F. P. Luyten, *et al.* (2014a). "Spatial optimization in perfusion bioreactors improves bone tissue-engineered construct quality attributes." Biotechnol Bioeng.
Papantoniou, I., M. Hoare and F. S. Veraitch (2011). "The release of single cells from embryoid bodies in a capillary flow device." Chemical Engineering Science **66**(4): 570-581.
Papantoniou, I., M. Sonnaert, L. Geris, F. P. Luyten, J. Schrooten, *et al.* (2014b). "Three-dimensional characterization of tissue-engineered constructs by contrast-enhanced nanofocus computed tomography." Tissue Eng Part C Methods **20**(3): 177-187.
Park, J. H., R. A. Perez, G. Z. Jin, S. J. Choi, H. W. Kim, *et al.* (2013). "Microcarriers Designed for Cell Culture and Tissue Engineering of Bone." Tissue Engineering Part B-Reviews **19**(2): 172-190.
Park, S. and G. I. Im (2014). "Embryonic stem cells and induced pluripotent stem cells for skeletal regeneration." Tissue Eng Part B Rev **20**(5): 381-391.
Pattabhi, S. R., J. S. Martinez and T. C. S. Keller (2014). "Decellularized ECM effects on human mesenchymal stem cell sternness and differentiation." Differentiation **88**(4-5): 131-143.
Pattappa, G., H. K. Heywood, J. D. De Bruijn and D. A. Lee (2011). "The Metabolism of Human Mesenchymal Stem Cells During Proliferation and Differentiation." Journal of Cellular Physiology **226**(10): 2562-2570.
Pauwels, E., D. Van Loo, P. Cornillie, L. Brabant and L. Van Hoorebeke (2013). "An exploratory study of contrast agents for soft tissue visualization by means of high resolution X-ray computed tomography imaging." J Microsc **250**(1): 21-31.
Pedersen, J. A., S. Lichter and M. A. Swartz (2010). "Cells in 3D matrices under interstitial flow: Effects of extracellular matrix alignment on cell shear stress and drag forces." Journal of Biomechanics **43**(5): 900-905.
Pei, M., F. He and V. L. Kish (2011). "Expansion on extracellular matrix deposited by human bone marrow stromal cells facilitates stem cell proliferation and tissue-specific lineage potential." Tissue Eng Part A **17**(23-24): 3067-3076.
Perez-Sanchez, M. J., E. Ramirez-Glindon, M. Lledo-Gil, J. L. Calvo-Guirado and C. Perez-Sanchez (2010). "Biomaterials for bone regeneration." Med Oral Patol Oral Cir Bucal **15**(3): e517-522.
Peyrin, F., M. Mastrogiacomo, R. Cancedda and R. Martinetti (2007). "SEM and 3D synchrotron radiation micro-tomography in the study of bioceramic scaffolds for tissue-engineering applications." Biotechnology and Bioengineering **97**(3): 638-648.
Pham, Q. P., F. K. Kasper, L. Scott Baggett, R. M. Raphael, J. A. Jansen, *et al.* (2008). "The influence of an in vitro generated bone-like extracellular matrix on osteoblastic gene expression of marrow stromal cells." Biomaterials **29**(18): 2729-2739.
Piscaer, T. M., J. H. Waarsing, N. Kops, P. Pavljasevic, J. A. N. Verhaar, *et al.* (2008). "In vivo imaging of cartilage degeneration using [mu]CT-arthrography." Osteoarthritis and Cartilage **16**(9): 1011-1017.
Porter, B. D., A. S. P. Lin, A. Peister, D. Hutmacher and R. E. Guldberg (2007). "Noninvasive image analysis of 3D construct mineralization in a perfusion bioreactor." Biomaterials **28**(15): 2525-2533.
Potter, K., J. J. Butler, C. Adams, K. W. Fishbein, E. W. McFarland, *et al.* (1998). "Cartilage formation in a hollow fiber bioreactor studied by proton magnetic resonance microscopy." Matrix Biology **17**(7): 513-523.
Prewitz, M. C., F. P. Seib, M. von Bonin, J. Friedrichs, A. Stissel, *et al.* (2013). "Tightly anchored tissue-mimetic matrices as instructive stem cell microenvironments." Nature Methods **10**(8): 788-+.
Provot, S. and E. Schipani (2005). "Molecular mechanisms of endochondral bone development." Biochem Biophys Res Commun **328**(3): 658-665.
Pyka, G., A. Burakowski, G. Kerckhofs, M. Moesen, S. Van Bael, *et al.* (2012). "Surface Modification of Ti6Al4V Open Porous Structures Produced by Additive Manufacturing." Advanced Engineering Materials **14**(6): 363-370.
Quent, V. M. C., D. Loessner, T. Friis, J. C. Reichert and D. W. Hutmacher (2010). "Discrepancies between metabolic activity and DNA content as tool to assess cell proliferation in cancer research." Journal of Cellular and Molecular Medicine **14**(4): 1003-1013.
Quinn, K. P., E. Bellas, N. Fourligas, K. Lee, D. L. Kaplan, *et al.* (2012). "Characterization of metabolic changes associated with the functional development of 3D engineered tissues by non-invasive, dynamic measurement of individual cell redox ratios." Biomaterials **33**(21): 5341-5348.

Rafiq, Q. A., K. M. Brosnan, K. Coopman, A. W. Nienow and C. J. Hewitt (2013). "Culture of human mesenchymal stem cells on microcarriers in a 5 l stirred-tank bioreactor." Biotechnology Letters **35**(8): 1233-1245.
Rampersad, S. N. (2012). "Multiple applications of Alamar Blue as an indicator of metabolic function and cellular health in cell viability bioassays." Sensors (Basel) **12**(9): 12347-12360.
Rauh, J., F. Milan, K. P. Gunther and M. Stiehler (2011). "Bioreactor systems for bone tissue engineering." Tissue Eng Part B Rev **17**(4): 263-280.
Rebulla, P., T. Montemurro and R. Giordano (2010). "Regulation of cell-based medicine: the European experience." State of the Art Presentations **5**(1): 249-251 323.

Rezwan, K., Q. Z. Chen, J. J. Blaker and A. R. Boccaccini (2006). "Biodegradable and bioactive porous polymer/inorganic composite scaffolds for bone tissue engineering." Biomaterials **27**(18): 3413-3431.
Rice, W. L., D. L. Kaplan and I. Georgakoudi (2010). "Two-Photon Microscopy for Non-Invasive, Quantitative Monitoring of Stem Cell Differentiation." PLoS One **5**(4).
Ringe, J., I. Leinhase, S. Stich, A. Loch, K. Neumann, *et al.* (2008). "Human mastoid periosteum-derived stem cells: promising candidates for skeletal tissue engineering." J Tissue Eng Regen Med **2**(2-3): 136-146.
Roberts, I., S. Baila, R. B. Rice, M. E. Janssens, K. Nguyen, *et al.* (2012). "Scale-up of human embryonic stem cell culture using a hollow fibre bioreactor." Biotechnology Letters **34**(12): 2307-2315.
Roberts, S. J., L. Geris, G. Kerckhofs, E. Desmet, J. Schrooten, *et al.* (2011). "The combined bone forming capacity of human periosteal derived cells and calcium phosphates." Biomaterials.
Roberts, S. J., H. C. Owen, W. L. Tam, L. Solie, S. J. Van Cromphaut, *et al.* (2014). "Humanized culture of periosteal progenitors in allogeneic serum enhances osteogenic differentiation and in vivo bone formation." Stem Cells Transl Med **3**(2): 218-228.
Robey, P. G., S. A. Kuznetsov, J. Q. Ren, H. G. Klein, M. Sabatino, *et al.* (2015). "Generation of clinical grade human bone marrow stromal cells for use in bone regeneration." Bone **70**: 87-92.
Rodrigues, C. A. V., T. G. Fernandes, M. M. Diogo, C. L. da Silva and J. M. S. Cabral (2011). "Stem cell cultivation in bioreactors." Biotechnology Advances **29**(6): 815-829.
Rojewski, M. T., N. Fekete, S. Baila, K. Nguyen, D. Furst, *et al.* (2013). "GMP-compliant isolation and expansion of bone marrow-derived MSCs in the closed, automated device quantum cell expansion system." Cell Transplant **22**(11): 1981-2000.
Sadr, N., B. E. Pippenger, A. Scherberich, D. Wendt, S. Mantero, *et al.* (2012). "Enhancing the biological performance of synthetic polymeric materials by decoration with engineered, decellularized extracellular matrix." Biomaterials **33**(20): 5085-5093.
Salter, E., B. Goh, B. Hung, D. Hutton, N. Ghone, *et al.* (2012a). "Bone Tissue Engineering Bioreactors: A Role in the Clinic?" Tissue Eng Part B Rev **18**(1): 62-75.
Salter, E. K., B. C. Goh, B. P. Hung, D. L. Hutton, N. V. Ghone, *et al.* (2012b). "Bone Tissue Engineering Bioreactors - A Role in the Clinic?" Tissue Eng Part B Rev **18**(1): 62-75.
Santoro, R., C. Krause, I. Martin and D. Wendt (2012). "On-line monitoring of oxygen as a non-destructive method to quantify cells in engineered 3D tissue constructs." Journal of Tissue Engineering and Regenerative Medicine **6**(9): 696-701.
Sart, S., S. N. Agathos and Y. Li (2014a). "Process engineering of stem cell metabolism for large scale expansion and differentiation in bioreactors." Biochemical Engineering Journal **84**: 74-82.
Sart, S., Y. J. Schneider, Y. Li and S. N. Agathos (2014b). "Stem cell bioprocess engineering towards cGMP production and clinical applications." Cytotechnology **66**(5): 709-722.
Scadden, D. T. (2006). "The stem-cell niche as an entity of action." Nature **441**(7097): 1075-1079.
Schaffler, A. and C. Buchler (2007). "Concise review: Adipose tissue-derived stromal cells - Basic and clinical implications for novel cell-based therapies." Stem Cells **25**(4): 818-827.
Schallmoser, K., C. Bartmann, E. Rohde, A. Reinisch, K. Kashofer, *et al.* (2007). "Human platelet lysate can replace fetal bovine serum for clinical-scale expansion of functional mesenchymal stromal cells." Transfusion **47**(8): 1436-1446.
Scherberich, A., R. Galli, C. Jaquiery, J. Farhadi and I. Martin (2007). "Three-dimensional perfusion culture of human adipose tissue-derived endothelial and osteoblastic progenitors generates osteogenic constructs with intrinsic vascularization capacity." Stem Cells **25**(7): 1823-1829.
Schneider, C. K., P. Salmikangas, B. Jilma, B. Flamion, L. R. Todorova, *et al.* (2010). "Challenges with advanced therapy medicinal products and how to meet them." Nat Rev Drug Discov **9**(3): 195-201.
Schulz-Mirbach, T., M. Hess and B. D. Metscher (2013). "Sensory epithelia of the fish inner ear in 3D: studied with high-resolution contrast enhanced microCT." Front Zool **10**(1): 63.

Scotti, C., E. Piccinini, H. Takizawa, A. Todorov, P. Bourgine, *et al.* (2013). "Engineering of a functional bone organ through endochondral ossification." Proceedings of the National Academy of Sciences of the United States of America **110**(10): 3997-4002.
Scotti, C., B. Tonnarelli, A. Papadimitropoulos, A. Scherberich, S. Schaeren, *et al.* (2010). "Recapitulation of endochondral bone formation using human adult mesenchymal stem cells as a paradigm for developmental engineering." Proceedings of the National Academy of Sciences of the United States of America **107**(16): 7251-7256.
Seeger, F. H., T. Tonn, N. Krzossok, A. M. Zeiher and S. Dimmeler (2007). "Cell isolation procedures matter: a comparison of different isolation protocols of bone marrow mononuclear cells used for cell therapy in patients with acute myocardial infarction." European Heart Journal **28**(6): 766-772.
Seeman, E. (2003). "Periosteal bone formation - A neglected determinant of bone strength." New England Journal of Medicine **349**(4): 320-323.
Seib, F. P., K. Muller, M. Franke, M. Grimmer, M. Bornhauser, *et al.* (2009). "Engineered extracellular matrices modulate the expression profile and feeder properties of bone marrow-derived human multipotent mesenchymal stromal cells." Tissue Eng Part A **15**(10): 3161-3171.
Sensebe, L., P. Bourin and K. Tarte (2011). "Good manufacturing practices production of mesenchymal stem/stromal cells." Hum Gene Ther **22**(1): 19-26.
Sheehy, E. J., C. T. Buckley and D. J. Kelly (2012). "Oxygen tension regulates the osteogenic, chondrogenic and-endochondral phenotype of bone marrow derived mesenchymal stem cells." Biochemical and Biophysical Research Communications **417**(1): 305-310.
Sikavitsas, V. I., G. N. Bancroft, H. L. Holtorf, J. A. Jansen and A. G. Mikos (2003). "Mineralized matrix deposition by marrow stromal osteoblasts in 3D perfusion culture increases with increasing fluid shear forces." Proc Natl Acad Sci U S A **100**(25): 14683-14688.
Sikavitsas, V. I., G. N. Bancroft, J. J. Lemoine, M. A. Liebschner, M. Dauner, *et al.* (2005). "Flow perfusion enhances the calcified matrix deposition of marrow stromal cells in biodegradable nonwoven fiber mesh scaffolds." Ann Biomed Eng **33**(1): 63-70.
Sivasubramaniyan, K., A. Harichandan, S. Schumann, M. Sobiesiak, C. Lengerke, *et al.* (2013). "Prospective Isolation of Mesenchymal Stem Cells from Human Bone Marrow Using Novel Antibodies Directed Against Sushi Domain Containing 2." Stem Cells and Development **22**(13): 1944-1954.
Smith, L. E., R. Smallwood and S. Macneil (2010). "A comparison of imaging methodologies for 3D tissue engineering." Microsc Res Tech **73**(12): 1123-1133.
Sonnaert, M., I. Papantoniou, V. Bloemen, G. Kerckhofs, F. P. Luyten, *et al.* (2014a). "Human periosteal-derived cell expansion in a perfusion bioreactor system: proliferation, differentiation and extracellular matrix formation." J Tissue Eng Regen Med.
Sonnaert, M., I. Papantoniou, F. P. Luyten and J. Schrooten (2014b). "Quantitative validation of the Presto Blue metabolic assay for on-line monitoring of cell proliferation in a 3D perfusion bioreactor system." Tissue Eng Part C Methods.
Spanholtz, J., F. Preijers, M. Tordoir, C. Trilsbeek, J. Paardekooper, *et al.* (2011). "Clinical-Grade Generation of Active NK Cells from Cord Blood Hematopoietic Progenitor Cells for Immunotherapy Using a Closed-System Culture Process." PLoS One **6**(6).
Stephens, J. S., J. A. Cooper, F. R. Phelan and J. P. Dunkers (2007). "Perfusion flow bioreactor for 3D in situ imaging: Investigating cell/biomaterials interactions." Biotechnology and Bioengineering **97**(4): 952-961.
Stoppie, N., J. P. van der Waerden, J. A. Jansen, J. Duyck, M. Wevers, *et al.* (2005). "Validation of microfocus computed tomography in the evaluation of bone implant specimens." Clinical Implant Dentistry and Related Research **7**(2): 87-94.
Stradiotti, P., A. Curti, G. Castellazzi and A. Zerbi (2009). "Metal-related artifacts in instrumented spine. Techniques for reducing artifacts in CT and MRI: state of the art." Eur Spine J **18 Suppl 1**: 102-108.
Tan, S. and N. Barker (2013). "Engineering the niche for stem cells." Growth Factors **31**(6): 175-184.
Tan, W., A. Sendemir-Urkmez, L. J. Fahrner, R. Jamison, D. Leckband, *et al.* (2004). "Structural and functional optical imaging of three-dimensional engineered tissue development." Tissue Eng **10**(11-12): 1747-1756.
Tandon, N., D. Marolt, E. Cimetta and G. Vunjak-Novakovic (2013). "Bioreactor engineering of stem cell environments." Biotechnol Adv **31**(7): 1020-1031.
Thibault, R. A., L. Scott Baggett, A. G. Mikos and F. K. Kasper (2010). "Osteogenic differentiation of mesenchymal stem cells on pregenerated extracellular matrix scaffolds in the absence of osteogenic cell culture supplements." Tissue Eng Part A **16**(2): 431-440.

Tigli, R. S., C. Cannizaro, M. Gumusderelioglu and D. L. Kaplan (2011). "Chondrogenesis in perfusion bioreactors using porous silk scaffolds and hESC-derived MSCs." Journal of Biomedical Materials Research Part A **96A**(1): 21-28.
Tonnarelli, B., M. Centola, A. Barbero, R. Zeller and I. Martin (2014). "Re-engineering Development to Instruct Tissue Regeneration." Mechanism of Regeneration **108**: 319-338.
Truscello, S., G. Kerckhofs, S. Van Bael, G. Pyka, J. Schrooten, *et al.* (2012). "Prediction of permeability of regular scaffolds for skeletal tissue engineering: A combined computational and experimental study." Acta Biomaterialia **8**(4): 1648-1658.
Tsao, Y. S., A. G. Cardoso, R. G. G. Condon, M. Voloch, P. Lio, *et al.* (2005). "Monitoring Chinese hamster ovary cell culture by the analysis of glucose and lactate metabolism." Journal of Biotechnology **118**(3): 316-327.
Tullberg-Reinert, H. and G. Jundt (1999). "In situ measurement of collagen synthesis by human bone cells with a sirius red-based colorimetric microassay: effects of transforming growth factor beta2 and ascorbic acid 2-phosphate." Histochem Cell Biol **112**(4): 271-276.
Uzunoglu, S., B. Karaca, H. Atmaca, A. Kisim, C. Sezgin, *et al.* (2010). "Comparison of XTT and Alamar blue assays in the assessment of the viability of various human cancer cell lines by AT-101 (-/- gossypol)." Toxicol Mech Methods **20**(8): 482-486.
Van Bael, S., G. Kerckhofs, M. Moesen, G. Pyka, J. Schrooten, *et al.* (2011). "Micro-CT-based improvement of geometrical and mechanical controllability of selective laser melted Ti6Al4V porous structures." Materials Science and Engineering a-Structural Materials Properties Microstructure and Processing **528**(24): 7423-7431.
van Gastel, N., M. Depypere, I. Stockmans, J. Schrooten, F. Maes, *et al.* (2012a). "Interactions between periosteal cells and blood vessels during bone autograft healing: implications for tissue engineering strategies." Journal of Tissue Engineering and Regenerative Medicine **6**: 310-310.
van Gastel, N., S. Torrekens, S. J. Roberts, K. Moermans, J. Schrooten, *et al.* (2012b). "Engineering Vascularized Bone: Osteogenic and Proangiogenic Potential of Murine Periosteal Cells." Stem Cells **30**(11): 2460-2471.
van Lenthe, G. H., H. Hagenmuller, M. Bohner, S. J. Hollister, L. Meinel, *et al.* (2007). "Nondestructive micro-computed tomography for biological imaging and quantification of scaffold-bone interaction in vivo." Biomaterials **28**(15): 2479-2490.
Vickerton, P., J. Jarvis and N. Jeffery (2013). "Concentration-dependent specimen shrinkage in iodine-enhanced microCT." Journal of Anatomy **223**(2): 185-193.
Voronov, R. S., S. B. Vangordon, R. L. Shambaugh, D. V. Papavassiliou and V. I. Sikavitsas (2012). "3D Tissue Engineered Construct Analysis via Conventional High Resolution MicroCT without X-Ray Contrast." Tissue Eng Part C Methods.
Wagner, W., P. Horn, M. Castoldi, A. Diehlmann, S. Bork, *et al.* (2008). "Replicative senescence of mesenchymal stem cells: a continuous and organized process." PLoS One **3**(5): e2213.
Ward, A., K. P. Quinn, E. Bellas, I. Georgakoudi and D. L. Kaplan (2013). "Noninvasive metabolic imaging of engineered 3D human adipose tissue in a perfusion bioreactor." PLoS One **8**(2): e55696.
Washburn, N. R., M. Weir, P. Anderson and K. Potter (2004). "Bone formation in polymeric scaffolds evaluated by proton magnetic resonance microscopy and X-ray microtomography." Journal of Biomedical Materials Research Part A **69A**(4): 738-747.
Weiss, H. E., S. J. Roberts, J. Schrooten and F. P. Luyten (2012). "A Semi-Autonomous Model of Endochondral Ossification for Developmental Tissue Engineering." Tissue Eng Part A.
Wendt, D., A. Marsano, M. Jakob, M. Heberer and I. Martin (2003). "Oscillating perfusion of cell suspensions through three-dimensional scaffolds enhances cell seeding efficiency and uniformity." Biotechnol Bioeng **84**(2): 205-214.
Wendt, D., S. A. Riboldi, M. Cioffi and I. Martin (2009). "Bioreactors in tissue engineering: scientific challenges and clinical perspectives." Adv Biochem Eng Biotechnol **112**: 1-27.
Wersinger, C., P. Vernier and A. Sidhu (2004). "Trypsin disrupts the trafficking of the human dopamine transporter by alpha-synuclein and its A30P mutant." Biochemistry **43**(5): 1242-1253.
Wilkins, S. W., Y. I. Nesterets, T. E. Gureyev, S. C. Mayo, A. Pogany, *et al.* (2014). "On the evolution and relative merits of hard X-ray phase-contrast imaging methods." Philos Trans A Math Phys Eng Sci **372**(2010): 20130021.
Wong, M. D., A. E. Dorr, J. R. Walls, J. P. Lerch and R. M. Henkelman (2012). "A novel 3D mouse embryo atlas based on micro-CT." Development **139**(17): 3248-3256.
Wung, N., S. M. Acott, D. Tosh and M. J. Ellis (2014). "Hollow fibre membrane bioreactors for tissue engineering applications." Biotechnol Lett **36**(12): 2357-2366.

Xie, L., A. S. P. Lin, R. E. Guldberg and M. E. Levenston (2010). "Nondestructive assessment of sGAG content and distribution in normal and degraded rat articular cartilage via EPIC-mu CT." Osteoarthritis and Cartilage **18**(1): 65-72.
Xie, L., A. S. P. Lin, M. E. Levenston and R. E. Guldberg (2009). "Quantitative assessment of articular cartilage morphology via EPIC-mu CT." Osteoarthritis and Cartilage **17**(3): 313-320.
Xu, H. H., S. F. Othman, L. Hong, I. A. Peptan and R. L. Magin (2006). "Magnetic resonance microscopy for monitoring osteogenesis in tissue-engineered construct in vitro." Physics in Medicine and Biology **51**(3): 719-732.
Xu, H. H., S. F. Othman and R. L. Magin (2008). "Monitoring Tissue Engineering Using Magnetic Resonance Imaging." Journal of Bioscience and Bioengineering **106**(6): 515-527.
Yang, C., M. W. Tibbitt, L. Basta and K. S. Anseth (2014a). "Mechanical memory and dosing influence stem cell fate." Nature Materials **13**(6): 645-652.
Yang, W., S. K. Both, G. J. V. M. van Osch, Y. Wang, J. A. Jansen, *et al.* (2014b). "Performance of Different Three-Dimensional Scaffolds for in Vivo Endochondral Bone Generation." European Cells & Materials **27**: 350-364.
Yeatts, A. B., D. T. Choquette and D. Fisher (2013). "Bioreactors to influence stem cell fate: Augmentation of mesenchymal stem cell signaling pathways via dynamic culture systems." Biochim Biophys Acta **1830**(2): 2470-2480.
Yonenaga, K., S. Nishizawa, Y. Fujihara, Y. Asawa, K. Sanshiro, *et al.* (2010). "The optimal conditions of chondrocyte isolation and its seeding in the preparation for cartilage tissue engineering." Tissue Eng Part C Methods **16**(6): 1461-1469.
Youssef, K., J. J. Mack, M. L. Iruela-Arispe and L. S. Bouchard (2012). "Macro-scale topology optimization for controlling internal shear stress in a porous scaffold bioreactor." Biotechnol Bioeng.
Zhang, X., C. Xie, A. S. Lin, H. Ito, H. Awad, *et al.* (2005). "Periosteal progenitor cell fate in segmental cortical bone graft transplantations: implications for functional tissue engineering." Journal of Bone and Mineral Research **20**(12): 2124-2137.
Zhang, X. P., H. A. Awad, R. J. O'Keefe, R. E. Guldberg and E. M. Schwarz (2008). "A perspective: Engineering periosteum for structural bone graft healing." Clinical Orthopaedics and Related Research **466**(8): 1777-1787.
Zhao, F., W. L. Grayson, T. Ma and A. Irsigler (2009). "Perfusion affects the tissue developmental patterns of human mesenchymal stem cells in 3D scaffolds." Journal of Cellular Physiology **219**(2): 421-429.
Zhao, F. and T. Ma (2005). "Perfusion bioreactor system for human mesenchymal stem cell tissue engineering: dynamic cell seeding and construct development." Biotechnol Bioeng **91**(4): 482-493.
Zhou, L., J. Kong, Y. Zhuang, J. Chu, S. Zhang, *et al.* (2013a). "Ex vivo expansion of bone marrow mesenchymal stem cells using microcarrier beads in a stirred bioreactor." Biotechnology and Biopocess Engineering **18**: 173-184.
Zhou, X., I. Holsbeeks, S. Impens, M. Sonnaert, V. Bloemen, *et al.* (2013b). "Non-invasive real-time monitoring by alamarBlue(R) during in vitro culture of 3D tissue engineered bone constructs." Tissue Eng Part C Methods **19**(9): 720-729.
Zoro, B. J. H., S. Owen, R. A. L. Drake, C. Mason and M. Hoare (2009). "Regenerative Medicine Bioprocessing: Concentration and Behavior of Adherent Cell Suspensions and Pastes." Biotechnology and Bioengineering **103**(6): 1236-1247.

Curriculum vitae

Personalia

Name:	Maarten Sonnaert
Date of birth:	22nd December 1988
Place of birth:	Leuven, Belgium
Address:	Maurits Noëstraat 20 3050 Oud-Heverlee
Email:	maarten.sonnaert@hotmail.com
Tel:	+32 474/84.71.68

Education

2010-2015:	PhD Student at Prometheus, Division of Skeletal Tissue Engineering, KU Leuven
2006-2010:	Bachelor and Master of Science in Industrial Sciences, Biochemical Engineering, Focus Biomedical applications Master thesis: 3D bioreactor cultuur van periostale cellen. Magna Cum Laude
2000-2006:	Science – Mathematics option Mathematics, Sint Albertus College, Haasrode

Awards

Best oral presentation award (3rd place) at the Tissue Engineering and Regenerative Medicine International Society conference for: 'Sonnaert, M., Papantoniou, I., Bloemen, V., Kerckhofs, G., Luyten, F., Schrooten, J. (2013). 3D perfusion bioreactor culture of human periosteum derived stem cells for bone tissue engineering.' TERMIS-EU 2013, Istanbul, Turkey, 17-20 June 2013.

Research publications

IT (Articles in internationally reviewed academic journals)

Sonnaert, M.*, Kerckhofs, G.*; Papantoniou, I., Van Vlierberghe, S., Boterberg, V., Dubruel, P., Luyten, F.P., Schrooten, J.$, Geris, L.$ (2015), Multifactorial optimization of contrast-enhanced nanoCT for quantitative analysis neo-tissue formation in tissue engineering constructs. PlosOne DOI: 10.1371/journal.pone.0130227

Papantoniou, I.*, Sonnaert, M.*, Geris, L., Luyten, F., Schrooten, J., Kerckhofs, G. (2014). Three-dimensional characterization of tissue-engineered constructs by contrast-enhanced nanofocus computed tomography. *Tissue Engineering Part C, Methods, 20* (3), 177-187.(* these authors share first authorship)

Papantoniou, I., Guyot, Y., Sonnaert, M., Kerckhofs, G., Luyten, F., Geris, L., Schrooten, J. (2014). Spatial optimization in perfusion bioreactors improves bone tissue-engineered construct quality attributes. *Biotechnology and bioengineering, 111* (12), art.nr. 10.1002/bit.25303, 2560-70.

Sonnaert, M., Papantoniou, I., Luyten, F., Schrooten, J. (2014). Quantitative validation of the Presto Blue™ metabolic assay for on-line monitoring of cell proliferation in a 3D perfusion bioreactor system. *Tissue engineering. Part C, Methods*, 2015 Jun; 21(6):519-529

Lambrechts, T., Papantoniou, I., Sonnaert, M., Schrooten, J., Aerts, J. (2014). Model-based cell number quantification using online single-oxygen sensor data for tissue engineering perfusion bioreactors. *Biotechnology and Bioengineering, 111* (10), art.nr. 10.1002/bit.25274, 1982-92.

Sonnaert, M., Papantoniou, I., Bloemen, V., Kerckhofs, G., Luyten, F., Schrooten, J. (2014). Human periosteal-derived cell expansion in a perfusion bioreactor system: proliferation, differentiation and extracellular matrix formation. *Journal of tissue engineering and regenerative medicine, Ahead of print*, art.nr. 10.1002/term.1951.

Papantoniou, I., Sonnaert, M., Lambrechts, T., Aerts, J., Geris, L., Luyten, F., Schrooten, J. (2014). Analysis of gene expression signatures for osteogenic 3D perfusion-bioreactor cultures based on a multifactorial DoE approach. *Processes*, 2 (3), 639-657.

Zhou, X., Holsbeeks, I., Impens, S., Sonnaert, M., Bloemen, V., Luyten, F., Schrooten, J. (2013). Non-invasive real-time monitoring by alamarBlue® during in vitro culture of 3D tissue engineered bone constructs. *Tissue engineering. Part C, Methods, 19* (9), 720-729.

Chen, Y., Sonnaert, M., Roberts, S., Luyten, F., Schrooten, J. (2012). Validation of a picogreen-based DNA quantification integrated in an RNA extraction method for two-dimensional and three-dimensional cell cultures. *Tissue Engineering Part C, Methods, 18* (6), 444-452.

IHb (Article in academic book, internationally recognised scientific publisher)

Papantoniou, I., Mantalaris, A., Sonnaert, M., Lambrechts, T., Aerts, J., Geris, L., Schrooten, J.. (2015). Product and Process Design: Toward Industrial TE Manufacturing. In: van Blitterswijk C. (Eds.), *Tissue Engineering*, Chapt. 22 Elsevier.

IC (Papers at international scientific conferences and symposia, published in full in proceedings)

Sonnaert, M., Kerckhofs, G., Papantoniou, I., Luyten, F., Schrooten, J., Geris, L. (2014). Contrast enhanced nanoCT parameter optimisation for volumetric analyses of in vitro manufactured tissue-engineered bone constructs. *Micro-CT User Meeting*. Bruker microCT User Meeting. Ostend, Belgium, 5-8 May 2014 (pp. 19-24).

Sonnaert, M., Papantoniou, I., Geris, L., Luyten, F., Schrooten, J., Kerckhofs, G. (2013). Contrast enhanced nanoCT for 3D quantitative and spatial analysis of in vitro manufactured extracellular matrix in metallic tissue engineering scaffolds. *Abstract Book Micro-Ct User Meeting Bruker microCT 2013*. User Meeting Bruker MicroCT. Hasselt, Belgium, 16-18 April 2013 (pp. 36-41).

IMa (Meeting abstracts, presented at international scientific conferences and symposia, published or not published in proceedings or journals)

Sonnaert, M., Luyten, F.P., Schrooten, J., Papantoniou, I. (2015). Bioreactor-based expansion and online recovery of a human periosteum derived cell population with uncompromised osteogenic potential. 3rd Belgian symposium on Tissue Engineering (BSTE). Leuven, 18-19 March 2015.

Sonnaert, M., Papantoniou, I., Luyten, F., Schrooten, J. (2014). Perfusion bioreactor expansion and dynamic harvest preserve in vivo bone forming capacity of osteoprogenitor cells. Tissue Engineering and Regenerative Medicine International Society. Genova, Italy, 10-13 June 2014.

Sonnaert, M., Papantoniou, I., Luyten, F., Schrooten, J. (2014). Integrated 3D bioprocessing for the expansion and recovery of a functional progenitor cell population with uncompromised osteogenic regeneration potential. Tissue Engineering Congress 2014. London, UK, 2-4 June 2014.

Papantoniou, I., Guyot, Y., Sonnaert, M., Kerckhofs, G., Luyten, F., Lies, G., Schrooten, J. (2013). Optimized bioprocess design for improved bone tissue-engineered construct quality in perfusion bioreactors. European Society of Biomechanics. Patras, 25-28 Aug 2013.

Sonnaert, M., Kerckhofs, G., Papantoniou, I., Luyten, F., Geris, L., Schrooten, J. (2013). Optimised contrast enhanced nanoCT for volumetric analyses of in vitro manufactured tissue-engineered bone constructs. 2nd Belgian Symposium on Tissue Engineering (BSTE). Leuven, 24-25 October 2013.

Papantoniou, I., Guyot, Y., Sonnaert, M., Geris, L., Luyten, F., Schrooten, J. (2013). Linking decoupled bioprocess design to tissue-engineered construct quality attributes: a stairway to robust manufacturing. European Interdisciplinary Summit on Cell-Based ATMPs. Vienna, Austria, 2-3 May, 2013.

Lambrechts, T., Papantoniou, I., Sonnaert, M., Schrooten, J., Aerts, J. (2013). Data-based Mechanistic Models for Bioprocess Monitoring in Tissue Engineering Bioreactors. 2nd Belgian Symposium on Tissue Engineering (BSTE). Leuven, 24-25 October 2013.

Kerckhofs, G., Papantoniou, I., Sonnaert, M., Sainz, J., Marechal, M., Wevers, M., Van de Putte, T., Luyten, F., Geris, L., Schrooten, J. (2013). Contrast-enhanced nanofocus computed tomography for virtual 3D histopathology and morphometric analysis of multiple skeletal tissues. 2nd Belgian Symposium on Tissue Engineering (BSTE) 2013. Leuven, Belgium, 24-25 October 2013.

Sonnaert, M., Papantoniou, I., Geris, L., Luyten, F., Schrooten, J., Kerckhofs, G. (2013). Contrast enhanced nanoCT for volumetric analyses of in vitro manufactured tissue-engineered bone constructs: a soft tissue case study. International Conference on Tomography of Materials and Structures. Ghent, Belgium, 1-5 July 2013.

Papantoniou, I., Guyot, Y., Sonnaert, M., Luyten, F., Geris, L., Schrooten, J. (2013). A Dynamic 3D Simulation of Tissue-Engineered Construct Growth in Perfusion Bioreactors: an Integrative Approach. Tissue Engineering and Regenerative Medicine International Society. Istanbul, Turkey,17-20 June 2013.

Sonnaert, M., Papantoniou, I., Bloemen, V., Kerckhofs, G., Luyten, F., Schrooten, J. (2013). 3D perfusion bioreactor culture of human periosteum derived stem cells for bone tissue engineering. TERMIS-EU 2013, Tissue Engineering and Regenerative Medicine International Society.Istanbul, Turkey, 17-20 June 2013.

Lambrechts, T., Papantoniou, I., Sonnaert, M., Schrooten, J. (2013). Non-Invasive On-Line Measurement of Stem Cell Proliferation in a 3D Perfusion Bioreactor Using Data-Based Modelling. Tissue Engineering and Regenerative Medicine International Society (TERMIS-EU 2013).Istanbul, Turkey, 17-20 June 2013.

Sonnaert, M., Papantoniou, I., Bloemen, V., Luyten, F., Schrooten, J. (2012). Wall shear stress and progenitor cell phenotype maintenance during 3D bioreactor

perfusion. Belgian Symposium on Tissue Engineering. Leuven, Belgium, 16-17 September 2012.

Lambrechts, T., Sonnaert, M., Impens, S., Bloemen, V., Holsbeeks, I., Schrooten, J., Aerts, J. (2012). Non-invasive on-line measurement of cell activity in a 3D perfusion bioreactor. Belgian Symposium on Tissue Engineering. Leuven, Belgium, 16-17 September 2012.

Zhou, X., Sonnaert, M., Bloemen, V., Impens, S., Holsbeeks, I., Schrooten, J. (2012). Perfusion bioreactors: a promising tool for the development of regulatory approvable bone tissue engineering constructs. Belgian Symposium on Tissue Engineering (BSTE) 2012. Leuven, Belgium, 17-18 September 2012.

Zhou, X., Sonnaert, M., Bloemen, V., Impens, S., Holsbeeks, I., Schrooten, J. (2011). Perfusion bioreactors: a promising tool for the development of regulatory approvable bone Tissue Engineered constructs. Biomedica. Eindhoven, The Netherlands, 7-8 April 2011.